

University of Louisville

ThinkIR: The University of Louisville's Institutional Repository

Electronic Theses and Dissertations

5-2018

Biophysical exploration of conformational environments in zymogen prothrombin and blood coagulant thrombin.

Ramya Billur
University of Louisville

Follow this and additional works at: <https://ir.library.louisville.edu/etd>



Part of the [Other Biochemistry, Biophysics, and Structural Biology Commons](#)

Recommended Citation

Billur, Ramya, "Biophysical exploration of conformational environments in zymogen prothrombin and blood coagulant thrombin." (2018). *Electronic Theses and Dissertations*. Paper 2904.
<https://doi.org/10.18297/etd/2904>

This Doctoral Dissertation is brought to you for free and open access by ThinkIR: The University of Louisville's Institutional Repository. It has been accepted for inclusion in Electronic Theses and Dissertations by an authorized administrator of ThinkIR: The University of Louisville's Institutional Repository. This title appears here courtesy of the author, who has retained all other copyrights. For more information, please contact thinkir@louisville.edu.

BIOPHYSICAL EXPLORATION OF CONFORMATIONAL ENVIRONMENTS IN
ZYMOGEN PROTHROMBIN AND BLOOD COAGULANT THROMBIN

By

Ramya Billur
B.Sc., Osmania University, 2008
M.Sc., Jawaharlal Nehru Technological University, 2010

A Dissertation
Submitted to the Faculty of the
College of Arts and Sciences of the University of Louisville
in Partial Fulfillment of the Requirements
for the Degree of

Doctor of Philosophy in Chemistry

Department of Chemistry
University of Louisville
Louisville, Kentucky

May 2018

Copyright 2018 by Ramya Billur

All rights reserved

BIOPHYSICAL EXPLORATION OF CONFORMATIONAL ENVIRONMENTS IN
ZYMOGEN PROTHROMBIN AND BLOOD COAGULANT THROMBIN

By

Ramya Billur
B.Sc., Osmania University, 2008
M.Sc., Jawaharlal Nehru Technological University, 2010

A Dissertation approved on

April 30, 2018

by the following Dissertation Committee:

Dissertation Chair
Dr. Muriel C. Maurer

Dr. Richard J. Wittebort

Dr. Robert M. Buchanan

Dr. Stanley E. D'Souza

DEDICATION

This dissertation is dedicated to my parents Mr. Vijay Kumar Billur and Mrs. Sharada Billur who always encouraged and allowed me to pursue higher education in Science

To
My spiritual teacher Bramhasri Chaganti Koteswara Rao

ACKNOWLEDGMENTS

I always believed in the credo “When your soul really wants something and desires for it, then the entire universe conspires in helping you to achieve it”. It is to this belief that I attribute all my accomplishments till today and still lean towards science.

I am extremely indebted to my dear mentor Dr. Muriel Maurer for allowing me to be the part of her protein biochemistry lab. I highly appreciate her time for training me from the basic biochemistry techniques to complex NMR methods. I am so grateful to her for being so encouraging even through the toughest times of graduate school. I cannot thank her enough for improving my professional career by encouraging and allowing me to attend several conferences. I always consider her as my role model in terms of planning and implementing ideas for productive results in both personal and professional life. Many thanks for being so patient and understanding from day one until today.

I want to convey my deepest appreciation to my favorite faculty Dr. Richard Wittebort for being so nice and helpful through the entire course of my dissertation. I admire the way he is not only expert in biophysical chemistry but also has skills in photography, shaping wood, dealing with electronics. It was fun traveling with his team to Columbus, Ohio for Gateway NMR conference and having spicy biryani on our way back to Louisville. I am so lucky to have registered for Dr. Robert Buchanan’s course and having him on my committee. His course on bioinorganic phenomenon led me to acquire knowledge on importance of metals for various physiological processes. I would like to thank Dr. Stanley D'Souza for being the external committee member and encouraging me to think out of the box to have a big and improvised picture of my research.

I would like to thank my crew in professor Maurer’s lab. Special mention to my dear friend Dr. Kelly Mouapi for always supporting, caring and encouraging. I cannot imagine how my research would go smooth without her pointers. She is more than a friend to me. Boris, thanks for being a strong critique during our lab meetings. This helped me improve my critical thinking during scientific paper reading. A big thanks to my little brother Dino Ablan who encouraged me during the final stages of research and dissertation writing. Omair and Mohammed, I am so impressed the way you read the research articles for our regular group meetings. Wish you all the best for your upcoming career plans. I really had great time working with several outstanding undergraduates during the past five years. Thanks for making research less stressful with your humor. Thank you Dr. Marina Malvichko for your professional guidance.

I would like to take time to thank exceptional NMR researchers- Dr. Neal Stolowich, Dr. Dr. Ying Li, and Faye for helping me during NMR crisis. I appreciate Michael Sabo, Dr. David Ban’s help with python code, intriguing data analysis, and K_D determination which

made a great impact in our PAR3 manuscript. I am lucky enough to meet Dr. Elizabeth Komives (UCSD) at Biophysical Society annual meetings. Discussions with her about studying thrombin ligand complexes by NMR are appreciated. Dr. Enrico Di Cera and Ms. Leslie Pelc (St. Louis University) your kind gift of thrombin R77aA mutant added a significant weightage to our PAR3 manuscript.

A big thanks to Dr. Eugene Mueller, Dr. Michael Nantz, Dr. Xiang Zhang, and Dr. Cecilia Yappert for the interesting and challenging coursework. Thank you, Dr. Danielle Franco, Dr. Mark Noble, Dr. Aleeta Powe, Dr. Lenore Hoyt, and Dr. Baldwin for making teaching labs less overwhelming. Dr. Mumiye Ogunwale, thanks for your advice and care all through these years. Steve, thanks for being the “fixer upper” of chemistry and surprising me with grapes and bike. Computer you found from surplus made my dissertation writing much easier. Sherry Nalley thanks for making our paper work easier in chemistry. Chemistry Graduate Student Association (CGSA) in chemistry is one of a kind, for organizing Derby lectures which always had awe inspiring talks. I appreciate UofL escort services which always ensured the safety of students during nights.

I like to thank Dr. Radhika Dasari, and Dr. Govi Reddy for being the crisis managers of my life. To my special friends Abdullah Al Mamum, and Anam Paul Opu, thanks for all the help. To my host family Debbie Ruehl and Dan Ruehl thanks for considering me as your daughter and showing your love all these years. I am lucky enough to have wonderful roommates who were like a family during my tenure as a graduate student. In particular, thanks a lot Sowmya and Swetha for being so nice. I would like to thank my UPA family and dearest friends in Louisville- Swathi, Raju, Aadhya, Chandu, Satya, Harish, Kolli, Manasa, Mani, Varshini, Arghya, Megan, Rupa, Kim and the list goes on.

Yash, Suhas, and Madhan I appreciate your care and suggestions during hardest times. Here I wanted to thank Dr. Sarabani pal, Gopi sir for being the best science teachers during masters and in high school. I also wanted to acknowledge the tremendous encouragement that I received from my dear uncle Sudheendra Billur and cousin Madhusudhan Dammur. Rupakka and Shilpakka, thanks for everything. You both are simply awesome. I am so glad to receive blessings from Billur, Karanam, Kottidinty, Dammur, and Bannai families.

Last but not the least is my loving family Appa, Amma and Uday. I cannot imagine my life without you. I would not have come this far and pursued my dreams without your selfless efforts. Thanks for having faith in me and let me continue my passion. I Love you and yes, we did it...!

ABSTRACT

BIOPHYSICAL EXPLORATION OF CONFORMATIONAL ENVIRONMENTS IN ZYMOGEN PROTHROMBIN AND BLOOD COAGULANT THROMBIN

Ramya Billur

April 30, 2018

The serine protease thrombin plays important roles in coagulation, anticoagulation, and platelet activation. Thrombin is initially expressed as the inactive zymogen prothrombin (ProT). The final cleaved and activated form of thrombin has mature anion binding exosites (ABEs) and several regulatory loops. Engagement with these exosites helps define the fate of thrombin as a procoagulant or an anticoagulant. Researchers previously reported that zymogen ProT may already bind exosite ligands. Little is known about conformational changes associated with ProT maturation, resultant ligand binding affinities, individual ligand-protein contacts, and long-range communication between thrombin exosites.

Protease Activated Receptors (PARs) play critical roles in controlling platelet activation. Using solution NMR methods, we demonstrated that PAR3 (44-56) and weaker binding version PAR3G (44-56, P51G) can already bind to immature pro-ABE I. 1D and 2D ^1H - ^{15}N HSQC titrations revealed that PAR3G ^{15}N -E48 and ^{15}N -D54 both entered into higher affinity, intermediate exchange regimes as ProT was converted into thrombin. The high affinity of PAR3G D54 suggests that the thrombin R77a region is better oriented for

binding than thrombin R75. PAR3G ¹⁵N-F47 and ¹⁵N-L52 experienced significant changes in chemical shift and thus chemical environment upon ABE I maturation. However, the ProT 30s loop made better contacts with PAR3 than the ProT hydrophobic cluster (F34, L65, and I82).

The project was extended to PAR1 (49-62). Both PAR1P and weaker version PAR1G (P54G) bound to ProT and proton NMR line broadening increased with thrombin. 1D and 2D ¹H-¹⁵N HSQC titrations revealed that unlike PAR3G (44-56), PAR1G (49-62) ¹⁵N- K51, E53, F55, D58, and E60 exhibited little interactions with ProT. Affinities increased with mature thrombin ABE I. NMR titrations could probe PAR1 (⁵⁸DEEKN⁶²), a region previously unresolved by X-ray crystallography. Interestingly, the ABE II ligand GpIb α (269-282, 3Y_P) influenced the NMR binding affinities of PAR1G and PAR3G supporting long-range communication between the ABE II and ABE I exosites. Finally, our studies shifted toward the thrombin active site region. Kinetic assays and 2D tr-NOESY studies provided clues on why Fibrinogen B β (5-16) is such a weak thrombin substrate. The Fibrinogen B β ¹⁰FFSAR¹⁴ sequence contributes towards hindering binding (K_m) and product turnover (k_{cat}).

TABLE OF CONTENT

ACKNOWLEDGEMENTS.....	IV
ABSTRACT.....	VI
LIST OF TABLES.....	IX
LIST OF FIGURES.....	X
LIST OF EQUATIONS.....	XIV

CHAPTER

1. INTRODUCTION.....	1
2. EXPERIMENTAL TECHNIQUES.....	26
3. DECIPHERING CONFORMATIONAL CHANGES ASSOCIATED WITH THE MATURATION OF THROMBIN ANION BINDING EXOSITES.....	40
4. BINDING INTERACTIONS OF PAR1 AND PAR3 FOR THROMBIN AND DISSECTING ALLOSTERIC LINKAGE BETWEEN THE EXOSITES.....	67
5. SECONDARY STRUCTURE INFORMATION AS A CLUE TO EXPLAIN THE WEAK KINETICS OF THROMBIN-CATALYZED RELEASE OF FIBRINOPEPTIDE B.....	102
6. RESEARCH SUMMARY AND FUTURE DIRECTIONS.....	119
REFERENCES.....	129
APPENDIX.....	148
CURRICULUM VITAE.....	203

LIST OF TABLES

1. Substrate sequences that bind thrombin active site region.....	14
2. Precessional frequencies of nuclei at various field strength.....	27
3. Binding affinity values for PAR3G _{FD} and PAR3G _{EL} when bound to ProT and thrombin.....	57
4. Binding affinity values for PAR1P _{FD} , PAR1G _{FD} , PAR1G _{ED} , and PAR1G _{KE} when bound to ProT and thrombin.....	82
5. Binding affinity values for PAR1G _{ED} when bound to thrombin and GpIb α + thrombin.....	93
6. Binding affinity values for PAR3G _{EL} when bound to thrombin and GpIb α + thrombin.....	93
7. Substrate sequences that bind thrombin active site region with site of cleavage indicated.....	110
8. Kinetic constants for hydrolysis of thrombin substrates.....	110

LIST OF FIGURES

1. Extrinsic and Intrinsic pathways.....	5
2. Modern blood coagulation cascade.....	6
3. Crystal structure of fibrinogen and fibrin formation.....	8
4. Activation of Prothrombin and its products.....	10
5. Crystal structures of ProT, PT-2, and IIa.....	10
6. Crystal structure of PPACK-IIa.....	12
7. Serine protease mechanism.....	12
8. Ligand binding modes of PAR3 and GpIb α with IIa.....	13
9. Crystal structure of PAR1 LDPR region bound to IIa.....	15
10. Crystal structure of FXIII A ₂	17
11. Conversion of FXIII A ₂ to FXIIIa.....	17
12. Crystal structure of GpIb α and GpIb α bound to von Willebrand factor.....	19
13. Mechanism of PAR1 activation.....	20
14. Sequence comparison of hPAR1, mPAR1, hPAR3, mPAR3, and Hirudin.....	20
15. Orientation of precessing nuclei in external magnetic field.....	27
16. Protein conformational change over broad timescales.....	29
17. General pulse sequence of 2D-NMR.....	30
18. Pulse sequence of 2D TOCSY.....	31
19. Schematic TOCSY spectrum of 3 spins.....	31
20. Pulse sequence of 2D tr-NOESY.....	32

21. Cartoon showing NOE and 1D line broadening of PAR3 (44-56).....	34
22. Three exchange regimes of protein-ligand interactions.....	35
23. Pulse sequence of 2D HSQC.....	36
24. ITC binding curve.....	37
25. Schematic representation of ITC.....	38
26. Dependence of ITC binding curve on <i>c</i> value.....	39
27. Crystal structure of IIa, and ProT shown in ribbon and surface formats.....	41
28. Crystal structure of PAR3 (44-56) bound to IIa.....	42
29. Structural alignment of (pro)-ABE I regions of 4HZH, 2PUX, and 1PPB.....	43
30. 1D proton line broadening of PAR3(44-56) and PAR3G (44-56) in the presence of ProT and PPACK-IIa.....	53
31. 2D ¹ H- ¹⁵ N HSQC of PAR3G _{FD} (44-56) in the presence of ProT and PPACK-IIa.....	56
32. Binding affinities of PAR3G _{FD} (44-56) F47 and D54 in the presence of ProT and PPACK-IIa.....	58
33. 1D and 2D ¹ H- ¹⁵ N HSQC of PAR3G _{FD} (44-56) in the presence of PPACK-R77Aa.....	60
34. 2D ¹ H- ¹⁵ N HSQC of PAR3G _{EL} (44-56) in the presence of ProT and PPACK-IIa.....	61
35. Crystal structure of PAR1 (49-62) bound to IIa.....	69
36. Structural alignment of (pro)-ABE I regions of 4HZH, 2PUX, 1PPB, 1P8V, and 1OOK.....	71
37. 1D proton line broadening of PAR1(49-62) and PARG (49-62) in the presence of ProT and PPACK-IIa.....	79
38. Selected NOE cross peaks of PAR1P (49-62) when bound to ProT and NOE showing <i>trans</i> conformation of Xaa-Pro bond.....	79
39. 1D, 2D ¹ H- ¹⁵ N HSQC, and K _D binding curve PAR1P _{FD} (49-62) F55 in the presence of ProT.....	81

40. 1D, 2D ^1H - ^{15}N HSQC of PAR1G _{FD} (44-56) F55 in the presence of ProT.....	83
41. 1D, 2D ^1H - ^{15}N HSQC, and K_D binding curve PAR1G _{FD} (49-62) F55 in the presence of PPACK-IIa.....	84
42. 1D HSQC of PAR1G _{ED} (49-62) in the presence of ProT and PPACK-IIa.....	86
43. Binding affinities of E53 and D58 of PAR1G _{ED} (49-62) in the presence of ProT and PPACK-IIa.....	87
44. 1D HSQC of PAR1G _{KE} (44-56) in the presence of ProT and PPACK-IIa.....	88
45. 2D ^1H - ^{15}N HSQC of PAR1G _{KE} (44-56) in the presence of ProT and PPACK-IIa.....	89
46. Binding affinities of K51 and E60 of PAR1G _{KE} (49-62) in the presence of ProT and PPACK-IIa.....	89
47. 1D, 2D ^1H - ^{15}N HSQC of PAR1G _{ED} (49-62) in the presence of GpIb α + PPACK-IIa.....	91
48. Binding affinities of E53 and D58 of PAR1G _{ED} (49-62) in the presence of GpIb α + PPACK-IIa.....	92
49. 1D, 2D ^1H - ^{15}N HSQC of PAR3G _{EL} (44-56) in the presence of GpIb α + PPACK-IIa.....	92
50. Comparison of interactions between PAR1 +IIa and PAR3 +IIa.....	96
51. Crystal structure of thrombin active region and interactions with P ₄ -P ₁ segment of FXIII AP.....	103
52. Mechanism of Fibrin formation.....	104
53. Chromatogram displaying Fbg B β (5-16) hydrolysis by thrombin.....	109
54. 1D proton line broadening of Fbg B β (5-16) when bound to thrombin.....	111
55. 2D tr-NOESY fingerprint region of Fbg B β (5-16) when bound to thrombin....	112
56. 2D tr-NOESY aliphatic region of Fbg B β (5-16) when bound to thrombin.....	113
57. 2D tr-NOESY amide region of FpB B β (5-16) when bound to thrombin.....	113

58. Cartoon displaying all possible NOEs of Fbg B β (5-16) when bound to thrombin.....	114
59. ITC binding curve of DNA aptamer +thrombin.....	124
60. ITC binding curve of PAR3 (44-56) +thrombin.....	125

LIST OF EQUATIONS

1. Dependence of resonance of the nuclei on external magnetic field.....	27
2. Relation between rotational correlation time and radius of the protein.....	28
3. The uncertainty principle.....	29
4. Relation between intensity of a NOE and distance between two spins.....	32
5. General equilibrium of protein-ligand interaction.....	35
6. Rate of chemical exchange of protein-ligand interaction.....	35
7. Quadratic equation for dissociation calculation.....	37
8. Gibbs fundamental equation.....	37
9. Dependence of c on ITC binding curve.....	39
10. Calculation of percent bound of protein.....	77

CHAPTER I

INTRODUCTION

Over time, an important host defense mechanism that highly evolved vertebrates adopted was hemostasis. Hemostasis can be defined as a mechanism for formation of a blood clot at the site of vascular injury, while not disturbing the blood flow throughout the rest of the body. During a vascular injury, platelet interactions with several clotting factors, red blood cells, and white blood cells forms a protective plug, which stops the flow of blood. To maintain balance, fibrinolytic mechanisms also evolved to degrade the clot and restore normal blood flow in the injured blood vessels.^{1,2}

Since the 1800s, blood coagulation has been recognized as an important biological phenomenon and has drawn the attention of many world class biochemists and physicians.³ Over the years, there were debates about the different nomenclatures being used for clotting factors. All this came to an end by the establishment of a standard nomenclature approved by an international committee and now regularly reviewed by the ISTH (International Society on Thrombosis and Hemostasis). For most of the clotting factors, a Roman Numeral nomenclature was assigned based on their time of discovery.⁴ This chapter will highlight the various coagulation pathways, the individual clotting factors, and the receptors that help control coagulation.

Blood coagulation cascade

Fibrinogen, also called factor I, was the first factor isolated and is an abundant glycoprotein in plasma.^{5,6} Fibrin is formed by the limited proteolysis of fibrinogen and followed by polymerization. Fibrin is the only coagulation protein whose existence has not been debated. Schmidt isolated fibrin ferment from fresh serum and later named the reactive component as thrombin. This thrombin was proposed to polymerize fibrinogen when tissue extracts could not convert fibrinogen to fibrin.³ The discovery of prothrombin (factor II or ProT), through differential precipitation strategies from blood, led the researchers to believe that thrombin cannot be extracted from blood. Thrombin must instead be generated from ProT following limited proteolysis.⁷⁻¹⁰ Morawitz developed a classical theory of blood coagulation. He proposed a four-factor theory, where tissue factor, also called thromboplastin (or thrombokinase), converts ProT to thrombin in the presence of calcium ions. Later, the activated thrombin converts fibrinogen into a meshy clot called fibrin. This four-factor theory was accepted for 50 years.^{4,11} However in 1947 based on a natural clotting defect, Owren put an end to the classical theory by concluding that normal plasma needs another factor to complete the action of thromboplastin. Further research led to the discovery of factor V (Proaccelerin).¹² Later, additional natural clotting defects led to the discovery of factors VII and X (Stuart-Prower factor). At the same time, a phospholipid environment was identified as being important in the conversion of prothrombin to thrombin. Biggs, Douglas, and Macfarlane demonstrated that haemophilic blood cannot produce fibrin.^{13,14} They also showed that fibrin production can be triggered by adding antihemophilic globulin that was later found to contain factor VIII (Antihemophilic factor).¹⁵⁻¹⁸ Characterizing several other clotting deficiencies led to the

discoveries of clotting factors IX (Christmas factor), XI (PTA, Plasma Thromboplastin Antecedant) and XII (Hageman factor). Laki and Lorand partially purified a fibrin-stabilizing factor which is now called factor XIII.¹⁹ Chen and Doolittle subsequently identified that factor XIII has transglutaminase activity and is responsible for the formation of cross links between fibrin monomers.²⁰

In 1964, Macfarlane incorporated the newly discovered proteins into an updated blood coagulation cascade.¹¹ He classified the cascade into two pathways: Intrinsic and Extrinsic. As the name suggests, the intrinsic pathway is triggered by the components which are already present in plasma. For the extrinsic pathway to occur, it requires exposure of tissue factors on the damaged cell wall. A clearer picture of coagulation evolved over time.

Intrinsic pathway

Upon encountering a negatively charged surface such as a membrane, Factor XII (FXII) in the presence of cofactor High Molecular Weight Kininogen HMWK or HK gets activated to FXIIa. The letter “a” indicates that FXII has been activated. The minute amounts of FXIIa produced then use HMWK as an anchor to convert prekallikrein to kallikrein. Newly formed kallikrein acts as a positive feedback to accelerate FXIIa production. FXIIa then proteolytically cleaves FXI to form FXIa consecutively forming FIXa from FIX with HMWK as a cofactor. A complex called “*tenase*” consisting of FVIIIa, FIXa, Ca^{+2} , and phospholipid membrane next converts FX to FXa. Finally, FXa with the help of cofactor FVa and in the presence of Ca^{+2} and phospholipid membrane forms a complex called “*prothrombinase*” which converts prothrombin (II) to thrombin (IIa) (**Figure 1**).²¹

Extrinsic pathway

The extrinsic pathway is initiated by the formation of a complex between FVII and TF (Tissue Factor). Tissue factor is a receptor for FVII and is located on cell surfaces. Whenever there is an injury to endothelium cells, FVII encounters TF and is nonproteolytically activated to FVIIa. Activated FVII proteolytically activates FIX, which accelerates the function of the *tenase* complex leading to the formation of FXa. With the formation of FXa, the *prothrombinase* complex is established leading to the formation of FIIa from FII. Biochemists have debated whether the extrinsic pathway is more physiologically relevant than the intrinsic pathway. Published results have provided evidence that even in the absence of FXII, the time taken for clot formation is not changed.

Both the intrinsic and extrinsic pathways merge at a common point where FX is converted to FXa from the *tenase* complex. FXa is then the first factor to trigger the rest of the cascade. As mentioned earlier, FXa is a key component of the *prothrombinase* complex that is responsible for thrombin (FIIa) formation. The resultant serine protease thrombin converts freely flowing fibrinogen into a fibrin network. This fibrin network is later susceptible to proteolysis by plasmin. To maintain complete hemostasis, FIIa converts FXIII to FXIIIa, which covalently cross links fibrin monomers into a hard clot. Interestingly, the production of thrombin acts as a positive feedback by helping to activate cofactors FV and FVIII.^{21,22}

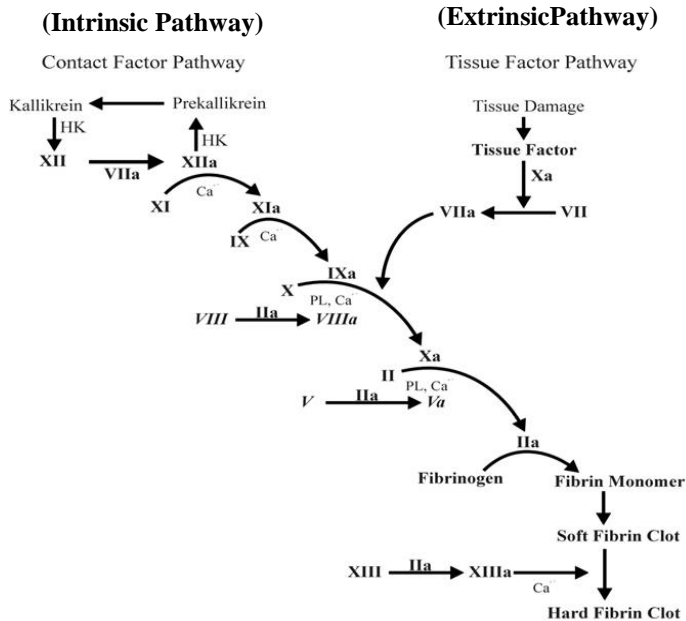


Figure 1: Blood coagulation factors are shown as Roman numerals. The letter “a” after the Roman numerals denotes the active form of the factor. Other abbreviations include: HK-High Molecular Weight Kininogen, Ca-Calcium ion and PL-phospholipid. The common final pathway for both extrinsic and intrinsic pathways is the formation of Xa and Va.

Modern blood coagulation and the importance of platelets

None of the above-mentioned pathways indicated the importance of platelets. From 1996 to 2001, several changes were made to generate a more general Modern Blood Coagulation Cascade (Figure 2).²³ The updated viewpoint involved three steps: a) Initiation b) Amplification, and c) Propagation. The initiation step involves exposure of Tissue Factor (TF) on injured endothelium cells and formation of a complex between FVIIa and TF. This assembly leads to generation of minute amounts of FIXa and FXa. FXa on the TF bearing cell accumulates the *prothrombinase* complex components to convert prothrombin (II) to thrombin (IIa). Later in the amplification stage, the small amount of thrombin that is formed in the initiation stage activates platelets, thereby exposing receptors for clotting factors to adhere on to platelets. The activated platelets slowly expose FVa and

FVIIIa which leads to positive feedback for higher amounts of thrombin generation. Meanwhile, platelet adhesion starts to develop to initiate the propagation step. A burst of thrombin production occurs during the propagation step. TF bearing cells sequentially activate FIX, FX, FVIII, and FV leading to the formation of thrombin in higher amounts. The resultant active thrombin finally converts fibrinogen to fibrin.^{23,24}

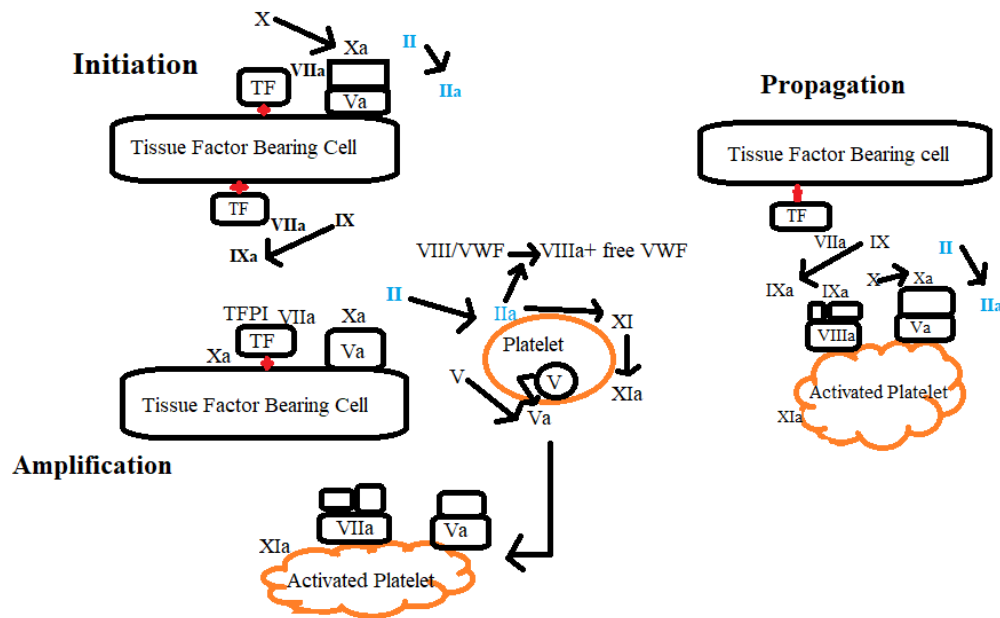


Figure 2: A) Initiation- TF on endothelium cell is exposed. FVIIa and TF interacts leading to the formation of IXa and Xa and minute amounts of FIIa. B) Amplification- Thrombin activates platelets, cofactors V and VIII and exposes various receptors on platelet surfaces. C) Propagation- platelet adhesion increases, factors IX, XI, X and VIII are activated to trigger thrombin burst which leads to the conversion of fibrinogen to fibrin.

Anticoagulation

To control the growth of unwanted thrombi in normal vascular areas, the anticoagulant pathway is triggered. Three anticoagulants that terminate the coagulation cascade are antithrombin (ATIII), Protein C, and Protein S.²⁵ ATIII in the presence of heparin inhibits the activities of serine proteases like FIIa, FIXa, FXa, FXIa, and FXIIa

Thrombomodulin (TM) when bound to endothelial cells accelerates the thrombin activation of Protein C by several thousand-fold. Protein C with the help of Protein S inhibit cofactors FVa and FVIIIa.^{26,27} Finally, Tissue Factor Pathway Inhibitor (TFPI) forms a complex with FXa and TF/FVIIa to hinder the start of the extrinsic pathway.

Fibrinogen

Fibrinogen (340 kDa) is an abundant glycoprotein composed of a dimer of nonidentical polypeptide chains ($A\alpha$, $B\beta$ and γ)₂. This protein is 450 Å long and is held together with several disulfide linkages (**Figure 3A**).^{1,6} The fibrinogen dimer of trimers is sigmoidal in shape due to the following features. The N-termini of all six polypeptides merge together to form a central globular “E” region. The C-termini of three chains meet at a point forming a globular “D”. This region is mainly composed of $B\beta$ and γ chains.^{28,29} During fibrin formation, adjacent knobs in the “E” region make favorable contacts with the holes in the “D” region which increases the stability of fibrin. An interesting feature of the $A\alpha$ chain is its C-terminus. It is a long flexible coiled-coil which ends with the αC domain. The αC regions (αC -connector and αC -domain) are not detected by X-ray crystallography and are considered as free-swimming appendages of fibrinogen. The αC domains associate to form a dimeric domain near the central E region (**Figure 3B**).^{5,30} Fibrin clot stability and mechanical stiffness is improved when αC is crosslinked by FXIIIa.³¹ This flexible αC region is susceptible to lysis by the actions of plasmin.³²

Another interesting feature of fibrinogen is the presence of 11 Asparaginyl- linked carbohydrates. Deglycosylation leads to an increase in the acceleration of fibrin formation,

however, desialidation resulted in the same rates of polymerization. Thus, it is the electrostatic charge effect that drives or dominates the events of polymerization.³³

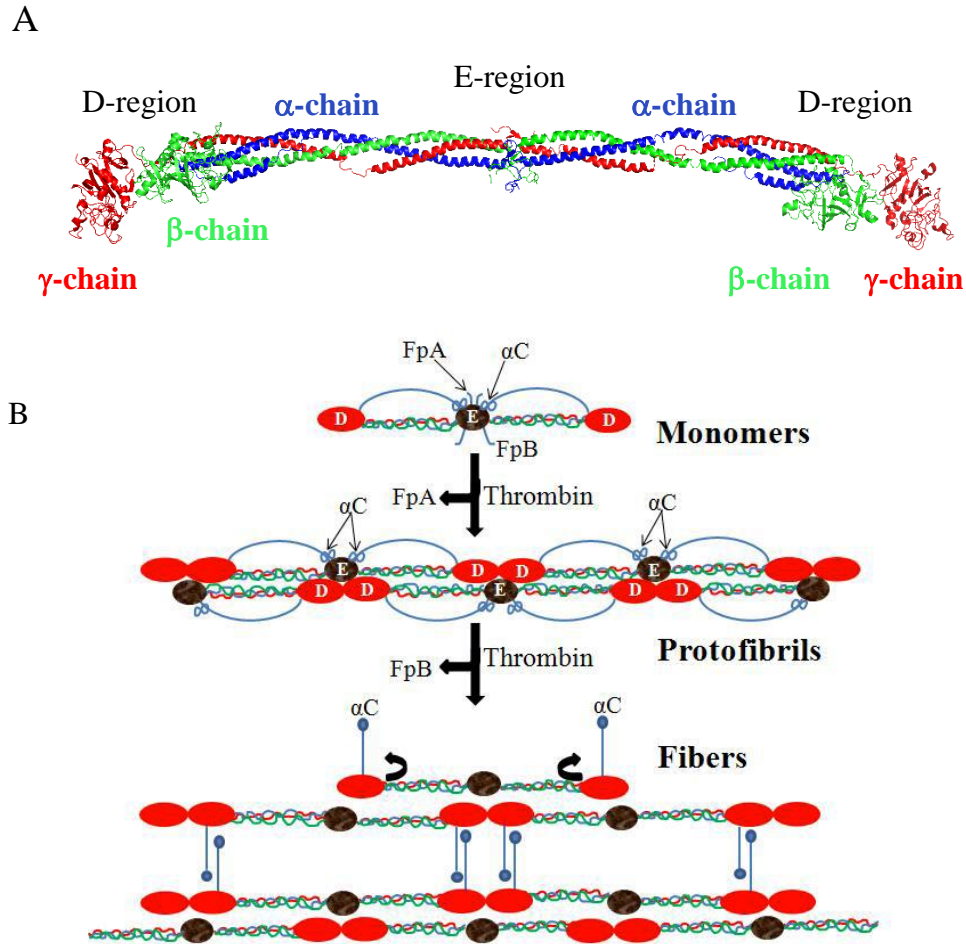


Figure 3: A) Fibrinogen α , β and γ are represented in blue, green and red. The cartoon includes coiled-coil connecting central E region and terminal D regions. Flexible α C and carbohydrates not shown. This cartoon is generated in Pymol through PDB code 3GHG. B) Fibrin clot formation is initiated by the cleavage of FpA leading to the formation of protofibrils, next the cleavage of FpB results in lateral aggregation of fibrin. Finally, FXIIIa imparts isopeptide bonds between two fibrin molecules thereby stabilizing fibrin architecture. Cartoon was adapted from Weisel, J.W. (2007).

The initial step of fibrin formation is triggered by the release of Fibrinopeptide A (FpA) by thrombin. Thrombin cleaves at the Arg16-Gly17 peptide bond of Fbg α , leading to the formation of protofibrils. This reaction is followed by thrombin cleavage of

Fibrinopeptide B (FpB) at the Arg14-Gly15 peptide bond. Release of these two N-terminal peptides within the central E region accelerates the lateral aggregation of fibrin (**Figure 3B**).³⁰ Activated FXIII (FXIIIa) is then responsible for the introduction of covalent γ -glutamyl- ϵ -lysine cross-links between the fibrin molecules.^{34,35} These cross links make the fibrin clot stiffer and less susceptible to fibrinolysis. Interactions observed in the crystal packing of human fibrinogen are end-to-end interactions between γ C domains, lateral antiparallel interactions between β C, and antiparallel association of coiled-coil regions. A and B knobs of the central E region are buried in β C and γ C holes.^{33,36}

Thrombin

The serine protease thrombin is originally produced as the 72 kDa zymogen, Prothrombin (ProT). ProT is a Vitamin K-dependent protein composed of Fragment-1 (1-155), Fragment-2 (156-271) and a protease domain (272-579). Fragment-1 contains a Gla domain (which contains 10 γ -carboxyglutamates) and disulfide containing Kringle-1. Fragment-2 contains a second disulfide containing Kringle-2, and the protease domain contains the A chain (272-320) and the catalytic B chain (321-579).³⁷ ProT is physiologically activated by the *prothrombinase* complex consisting of the serine proteinase Factor Xa and the cofactor Factor Va, a phospholipid membrane, and Ca^{2+} . ProT is anchored to the membrane surface through the Gla domain of Fragment 1 (F1). The membrane-associated prothrombinase complex can first be cleaved at ProT R320 leading to formation of an active intermediate Meizothrombin or cleavage at ProT R155 to form another inactive intermediate called Prethrombin-1 (PT1) (**Figure 4**). In platelets, cleavage of ProT at R271 leads to the formation of the inactive precursor Prethrombin-2 (PT2) and

Fragment 1.2 (Gla, Kringle 1, and Kringle 2). Subsequent cleavage at R320 gives rise to the active protease thrombin (36.7 kDa). (**Figure 4, 5**).³⁸⁻⁴⁰ Autolysis of α -thrombin generates β -thrombin. Further autolysis leaves γ -thrombin.⁴¹

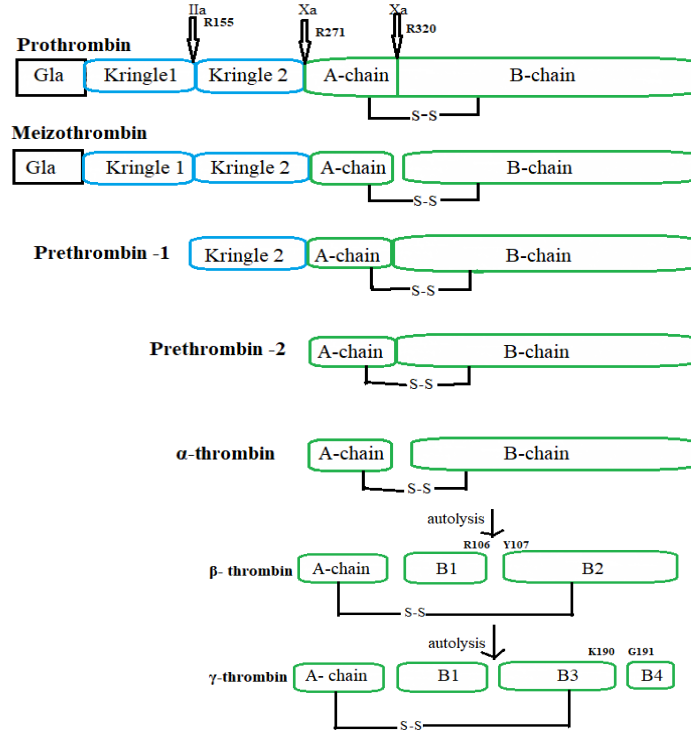


Figure 4: Schematic representation showing cleavages that occur in the conversion of prothrombin to meizothrombin or prethrombin-2 and then to thrombin. Autolysis leads to β -thrombin and then to γ -thrombin (Straight numbering is presented for β and γ -thrombin).

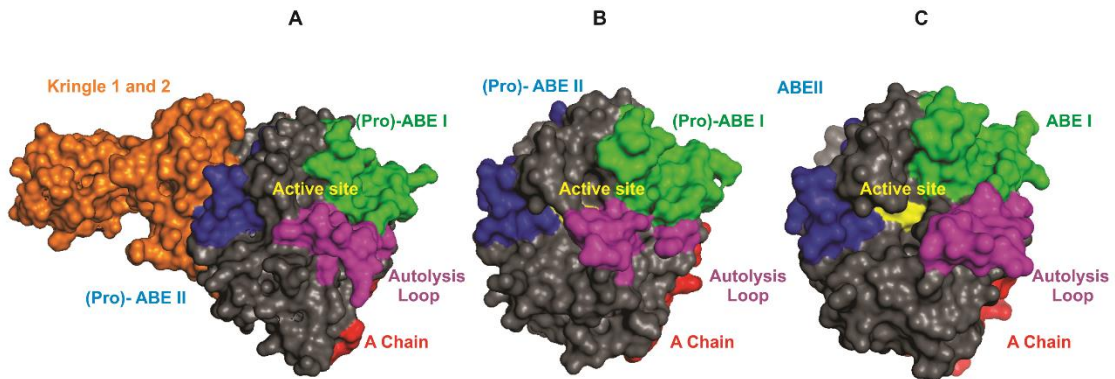


Figure 5: Surface structures of A) Prothrombin (4HZH), B) Prethrombin-2 (1MKX), C) Thrombin (1PPB). Active site is represented in yellow color. Anion Binding Exosite I and II are represented in green and blue colors. A-chain oriented in the back is in red, Autolysis Loop is in purple. All the structures were generated with Pymol.

α -thrombin is highly homologous to serine proteases such as trypsin and chymotrypsin with His 57, Asp 102 and Ser 195 (chymotrypsin numbering) forming the catalytic triad of the active site (**Figure 6**). Hydrolysis of the R-X or K-X substrate bond occurs by the mechanism shared with trypsin, chymotrypsin, and other serine proteases. This mechanism is shown in Figure 7. A nucleophilic attack of Ser 195 on the carbonyl atom of the scissile peptide bond initiates the reaction. As the carbonyl rearranges to give an acyl-enzyme intermediate, the new N-terminus of the hydrolyzed peptide chain is released. A water molecule enters the active site and participates in the reverse sequence, releasing the new C-terminus of the hydrolyzed substrate and regenerating the active enzyme.^{42,43}

Thrombin enzyme specificity is controlled through several loops including the 60s loop (or β insertion loop), autolysis loop (or γ loop), and the 220s loop (or Na⁺ binding loop) (**Figure 6**). The presence of prolines, tryptophans, and tyrosines in the β -insertion loop serves as a rigid hydrophobic cap over the active site and mediates contacts with the hydrophobic substrate residues N-terminal to the scissile bond.³⁷ The autolysis loop is more hydrophilic and flexible in nature and makes contact with residues C-terminal to the active site thereby influencing the substrate specificity. A third important loop (220s loop) contains a site for Na⁺ binding, which controls the activities of thrombin and is important for considering allostery. Na⁺ bound thrombin is denoted as “fast” thrombin and whereas the Na⁺ free enzyme is denoted as “slow” thrombin. The chymotrypsin numbering is followed for thrombin.⁴⁴⁻⁴⁶ For example, the 9-residue insertion between thrombin residues 60 and 61 is known as the Trp60s insertion loop. Residue 60 is followed by 60a, 60b, 60c, and so forth until residue 61 is reached.

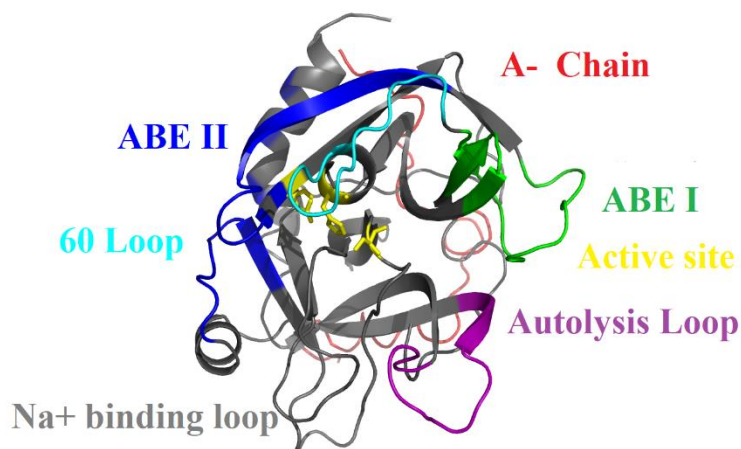


Figure 6: PDB structure of Thrombin (1PPB). Active site (His 57, Asp 102 and Ser 195) is represented in yellow color. Anion Binding Exosite I and II are represented in green and blue colors. A-chain oriented back is in red, 60 Loop is in cyan, Autolysis Loop is in purple.

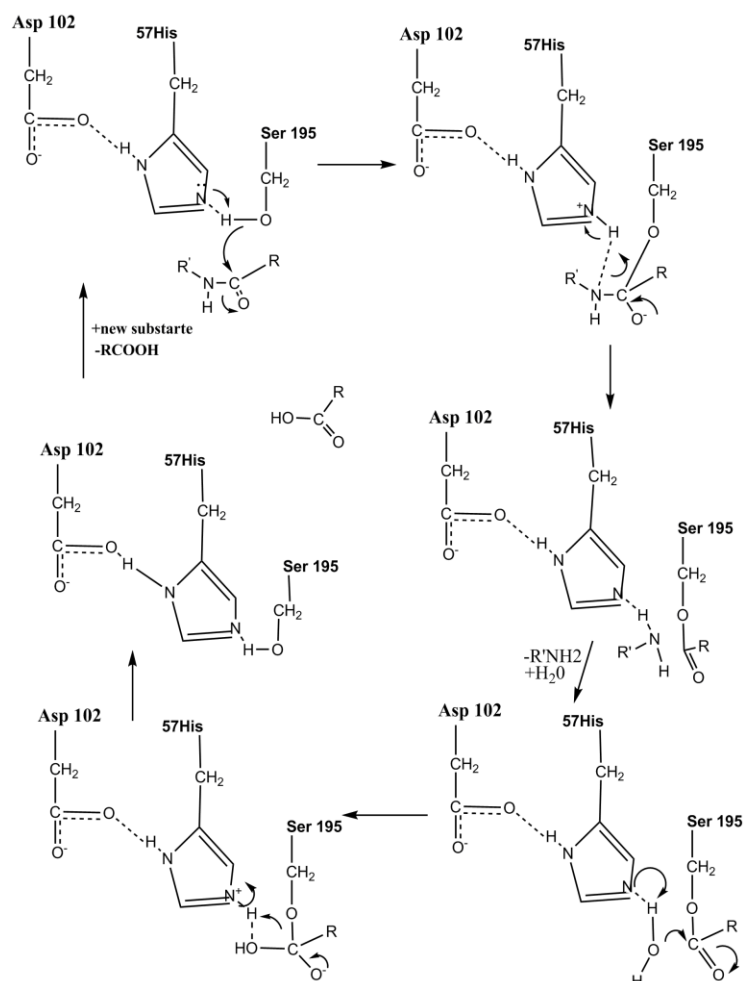


Figure 7: The Serine Protease Mechanism. Product from second reaction is the acyl intermediate.

Apart from the insertion loops, thrombin specificity is also dictated by secondary anchoring sites called exosites. Anion Binding Exosites I and II are rich in positively charged residues and are located on the opposite sides of the active site.^{47,48} Residues from ABE-I include F34, K36, R67, R75, R77a, K81, K109, K110, and K149e. Ligands that bind to ABE- I include the Protease Activated Receptors PAR1 (49-62)⁴⁹ and PAR3 (44-56),⁵⁰ and the leech derived thrombin inhibitor Hirudin (54-65).⁵¹ Residues from ABE-II include R93, R97, R101, R126, R173, R175, R233, K235, K236, and K240. Ligands binding to ABE-II include glycoprotein GpIb α (269-286),⁵² fibrinogen γ' (410-427),⁵³ another leech derived thrombin inhibitor Haemadin (45-57),⁵⁴ and heparin.⁵⁵ X-ray crystal structures shown below display the binding modes of PAR3 and GpIb α ligands to their respective exosites is shown below (Figure 8):

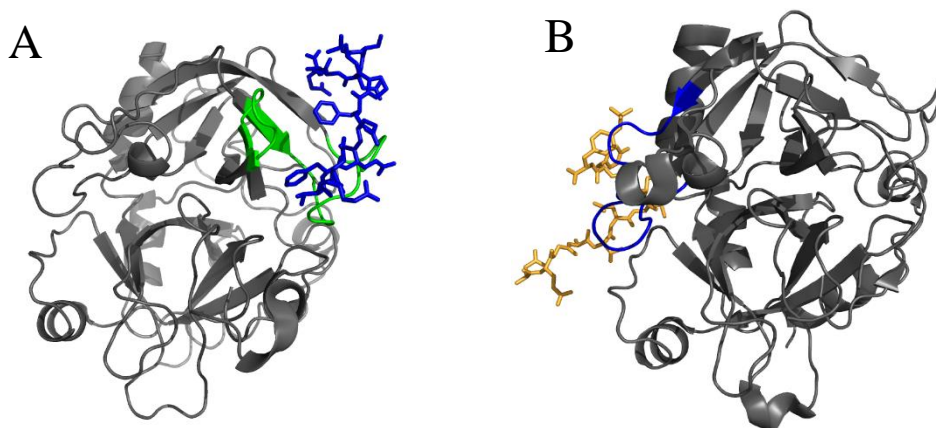


Figure 8: Ligands bound to thrombin A) PAR3 (44-56) B) GpIb α (269-286), PDB structures include 1P8V for GpIb α and 2PUX for PAR3. Anion Binding Exosite I and II are represented in green and blue colors. GpIb α (269-286) is depicted in orange sticks, PAR3 (44-56) is depicted in blue sticks.

Published literature supports the hypothesis that communication is possible between the exosites and with the catalytic center.⁵⁶⁻⁵⁹ Amide hydrogen/deuterium exchange coupled with mass spectrometry revealed that ligand binding at the exosites

promoted both local and long-range effects, but the ligands did not exhibit identical conformational changes to thrombin.⁶⁰ When considering ABE I ligands, Hirudin could show local effects but PAR3 and PAR1 showed both local and long-range effects. Turning to ABE II ligands, GpIb α and fibrinogen γ' could both show local and long-range effects.⁶⁰

The substrate amino acid sequence on the N-terminal side of the scissile bond makes significant contributions to thrombin binding and hydrolysis rates. The P nomenclature system ($P_3 P_2 P_1 \downarrow P_1' P_2' P_3'$) is used to assign the individual amino acid positions on the substrate peptides.⁶¹ The scissile bond is designated as P₁-P₁'. The serine protease thrombin specifically cleaves after arginine or lysine residues located at the P₁ position. A deep active site cleft accommodates the positively charged side chains of R and K. Sequences of some thrombin substrates and an inhibitor are shown in Table 1.

Table 1: Substrate sequences that target thrombin active site region. \downarrow indicates the cleavage between R-X bond.

	$P_3 P_2 P_1 \downarrow P_1' P_2' P_3'$
Factor XIII (28-41) V34 AP	²⁸ T V E L Q G V V P R \downarrow G V N L ⁴¹
Fibrinogen A α (7-20)	⁷ D F L A E G G G V R \downarrow G P R V ²⁰
Fibrinogen B β (5-16)	⁵ D N E E G F F S A R \downarrow G H
PAR1 (29-45)	²⁹ K A T N A T L D P R \downarrow S F L L ⁴⁵
PAR4 (38-51)	³⁸ S T P S I L P A P R \downarrow G Y P G ⁵¹
PPAck	<i>D-F P R-ck</i>

Human sequences were taken from the following sources: PPAck is D-phe-Pro-Arg-chloromethylketone,³⁷ Factor XIII,⁶² Fibrinogen A α and B β chains,⁶³ and thrombin receptors PAR1⁶⁴ and PAR4⁶⁵.

Interactions between thrombin and PAR1 (³⁸LDPR⁴¹) are shown in Figure 9. The Arg 41 residue at the P₁ position forms a salt bridge with thrombin D189, Pro 40 at P₂ makes extensive IIa contacts (Y60a and W60d), P₃ does not necessarily contact thrombin, and Leu 38 at P₄ contacts the aryl binding pocket (L99, I174, and W215).⁶⁶

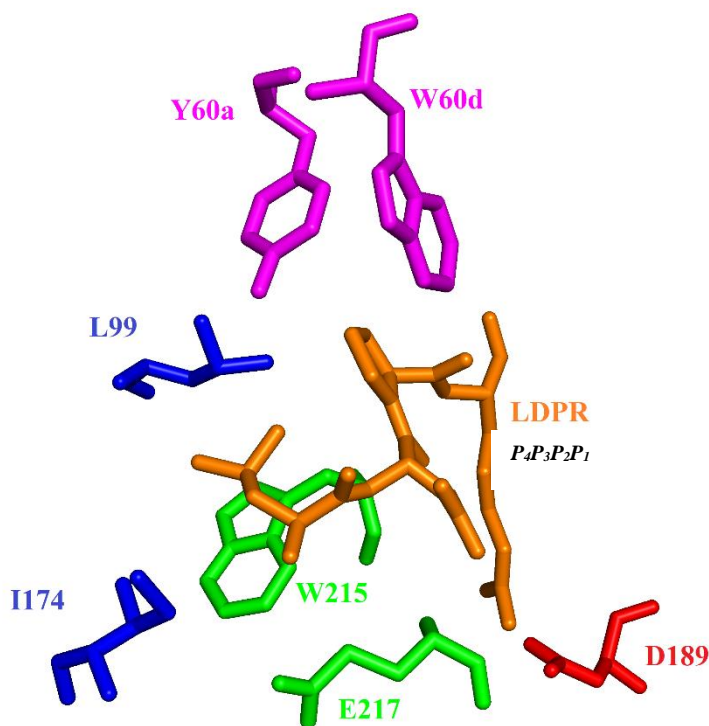


Figure 9: Thrombin receptor PAR1 segment ³⁸LDPR⁴¹ bound to thrombin, PAR1 can accommodate thrombin's active site effectively with the P₁-P₄ residues. PDB code 1NRS.

Fibrin-stabilizing factor: FXIIIa

Transglutaminase FXIIIa is involved in crosslinking the fibrin monomers that are generated by thrombin cleavage of fibrinogen. The major crosslinking sites include the γ - γ and α - α contacts that are crucial for stabilizing the fibrin clot structure. FXIIIa also crosslinks clot stabilizing proteins like α_2 -antiplasmin and Plasminogen Activator Inhibitor 1 (PAI1) to protect the clot from premature lysis. Besides its role in blood coagulation,

FXIII has also been identified as an important enzyme in maintaining pregnancy, vascular permeability, bone biology, and wound healing.⁶⁷

In plasma, pFXIII exists as a hetero tetramer, consisting of two catalytic A subunits and two carrier B subunits (FXIII_{A₂B₂}) (**Figure 10A**). The FXIII- A subunit contains an activation peptide- AP (1-37), a β - sandwich domain (38-184), a catalytic domain (185-515), and two β -barrel domains (516-628, 629-731) (**Figure 10B**).⁶⁸ V34L is a notable polymorphism within the AP region which seems to have cardioprotective functionality.⁶⁹ The FXIII- A subunit has 9 cysteine residues, and among them is Cys314 a key residue of the catalytic traid. C314, along with H373 and D396, form the FXIII active site. The Cys 314 residue is protected from the solvent by the FXIII AP. This thiol amino acid is also hydrogen bonded with Tyr 560. None of the 9 cysteine residues form disulfide linkages. Arg260 of one FXIII monomer is involved in a salt bridge with Asp404 of another monomer. Asp 11 of one FXIII AP forms a salt bridge with Asp 343 on the opposite monomer, thereby demonstrating how the AP of FXIII covers the active site. The FXIII-B subunit is a glycoprotein consisting of 10 sushi domains held together by disulfide bonds. The FXIII B subunits protect the catalytic FXIII A₂ from degradation and premature activation.^{70,71}

During the activation of plasma FXIII A₂B₂, thrombin first cleaves the FXIII A₂ activation peptides between Arg37-Gly38. In the presence of Ca⁺² ions, the regulatory/ carrier FXIII- B subunits dissociate from FXIII-A. The resultant FXIII-A subunits undergo conformational change to create active FXIIIa. In the cellular form found in platelets, cFXIII is only a dimer of A subunits. cFXIII can be activated by thrombin in the presence of low mM Ca⁺² ions or nonproteolytically with high mM Ca⁺² ions (**Figure 11**).⁷² Recently

analytical ultracentrifugation (AUC) and size-exclusion chromatography studies revealed that the FXIII A₂ dimer becomes monomeric following both proteolytic and nonproteolytic activation.⁷³

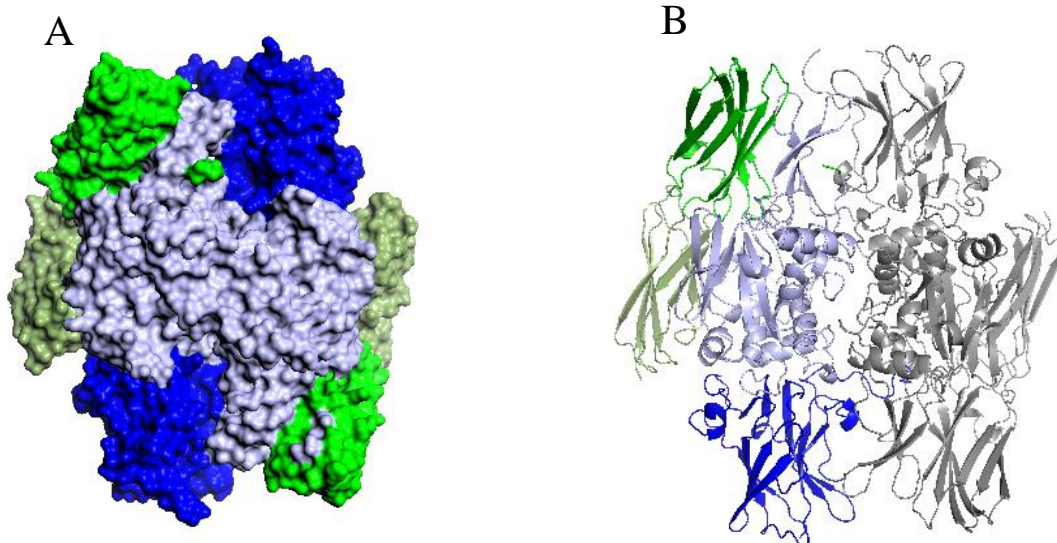


Figure 10: A) structure of cellular FXIII A₂ subunit rendered in surface model. Catalytic domain shown in light turquoise, β - sandwich is in blue, β - barrel 1 and 2 shown in light and dark green colors. B) structure of cellular FXIII A₂ subunit rendered in ribbon model. Catalytic domain shown in light turquoise, β - sandwich is in blue, β - barrel 1 and 2 shown in light and dark green colors. Other A monomer is shown in grey. Structure was generated with Pymol using PDB code 1GGU.

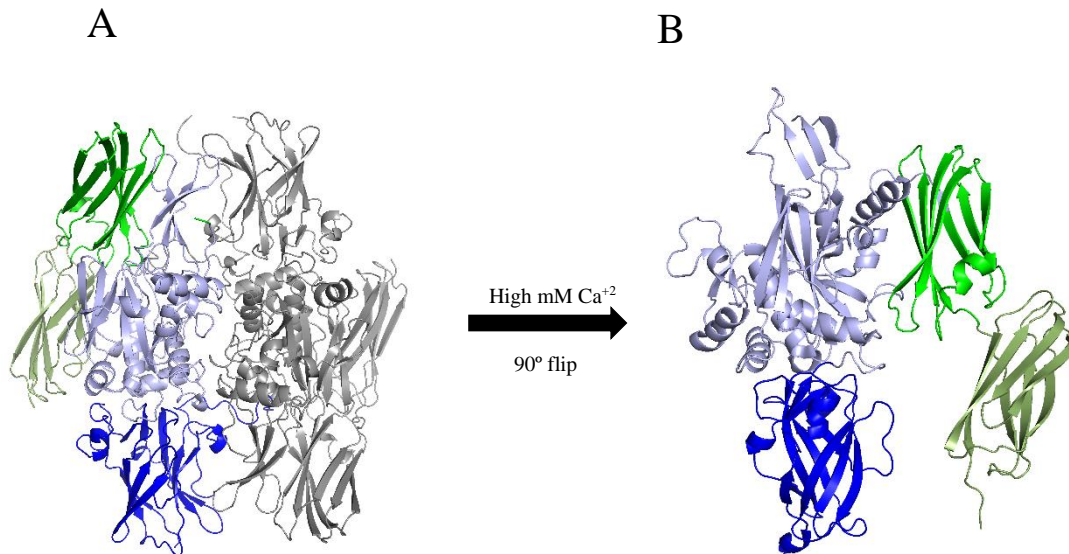


Figure 11: A) structure of catalytic A₂ subunit. Catalytic domain shown in light turquoise, β - sandwich is in blue, β - barrel 1 and 2 shown in light and dark green colors. Other A monomer is shown in grey. B) Conversion of inactive FXIII A₂ to FXIIIa in the presence of high mM (40 mM) Ca⁺² ion. Structure was generated with Pymol using PDB codes 1GGU and 4KTY.

Glycoprotein- GpIb α

To form the platelet plug during vascular injury, several receptors are involved in platelet adhesion. GpIb α is an important platelet adhesion receptor that belongs to the leucine-rich repeat family. Before the thrombin burst is generated, GpIb α binds to von Willebrand factor on the endothelial cells lining the vasculature which accelerates platelet activation. Activated platelets expose the procoagulant/ negatively-charged phospholipids for attracting several coagulation factors to trigger the blood coagulation cascade.⁷⁴⁻⁷⁶ Other important ligands of this receptor include thrombin, FXIa, FXIIa, and High Molecular Weight Kininogen (HMWK). By interacting with these ligands, GpIb α plays an important role in maintaining hemostasis. This glycoprotein also contributes a role in inflammation through leukocyte recruitment to fight infection. The absence or low expression of GpIb α leads to a severe bleeding disorder called Bernard-Soulier syndrome.^{75,77} There are two unique features of the GpIb α receptor. The N-terminus (1-267) has the Leucine-Rich repeat (LRR) which is responsible for curvature of the protein, whereas the C-terminus has a highly anionic cluster (269- 286) that is responsible for binding several clotting factors (**Figure 12A and B**) including thrombin.⁵²

The present research mainly focuses on interactions of GpIb α (269-286) with thrombin. The C-terminal region of the N-terminal fragment (1-290) is rich in anionic residues (²⁶⁹DEGDTDLY_sDY_sY_sPEEDTEGD²⁸⁷) and includes three sulfated tyrosines. In biochemical studies, the sulfated tyrosines are often replaced with phosphorylated tyrosines. X-ray, solution NMR, and HDX-MS studies proved that the anionic cluster of GpIb α (269-286) binds to ABE II of thrombin.^{78,79} Through HDX-MS studies, Malovichko *et al.*, showed that GpIb α (269-286) containing up to 3 phosphorylated tyrosines bound to

thrombin ABE II and can allow for inter-exosite communication over to ABE I.⁶⁰ Additional studies demonstrated that the presence of GpIb α increases thrombin-catalyzed hydrolysis of PAR1 (38-60). Such results provide evidence that binding of GpIb α (269-286) can influence binding and hydrolysis of substrates at the active site.⁸⁰

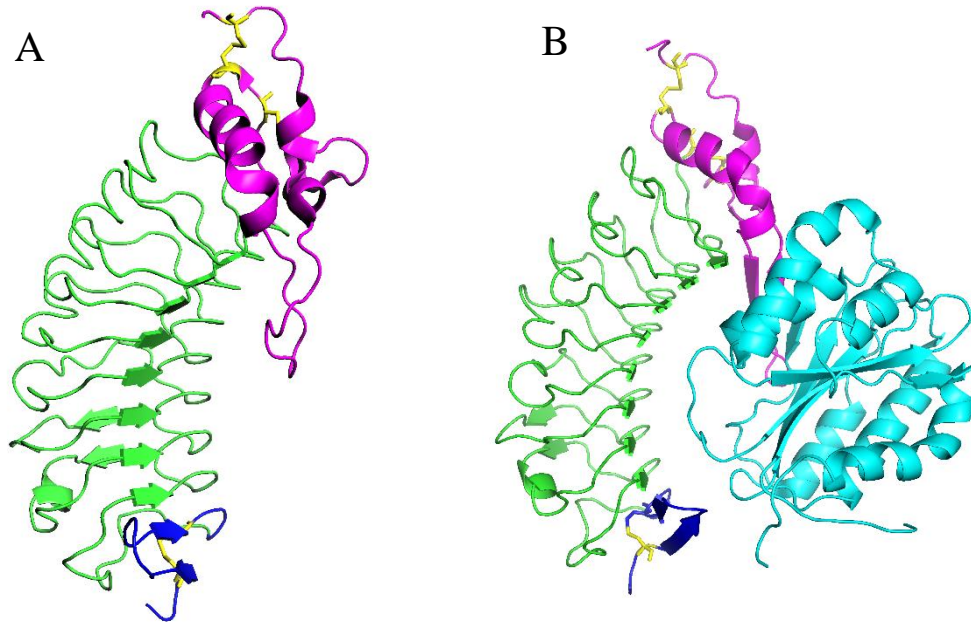


Figure 12: A) Ribbon structure of GpIb α (1-267). N-terminus is in blue, LRR is in green, and C-terminus is in purple. B) von-Willebrand factor shown in cyan (478-705) is complexed at the C-terminus region. Structures were generated with Pymol using PDB codes 1MOZ and 1M10.

Protease Activated Receptors (PARs)

Platelets play an important role in hemostasis, inflammation, angiogenesis, and cancer metastasis. At the site of vascular injury, platelet accumulation, activation, and aggregation are quite essential to prevent major blood loss. Platelet activation can be mediated through the small family of G-protein coupled Protease Activated Receptors PARs. PAR1, PAR2, PAR3, and PAR4 have been identified. PAR1, PAR3, and PAR4 are activated by thrombin whereas PAR2 is activated by trypsin, FVIIa, and FXa.^{64,81,82}

Human platelets use PAR1 and PAR4 to trigger platelet secretion and aggregation. In contrast, murine platelets express PAR3 and PAR4 for platelet activation and accumulation. In humans PAR3 is known to play a regulatory role in megakaryocytic and endothelial cell development.⁸³

Thrombin cleaves the N-terminal extracellular domain of PARs at a specific R-X peptide bond leading to the formation of a tethered ligand which intramolecularly binds to the body of the receptor to elicit transmembrane signaling (**Figure 13**).⁸² However, the complete mechanisms for the transmembrane signaling of all PARs are not yet known.

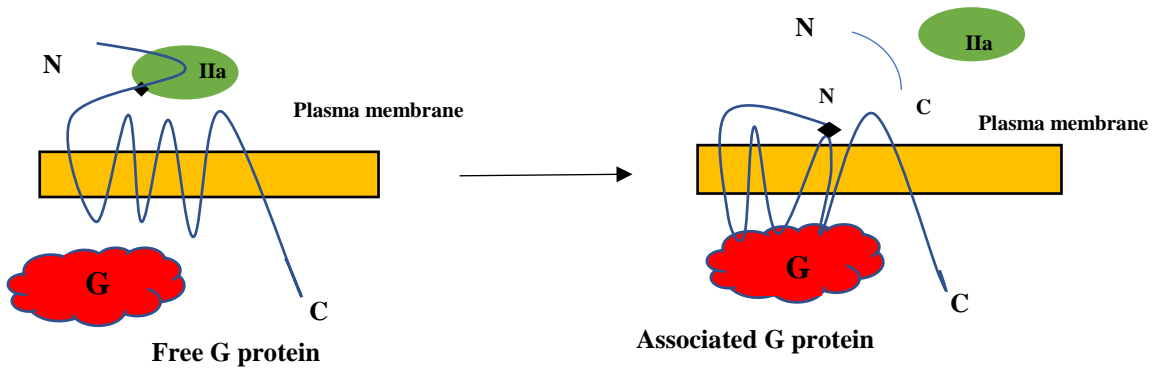


Figure 13: Mechanism of activation of PAR1. Thrombin is visualized as green sphere, identifying N-terminal exodomain. Thrombin cleaves at R41-S42 to produce a new tethered ligand to elicit transmembrane signaling. Picture was adapted from Coughlin, S.R (2000).

	Thrombin cleavage site				Hir	WEDEE
	30	40	50	60		
h PAR1	ARRPESKATNAT	LDPRS	FLLRNPND	KYEPF	WEDEE	-----
m PAR1	MSQPESERTDAT	VNPRS	FLLRNPSEN	FELVPLG	DEEEEE	
h PAR3	MENDTNNLAKPT	LPIKT	FRGAPPN	SFEFP	SALE	-----
m PAR3	GINVSDNSAKPT	LTIKS	FNGGPQN	TFEEF	PLSDIE	-----
Hirudin	TGE	GTPK	PQSH	NDG	DFEEIP	EEYLQ
						SO ₄ ²⁻

Figure 14: Sequence comparison between human and murine versions of PARs. Picture shows the Thrombin cleave site (yellow), and hirudin- like sequence (purple and cyan) binds at ABE-I of thrombin

Located beyond the thrombin cleavage sites, PAR1 and PAR3 both contain hirudin-like sequences.^{49,50,84,85} Hirudin is a leech derived inhibitor that utilizes a DFEEI sequence to anchor on to thrombin ABE I. Human and murine versions of PAR1 and PAR3 also contain segments with highly anionic residues (⁵¹KYEPEF⁵⁵ in PAR1 and ⁴⁶TFEEF⁵⁰ in PAR3) that target ABE I (**Figure 14**).⁸⁴ These residues help increase the affinities of PAR1 and PAR3 for thrombin. PAR1 is the best substrate for thrombin in terms of k_{cat}/K_m . In murine models, PAR3 acts as cofactor for PAR4 activation at low thrombin concentration. PAR3 has been documented to dimerize with PAR4 for further transmembrane signaling.⁸⁶

Physiological relevance and research goals

25% of deaths worldwide are due to ischaemic heart disease and strokes. Being a global disease burden, this health issue attracted many biochemists to decipher the mechanism involved in hemostasis.⁸⁷ Hemostasis is an important physiological process to control the unwanted loss of blood during trauma. The three-step process begins with vasoconstriction of the blood vessel. Next, platelet plug formation to reduce the gap and minimize the blood flow occurs. The last and most important step involves the 30 important biomolecules that are part of the blood coagulation cascade.^{88,89} The coagulation factors and cofactors work together to convert the liquid blood to an insoluble fibrin network which is less susceptible to lysis.³⁰ Imbalances in the blood coagulation pathway may lead to deleterious effects like stroke, heart attacks, and pulmonary embolism. To control the unwanted formation of blood clots, anticoagulation events are in place. Key features about blood coagulation including the various factors involved in coagulation and anticoagulation were described in detail earlier in this chapter. Therapeutic anticoagulants

are administered to the patients when the physiological levels of natural anticoagulants are not enough to elicit their functions. Several anticoagulant drugs have been developed and new generation versions have been developed in recent years. Some intriguing therapeutic strategies are currently being developed to reduce the side effects of anticoagulants and to actually reverse the anticoagulation event.⁹⁰

A few blood coagulation factors utilize a Gla domain to anchor on to a phospholipid membrane. This Gla domain contains the specialized amino acid γ -carboxy glutamate that is generated with the help of Vitamin K. Vitamin K antagonists acts as competitive inhibitors, hindering the the formation of the Gla residue and thus hindering zymogen activation. Dicoumarol and its synthetic analog Warfarin are the most famous Vitamin K antagonists. They inhibit the redox step of the Vitamin K cycle and hamper the generation of vitamin K, and thus induce their anticoagulation activity. A well-known side effect in patients administered Vitamin K antagonists is excessive bleeding.⁹¹

Heparin is another anticoagulant that is administered to patients with cardiovascular abnormalities. Heparin is known to promote conformational changes to Antithrombin III. The properly oriented antithrombin-heparin complex then binds to factors Xa and IIa to hinder their serine protease activities. However, heparin induces thrombocytopenia and dysfunction of platelet activation. Heparin is also known to have non-specific plasma binding effects. Because of these concerns, research slowly shifted towards targeting specific factors and binding sites in blood coagulation.⁹²

Factor X is a common factor of both the intrinsic and extrinsic pathways and is involved in activating the final serine protease thrombin. As a result, several drugs are available on the market which directly bind to the active site of Xa. Among them are

Fondaparinux, Rivaroxaban, Apixaban, and Endoxaban. These drugs work more efficiently than Vitamin K antagonists and heparin and have fewer side effects. However, a critical issue concerned with FXa inhibitors is the lack of an antidote to reverse the anticoagulant activity.⁹³

Since thrombin is known to have more than a dozen substrates that are involved in both coagulation and anticoagulation, extensive time has been dedicated toward developing direct thrombin inhibitors. Three types of direct thrombin inhibitors are available on the market. The first type is the univalent inhibitor which binds to the thrombin active site and includes drugs like Argatroban, Melagatran, and Dabigatran. Like FXa inhibitors, such IIa inhibitors do not have a universal antidote to reverse the anticoagulant effect.⁹⁴ Also, univalent inhibitors lead to coagulopathy. The second inhibitor type is the bivalent inhibitor where the drugs take advantage of ABE I in addition to the active site to improve affinity with thrombin. Bivalirudin is known to bind reversibly to thrombin and bridge both the ABE I and the active site.⁹⁵ However, the half-life of bivalirudin is low due to spontaneous chemical degradation by proteases in the body.

Allosteric inhibitors are the third class of direct thrombin inhibitors and include DNA⁹⁶ and RNA aptamers,⁹⁷ benzofuran dimers, benzofuran trimers, and heparin based analogs.⁹⁸ These molecules take advantage of ABE I, ABE II, and the sodium ion binding loop. The best DNA aptamers are selected from a pool of nucleic acids through a technique called “SELEX” (systematic evolution of ligands by exponential enrichment) to elicit the anticoagulation activity.⁹⁹ The SELEX approach is still evolving and might take several decades to make a “*druggable*” form. Meanwhile, a non-enzymatic protein called Bothrojaracin has been isolated from snake venom which binds to pro-ABE I of ProT and

blocks the thrombin activation.^{100,101} This venom protein is also known to compete with ProT F2. Such an effect would indicate that bothrojaracin can also bind to ABE II of thrombin. However, bothrojaracin is known for its toxicity.

A few antagonists targeting the physiological substrate ligands have also been developed. PAR targeted therapy is taking shape to inhibit PAR activation and platelet aggregation. RWJ-56110 acts as antagonist to PARs which not only blocks platelet aggregation but also hinders PAR1 and PAR4 dimerization responsible for several signaling events.^{102,103}

Keeping these different anticoagulant functionalities in mind, researchers will want to develop future drug candidates that regulate hemostasis with fewer side effects and enable reversal of their functionalities with effective antidotes. Considering this big picture and the use of (pro)thrombin as the drug target, we wanted to better understand the conformational changes of the active site region and the (pro)-ABEs of (pro)thrombin that lead to different physiological processes. Understanding different conformations of biomolecules can help develop novel therapeutics that target specific hot spots on (pro)thrombin. Also, binding affinities between the drug and its binding partner plays a key role in improving the efficacy. Probing the binding affinities of individual residues within the physiological peptide ligand will be a big asset for developing better therapeutics.

Hence, the dissertation is divided into the following chapters. Chapter 2 mainly focuses on different techniques employed in this research and includes the theory behind 1D proton line broadening, 2D TOCSY, 2D tr-NOESY, and 2D HSQC. These solution based techniques are used as complementary methods to X-ray crystallography to evaluate different conformations and binding interactions involving (pro)thrombin and PARs. Also,

the principle behind ITC (Isothermal Titration Calorimetry) is explained as it is used as a supplementary technique to evaluate the global K_{DS} between two binding partners. Chapter 3 then emphasizes on how a PAR based ligand (PAR3) probes exosite maturation at single amino acid levels. This chapter will also include the quantitative measurements of binding affinities of ^{15}N - labeled PAR3 amino acids towards zymogen ProT vs mature thrombin. As a continuation of this study, Chapter 4 discusses the comparative studies between the binding affinities of two PAR based ligands (PAR1 and PAR3) towards (pro)-exosites. The most striking segment in this chapter is further proof of allosteric communication between exosites ABE I and ABE II. Chapter 5 describes the thrombin catalyzed hydrolysis of Fbg B β (5-16) and compares the kinetic parameters with common substrates of thrombin. In addition, 1D and 2D solution NMR results are used to explain secondary structural information for the thrombin bound FpB (5-14) and the weak kinetics associated with thrombin- catalyzed release of FpB (5-14). As a wrap up, Chapter 6 includes a summary of all the different research projects, some new preliminary results attained so far, and possible future directions for the above discussed research projects.

CHAPTER II

EXPERIMENTAL TECHNIQUES

NUCLEAR MAGNETIC RESONANCE (NMR)

Nuclear Magnetic Resonance (NMR) examines the magnetic properties of such nuclei as the proton (^1H), the carbon 13 isotope of carbon, and the nitrogen 15 isotope of nitrogen. Unlike some other biophysical methods, NMR is a non-destructive technique which enables us to deduce the positions of the nuclei within the molecule, identify different types of environments, and assess the types of atoms within the molecule.¹⁰⁴

Any charged particle that spins behaves like a tiny bar magnet, and it generates a magnetic field. The proton in the hydrogen atom being a charged particle also behaves as a tiny magnet, generating its own magnetic field. In the presence of an external magnetic field, the spin $\frac{1}{2}$ proton can adopt two orientations with respect to the applied magnetic field. One is the lower energy state where it aligns with the magnetic field, and the other is the higher energy state, opposing the magnetic field. The spinning proton can move under the influence of the external magnetic field. A spinning proton can be considered as a spinning top. If the spinning axis is not parallel to the applied magnetic field it will precess around the axis of the external field (**Figure 15**). The precessional frequency ν , is directly proportional to the strength of the external magnetic field B_0 . When nuclei are irradiated with radiowaves whose frequency is the same as the precession frequency, the spinning

axis is tilted away from the axis of B_0 . If the radio frequency field is pulsed on for a time such that the spinning axis and the magnetic field axis are perpendicular, the pulse is known as a 90° pulse.

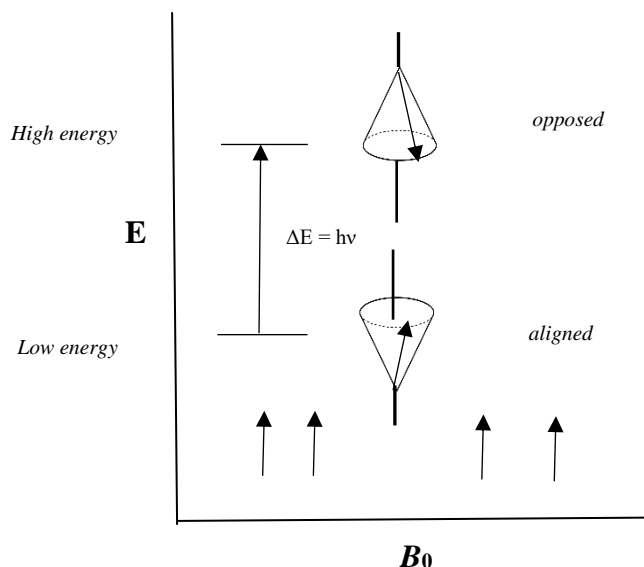


Figure 15: Types of orientation a precessing nuclei can adopt in presence of external magnetic field.

$$\nu \propto B_0 \quad (1a)$$

$$\nu = \frac{\gamma B_0}{2\pi} \quad (1b)$$

γ is the gyromagnetic ratio between the nuclear magnetic moment μ and the nuclear angular momentum I . The ν values for a few magnetic nuclei with different field strengths is given in Table 2.¹⁰⁵

Table 2: Precessional frequencies (in MHz) as a function of field strength (Tesla).¹⁰⁵

B_0 (Tesla)	1.4	1.9	2.3	4.7	7.1	11.7	14.1
<i>Nucleus</i>							
^1H	60	80	100	200	300	500	600
^2H	9.2	12.3	15.3	30.6	46.0	76.8	92
^{13}C	15.1	20.1	25.1	50.3	75.5	125.7	151
^{15}N	6.1	8.1	10.1	20.3	30.4	50.7	61
^{19}F	56.5	75.3	94.1	188.2	288.2	470.5	565
^{31}P	24.3	32.4	40.5	81.0	121.5	202.4	243

When the nuclei precess, they emit radiowaves, which can be recorded by a radiofrequency detector. However, there can be two types of radiationless mechanisms for a high-energy state nucleus to lose (relax) energy.¹⁰⁴ The first type of relaxation is the spin-lattice relaxation or longitudinal relaxation with time constant T_1 . In this process, the nuclei transfer energy to the surrounding lattice. Surrounding molecules can be from the solvent or from the same molecule. The second type of relaxation is spin-spin relaxation or transverse relaxation with time constant T_2 . Here, the energy is transferred to neighboring nuclei. In this mechanism, one nucleus loses energy whereas another nucleus gains energy and hence both nuclei are coupled. In protons, spin-spin relaxation is the predominant way for radiationless energy transfer.¹⁰⁵

Molecular weight plays an important role in dipolar coupling. The rotational correlational time (τ_c) is the time required for a molecule to rotate 1 radian, which is proportional to the size of a protein and the viscosity of the solution. τ_c is $1 \text{ nsec} / 2.6 \text{ kDa}$ of protein mass at $T = 300 \text{ K}$. Thus, a smaller protein can fluctuate/tumble ($\omega\tau_c \ll 1$) more rapidly than a larger protein ($\omega\tau_c \gg 1$), where a is the radius of the protein, and η is the viscosity

$$\tau_c = \frac{4\pi\eta a^3}{3kT} \quad (2)$$

The rates of relaxation are important. They determine the width of the NMR peaks. If both T_1 and T_2 are small, the lifetime of the high energy nucleus is short and will lead to broad spectral lines. If both T_1 and T_2 are large, then sharp spectral lines can be seen. The uncertainty principle can give us a qualitative relation between relaxation time and frequency spread in NMR spectra. If Δt (life time of particular energy state) is large, $\Delta\nu$

(frequency) must be small, which means the frequency spread is small thus leading to narrow lines. By contrast, if Δt is small, the large $\Delta \nu$ will result in large spread of frequency.¹⁰⁵

$$\Delta E * \Delta t \sim \frac{h}{2\pi} \quad (3a)$$

$$as E = h\nu \quad (3b)$$

$$\Delta \nu * \Delta t \sim \frac{1}{2\pi} \quad (3c)$$

Proteins in solution are highly dynamic. Folded proteins reorient due to rotational diffusion. In addition, proteins can have internal degrees of flexibility. Different conformations can lead to different protein functions. A protein can be defined as an ensemble of different conformations that sample between various spatial and temporal scales ranging from nanometers to micrometers and femtoseconds to hours. In short, proteins are highly “dynamic molecules”. NMR provides the greatest advantage to study different structural changes ranging from bond breakage/formation to domain motions which fall within a time scale from 10^{-15} secs to 10^3 secs. Figure 16 provides a range of timescales enabling various biological functions.¹⁰⁶

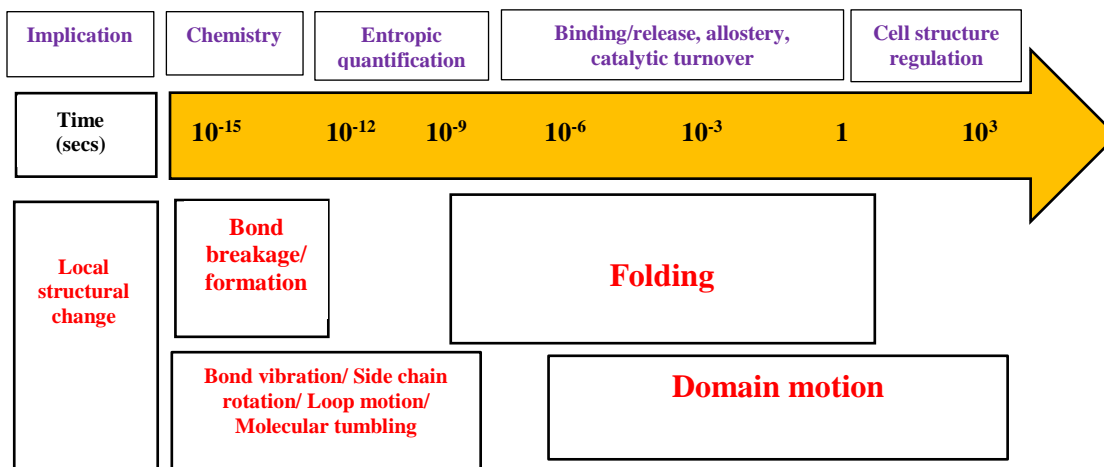


Figure 16: Protein conformational changes over a broad range of timescales. Adapted from Kleckner I.R. et al. (2011)

The remainder of this chapter focuses on 2D TOCSY, 2D tr-NOESY, and 2D HSQC experiments and how these NMR techniques can be used to obtain structural information about a protein or the ligand. Any 2D NMR experiment requires four essential steps. The first step is recovery, during which spins return to equilibrium. This phase typically ranges from 0.5-5.0 secs. Exciting the first spin type (let suppose A) by applying a single 90° pulse will end this phase. The second phase is the evolution period (t_1) which can encode the chemical shift of A. This period measures the A chemical shift indirectly i.e., it is not directly detected by the receiver coil. This evolution phase ranges from 0-5 secs. In the third phase, the magnetization of A spins is transferred to coupled B spins. The coupling is either J-coupling or dipolar coupling. The fourth and final phase is the detection period, where the FID of B spins is observed directly. This period ranges from 50-200 ms. These four steps are typically repeated 2 to 32 times to increase the signal to noise ratio several fold (**Figure 17**).¹⁰⁶

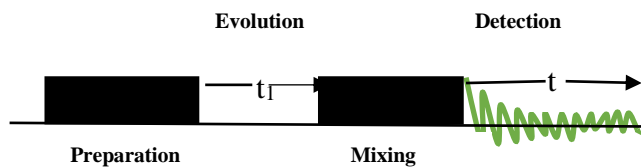


Figure 17: General pulse sequence of 2D- NMR.

2D TOCSY (Total Correlation Spectroscopy)

2D TOCSY is used to identify networks of spins that are scalar coupled. Spectra from this homonuclear experiment reveal the cross peaks between spins which are connected by bonds. The TOCSY pulse sequence involves a 90° pulse in the beginning, a frequency labeling time t_1 , followed by series of 180° (Π) pulses during which scalar coupled spins exchange magnetization. This pulse sequence is then followed by detection

of the FID. 2D transformation of the data table shows both diagonal and off diagonal peaks. The off diagonal peaks correlate scalar coupled spin pairs(**Figure 18**).¹⁰⁵

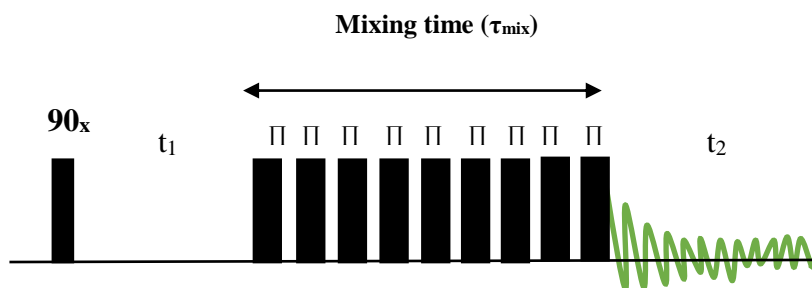


Figure 18. Pulse sequence of 2D TOCSY experiment.

Consider three different spins, A, B, and C. If spin A is coupled with spin B, and spin B is coupled with spin C, then in the TOCSY spectrum one can see a cross peak between A and C, even though there is no direct coupling between these two spins. In Figure 19, black peaks correspond to cross-peaks between spins A and B due to 3J coupling, orange peaks correspond to cross-peaks between spins B and C due to 3J coupling, grey peak correspond to cross-peaks between spins A and C. Cross-peaks between A and C are due to an unbroken chain of couplings. Green peaks on the diagonal indicate that they are connected through bond.¹⁰⁷

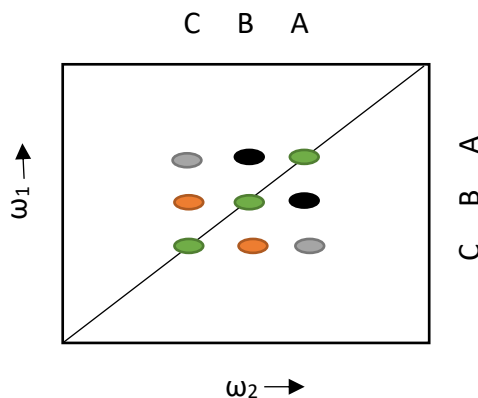


Figure 19: Schematic TOCSY spectrum for the three spins.

2D tr-NOESY (2D transferred nuclear overhauser enhancement spectroscopy)

Nuclear spins also interact through space via dipolar coupling making it possible to learn interesting structural information about a biomolecule. The magnitude of the dipolar coupling depends on the strength of the magnetic field generated by one spin and the magnetic moment of the other spin. If the cross-peak is seen between two dipolar coupled spins which are spatially interacting, then it leads to the nuclear Overhauser effect and the peak is referred to as an NOE. The NOE intensity is related to the distance “r” between two coupled spins which can be derived with the following equation. Ideally if two spatially interacting protons are separated by a distance of less than 5 Å, then a NOE can be observed.¹⁰⁸

$$NOE \propto \frac{1}{\langle r^6 \rangle} * f(\tau_c) \quad (4)$$

In the pulse sequence of an NOE experiment, a 90° - t_1 - 90° pulse is used to frequency label the spins and return the magnetization to the z-axis. Subsequently, dipolar coupled exchange longitudinal magnetization occurs during the τ_m phase. The observed transverse relaxation time is created by the final 90° pulse. Like the TOCSY experiment, 2D transformation of the data table shows both diagonal and off diagonal peaks. Here, the off-diagonal peaks correlate to dipolar coupled spin pairs (**Figure 20**).¹⁰⁴

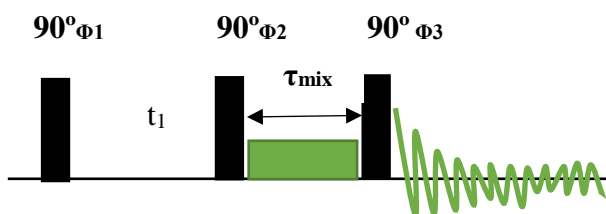


Figure 20. Pulse sequence of 2D tr-NOESY experiment.

For 2D tr-NOESY experiments, protein-ligand complexes are examined that contain less than stoichiometric amounts of a large binding protein. A free peptide ligand of up to 20 amino acids can tumble very fast in solution due to the absence of conformational restraints. This property results in $\omega\tau_c \leq 1$ and longer transverse relaxation (T_2) time. The 1D proton spectrum displays very sharp peaks and the 2D tr-NOESY will have very few NOEs. Once the peptide binds to the protein, the conformations accessible to the ligand become restricted by the geometry of the binding protein partner, and the peptide becomes part of a larger protein-ligand complex. The peptide may also adopt some secondary structure. These properties result in an increase in correlation time $\omega\tau_c \gg 1$ and a shorter T_2 time. As a result, many NOEs (**Figure 21**)¹⁰⁹⁻¹¹² can be observed. Intramolecular NOEs for the bound state of the peptide can be observed.

The use of 2D tr-NOESY for structural determination is based upon the assumption that the ligand is under fast exchange conditions (higher k_{on} and k_{off} rates from the protein surface). For a typical 2D tr-NOESY experiment, 10:1 ligand to protein ratios are preferred to increase the exchange rates. Increased exchange rates will make it possible for the peptide to associate and dissociate at least a few times during the NOE mixing time. During this time, NOE information is transferred from the bound to the free state. Typically, a 100-200 ms mixing time is employed to obtain sufficiently intense cross peaks that can be correlated to inter-proton distances. If the ligand has relatively low exchange rates, then changes to pH, ionic strength, or temperature can alter the exchange rates to enable the tr-NOESY experiments to reveal more productive information. Other modifications that can alter the exchange rate include removal of phosphate groups from tyrosines or serines, and

amidation of a C-terminal carboxyl group. Individual amino acid substitution within a peptide ligand can also be used to alter the affinities of protein-ligand complexes.¹¹⁰

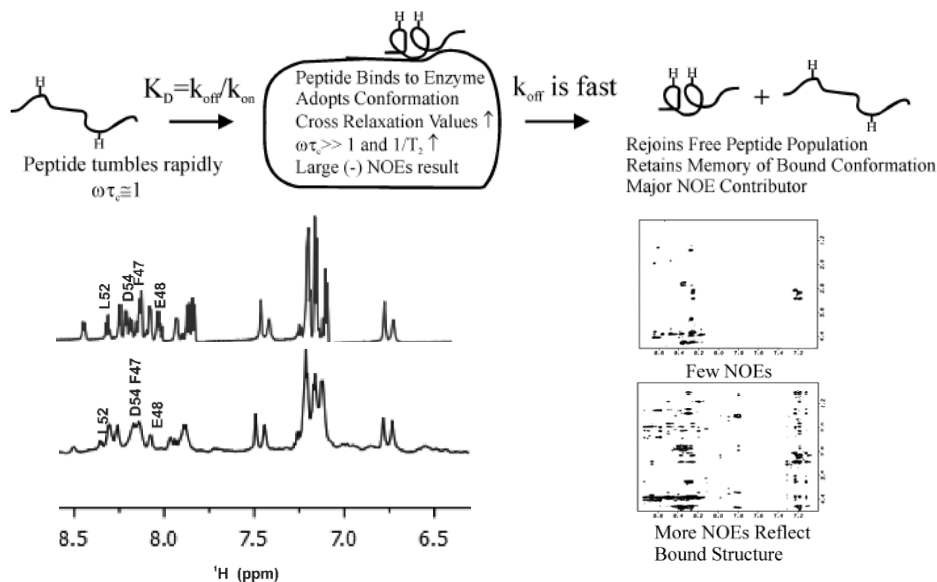
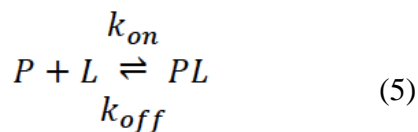


Figure 21: Cartoon showing NOE and 1D line broadening of free and bound form of PAR3 (44-56).

Ligand Binding Kinetics

Studying enzyme-ligand interactions through NMR is achieved through observing the changes in chemical shift with respect to changing either protein or ligand concentrations. These types of chemical shift changes fall under three regimes- fast, intermediate, and slow exchange (Fig 22). For the fast exchange regime ($k_{ex} \gg |\Delta\omega|$), only one signal is observed reflecting the population-weighted averages of chemical shift, intensity, and linewidth. For the intermediate exchange regime ($k_{ex} \approx |\Delta\omega|$), only one signal with anomalous peak broadening and an intermediate chemical shift is seen. Finally, for slow exchange regime ($k_{ex} \ll |\Delta\omega|$), signals from both states are observed reflecting their distinct chemical shifts, intensities, and line widths. $\Delta\omega = \omega_P - \omega_{PL}$, where $\Delta\omega$ is the change

in resonance frequencies of nuclear spins calculated as a difference between the resonance frequencies of free (ω_P) and bound (ω_{PL}) (**Figure 22**).^{106,111}



$$k_{ex} = k_{on} [L] + k_{off} \quad (6)$$

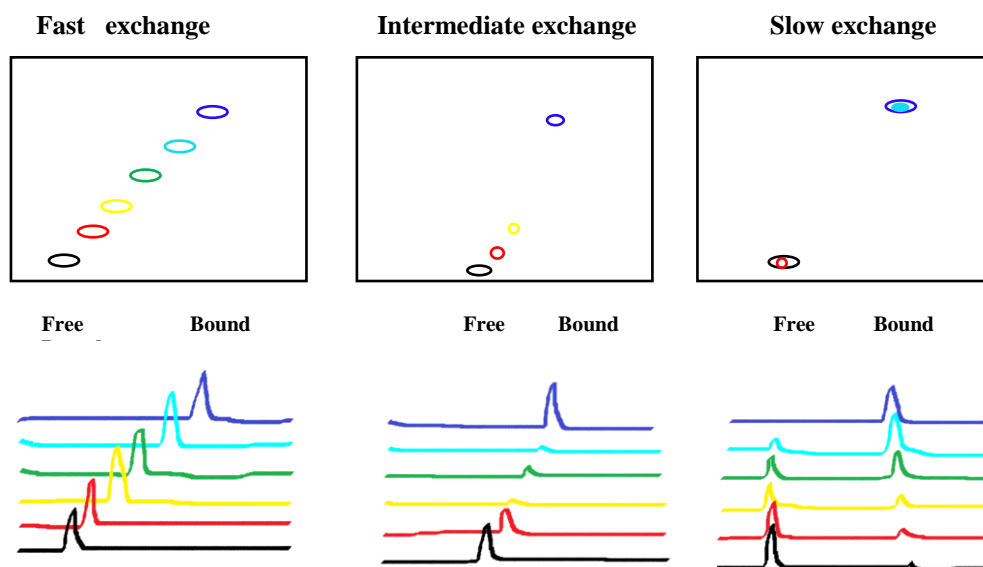


Figure 22: Three different exchange regimes: Fast, Intermediate, and Slow regimes in 2D and 1D NMR spectra.

The chemical shifts of homonuclear spins mostly overlap. To detect the correlation between protons and their attached heteronuclear spins, heteronuclear J-correlated spectroscopy is employed. HMQC (Heteronuclear Multiple-Quantum Coherence) and HSQC (Heteronuclear Single-Quantum Coherence) are two methodologies that provide this type of information. Our research has mainly employed 2D- HSQC to examine protons that are directly attached to particular nitrogens or carbons. The HSQC pulse sequence involves the transfer of magnetization from ^1H to usually ^{15}N or ^{13}C through INEPT (insensitive nuclei enhanced by polarization transfer). After a time delay of t_1 , the

magnetization is transferred back to the proton through the retro-INEPT step. The ^1H signal is detected in the direct dimension, and the heteroatom ^{15}N or ^{13}C is detected in the indirect dimension (**Figure 23**).¹⁰⁴

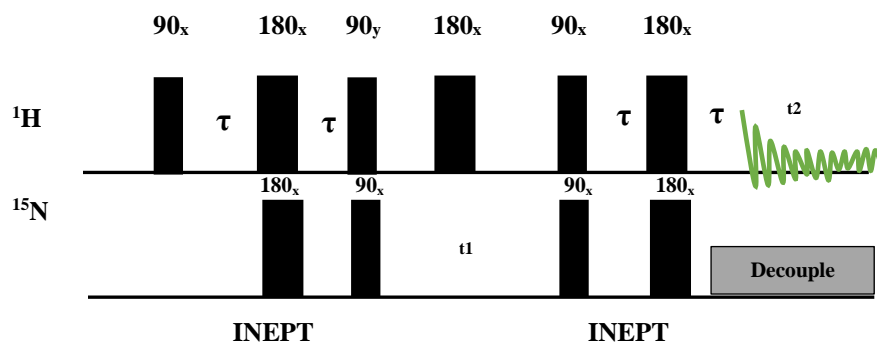


Figure 23: Pulse sequence of 2D HSQC

Chemical shift perturbations (CSP) reflect the changes in chemical shift that occur to a ligand or protein when the binding partner is added. These CSP provide a tremendous wealth of information about the environment of the binding site, the binding affinity, and/or possible structural features of the complex. For the current research, one use of CSP was to calculate the binding affinities between the ligand and the protein. CSP can be recorded for different nuclei like protons (^1H), ^{13}C , and ^{15}N . The CSP for ^1H are affected by several factors including paramagnetic effects, magnetic anisotropy around bonds, aromatic ring currents, and electrostatic field effects. Carbons are mainly affected by local dihedral angles. Nitrogens and carbonyl groups depend on hydrogen bonding and on the identity and side chain conformation of the preceding amino acid.¹¹³

CSP can be an asset in determining weak binding affinities if the protein-ligand kinetics fall under the fast exchange regime. Under such conditions, there are often enough titration

points in the Δ_{obs} versus the protein/ligand concentration plot to approach saturation and thus obtain a more accurate K_D value. Binding affinities are calculated using the equation shown below, where K_D is binding affinity, $[L_0]$ is the ligand concentration, $[P_0]$ is the total protein concentration, and Δ_{obs} is the CSP between the free and bound form.¹⁰⁶

$$\Delta_{\text{obs}} = \Delta_{\text{max}} * \frac{(K_D + [L_0] + [P_0]) - \sqrt{(K_D + [L_0] + [P_0])^2 - (4[P_0][L_0])}}{2[P_0]} \quad (7)$$

ISOTHERMAL TITRATION CALORIMETRY (ITC)

Interactions between a series of biological molecules can lead to important biological processes like immune response, signal transduction, and gene expression. It is therefore important to know the nature of forces that help in stabilizing the individual interactions. Isothermal Titration Calorimetry (ITC) is an excellent biophysical technique which not only gives binding affinities K_D but also gives information about the thermodynamic parameters like free energy of binding (ΔG), enthalpy of binding (ΔH), and stoichiometry (n). The entropy of the system (ΔS) can be calculated from the well-known Gibbs fundamental equation (Figure 24).¹¹⁴

$$\Delta G = - RT \ln K_a \quad (8a)$$

$$\Delta G = \Delta H - T\Delta S \quad (8b)$$

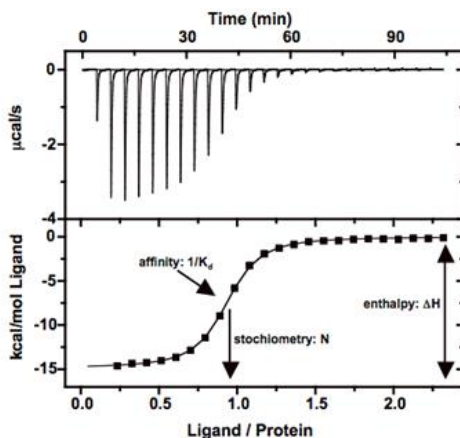


Figure 24: ITC binding curve. Picture taken from <http://www.endocytosis.org>

An ITC instrument consists of two identical cells composed of a highly efficient thermal conducting material, mostly hasteloy or gold, that is surrounded by an adiabatic jacket. A sensitive thermopile/thermocouple detects the temperature differences between the two cells and between the cells and the jacket. Heaters in both cells are activated when there is a temperature difference between the cells. Furthermore, these heaters seek to maintain identical temperatures between the two cells (**Figure 25**). In a typical ITC experiment, the macromolecule is placed in the sample cell, whereas the reference cell has either water or buffer. During the experiment, titrant will be injected into the sample cell, and based upon the type of association, heat will be evolved or taken up. If the association is exothermic, temperature of the sample cell will increase, and for an endothermic reaction, the temperature will decrease. Over the course of an ITC experiment, there is a time-dependent input of power applied to maintain equal temperatures in the sample and reference cell.^{115,116}

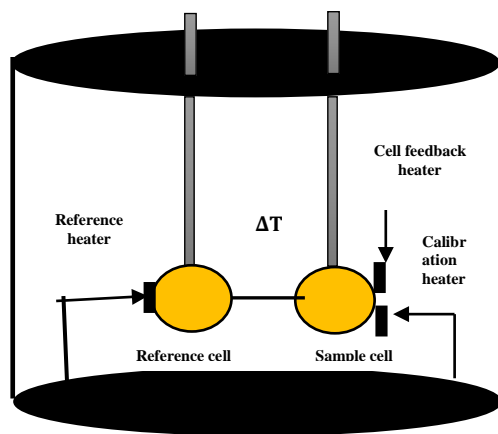


Figure 25: Schematic diagram of an ITC experiment.

The isothermal titration calorimeter is an extremely sensitive instrument and utmost care should be taken from sample preparation to data analysis. The experimental binding

isotherm can be characterized by a unitless value c (wiseman parameter), which is the product of the association constant K_a , the macromolecular concentration $[M]$, and the stoichiometry n (**Figure 26**).¹¹⁷ A large c is seen for complexes where saturation is achieved already at 2 or 3 injections of ligand. A smaller c occurs when the characteristic sigmoidal curve is completely lost. For a single-site binding model, a c value between 10 and 500 is said to be optimal for curve fitting.¹¹⁸ The fitting process is erroneous if $c < 10$, and finally it is said to be not feasible if $c < 1$. For accurate measurements of affinities and thermodynamic parameters $10 \leq c \leq 500$ is preferable.

$$c = K_a * [M] * n \quad (9)$$

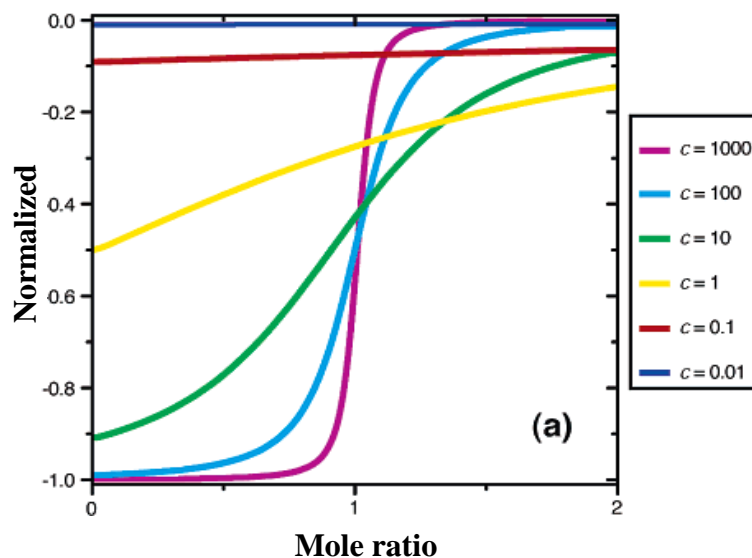


Figure 26: Dependence of ITC binding curve on c value. Picture adapted from Turnbull (2003).

CHAPTER III
DECIPHERING CONFORMATIONAL CHANGES ASSOCIATED WITH THE
MATURATION OF THROMBIN ANION BINDING EXOSITE I

INTRODUCTION

Thrombin (factor IIa) is a multifunctional enzyme that plays critical roles associated with procoagulation and anticoagulation. Procoagulant functions of thrombin include activating other coagulation proteins (zymogen factors V, VIII, and XIII), converting fibrinogen into fibrin that then polymerizes into a blood clot, and helping to activate platelets by cleaving the protease-activated receptors (PARs). An important anticoagulant function of thrombin is to activate protein C and thereby help inhibit a set of coagulant proteins.⁴⁷

Thrombin also has two anion binding exosites, ABE I and ABE II, located on opposite sides of the serine protease active site (Figure 27A). These exosites have been shown to direct substrates to the active site, contribute to opening of the active site region, and help in attracting other regulatory molecules. Direct allosteric linkage may exist between ABE I and ABE II to modulate thrombin activity.⁶⁰

Thrombin is expressed as the zymogen Prothrombin (ProT) (Figure 27B).^{38,119} As ProT is proteolytically converted to thrombin, the immature pro-ABEs develop into the mature, active ABEs I and II^{38,39} (Figure 27C). In ProT, access to pro-ABE II is blocked

by the kringle-containing Fragment 1.2 (F1.2). This pro-ABE II region becomes exposed during the cleavage and activation process.^{38,120,121} By contrast, the pro-ABE I region is not directly affected by a cleavage event. Instead, subsequent conformational changes likely lead to ABE I maturation.^{38,122}

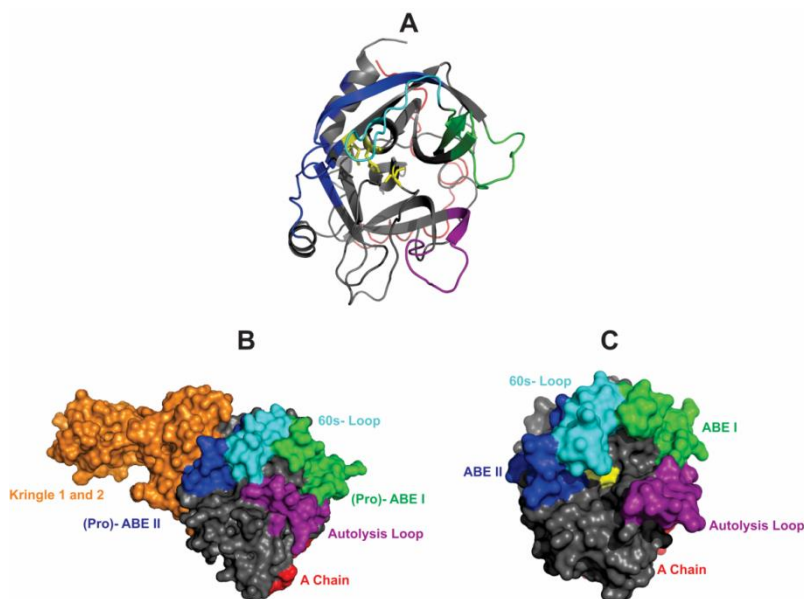


Figure 27: Crystal structures of thrombin [Protein Data Bank (PDB) entry 1PPB] and prothrombin (PDB entry 4HZH). A) Ribbon diagram of thrombin in which the catalytic triad (His 57, Asp 102, and Ser 195) is colored yellow, (Pro)- ABE I is colored green, (Pro)- ABE II is colored blue, the autolysis Loop is colored purple, the 60s Loop is colored cyan, and the A chain is colored red. B) Space filling model of zymogen prothrombin missing the Gla domain. Kringles 1 and 2 are colored orange. The other colored regions match those shown in panel A. C) Thrombin is generated from prothrombin following cleavages after Arg 271 and Arg 320. The space filling model highlights the removal of the kringles (orange), the exposure of the active site (yellow), and full maturation of ABE I (green) and ABE II (blue).

Designing new therapeutic anticoagulants that are directed toward individual thrombin exosites is a promising area of investigation.^{98,123,124} Different segments of the mature exosite surfaces could be targeted without directly occluding the active site with a small molecule. Unexpectedly, there are reports that ABE I - directed ligands based on

hirudin^{125,126} and DNA/RNA aptamers^{127,128} can already bind to the immature pro-ABE I on ProT.

Similar to hirudin and the aptamers, PAR3 also contains a binding region directed to thrombin ABE I.⁵⁰ PARs are members of the G protein-coupled receptor family and are involved in platelet activation¹²⁹ vascular remodeling, and vascular permeability.¹³⁰ A fragment of PAR3 including amino acid residues ⁴⁴QNTFEEFPLSDIE⁵⁶ has been confirmed to bind in a specific manner to thrombin ABE I by X-ray crystallography.⁵⁰ A review of the crystal structure reveals that thrombin residues located < 4 Å from the PAR3 include F34, L65, R75, Y76, R77a, I82, and K110. Chymotrypsin numbering is used to define the thrombin sequence. Thrombin R77a is an extra amino acid residue located after E77, which is not found in chymotrypsin.

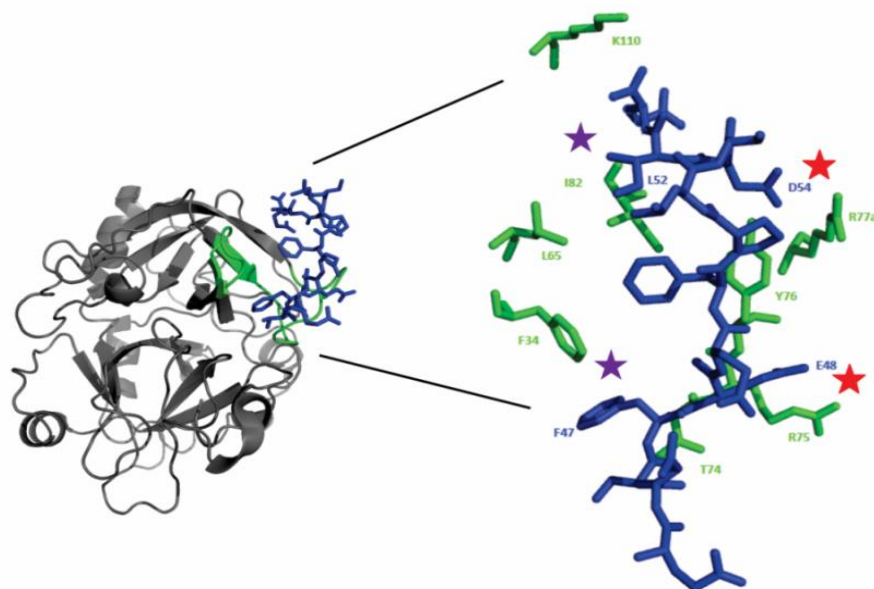


Figure 28: Crystal structure of thrombin in complex with murine PAR3 fragment (44-56). The thrombin surface is rendered as gray ribbons and the PAR3 peptide as blue sticks. Thrombin ABE-I residues that are located < 4 Å from PAR3 (44-56) are displayed as green ribbons or green sticks. The PAR3 residues later chosen for ¹⁵N-HSQC titration studies include acidic residues D54 and E48 (red stars) and hydrophobic residues F47 and L52 (purple stars).

The PAR3 (44-56) sequence is similar to the ABE I-directed region found within the leech-derived inhibitor hirudin (Figure 28).⁵¹ PAR3 could thus be a valuable new system for helping decipher the specific conformational changes that occur as pro-ABE I on prothrombin matures to ABE I on thrombin. An examination of the X-ray crystal structures of prothrombin,¹²⁰ thrombin-PAR3,⁵⁰ and active site -inhibited PPACK-thrombin³⁷ reveals no striking differences between their pro-ABE I and ABE I regions (Figure 29).

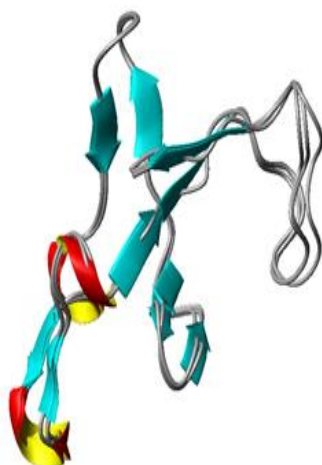


Figure 29: Structural alignment of the ABE I regions of prothrombin (PDB entry 4HZH), thrombin-PAR3 (PDB entry 2PUX), and PPACK-thrombin (PDB entry 1PPB). Regions encompassing exosite I (residues F34-M84, thrombin straight numbering) were selected, and then a backbone alignment was performed using MolMol. The backbone ABE I root-mean-square deviation values for the different protein-protein comparisons were then determined: 0.79 Å for ProT and thrombin-PAR3, 0.47 Å for PPACK-thrombin and thrombin-PAR3 and 0.63 Å for ProT and PPACK-thrombin. This analysis reveals no striking differences for the backbone atoms located in ABE I.

The backbone root-mean-square deviation¹³¹ values for these three anion binding exosite regions were <0.8 Å. These values indicate that conformational changes may have been missed by crystallographic studies and are transient in nature. Nuclear magnetic resonance (NMR) could thus provide a critical alternative strategy for directly monitoring exosite maturation. To achieve this goal, we have performed NMR titration projects

comparing the binding of PAR3 amino acid residues (44-56) to the original zymogen state ProT versus the final active protease thrombin. For the first time, the ability of the PAR3 fragment (44-56) to target the immature (pro)-ABE I site on ProT could be explored.

Previous hydrogen-deuterium exchange studies coupled with mass spectrometry (HDX-MS) demonstrated that regions of pro-ABE I experience increases in their level of solvent exposure as ProT is converted to thrombin.³⁹ These exposures are hypothesized to be part of the exosite maturation process. NMR removes the issue of only probing segments of a protein and would allow for single -amino acid residue analysis. Moreover, NMR has the unique advantage of allowing K_D measurements in solution at this individual residue level.

Thrombin is highly dynamic and adopts distinct states in the presence of ligands, which enable this enzyme to fulfill its array of protease activities.^{56,132-135} Previous NMR studies of thrombin revealed that there are key residues within the 30s and 70s loop regions of ABE I that cannot be monitored by NMR.^{56,132-135} Some of these thrombin residues become NMR-visible following introduction of ABE I ligands, whereas others do not. Intriguingly, surface loops and the ABE I region can remain flexible even when the active site of thrombin is inhibited.¹³³⁻¹³⁵ Because of the flexible nature of thrombin, development of the mature 30s and 70s loop regions can be challenging to probe. To overcome this issue, a novel NMR titration approach was needed. For the current project, the PAR3 (44-56) peptides were labeled with ^{15}N at the amide nitrogen of specific amino acid residues, and ProT and thrombin remained unlabeled.¹³⁶

Critical NMR information about how the PAR3 peptide (44-56) responds to the changing environment that occurs upon exosite maturation could now be collected. NMR

titration studies first revealed that the native PAR3 (44-56) sequence bound too tightly to be monitored by NMR. A P51G substitution was successful in decreasing the PAR3 affinity. One-dimensional (1D) ^1H line broadening NMR studies revealed that PAR3G (44-56) could bind to immature pro-ABE I on ProT and also mature ABE I on thrombin. ^1H - ^{15}N - heteronuclear single -quantum coherence (HSQC) NMR titrations were then performed with selectively labeled PAR3G peptides. Acidic PAR3G ^{15}N -E48 and ^{15}N -D54 both entered into higher affinity, intermediate exchange regimes as ProT was converted to thrombin. Strong binding events involving PAR3G D54 could be weakened with thrombin mutant R77aA, thus supporting the presence of a salt bridge. By contrast, PAR3G [^{15}N -] F47 and [^{15}N -] L52 both bound more weakly to ProT/thrombin than the acidic PAR3G residues did. Furthermore, [^{15}N -] F47 and [^{15}N -] L52 were able to document important changes to the hydrophobic exosite environment as pro-ABE I matures to ABE I.

MATERIALS AND METHODS

Materials

Human plasma Prothrombin (ProT) and thrombin were purchased from Haematologic Technologies, Inc (Essex Junction, VT). Recombinant thrombin mutant R77aA (chymotrypsin numbering) was a kind gift from E. Di Cera and L. Leslie Pelc (St. Louis University School of Medicine, St. Louis, MO).¹³⁷ R77a is an extra thrombin amino acid residue located after E77, which is not found in chymotrypsin. For the R77aA project, the basic R77a was replaced with a small, neutral A. The active sites of the thrombin species were protected from autolysis by blocking with PPACK (D-phenylalanyl-L-prolyl-L-arginine chloromethyl ketone). This serine protease active site inhibitor was purchased

from Calbiochem (San Diego, CA). D₂O (99.96%) was from Cambridge Isotope Laboratories (Andover, MA)

Synthetic Peptides

A series of PAR3 -based peptides were custom synthesized by New England Peptide (Gardner, MA). PAR3 (⁴⁴Q N T ¹⁵F E E F P L S ¹⁵D I E⁵⁶), abbreviated as PAR3 (44-56), is the original PAR3 sequence, and amino acid residues F47 and D54 were labeled with ¹⁵N at their amide nitrogens. PAR3 (44-56, P51G, ¹⁵F47, ¹⁵D54) (⁴⁴Q N T ¹⁵F E E F G L S ¹⁵D I E⁵⁶), abbreviated as PAR3G_{FD} (44-56), contains a Pro51 to Gly substitution (G) and furthermore, F47 and D54 were labeled with ¹⁵N. PAR3 (44-56, P51G, ¹⁵E48, ¹⁵L52) (⁴⁴Q N T F ¹⁵E E F G ¹⁵L S D I E⁵⁶), abbreviated as PAR3G_{EL} (44-56), also contains the P51G substitution (G) but now E48 and L52 are labeled with ¹⁵N. The purity of each synthesized peptide was verified by high-performance liquid chromatography and matrix-assisted laser desorption ionization time-of-flight mass spectrometry. Initial stock solutions of peptide were solubilized in deionized water, and the concentration was determined by amino acid analysis (AAA Service Laboratory, Inc., Damascus, OR). Peptides were later diluted into 25 mM H₃PO₄, 150 mM NaCl, and 0.2 mM EDTA (pH) 6.5 for NMR studies.

The proton chemical shift values for all the PAR3 peptide amino acid residues were determined using a combination of two-dimensional (2D) TOCSY and 2D-transferred NOESY ^{65,109} experiments performed on a Varian Inova 700 MHz NMR spectrometer. Standard TOCSY and NOESY pulse sequences were employed. As is typical for trNOESY experiments, the ligand-protein complex contained a 10-fold excess of PAR3 (44-56) peptide fragment, and the chemical shifts report on the solution environment encountered by the peptide in the presence of the target protein.⁶⁵ The amide proton ¹H chemical shift

assignments derived from the TOCSY and trNOESY experiments were later matched with their respective peaks found in ^1H - ^{15}N HSQC NMR experiments. Both ^1H and ^{15}N values could be followed in the HSQC titrations.

Theoretical Basis for 1D Proton Line Broadening NMR and ^1H - ^{15}N HSQC NMR

1D proton line broadening studies were performed to monitor binding of the PAR3/PAR3G (44-56) peptide fragment to prothrombin versus thrombin.¹⁰⁹⁻¹¹¹ Protein-peptide complexes were prepared with a 10-fold excess of peptide. Peptide protons that undergo interactions experience transient on/off events that cause an increase in the proton transverse relaxation rate and/or cause changes in the observed chemical shift position depending on the time scale of the interaction. The resultant alterations in peptide proton line width/shape reflect the weighted contributions of bound and free populations. This NMR line broadening approach can help map the peptide residue protons that come into direct contact with the protein surface.^{109,110}

^1H - ^{15}N HSQC NMR titrations were used to assess whether specific ^{15}N -labeled residues located within a peptide ligand exhibited fast, intermediate, or slow exchange on/off a protein surface.¹³⁸ In these titrations, changes in chemical shift are monitored as a function of protein-ligand ratios. For weak binding, the interaction is under the fast exchange regime ($k_{\text{ex}} \gg |\Delta\omega|$) where k_{ex} is the exchange rate of the interaction and $\Delta\omega$ is the resonance frequency difference between the bound and free states. Only one signal per ^{15}N -labeled residue is observed reflecting the population-weighted average of bound and free states in terms of chemical shift, intensity, and line width. Furthermore, NMR chemical shifts can be used to quantitatively evaluate affinities for individual ^{15}N labeled residues.^{106,139} For the moderate affinity, intermediate exchange regime ($k_{\text{ex}} \approx |\Delta\omega|$), the

^{15}N peak may disappear during the titration because of extensive line broadening and with an increase in the bound population will later reappear. Finally, for tight binding in which the interaction is described by the slow exchange regime ($k_{\text{ex}} \ll |\Delta\omega|$), two sets of resonances are observed: one corresponding to the free and the other to the bound state. Under this situation, the change in the intensity of the peaks will correspond to the relative population of each state during the course of the titration.

Sample Preparation and Analysis for 1D Proton Line Broadening Experiments

All NMR experiments were performed at pH 6.5 and at 25 °C. Under these conditions, the highly exchangeable [^{15}N -] amide proton could still be readily observed by NMR at pH was not far from physiological (7.4). To prevent autolysis, the serine protease inhibitor PPACK was added to thrombin at a ratio of 4:1, and the mixture was incubated at 37 °C for 30 min. Previous NMR relaxation studies have confirmed that the ABE I region remains flexible in PPACK-inhibited IIa and can engage in long-range communication across the enzyme surface.¹³⁵ Plasma versions of ProT and PPACK- thrombin were buffer exchanged into NMR buffer- [25 mM H_3PO_4 , 150 mM NaCl, 0.2 mM EDTA, (pH 6.5)] using a Vivaspin 2 ultrafiltration unit with a 5000 Da molecular weight cutoff (Sartorius, Göttingen, Germany). Protein concentrations were determined using extinction coefficients ($E^{1\%}_{280\text{ nm}}$) of 18.3 for thrombin and 13.8 for ProT.

Ligand-protein complexes with ratios of at least 10:1 were then prepared. The complexes included 1 mM PAR3 (44-56) with 74 μM ProT, 1 mM PAR3 (44-56) with 77 μM PPACK-thrombin, 960 μM PAR3G (44-56) with 76 μM ProT, and 1 mM PAR3G (44-56) with 76 μM PPACK-thrombin. The peptide at a minimum concentration of 1 mM was used as a free ligand control. The resultant NMR experiments and all others in this project

were performed on a Varian Inova 700 MHz spectrometer with a triple resonance cold probe and pulsed-field Z-axis gradients run at 25 °C. The ^1H NMR spectra were processed using Mnova NMR (Mestrelab Research software).

2D ^1H - ^{13}C HSQC Natural Abundance Experiments

Before proceeding to ^1H - ^{15}N HSQC NMR titrations, we performed ^1H - ^{13}C HSQC natural abundance experiments on both PAR3 (44-56) and PAR3G (44-56) to assess whether the proline to glycine substitution would change the PAR3 peptide conformations. For this project, 1 mM PAR3 and 1 mM PAR3G were prepared in NMR buffer- ([25 mM H_3PO_4 , 150 mM NaCl, and 0.2 mM EDTA, (pH 6.5)]. Parameters for the 2D ^1H - ^{13}C HSQC project included 128 transients with 64 complex points in the indirect dimension, sweep widths of 8064.5 and 24635.3 Hz for the direct and indirect dimensions, respectively, and 3000 complex points acquired in the direct dimension. 2D ^1H - ^{13}C HSQC data were processed using NMRPipe and nmrDraw and then further visualized using Sparky. The ability to superimpose the spectra of PAR3 (red) and PAR3G (black) confirmed that replacement of proline with flexible glycine did not change the overall peptide structure (Appendix 1)

1D and 2D ^1H - ^{15}N HSQC NMR Titration

ProT and active site inhibited PPACK- thrombin were exchanged into NMR buffer using Vivaspin 2 ultrafiltration units with a 5000 Da molecular weight cutoff. A series of protein–ligand complexes were then prepared involving PAR fragments PAR3 (44-56), PAR3G_{FD} (44-56), and PAR3G_{EL} (44-56). ProT and PPACK-thrombin exhibit limited solubility at the high concentrations typically used for NMR titrations. As a result, an alternative titration strategy was employed for the current NMR project. The protein

concentration typically started in the range of 100-200 μM and was serially diluted while maintaining a constant concentration of ^{15}N -labeled ligand. These conditions were achieved by removing a certain volume of the protein-ligand solution and replacing it with the same volume of the ligand solution. The titrations were thus initiated with a high protein: ligand ratio and ended with low protein: ligand ratios all while maintaining a constant peptide ligand concentration. The NMR titrations were therefore monitoring the ability of ProT or thrombin to bind to the ^{15}N -labeled PAR3 fragment.

For the first PAR3 binding studies, the starting complexes included 50 μM PAR3 (44-56) in either 137 μM ProT or 210 μM PPACK-thrombin. The serial dilutions resulted in ProT: PAR3 ratios that spanned from 3:1 to 0.1:1. PPACK-thrombin: PAR3 ratios spanned from 4:1 to 0.1:1. For the PAR3_{G_{FD}} binding studies, starting complexes included 37.5 μM PAR3_{G_{FD}} (44-56) in 70 μM ProT or in PPACK-thrombin. ProT: PAR3_{G_{FD}} ratios during the titrations then spanned from 2:1 to 0.3:1. PPACK-thrombin: PAR3_{G_{FD}} ratios spanned from 2:1 to 0.05:1.

To evaluate the importance of electrostatic interactions between the ^{15}N -labeled D54 of PAR3_{G_{FD}} and R77a of wild-type thrombin, a series of 1D and 2D ^1H - ^{15}N HSQC titrations involving recombinant thrombin mutant R77aA and PAR3_{G_{FD}} were performed. The stock solution of R77aA thrombin was in 20 mM Tris (pH 7.4) and 400mM NaCl. After PPACK treatment, active site inhibited R77aA thrombin was buffer exchanged into 25 mM H_3PO_4 , 150 mM NaCl, 0.2 mM EDTA, (pH 6.5) using a 3 mL Slide-A-Lyzer Dialysis cassette G2 (Thermo Scientific, Rockford, IL) with a 3500 Da molecular weight cutoff and then concentrated using a 5000 Da molecular Weight Cut Off Vivaspin 2 ultrafiltration unit. Starting complexes included 50 μM PAR3_{G_{FD}} (44-56) with 150 μM

PPACK-thrombin (R77aA). PPACK-thrombin (R77aA) to PAR3G_{FD} ratios spanned from 3:1 to 0.1:1.

For the PAR3G_{EL} binding studies, the starting complexes included 50 μ M PAR3G_{EL} (44-56) with either 180 μ M ProT or 211 μ M PPACK-thrombin. The protein: ligand ratio of ProT to PAR3G_{EL} and PPACK to thrombin to PAR3G_{EL} complexes spanned from 4:1 to 0.1:1.

Parameters for the 1D ^1H - ^{15}N HSQC titrations included 512 transients, sweep width of 7022.5 Hz, and 1242 complex points in the direct dimension with PAR3 and 4096 with the PAR3G complexes. Parameters for the 2D ^1H - ^{15}N HSQC titrations included 16 transients with 64 complex points in the indirect dimension, sweep widths of 7022.5 Hz and 1944.3 Hz for the direct and indirect dimensions, respectively, and 1242 complex points acquired in the direct dimension. The ^{15}N labeled free peptide was used as a control for each titration. 1D ^1H - ^{15}N HSQC data were stacked using Mnova NMR and 2D ^1H - ^{15}N HSQC data were processed using NMRPipe and nmrDraw and then further visualized using Sparky.

Quantitative estimates of binding interactions between individual ^{15}N -labeled peptide ligand residues and specific proteins were determined using in-house scripts written using Python.¹⁴⁰ Information provided to such scripts included the total enzyme ($[P_0]$) and total peptide ($[L_0]$) concentrations employed in the different steps of the HSQC titrations. In addition, the NMR chemical shift difference (Δ_{obs}) between each set of free and bound conditions was provided. For the current NMR project, it is important to note that the peptide ligand concentration was kept constant and the protein was serially diluted. As a result, the NMR titrations were measuring the binding of protein to a defined peptide ligand

concentration. The equation for determining the binding affinity values (K_D) was thus modified so that the denominator now contains $[L_0]$ instead of the more typical $[P_0]$.^{138,139}

$$\Delta_{obs} = \Delta_{max} * \frac{(K_D + [L_0] + [P_0]) - \sqrt{(K_D + [L_0] + [P_0])^2 - (4[P_0][L_0])}}{2[L_0]} \quad (1)$$

NMR titrations were performed at least in triplicate to determine K_D values involving plasma-derived ProT and thrombin. Duplicate titrations were performed for thrombin R77aA. An error analysis of the K_D values was performed using a Monte-Carlo approach in which a 10% error was imposed on the serially diluted thrombin concentration.¹⁴⁰

RESULTS

1D Proton Line Broadening NMR Studies with PAR3 (44-56)

One dimensional ^1H line broadening NMR experiments were performed on PAR3 (44-56) in the presence of ProT versus PPACK-thrombin (Figure 30 A-C). The active site inhibitor PPACK (D-phenylalanyl-L-prolyl-L-arginine chloromethyl ketone) was used to protect thrombin from autolysis during the NMR experiments. Proton (^1H) peak broadening could be detected for aliphatic, amide, and aromatic protons of PAR3 in complex with ProT. Such results indicate that a binding surface for PAR3 (44-56) is already available within the immature pro-ABE I on ProT. Substantial peak line broadening was also observed when the peptide was introduced into a solution of PPACK-thrombin containing mature exosite ABE I. Such broadening is impressive considering the lower molecular weight of thrombin (37 kDa) versus that of ProT (72 kDa).¹⁴¹ The overall, extensive thrombin-induced peak broadening provides further justification that mature ABE I is well suited for accommodating PAR3 (44-56). The ^1H chemical shift overlaps

observed across the different Figure 30 panels make it difficult to quantitatively evaluate individual proton line effects.

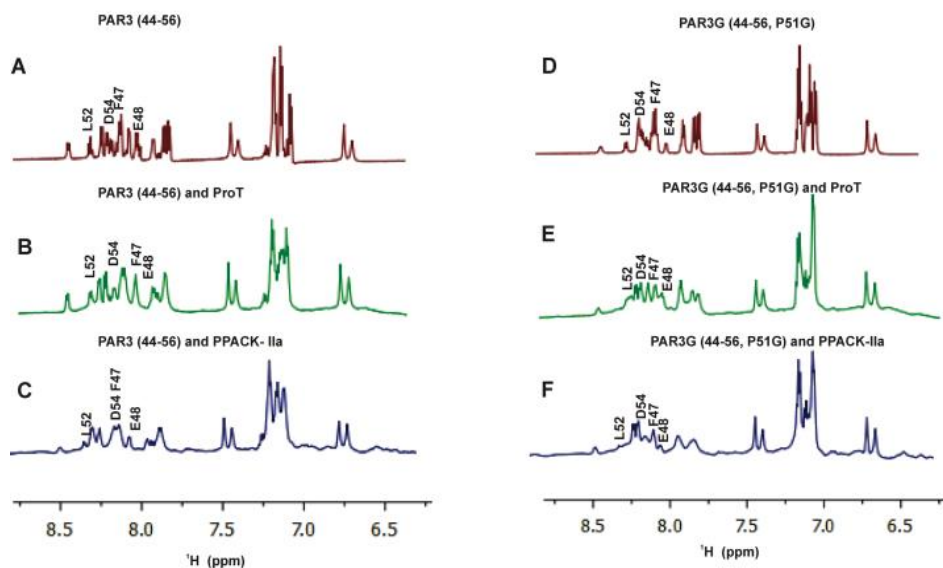


Figure 30: Proton line broadening spectra for PAR3 and PAR3G peptides in the presence of prothrombin and PPACK-thrombin. All NMR samples were in 25 mM H_3PO_4 , 150 mM NaCl, 0.2 mM EDTA and 10 % D_2O (pH 6.5). **A)** 1D ^1H -NMR spectrum of 1 mM PAR3 (44- 56) peptide in solution **B)** 1D ^1H -NMR spectrum of 1 mM PAR3 (44-56) in the presence of 74 μM ProT **C)** 1D ^1H NMR spectrum of 1 mM PAR3 (44-56) in the presence of 77 μM PPACK-IIa **D)** 1D NMR spectrum of 1 mM PAR3G (44- 56) in solution **E)** 1D ^1H NMR spectrum of 960 μM PAR3G (44-56) in the presence of 76 μM ProT. **F)** 1D NMR spectrum of 1 mM PAR3G (44-56) in the presence of 76 μM PPACK-IIa. Line broadening was observed for residues of PAR3 (44-56) and PAR3G (44-56) when either peptide was bound to prothrombin and PPACK- IIa. The amide protons that were later selected for HSQC titrations are labeled.

^{15}N -HSQC Titration Studies with PAR3 (44-56) Labeled at D54 and F47

An HSQC titration project was designed to systematically characterize binding of PAR3-based peptides that are selectively labeled at amide nitrogen locations. The X-ray crystal structure of the thrombin - PAR3 (44-56) complex was first consulted to select sets of acidic and hydrophobic amino acid residues of PAR3 that display interactions with the 30s and 70s loop regions on thrombin (Figure 28).⁵⁰ 2D total correlation spectroscopy (TOCSY) spectra of the bound PAR3 peptide then provided a valuable guide for choosing

amino acid residues with amide chemical shift positions that would be less likely to overlap in the proton dimension during the course of the PAR3-protein ^1H - ^{15}N HSQC titrations.

The first amino acid residues selected included PAR3 F47 and D54. According to the X-ray crystal structure, acidic PAR3 D54 makes a salt bridge contact with thrombin R77a of the 70s ABE I loop whereas PAR3 F47 exhibits π - π stacking interactions with thrombin F34 in the 30s ABE I loop region (Figure 28).⁵⁰ ^{15}N -HSQC NMR titrations were thus performed with PAR3 (44-56) labeled with ^{15}N at D54 and F47. These two PAR3 residues both exhibited proton line broadening in the presence of ProT and PPACK-thrombin confirming contact with the target protein in solution (Figure 30A-C).

The HSQC titrations started out with a 3:1 ProT: PAR3 ratio (containing the [^{15}N]D54 and [^{15}N]-F47 residues). Extensive peak broadening was observed for both [^{15}N]-D54 and [^{15}N]-F47 until the ProT:PAR3 ratios were serially diluted to 0.3:1 (D54) or 0.6:1 (F47) and lower. With PPACK-thrombin, peaks for both PAR3 residues could not be detected until ratios of $\leq 0.3:1$ were reached (Appendix 2 and 3). These NMR results suggest that PAR3 D54 and F47 can already interact with pro-ABE I on ProT, and tightens in the presence of PPACK-thrombin with a mature ABE I.

Proton Line Broadening NMR and ^{15}N -HSQC NMR Titration Studies with PAR3_{GF_D} (44-56) Labeled at D54 and F47

The extensive line broadening observed for PAR3 (44-56) bound to PPACK-IIa was a major hindrance for ^{15}N -NMR titration studies, and binding affinities could not be determined. To weaken this interaction, a modified sequence was designed in which the P51 was replaced with a flexible glycine (P51G). The resultant PAR3_{GF_D} (44-56) showed 1D proton line broadening with both ProT and PPACK- thrombin (Figure 30 D-F). Natural

abundance ^{13}C HSQC spectra were recorded for both PAR3 peptides. As seen Appendix 2, the two spectra show good overlap suggesting that the Pro to Gly substitution has not caused substantial changes to the conformation or the chemical environments of the two peptides.

^1H - ^{15}N HSQC titrations were then performed with PAR3G_{FD} containing ^{15}N -labeled D54 and F47. The ProT:PAR3G_{FD} ratios spanned from 2:1 to 0.3:1 and PPACK thrombin: PAR3G_{FD} ratios spanned from 2:1 to 0.05:1. Results from 1D displays of the ^{15}N -HSQC studies revealed that the PAR3G_{FD} D54 peak became more broadened than the F47 peak in the presence of ProT and PPACK-thrombin (Appendix 4). Further information about interactions occurring with these two proteins was obtained by examining the 2D HSQC titrations (Figures 31A and 31B). In the presence of ProT, the PAR3G_{FD} residue D54 exhibited changes in chemical shift that resemble a fast exchange scenario corresponding to an interaction with weakened affinity. This interaction creates a new protein environment for the ligand. By contrast, PAR3G_{FD} residue F47 residue exhibited little change in chemical shift during the ProT titration suggesting this residue did not experience a substantial change in its chemical environment relative to that of the free peptide (Figure 31A). The project then proceeded to titrations with PPACK-thrombin where additional new effects were observed. The 2D HSQC crosspeak for D54 underwent extensive line broadening and could only be observed for thrombin: PAR3G_{FD} ratios of 0.16:1 to 0.05:1 (Figure 31B). Such a peak broadening reflects improved interactions with the mature ABE I site and is consistent with intermediate exchange conditions. Interestingly, the F47 residue was observed to undergo a wider range of chemical shift changes for the 2:1 to

0.05:1 titration series. F47 was now experiencing a chemical environment different from what had been observed with ProT containing an immature (pro)-ABE I.

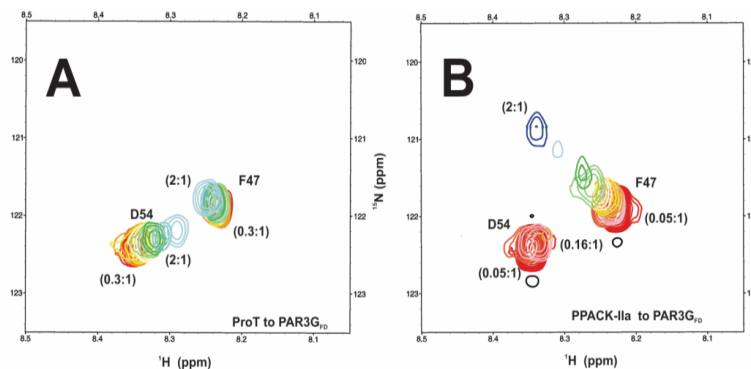


Figure 31: 2D ^1H - ^{15}N HSQC NMR titrations of PAR3G_{FD} (44-56) in the presence of ProT and PPACK- IIa. All NMR samples were in 25 mM H_3PO_4 , 150 mM NaCl, 0.2 mM EDTA, and 10 % D_2O (pH 6.5). A) For the PAR3G_{FD} binding studies with ProT, starting complexes included 37.5 μM PAR3G_{FD} (44-56, [^{15}N]-F47, [^{15}N]-D54) in 70 μM ProT. The serial dilutions resulted in ProT:PAR3G_{FD} ratios that spanned from 2:1 to 0.3:1. B) For PPACK- IIa, starting complexes included 37.5 μM PAR3G_{FD} (44-56, [^{15}N]-F47, [^{15}N]-D54) in 70 μM PPACK- IIa. The serial dilutions resulted in PPACK- IIa:PAR3G_{FD} ratios that spanned from 2:1 to 0.05:1. Representative data sets are shown. Colors for the HSQC crosspeaks span from blue (highest protein:peptide ratio) to red (free peptide).

The chemical shift changes for the D54 and F47 titrations proceed in the same directions across the NMR panels when probing ProT versus PPACK- IIa (upfield for F47 and downfield for D54). These similarities are consistent with the PAR3 and PAR3G peptides interacting within the same binding region of ProT versus PPACK- IIa. Nonspecific binding to a separate area on ProT is not evident. In further support of this proposal, Andersen et al. confirmed that hirudin (54-65) can bind specifically to the (pro)-exosites of prothrombin and thrombin.¹²⁶ Moreover, HDX-MS studies demonstrated that hirudin and PAR3 (44-56) both bind to thrombin ABE I region 65-84.⁶⁰

NMR HSQC titrations can be used to quantitatively characterize binding interactions for individual ^{15}N -labeled amino acid residues. These calculations work the best when there are distinct changes in chemical shift position when ^{15}N -labeled peptide amino acid

residues interact with a target protein. Furthermore, the binding curves should approach saturation.^{138,139} With the current project, the peptide concentration remained constant, and the protein solutions were serially diluted. For these protein- peptide ligand systems, affinity estimates could be made for some of the ¹⁵N-labeled PAR3G (44-56) amino acid residues. On the basis of the titration data that were collected, D54 had a binding affinity (K_D) of $65 \pm 12 \mu\text{M}$ in the presence of ProT and a maximal chemical shift difference ($\Delta\omega_{\text{max}}$) of 0.39 ± 0.03 ppm. (Table 3, and Figure 32B). The interaction became stronger with thrombin, however, the binding of D54 was too tight and the peak broadening was too severe to determine a K_D value from the titration curve. The labeled PAR3 F47 residue had an estimated K_D value of $64 \pm 8 \mu\text{M}$ and a $\Delta\omega_{\text{max}}$ of 0.23 ± 0.01 ppm for ProT and a K_D value of $40 \pm 10 \mu\text{M}$ and a $\Delta\omega_{\text{max}}$ of 1.98 ± 0.19 ppm with thrombin (Table 3, and Figures 32A and C). Curiously, F47 experienced a marginal increase in affinity upon exosite maturation even though this residue clearly encountered a new environment reflected by its now larger chemical shift spread ($\Delta\omega_{\text{max}}$) (Table 3, and Figure 32C)

Table 3: K_D and $|\Delta\omega_{\text{max}}|$ Values Determined from 2D HSQC Titrations for ¹⁵N Labeled PAR3G_{FD} and PAR3G_{EL} Bound to Human Prothrombin and Thrombin (wild type and mutant)^a

Peptide	Residue	[ProT] (μM)	$ \Delta\omega_{\text{max}} $ (ppm)	wild type PPACK- IIa	$ \Delta\omega_{\text{max}} $ (ppm)	R77aA PPACK- IIa
PAR3G _{FD}	F47	64 ± 8	0.23 ± 0.01	$40 \pm 10 \mu\text{M}$	1.98 ± 0.2	$173 \pm 85 \mu\text{M}$
PAR3G _{FD}	D54	65 ± 12	0.39 ± 0.03	too tight to calculate	insufficient data points	$168 \pm 88 \mu\text{M}$
PAR3G _{EL}	L52	124 ± 27	0.37 ± 0.04	$47 \pm 6 \mu\text{M}$	1.84 ± 0.08	salt bridge not involved
PAR3G _{EL}	E48	>200	NA	too tight to calculate	insufficient data points	salt bridge not involved

^aFor these NMR titrations, the peptide ligand concentrations were kept constant and the protein concentrations were serially diluted. Estimated K_D were calculated using in house scripts written in Python. Experimental data employed in the calculations include the individual protein and peptide concentrations and also the ¹⁵N NMR chemical shift differences between each set of free and bound conditions. The plasma-derived ProT and IIa titration series were carried out at least in triplicate. The studies with recombinant R77aA-IIa were done in duplicate. Error analysis was carried out using a Monte-Carlo approach assuming a 10% error in the serially diluted protein samples. See Materials and Methods for more details.

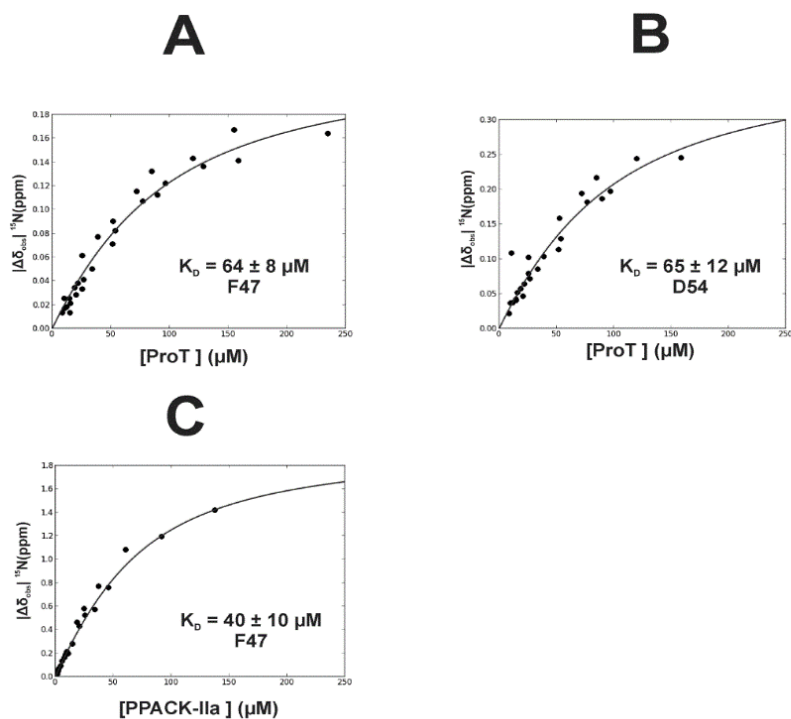


Figure 32: Determination of the binding Affinity (K_D) for ^{15}N -labeled F47 and D54 of PAR3G_{FD} interacting with prothrombin and PPACK-IIa. For this NMR titration series, the peptide ligand concentration was kept constant and the ProT and PPACK-IIa concentrations were serially diluted. As a result, the NMR titrations were measuring the binding of protein to a defined peptide concentration. Interactions between A) ProT and PAR3G [^{15}N]-F47 led to a K_D of $64 \pm 8 \mu\text{M}$, B) ProT and PAR3G [^{15}N]-D54 led to a K_D of $65 \pm 12 \mu\text{M}$, and C) PPACK-IIa and PAR3G [^{15}N]-F47 led to a K_D of $40 \pm 10 \mu\text{M}$. NMR titrations were performed in triplicate. The reported K_D values were determined using in-house scripts written using Python. The term $|\Delta\delta_{\text{obs}}|^{15}\text{N ppm} = \delta^{15}\text{N}_{\text{bound}} - \delta^{15}\text{N}_{\text{free}}$ reflects the absolute difference in chemical shift between the bound and free states of the particular ^{15}N -residue. Error analysis was performed using a Monte-Carlo approach assuming a 10% error in the serially diluted protein samples. See Materials and Methods for more details.

^{15}N -HSQC NMR Titration Studies with PAR3G (44-56) Labeled at D54 and F47

Interacting with the Thrombin Mutant R77aA

The HSQC titrations described above revealed a significant increase in affinity for PAR3 residue D54 as ProT is converted to thrombin. Acidic PAR3 D54 has been reported to make salt bridge contact with basic thrombin residue R77a (Figure 28).⁵⁰ Interactions between these two residues likely become more effective once the mature ABE I is formed. To probe whether electrostatic interactions are occurring between R77a and D54, ^1H - ^{15}N HSQC titrations were performed with a thrombin R77aA - PAR3G_{FD} complex (Figure 33).

Unlike the wild-type PPACK-thrombin titrations, D54 and F47 chemical shifts could be followed for the full titration series for PPACK-thrombin R77aA: PAR3G_{FD} ratios of 3:1 to 0.13:1. The D54 crosspeak exhibited a broad range of chemical shifts and even overlapped with the F47 crosspeak for a portion of the titration (Figures 33A and 33B). Note in Figure 33A that at the start of the titration (3:1 protein:peptide ratio) the amide proton for PAR3G F47 was at 8.3 ppm and for PAR3G D54 at 8.2 ppm. By a ratio of 0.7:1, the two peaks overlapped into a single peak. As the PPACK-R77aA was further diluted, the F47 and D54 peaks continued to change resonance positions and eventually matched those of the free PAR3G_{FD} peptide. A similar set of trends can be observed in the 2D HSQC crosspeaks shown in Figure 33B. Overall, the 2D crosspeak patterns for both F47 and D54 were consistent with fast exchange conditions. For PAR3G D54, the estimated K_D was $168 \pm 88 \mu\text{M}$ and the $\Delta\omega_{\text{max}} = 1.83 \pm 0.62$ ppm, whereas for PAR3G F47 the values were a K_D of $173 \pm 85 \mu\text{M}$ and the $\Delta\omega_{\text{max}} = 1.79 \pm 1.05$ ppm (Table 3, and Appendix 6A and, B). The removal of the salt bridge between PAR3 D54 and thrombin R77a clearly weakened the interaction of D54 with the ABE I surface, and a K_D value could now be estimated. In addition, an ~3-fold loss of affinity was observed for PAR3G F47 in the presence of the R77aA thrombin mutant. Even with the weakened affinity, thrombin R77aA still incurred large structural changes as reflected in the >1.8 ppm changes in the maximal chemical shift.

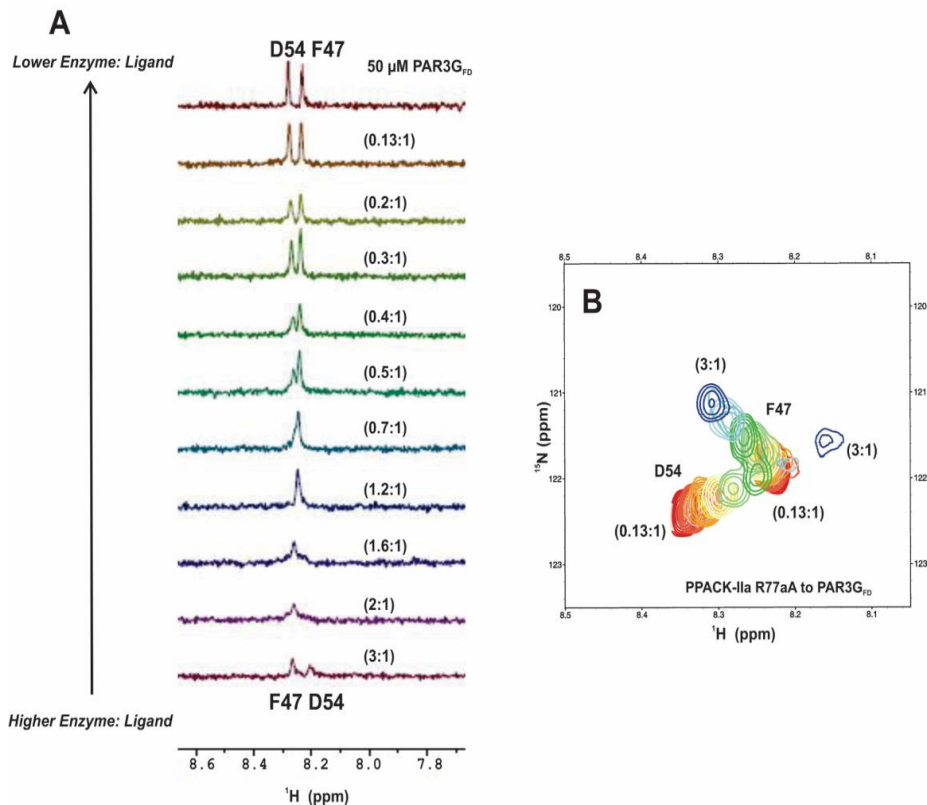


Figure 33: 1D and 2D ^1H - ^{15}N HSQC NMR titrations of PAR3G_{FD} (44-56) in the presence of PPACK- R77aA. All NMR samples were in 25 mM H_3PO_4 , 150 mM NaCl, 0.2 mM EDTA, and 10 % D_2O (pH 6.5). A) For the 1D HSQC NMR titrations, the starting complexes included 50 μM PAR3G_{FD} (44-56, ^{15}N -F47, ^{15}N -D54) in 150 μM PPACK- R77aA. The serial dilutions resulted in PPACK- R77aA:PAR3G_{FD} ratios that spanned from 3:1 to 0.1:1. Note that at the start of the titration (3:1 protein to peptide) the amide proton for PAR3G F47 was at 8.3 ppm and for PAR3G D54 at 8.2 ppm. By a ratio of 0.7:1, the two peaks overlapped into a single peak. As the PPACK-R77aA thrombin was further diluted, the F47 and D54 peaks continued to change resonance positions and eventually matched those of the free PAR3G_{FD} peptide. Representative data sets are shown. B) For the 2D ^1H - ^{15}N HSQC titrations, starting complexes included 50 μM PAR3G_{FD} (44-56, [^{15}N]-F47, [^{15}N]-D54) in 150 μM PPACK- R77aA. The serial dilutions resulted in PPACK-thrombin: PAR3G_{FD} ratios that spanned from 3:1 to 0.1:1. Representative data sets are shown. Colors for the 2D ^1H - ^{15}N HSQC crosspeaks span from blue (highest protein:peptide ratio) to red (free peptide).

^{15}N -HSQC NMR Titration Studies with PAR3G (44-56) Labeled at L52 and E48

Two additional PAR3 residues were chosen to probe the environments of the 30s and 70s loop regions of (pro)-ABE I. E48 of PAR3 (44-56) makes a salt bridge with R75 of thrombin, and L52 of PAR3 (44-56) is positioned within a hydrophobic pocket containing thrombin residues F34, L65, and I82 (Figure 28).⁵⁰ As observed with F47 and D54, the two new PAR3 residues E48 and L52 also exhibited 1D proton line broadening when

complexed with ProT and PPACK-IIa (Figure 30). Thus, HSQC NMR titrations could be performed with PAR3G (44-56) labeled at [¹⁵N]-E48 and [¹⁵N]-L52.

The titration ratios for ProT-PAR3G_{EL} and (PPACK-thrombin)-PAR3G_{EL} spanned from 4:1 to 0.1:1. For the ProT bound complex, 1D and 2D displays of HSQC titration peaks could be followed for all the titrations points (Appendix 5A and Figure 34). Unlike those of PAR3G_{FD}, the binding affinities for L52 and E48 were weaker resulting in K_D values of 124 ± 27 and > 200 μM, respectively (Table 3, Figure Appendix 7A and Appendix 8B). Moreover, both E48 and L52 exhibited fewer changes in chemical shift position. These results suggested that E48 and L52 did not encounter much of a change in binding environment when they were tethered weakly to the surface of ProT.

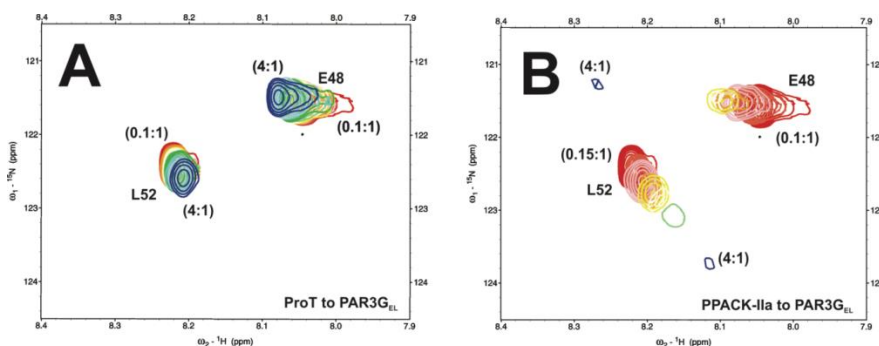


Figure 34: 2D ¹H-¹⁵N HSQC NMR titrations of PAR3G_{EL} (44-56) in the presence of ProT and PPACK- IIa. All NMR samples were in 25mM H₃PO₄, 150 mM NaCl, 0.2 mM EDTA and 10 % D₂O (pH 6.5).A) For the PAR3G_{EL} binding studies with ProT, starting complexes included 50 μM PAR3G_{EL} (44-56, ¹⁵N-E48, ¹⁵N-L52) in 180 μM ProT. The serial dilutions resulted in ProT to PAR3G ratios that spanned from 4:1 to 0.1:1. B) For the PPACK - IIa, starting complexes included 50 μM PAR3G_{EL} (44-56, ¹⁵N-E48, ¹⁵N-L52) in 211 μM PPACK- IIa. The serial dilutions resulted in PPACK- IIa to PAR3G_{EL} ratios that spanned from 4:1 to 0.1:1. Representative data sets are shown. Colors for the 2D ¹H-¹⁵N HSQC crosspeaks span from blue (highest protein-peptide ratio) to red (free peptide).

Furthermore, we propose that ProT R75 is less available for interacting with E48 of PAR3 than the distinct interactions already observed between ProT R77a and D54 of PAR3. When the peptide was titrated with PPACK- thrombin (Appendix 6B and Figure 34B), L52 exhibited a greater change in chemical shift position. By contrast, E48

resembled intermediate exchange on/off the thrombin surface. Extensive peak broadening could already be observed at 1.2:1 protein: ligand ratios. In the presence of PPACK-thrombin, L52 showed a 3-fold improvement in K_D ($47 \pm 6 \mu\text{M}$) and E48 underwent extensive peak broadening preventing a K_D value from being calculated. For L52, a $\Delta\omega_{\text{max}}$ of 0.37 ± 0.04 ppm was obtained for ProT and increased to 1.84 ± 0.08 ppm upon conversion to thrombin (Table 3, and Figures Appendix 7A, C).

DISCUSSION

With thrombosis becoming a global disease burden, the urge to develop better anticoagulants has increased.⁸⁷ Novel oral anticoagulants^{141,142} that target the active sites of FXa and thrombin¹⁴³ have shown much medical promise but reversing their therapeutic activities during heavy bleeding scenarios can be challenging.^{144,145} Drug candidates^{123,124,146} that target thrombin ABE I are an alternative strategy. Thrombin is, however, proteolytically derived from the zymogen prothrombin (Figure 27). Unexpectedly, some ABE I ligands can already bind to the immature pro-ABE I site on this zymogen.^{101,125,126,128,147} Future ABE I directed therapeutics might therefore be designed to target or avoid specific regions of pro-ABE I on ProT versus ABE I on thrombin.

With our NMR titration approaches, we characterized, for the first time, the binding of ABE I directed PAR3 peptides to ProT versus PPACK-thrombin. Previous NMR relaxation studies had already revealed that communication from ABE I toward the active site region is still preserved with PPACK-thrombin.¹³³ Our 1D ^1H line broadening NMR results demonstrated that PAR3 (44-56) and its weaker binding version PAR3G (44-56) could interact with both ProT and PPACK-thrombin (Figure 30).⁵⁰ NMR ^1H - ^{15}N -HSQC titration studies were then performed with a series of ^{15}N -labeled PAR3 peptides to characterize our

ability to bind ProT versus PPACK-thrombin (Figure 31-34, and Figure Appendix 1-8). Such an approach has the distinct advantage of monitoring exosite maturation at the individual amino acid residue level. Isothermal titration calorimetry, fluorescence, and surface plasmon resonance all provide a global K_D fit using all peptide amino acid residues. NMR, by contrast, preserves the ability to measure individual binding interactions in solution and thus document their contributions. Moreover, NMR works best with weaker affinity systems.

For the current NMR project, PAR3 peptides were prepared with [^{15}N -] amide labeling of F47, E48, L52, and D54. HSQC titrations were performed at the typical NMR pH of 6.5. The acidic and hydrophobic residues [^{15}N -] D54 and [^{15}N -]F47 on PAR3 (44-56) were examined first. This native PAR3 sequence bound too tightly to thrombin hindering ability to assess K_D values by NMR titration methods. Prior fluorescence titrations revealed a K_D of 2 μM for a related PAR3 sequence thus confirming our observation of intermediate/slow exchange conditions in the NMR titrations.¹⁴⁸ Greater success was achieved with PAR3G_{FD} (44-56) in which P51 was replaced with G51. With ProT, PAR3G D54 and F47 both had individual K_D values in the range of 65 μM . The immature pro-ABE I can thus accommodate both residues to a similar extent. Upon maturation to ABE I, PAR3G D54 bound too tightly to PPACK-thrombin for binding affinity calculation. By contrast, the F47 binding affinity increased only modestly as ProT was converted to thrombin. Interestingly, the F47 also documented a substantial change in the chemical environment ($\Delta\omega_{\text{max}} = 1.8$ ppm) within the 30s loop region following activation to thrombin. Structural rearrangements are proposed to occur in the vicinity of ProT/thrombin residue F34 but do not result in a significant change in affinity (Figure 28).

The PAR3G D54 residue was hypothesized to be influenced by its electrostatic interaction with thrombin R77a (Figure 28).⁵⁰ This acidic PAR3 residue may have properties similar to those of hirudin.¹⁴⁹ The hirudin sequence (⁵⁶FEEI⁵⁹) has already been proposed to electrostatically steer toward the ABE I surface.^{149,150} Ionic tethering between acidic hirudin residues and specific basic residues on ABE I might then be promoted followed by stabilizing hydrophobic interactions.^{149,150} These hypotheses could now be tested with the PAR3G sequence and thrombin R77aA. As predicted, the affinity for D54 weakened 3-fold upon loss of its salt bridge partner. In response, the F47 also displayed a much weaker affinity value.

PAR3G residues E48 and L52 provided the opportunity to probe two additional regions of ProT versus PPACK-thrombin. E48 makes a salt bridge with thrombin R75, a neighboring region of the 70s loop. PAR3G L52 interacts with a cluster of hydrophobic residues including thrombin F34, L65, and I82 (Figure 28).⁵⁰ Curiously, both E48 and L52 exhibited only minor changes in chemical shift upon binding to ProT. Furthermore, the estimated individual K_D values for L52 and E48 bound to ProT were ≥ 2 -fold weaker than those for D54 and F47. The pro-ABE I surface on ProT may not accommodate these two residues as well as it does PAR3 D54 and F47. Similar to PAR3G D54, there was extensive line broadening for E48 upon conversion to thrombin and K_D values could not be determined. By contrast, L52 exhibited a broad series of chemical shift changes during the thrombin titration ($\Delta\omega_{\max} = 1.8$ ppm). Interestingly, the estimated K_D for binding of L52 ($K_D = 47 \pm 6 \mu\text{M}$) to PPACK-thrombin was similar to the value determined for F47 ($K_D = 40 \pm 10 \mu\text{M}$). Both L52 and F47 interact at the more hydrophobic surface area of ABE I with a common overlapping influence from thrombin F34 (Figure 28).

CONCLUSIONS

Overall, our solution NMR studies have elucidated changes in the exosite environment that occur as zymogen ProT is converted to active thrombin. 1D proton line broadening NMR and ^1H - ^{15}N -HSQC studies demonstrated that PAR3G E48 and D54 could already interact with ProT and the affinity increased upon maturation to thrombin. In the NMR studies, the 3-fold tighter binding affinity for D54 versus that of E48 suggests that the 70s loop region surrounding thrombin R77a may be better oriented to bind PAR3G D54 than the interaction between thrombin R75 and PAR3G E48 (Figure 28). Moreover, a close review of the crystal structure overlays in Figure 3 suggests that the 70s loop region of ProT may assume an orientation that is preconfigured to that of PAR3-thrombin and PPACK-thrombin. As the ionic PAR3G D54 – ProT/IIa R77a and PAR3G E48- ProT/IIa R75 interactions are stabilized, PAR3G F47 and L52 are proposed to take further advantage of interacting with thrombin F34 (within the 30-40s loop) and the thrombin hydrophobic cluster F34, L65, and I82 (Figure 28). Aromatic PAR3G F47 and aliphatic PAR3G L52 both reported on significant changes in the chemical environment upon conversion of ProT to thrombin. The region surrounding the ProT/IIa 30s loop appears to be more affected than the hydrophobic pocket containing F34, L65, and I82.

Curiously, no striking differences are observed between the crystal structures of immature pro-ABE I in ProT versus the mature ABE I regions of thrombin-ligand complexes (Figure 29). Moreover, there are no X-ray crystal structures for a ligand bound to the pro-ABE I region of ProT. We can speculate that there are transient structural states within this coagulation protein system that are differentially explored by ProT and thrombin. Some of these states may be shared whereas others may be unique.

Interestingly, ProT already possesses a binding competent state. Additional research has implicated transient, or lowly populated, structures as playing an essential role in molecular interactions.¹⁵¹⁻¹⁵³ Thus, we believe that the mature thrombin likely visits a binding competent state more often than ProT does, thereby promoting the higher affinity of PAR3 for thrombin.

In conclusion, our NMR titration studies have clearly revealed that individual PAR3 amino acid residues are documenting structural rearrangements that occur upon ABE I maturation. Moreover, these amino acid residues make individual contributions to the overall binding affinity. The knowledge gained from this NMR project may be used to help decipher the characteristic features of pro-ABE I versus ABE I that become accessible to physiological ligands or future drug candidates.

NOTE:

1.) 2D ¹H-¹⁵N HSQC titration for PAR3_{G_{FD}} and thrombin without PPACK incubation was performed as a control experiment to verify whether chemical shift pattern of ¹⁵N-labeled F47 and D54 are in the same direction as the one with PPACK-incubation (Appendix 8).

2.) This chapter is reproduced in part from the published manuscript:

Ramya Billur, David Ban, T. Michael Sabo, Muriel C. Maurer. (2017). “Deciphering the Conformational Changes Associated with the Maturation of Thrombin Anion Binding Exosite I”, *Biochemistry*, 56, 6343- 6354.¹⁵⁴

CHAPTER IV
BINDING INTERACTIONS OF PAR1 AND PAR3 FOR THROMBIN AND
DISSECTING ALLOSTERIC LINKAGE BETWEEN THE EXOSITES

INTRODUCTION

Thrombin is a serine protease whose functions are controlled by surface loops and two anion binding exosites.⁴⁸ These exosites ABE I and ABE II are located on opposite sides of the active site region (**Figure 6 from chapter 1**).³⁷ Thrombin is originally expressed as the zymogen prothrombin (ProT) that contains immature exosites pro-ABE I and pro-ABE II (**Figure 5 from chapter 1**).³⁸ These immature exosites convert into mature ligand binding sites upon activation of ProT to thrombin.^{48,57,89}

Unexpectedly, there are reports that ABE I directed ligands can already bind to immature pro-ABE I on ProT.^{125,126,128} In the previous chapter, we successfully demonstrated how NMR titrations could be used to decipher conformational changes that occur as pro- ABE I on ProT is converted into thrombin. In that project, a peptide based on the protease activated receptor PAR3 (46-54) was successfully shown to bind to ProT and affinity increased upon thrombin maturation.¹⁵⁴ Moreover, the valuable roles that individual ¹⁵N-labeled PAR3 residues play in the binding process were determined. Both electrostatic (E48, D54) and hydrophobic residues (F47, L52) of PAR3 (46-54) made unique contributions toward interacting with pro-ABE I and ABE I.

PAR3 is just one member of the protease activated receptor family. PARs are membrane bound proteins containing seven transmembrane domains. Among this family, thrombin exhibits the greatest substrate specificity towards PAR1 reflected by its highest k_{cat}/K_m .¹⁵⁵ PAR1 is well known for its roles in platelet activation, aggregation, and for helping to trigger inflammatory processes.^{81,102,156,157} PAR1 has gained attention for its role in controlling the metastasis of cancer cells.^{158,159}

PAR1 needs to be activated for this receptor to initiate its biosignaling functions. Thrombin cleaves PAR1 at the R41-S42 peptide bond, and a portion of the new N-terminus then serves as a tethered ligand to help activate PAR1. The required cleavage of PAR1 at the thrombin active site is helped by having a portion of PAR1 also bind to thrombin ABE I. Interestingly, PAR3 and PAR1 have both been shown to bind at ABE I and assist in cleavage of PAR4 which lacks an ABE I binding segment. Following their activations, PAR1 and PAR4 can illicit transmembrane signaling events like coupling to heterotrimeric G-proteins, regulating kinase signaling cascades, and promoting receptor phosphorylation and internalization.^{156,160}

Gandhi and coworkers reported the X-ray crystal structure of PAR1 (33-62, ³³ATNATLDPRSFLLRNPNDKYEPFWEDEEKN⁶²) bound to catalytically inactive thrombin S195A.^{49,85} The ³⁸LDPRSFLLRNP⁴⁸ segment spans the active site with thrombin cleavage occurring at the R41-S42 peptide bond. The segment ⁵⁰DKYEPF⁵⁵ is hypothesized to be important for binding to ABE I.¹⁴⁹ Similar to other ABE I directed ligands such as hirudin^{51,161} and PAR3, this PAR1 sequence has both electrostatic and hydrophobic residues to interact with thrombin. A careful review of the X-ray crystal

structure revealed that key thrombin sites located $< 4 \text{ \AA}$ away from PAR1 include F34, R35, Q38, L40, L65, R67, R73, T74, Y76, and I82 (**Figure 35**).

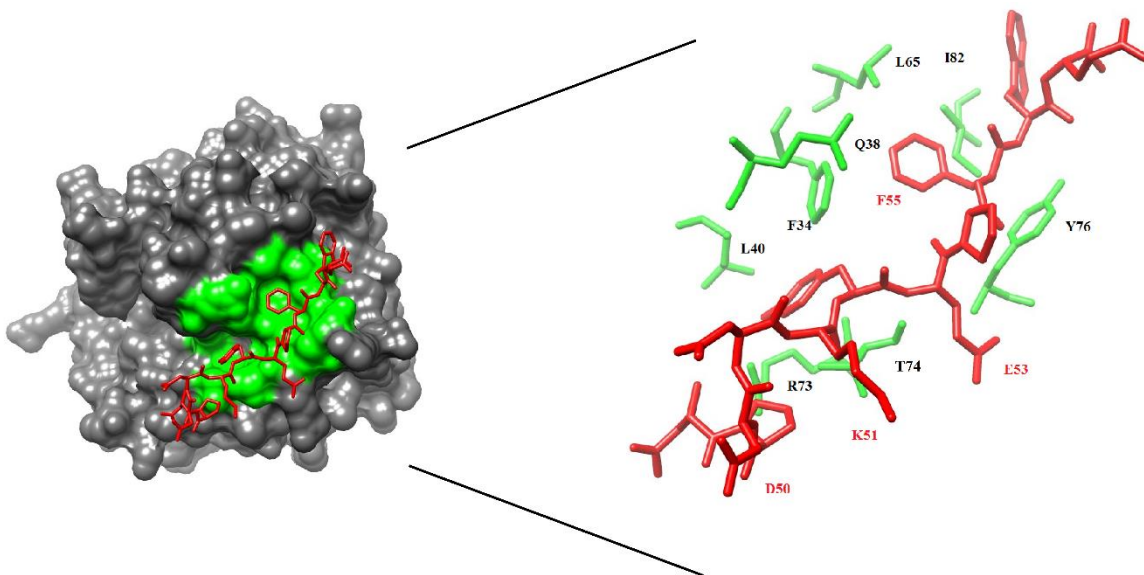


Figure 35: Crystal structure of thrombin in complex with human PAR1 fragment (49-57) PDB code 3LU9. The thrombin surface is rendered in gray. ABE-I residues that are located $< 4 \text{ \AA}$ from PAR1 (49-57) are displayed as green ribbons or green sticks and PAR1 (49-57) in red sticks. The PAR1 residues later chosen for ^{15}N -HSQC titration studies include residues D50, K51, E53 and F55 (highlighted in red).

PAR1 $^{50}\text{DKYEP}^{54}$, similar to $^{56}\text{FEEI}^{59}$ of hirudin,¹⁶¹ is proposed to be responsible for docking PAR1 on to thrombin ABE I. The next step is thought to be locking of $^{38}\text{LDPR}^{41}$ on to the thrombin active site for cleavage. Molecular modeling studies have suggested that the C-terminal $^{58}\text{DEEKN}^{62}$ binds to ABE I, but this flexible PAR1 segment is not observed in the Gandhi X-ray crystal structure.^{49,85} Similar to our previous work with PAR3 peptides, solution NMR could provide a successful strategy to further map the binding of PAR1 to ABE I.¹⁵⁴ Moreover, exosite maturation from ProT to thrombin could be explored.

Events at thrombin ABE I can also be influenced by occupancy at ABE II. Similar to PAR1 and PAR3, glycoprotein GpIb α is also found on the surface of platelets. GpIb α recruits thrombin to the platelet environment by binding an anionic cluster (269-286) to thrombin ABE II (R93, R101, R126, K235, K236, and K240).⁷⁹ GpIb α binding then affects a variety of thrombin functions. The GpIb α -thrombin complex enhances PAR1 hydrolysis,⁸⁰ hinders release of FpA,¹⁶² and decreases affinity for FVIII.¹⁶³ Previous HDX-MS studies demonstrated that GpIb α binding at thrombin ABE II can influence the solvent accessibility of thrombin ABE I regions.^{60,78} There have been reports that Prothrombin F2 and Fibrinogen γ' can each bind to ABE II and also elicit both local and long range allosteric effects.¹⁶⁴ Keeping these observations in mind, we wanted to further probe how GpIb α is involved in allosteric communication with ABE I bound ligands.

X-ray crystal structures are available for prothrombin,¹²⁰ active site inhibited thrombin,³⁷ PAR1 bound thrombin,⁴⁹ PAR3 bound thrombin,⁵⁰ and GpIb α bound thrombin.⁵² An overlay of ABE-I regions for these proteins reveals no striking structural differences across the series (**Figure 36**). The backbone root mean square deviation for those five ABE-I regions range from 0.47 to 0.76 Å.¹³¹ Our current solution NMR titration methods have the ability to reveal conformational changes that occur upon activation of prothrombin to thrombin and to monitor how individual peptide ligand residues respond to the new environments. Conformational changes that are transient in nature and may have been missed by X-ray crystallography can be identified.

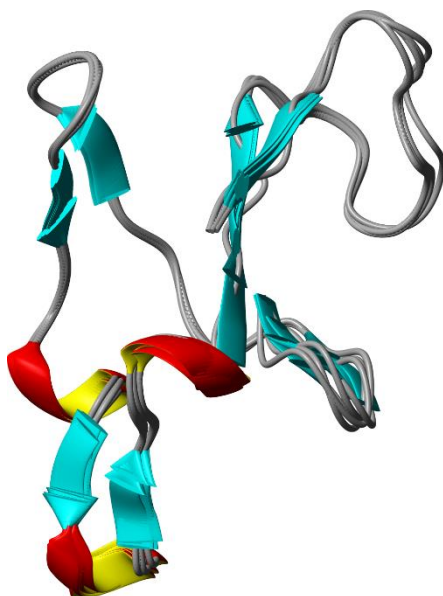


Figure 36: Structural alignment of the ABE I regions of prothrombin (PDB entry 4HZH), thrombin-PAR1 (PDB entry 3LU9), and PPACK-thrombin (PDB entry 1PPB), thrombin- GpIb α (PDB entry 1PBV and 1OOK). Regions encompassing exosite I (residues F34-M84, thrombin straight numbering) were selected, and then a backbone alignment was performed using MolMol. The backbone ABE I root-mean-square deviation values for the different protein -protein comparisons were then determined: 0.79 Å for ProT and thrombin-PAR1, 0.47Å for PPACK-thrombin and thrombin-PAR1, 0.63 Å for ProT and PPACK-thrombin, 0.76Å and 0.62Å for ProT and two crystal structures of GpIb α , 0.48Å and 0.50Å for thrombin-PAR1 and two crystal structures of GpIb α . Finally, 1PBV and 1OOK had an RMSD of 0.34Å.

Important information on how individual PAR1 amino acids interact with ProT and mature IIa were obtained in this second NMR titration project. With our 1D ^1H line broadening NMR experiments, we successfully monitored the native PAR1P sequence (49-62) binding to immature zymogen Prothrombin (ProT) versus the mature protease thrombin (IIa). Proton line broadening for PAR1P (49-62) increased when bound to PPACK-IIa. 2D trNOESY suggested an extended conformation for PAR1 (49-62) with the Xaa-Pro adopting a *trans* conformation. Studies then proceeded to ^1H - ^{15}N HSQC titrations using selectively labeled PAR1 peptides. ^{15}N - labeled F55 of PAR1P interacted already with ProT indicating the existence of hydrophobic interactions with the immature exosite. However, NMR titrations with ^{15}N - labeled PAR1P with PPACK-IIa could not be followed

due to severe exchange broadening. Hence, a weaker binding version PAR1 (P54G) was employed for all ^{15}N -labeled titrations. Upon ABE I maturation, the affinities increased for ^{15}N -labeled K51, F55, and D58 of PAR1G (49-62) owing to the formation of more optimal contacts. For the first time, thrombin binding interactions could be monitored for PAR1G D58 and E60 which were missed in X-ray structures. By having GpIb α bind at ABE II, long-range communication between exosites could be explored and effects on binding affinities determined. Both PAR1 (49-62) and PAR3 (44-56) responded to the presence of the ABE II ligand GpIb α (269-286). New evidence is available that interactions between PARs and thrombin are ligand dependent.

MATERIALS AND METHODS

Materials

Human plasma Prothrombin (ProT) and thrombin were purchased from Haematologic Technologies, Inc (Essex Junction, VT). The active sites of the thrombin species were protected from autolysis by blocking with PPACK (D-phenylalanyl-L-prolyl-L-arginine chloromethyl ketone). This serine protease active site inhibitor was purchased from Calbiochem (San Diego, CA). D_2O (99.96%) was from Cambridge Isotope Laboratories (Andover, MA).

Synthetic Peptides

A series of PAR1 -based peptides was custom synthesized by New England Peptide (Gardner, MA). PAR1 (^{49}N ^{15}D K Y E P ^{15}F W E D E E K N 62), abbreviated as PAR1P (49-62), is the original PAR1 sequence, and amino acid residues D50 and F55 were labeled with ^{15}N at their amide nitrogens. PAR1 (^{49}N ^{15}D K Y E G ^{15}F W E D E E K N 62) abbreviated as PAR1G_{FD} (49-62), contains a Pro54 to Gly substitution (G) and furthermore,

the D50 and F55 were labeled with ^{15}N . PAR1 (49-62, P54G, $^{15}\text{E}53$, $^{15}\text{D}58$) ($^{49}\text{N D K Y }^{15}\text{E } \underline{\text{G}} \text{ F W E }^{15}\text{D E E K N}^{62}$), abbreviated as PAR1G_{ED} (49-62), also contains the P54G substitution (G) but now E53 and D58 are labeled with ^{15}N . PAR1 (49-62, P54G, $^{15}\text{K}51$, $^{15}\text{E}60$) ($^{49}\text{N D }^{15}\text{K Y E } \underline{\text{G}} \text{ F W E D E }^{15}\text{E K N}^{62}$), abbreviated as PAR1G_{KE} (49-62), also contains the P54G substitution (G), where K51 and E60 are labeled with ^{15}N . PAR3 (44-56), P51G, $^{15}\text{E}48$, $^{15}\text{L}52$) ($^{44}\text{Q N T F }^{15}\text{E E F G }^{15}\text{L S D I E}^{56}$), abbreviated as PAR3G_{ED} (44-56), contains the P51G substitution (G), where E48 and L52 are labeled with ^{15}N . GpIb α (269- 286) ($^{269}\text{D E G D T D L Y}_P \text{ P D Y}_P \text{ P Y}_P \text{ P P E E D T E G}^{289}$) with the three tyrosines phosphorylated was synthesized by Bachem Bioscience Inc. The purity of each synthesized peptide was verified by high-performance liquid chromatography and matrix-assisted laser desorption ionization time-of-flight mass spectrometry. Initial stock solutions of peptide were solubilized in deionized water, and the concentrations were determined by amino acid analysis (AAA Service Laboratory, Inc., Damascus, OR). Peptides were later diluted into 25 mM H_3PO_4 , 150 mM NaCl, and 0.2 mM EDTA (pH 6.5) for NMR studies.

The ^1H chemical shift assignments for all PAR1 peptide residues were derived from 2D TOCSY and 2D trNOESY experiments. Standard pulse sequences were employed. Since the aromatic residues (F55 and W56) were challenging to assign for PAR1 (49-62), 2D ^1H - ^{13}C HSQC natural abundance experiments were also employed. For this project, 1 mM PAR1P and 1 mM PAR1G were prepared in NMR buffer- [25 mM H_3PO_4 , 150 mM NaCl, and 0.2 mM EDTA, (pH 5.4-6.5)]. Parameters for the 2D ^1H - ^{13}C HSQC project included 128 transients with 64 complex points in the indirect dimension, sweep widths of 8064.5 and 24635.3 Hz for the direct and indirect dimensions, respectively, and 3000 complex points acquired in the direct dimension. Each aromatic carbon and hydrogen of

F55, W56, and Y52 were first assigned in 2D ^1H - ^{13}C HSQC spectra. Later, aromatic hydrogens were matched with the fingerprint and amide- amide regions of 2D TOCSY and 2D tr-NOESY spectra.

Sample Preparation and Analysis for 1D Proton Line Broadening and 2D Transferred NOESY Experiments

All NMR experiments were performed at pH 6.5 and at 25 °C. To prevent autolysis, the serine protease inhibitor PPACK was added to thrombin at a ratio of 4:1, and the mixture was incubated at 37 °C for 30 min. Plasma versions of ProT and PPACK- thrombin were buffer exchanged into NMR buffer- [25 mM H_3PO_4 , 150 mM NaCl, 0.2 mM EDTA, (pH 6.5)] using a Vivaspin 2 ultrafiltration unit with a 5000 Da molecular weight cutoff (Sartorius, Göttingen, Germany). Protein concentrations were determined using extinction coefficients ($E^{1\%}_{280\text{ nm}}$) of 18.3 for thrombin and 13.8 for ProT. Ligand-protein complexes with ratios of at least 10:1 were then prepared.

As is typical for trNOESY experiments, the ligand-protein complex contained a 10-fold excess of PAR1 (49-62) peptide fragment, and the chemical shifts report on the solution environment encountered by the peptide in the presence of the target protein. The complexes included 780 μM PAR1 (49-62) with 59 μM ProT, 900 μM PAR1P (49-62) with 97 μM PPACK-thrombin, 830 μM PAR1G (49-62) with 83 μM ProT, and 870 μM PAR1G (44-56) with 87 μM PPACK-thrombin. Peptide at a minimum concentration of 1 mM was used as a free ligand control.

All NMR experiments in this project were performed on a Varian Inova 700 MHz spectrometer with a triple resonance cold probe and pulsed-field Z-axis gradients run at 25 °C. The ^1H NMR spectra were processed using Mnova NMR (Mestrelab Research

software). 2D TOCSY, 2D tr-NOESY, and 2D ^1H - ^{13}C HSQC data were processed using NMRPipe and nmrDraw and then further visualized using Sparky.

1D and 2D ^1H - ^{15}N HSQC NMR Titration

ProT and active site inhibited PPACK- thrombin were exchanged into NMR buffer using Vivaspin 2 ultrafiltration units with a 5000 Da molecular weight cutoff. A series of protein–ligand complexes was then prepared involving PAR fragments PAR1P (49-62), PAR1G_{FD} (49-62), PAR1G_{ED} (49-62), and PAR1G_{KE} (49-62). ProT and PPACK-thrombin exhibit limited solubility at the high concentrations typically used for NMR titrations. As a result, an alternative titration strategy was employed for the current NMR project. The protein concentration typically started in the range of 100-200 μM and was serially diluted while maintaining a constant concentration of ^{15}N -labeled ligand. These conditions were achieved by removing a certain volume of the protein-ligand solution and replacing it with the same volume of the ligand solution. The titrations were thus initiated with a high protein: ligand ratio and ended with low protein: ligand ratios all while maintaining a constant peptide ligand concentration. The NMR titrations were therefore monitoring the ability of ProT or PPACK inhibited thrombin to bind to the ^{15}N -labeled PAR1 fragment.

For the first PAR1 binding studies, the starting complexes included 50 μM PAR1P (49-62) with 150 μM ProT and 150 μM PPACK-thrombin. The serial dilutions for both ProT: PAR1P and PPACK-thrombin: PAR1P resulted in ratios that spanned 3:1 to 0.1:1. To weaken the affinity of the PAR1P peptide for PPACK-IIa, P54 was replaced with the still flexible Glycine. For these PAR1G_{FD} binding studies, starting complexes included 50 μM PAR1G_{FD} (49-62) with 150 μM ProT and with 175 μM PPACK-thrombin. Serial dilutions

for both ProT: PAR1G_{FD} (49-62) and PPACK-thrombin: PAR1G_{FD} resulted in protein-peptide ratios that spanned 3:1 to 0.1:1.

To evaluate the electrostatic binding contributions at (pro)- ABE I, a series of acidic and basic PAR1 residues were ¹⁵N labeled. For the PAR1G_{ED} binding studies, the starting complexes included 50 μM PAR1G_{ED} (49-62) with 150 μM ProT or PPACK-thrombin. The protein:ligand ratio of ProT:PAR1G_{EL} and PPACK-thrombin: PAR3G_{EL} complexes spanned from 3:1 to 0.1:1. For the PAR1G_{KE} binding studies, starting complexes included 50 μM PAR1G_{KE} (49-62) with 150 μM ProT and with 185 μM PPACK-thrombin. The serial dilutions for both ProT: PAR1G_{KE} (49-62) and PPACK-thrombin: PAR1G_{KE} resulted in ratios that spanned 3:1 to 0.1:1.

Parameters for the 1D ¹H-¹⁵N HSQC titrations for both PAR1P and PAR1G complexes included 512 transients, a sweep width of 9000 Hz, and 4096 complex points in the direct dimension. Parameters for the 2D ¹H-¹⁵N HSQC titrations included 16 transients with 64 complex points in the indirect dimension, sweep widths of 9000Hz for both direct and indirect dimensions, and 1242 complex points acquired in the direct dimension. The ¹⁵N labeled free peptide was used as a control for each titration. 1D ¹H-¹⁵N HSQC data were stacked using Mnova NMR and 2D ¹H-¹⁵N HSQC data were processed using NMRPipe and nmrDraw and then further visualized using Sparky. Quantitative estimates of binding interactions between individual ¹⁵N-labeled peptide ligand residues and specific proteins were determined using in-house scripts written using Python. All the titrations were repeated at least twice. A Monte-Carlo approach was employed to calculate the errors in K_D values (Refer to Chapter 3).

1D and 2D ^1H - ^{15}N HSQC NMR Titration for Long-Range Communication Studies

To elucidate whether long-range communication existed between the two exosites of thrombin, two PAR based ^{15}N -labeled peptide ligands were chosen that included PAR1_{G_{ED}} (49-62) and PAR3_{G_{EL}} (44-56). In this titration, triply phosphorylated GpIb α (269- 286) is expected to bind at ABE II and ^{15}N -labeled PARs at ABE I. Even though GpIb α (269- 286) is reported to have a K_D of 5.9 nM for IIa,¹⁶⁵ we still made sure that GpIb α (269-286) was at least 99.7 % bound during the entire course of the titration. The following equation was used to determine the % GpIb α ligand (L) bound to protein/receptor (R).

$$\% \text{ Bound} = \frac{(K_D+L+R) - \sqrt{(K_D+L+R)^2 - (4LR)}}{2R} \quad (9)$$

The experimental strategies employed for the NMR titrations were similar to the previously described project. The only difference was adding the GpIb α to the thrombin prior to starting the PAR titration. For both PAR1_{G_{ED}} and PAR3_{G_{EL}} binding studies, the starting complexes included 150 μM PPACK-IIa, 200 μM GpIb α , and 50 μM of ^{15}N -labeled PAR peptide. The protein: ligand ratio of PPACK-thrombin: PAR1_{G_{ED}}/PAR3_{G_{EL}} complexes spanned from 3:1 to 0.1:1. PPACK- thrombin concentration was diluted from 150 μM to 6 μM and GpIb α concentration were diluted from 200 μM to 8 μM . At each titration point, the concentration of ^{15}N -labeled PAR ligands was kept constant. The same instrument, parameters, and processing software were used to elucidate long-range communication in the serine protease thrombin as used for the single ligand binding sites.

RESULTS

1D Proton Line Broadening Experiments with PAR1 (49-62)

1D ^1H - NMR experiments were performed for PAR1P (49-62) in the presence and absence of enzyme. The appearance of peak broadening can be correlated with particular peptide protons that come in direct contact with the enzyme surface. Decent amide proton broadening was seen for both PAR1P (49-62) and PAR1G (49-62) in the presence of ProT (Figure 37B and 37E). PAR1 residues which had effective line broadening included D50, K51, E53, F55, D58, and E60. To rule out that line broadening was only due to the increased relaxation effects of higher molecular weight ProT (72 kDa), we also examined whether line broadening occurred with lower molecular weight thrombin (37 kDa). The further line broadening seen with PPACK-IIa supported the proposal for additional contact with the mature exosite (Figure 37C and 37F). Careful examination of the different line broadening effects led to the conclusion that PAR1P (49-62) showed better line broadening and thus enhanced binding than PAR1G (49-62). Later, individual residues with substantial line broadening (D50, K51, E53, F55, D58, and E60) were selected for ^{15}N labeling.

2D trNOESY revealed that the PAR1P (49-62) is mostly in an extended conformation when bound to ProT (Figure 38A) as evident from having only nearest neighbor NOEs. Another feature that was identified was the orientation of the PAR1 Xaa-Pro bond. NOEs resulting from through space interactions between $\text{E53C}_{\alpha\text{H}}$ and $\text{P54C}_{\delta\text{H}}$ confirmed that the Xaa-Pro adopts a *trans* conformation when PAR1P (49-62) is bound to ProT (Figure 38A and 38B).

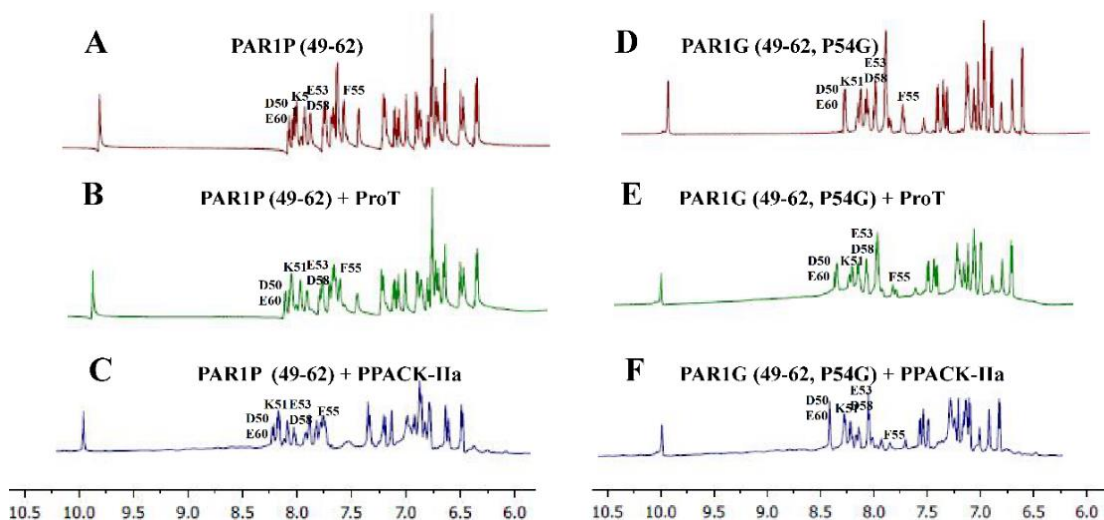


Figure 37: Proton line broadening spectra for PARIP and PARIG peptides in the presence of prothrombin and PPACK-thrombin. All NMR samples were in 25 mM H_3PO_4 , 150 mM NaCl, 0.2 mM EDTA and 10 % D_2O (pH 6.5). A) 1D ^1H -NMR spectrum of 1 mM PAR1 (49- 62) peptide in solution B) 1D ^1H -NMR spectrum of 780 μM PAR1 (49-62) in the presence of 59 μM ProT C) 1D ^1H NMR spectrum of 700 μM PAR1 (49-62) in the presence of 97 μM PPACK-IIa D) 1D NMR spectrum of 1 mM PAR1G (49- 62) in solution E) 1D NMR spectrum of 830 μM PAR1G (49-62) in the presence of 83 μM ProT. F) 1D NMR spectrum of 870 μM PAR1G (49-62) in the presence of 87 μM PPACK-IIa.

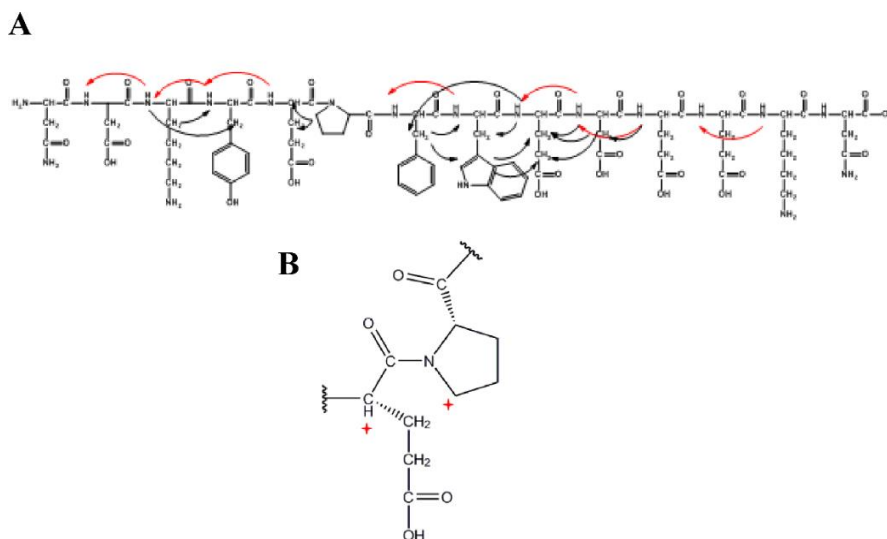


Figure 38. A) selected NOE cross peaks of PARIP (49-62) when bound to ProT. B) Red pointers indicate NOE between E53 $\text{C}_{\alpha\text{H}}$ and P54 $\text{C}_{\delta\text{H}}$.

^{15}N -HSQC Titration Studies with PAR1_{FD} (49-62) Labeled at D50 and F55

To further evaluate differences in the binding affinities of ABE I directed ligands and to decipher exosite maturation, we selected PARIP (49-62) as our next test PAR

candidate. Results could later be compared with our earlier PAR3 NMR titration studies. 2D TOCSY and 2D tr-NOESY had been performed on PAR1P to obtain chemical shift values for the amide protons of the amino acid residues. Identifying aromatics like W and F were however challenging as their side chain protons overlapped in the fingerprint region. To increase the accuracy of peak assignments, ^1H - ^{13}C 2D HSQC was employed (**Appendix 9**). Once all proton chemical shifts were successfully assigned, the best residues for ^{15}N labeling were chosen and correlated with the X-ray structures.

For the first HSQC titration studies, PAR1 D50 and F55 were selected for ^{15}N labeling. Figure 36 shows that PAR1 D50 is in ionic interaction with R73 of thrombin and F55 is surrounded by the hydrophobic cluster (F34, L65 and I82) of ABE I.^{49,85} Thrombin ABE I is mainly composed of the 30 and 70 loops which are responsible for electrostatic and hydrophobic interactions with physiological ligands. HSQC titrations started with ProT: PAR1P_{FD} ratios of 2.3:1, where D50 and F55 were ^{15}N labeled. Unfortunately, the [^{15}N]-D50 amide proton was not seen throughout the NMR titration series due to fast exchange with the solvent. This amide proton could be detected at pH 3.0, a more acidic environment than what ProT/IIa encounters physiologically. By contrast, [^{15}N]-F55 could be detected during the full NMR titration series at pH 6.5. 1D HSQC titration revealed that the [^{15}N]-F55 peak exhibited line broadening at higher ProT: PAR1P_{FD} ratios and sharper peaks started to develop as the enzyme was diluted with a constant amount of ^{15}N - labeled PAR1P_{FD} (Figure 39A).

2D ^1H - ^{15}N - HSQC cross peaks could be followed for all the titration points of [^{15}N]-F55, consistent with this residue being in fast exchange with ProT (Figure 39B). Moreover, there was a clear change in F55 chemical shift position (and thus chemical environment)

resulting in a binding affinity (K_D) of $99 \pm 39.4 \mu\text{M}$ and a maximal chemical shift difference ($\Delta\omega_{\text{max}}$) of $0.47 \pm 0.09 \text{ ppm}$ (Figure 39C and Table 4). Upon exosite maturation, $[^{15}\text{N}]$ -F55 showed extensive line broadening even at the very lower PPACK-IIa: PAR1P_{FD} (0.1:1) ratios thus hindering the ability to calculate a K_D (data not shown). Such line broadening was due to extensive contacts with the mature ABE I surface of thrombin.

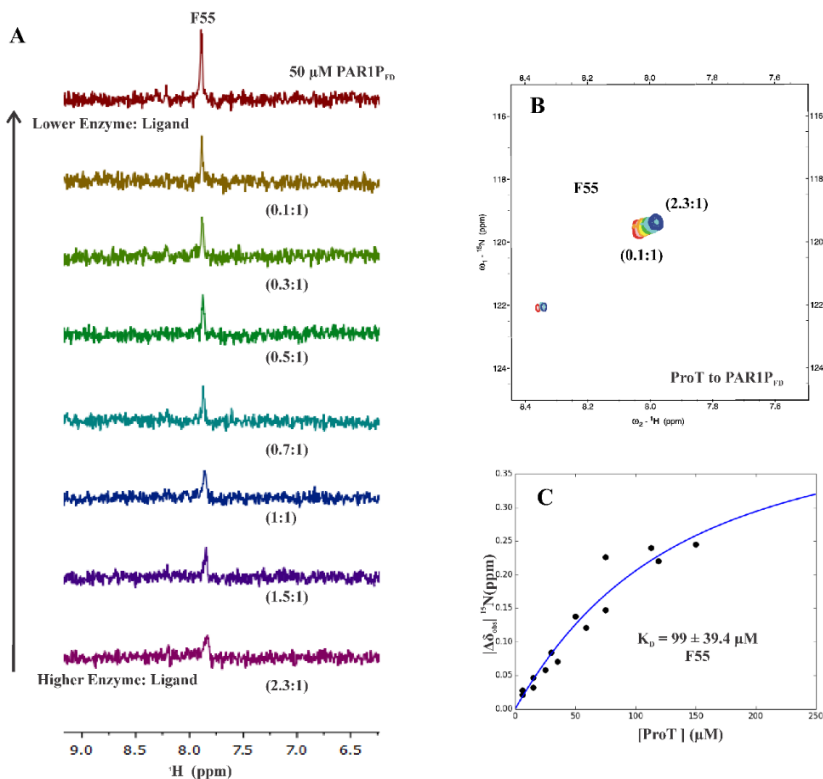


Figure 39: 1D, 2D ^1H - ^{15}N HSQC NMR titrations, and K_D value of PAR1P_{FD} (49-62) in the presence of ProT. All NMR samples were in 25 mM H_3PO_4 , 150 mM NaCl, 0.2 mM EDTA, and 10 % D_2O (pH 6.5). A) 1D HSQC of PAR1P_{FD} binding studies with ProT, starting complexes included 50 μM PAR1P_{FD} (49-62), $[^{15}\text{N}]$ -D50, $[^{15}\text{N}]$ - F55 in at least 115 μM ProT. The serial dilutions resulted in ProT: PAR1P_{FD} ratios that spanned from 2:1 to 0.1:1. B) 2D ^1H - ^{15}N HSQC PAR1P_{FD} binding studies with ProT, starting complexes included 50 μM PAR1P_{FD} (49-62), $[^{15}\text{N}]$ -D50, $[^{15}\text{N}]$ - F55 in at least 115 μM ProT. The serial dilutions resulted in ProT: PAR1P_{FD} ratios that spanned from 2:1 to 0.1. Representative data sets are shown. Colors for the HSQC crosspeaks span from blue (highest protein:peptide ratio) to red (free peptide). C) Determination of the binding Affinity (K_D) for ^{15}N -labeled F55 of PAR1P_{FD} interacting with prothrombin. ProT and PAR1P $[^{15}\text{N}]$ - F55 led to a K_D of $99 \pm 39.4 \mu\text{M}$. NMR titrations were performed in duplicate. The reported K_D values were determined using in-house scripts written using Python. The term $|\Delta\delta_{\text{obs}}|$ ^{15}N ppm = $\delta^{15}\text{N}_{\text{bound}} - \delta^{15}\text{N}_{\text{free}}$ reflects the absolute difference in chemical shift between the bound and free states of the particular ^{15}N -residue. Error analysis was performed using a Monte-Carlo approach assuming a 10% error in the serially diluted protein samples.

Peptide	Residue	[ProT] (μM)	$ \Delta\omega_{\text{max}} $ (ppm)	[PPACK-IIa] (μM)	$ \Delta\omega_{\text{max}} $ (ppm)	IIa residues in contact with PAR1 (49-62)
PAR1P _{FD}	F55	99 ± 39.4	0.47 ± 0.09	Too tight for NMR	NA	F34, L65, I82
PAR1P _{FD}	D50	Solvent exchange	NA	Solvent exchange	NA	R73
PAR1G _{FD}	F55	Too weak for NMR	NA	251	NA	F34, L65, I82
PAR1G _{FD}	D50	Solvent exchange	NA	Solvent exchange	NA	R73
PAR1G _{ED}	E53	Too weak for NMR	NA	Too weak for NMR	NA	T74, Y76, and R75
PAR1G _{ED}	D58	Too weak for NMR	NA	36 ± 6.6	0.41 ± 0.05	Not seen in X-ray (might see R77a)
PAR1G _{KE}	K51	Too weak for NMR	NA	167 ± 49	0.09 ± 0.02	In vicinity of R73
PAR1G _{KE}	E60	Too weak for NMR	NA	280	NA	Not seen in X-ray (might see I82, K110)

Table 4: K_D and $|\Delta\omega_{\text{max}}|$ Values Determined from 2D HSQC Titrations for ^{15}N Labeled PAR1P_{FD}, PAR1G_{FD} and PAR3G_{EL} bound to prothrombin and PPACK-IIa.

^{15}N -HSQC Titration Studies with PAR1G_{FD} (49-62) Labeled at D50 and F55

The strategy to evaluate individual K_D values was hindered due to extensive line broadening of PAR1P_{FD} [^{15}N]-F55 when bound to PPACK-IIa. Hence, a weaker binding version of PAR1 (49-62) [P54G] was used to probe the availability of (pro)- ABE I for binding. A similar P to G substitution had been utilized in our previous PAR3 peptide project. The titration was initiated with a 3:1 (ProT: PAR1G_{FD}) protein: ligand ratio where D50 and F55 were ^{15}N labeled. Both 1D and ^1H - ^{15}N 2D HSQC titrations revealed that the [^{15}N]-F55 peak showed no change in chemical shift position with ProT (Figure 40A and 40B) indicating that the new PAR1G_{FD} [^{15}N]-F55 sequence exhibited less effective interactions with the hydrophobic cluster (F34, L65, I82) of zymogen ProT. The replacement of PAR1 proline to glycine (P54G) had caused a definite weakening of binding

affinity. With such a change, the mature thrombin ABE I environment might be able to be probed.

A

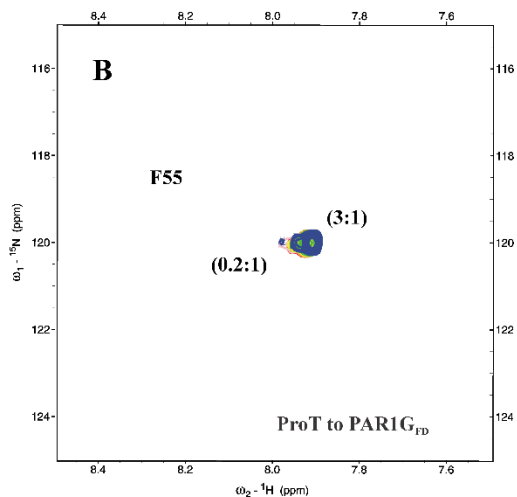
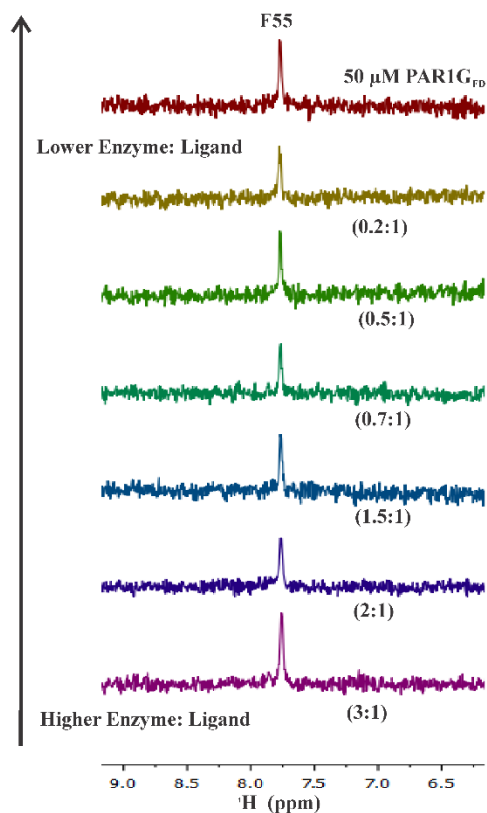


Figure 40: 1D and 2D ^1H - ^{15}N HSQC NMR titrations of PAR1G_{FD} (49-62) in the presence of ProT. All NMR samples were in 25 mM H_3PO_4 , 150 mM NaCl, 0.2 mM EDTA, and 10 % D_2O (pH 6.5). A) 1D HSQC of PAR1G_{FD} binding studies with ProT, starting complexes included 50 μM PAR1G_{FD} (49-62, [^{15}N]-D50, [^{15}N]- F55) in at least 150 μM ProT. The serial dilutions resulted in ProT: PAR1G_{FD} ratios that spanned from 3:1 to 0.1:1. B) 2D ^1H - ^{15}N HSQC PAR1G_{FD} binding studies with ProT, starting complexes included 50 μM PAR1G_{FD} (49-62, [^{15}N]-D50, [^{15}N]- F55) in at least 150 μM ProT. The serial dilutions resulted in ProT: PAR1G_{FD} ratios that spanned from 3:1 to 0.1. NMR titrations were performed in duplicate.

Upon exosite maturation, [^{15}N]-F55 did indeed undergo a substantial increase in chemical shift during the titration series. The presence of a new binding environment around the hydrophobic cluster (F34, L65, I82) of thrombin was thus detected upon ABE I maturation (Figure 41A and 41B). Also, the chemical shift changes for [^{15}N]-F55 of

PAR1G_{FD} titrations proceeded in the same direction as [¹⁵N]-F55 of PAR1P_{FD} across the panels. This common pattern is consistent with the idea that both versions of PAR1 are encountering the same environment when bound to PPACK-IIa. The estimated binding affinity (K_D) of PAR1G_{FD} [¹⁵N]-F55 for PPACK-IIa was 251 μM (Figure 41C, Table 4). The PAR1 P54G sequence was next used to explore binding affinities of other key PAR1 (49-62) residues in the presence of immature prothrombin versus mature thrombin.

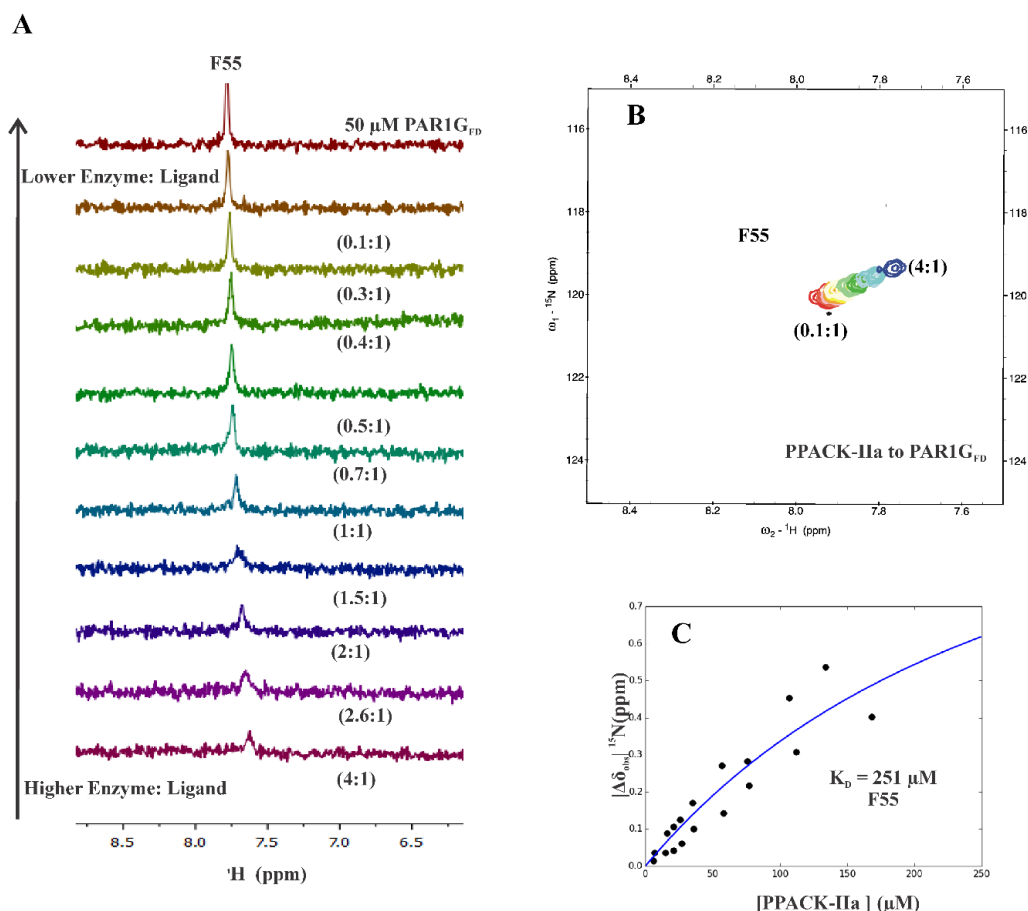


Figure 41: 1D, 2D ¹H-¹⁵N HSQC NMR titrations, and K_D value of PAR1G_{FD} (49-62) in the presence of PPACK-IIa. All NMR samples were in 25 mM H₃PO₄, 150 mM NaCl, 0.2 mM EDTA, and 10 % D₂O (pH 6.5). A) 1D HSQC of PAR1G_{FD} binding studies with PPACK-IIa, starting complexes included 50 μM PAR1G_{FD} (49-62), [¹⁵N]-D50, [¹⁵N]- F55) in at least 150 μM PPACK-IIa. The serial dilutions resulted in PPACK: PAR1G_{FD} ratios that spanned from 3:1 to 0.1:1. B) 2D ¹H-¹⁵N HSQC PAR1G_{FD} binding studies with PPACK-IIa, starting complexes included 50 μM PAR1G_{FD} (49-62), [¹⁵N]-D50, [¹⁵N]- F55) in at least 150 μM PPACK-IIa. The serial dilutions resulted in PPACK-IIa: PAR1P_{FD} ratios that spanned from 3:1 to 0.1:1. C) Determination of the binding Affinity (K_D) for ¹⁵N-labeled F55 of PAR1G_{FD} interacting with prothrombin. PPACK and PAR1G [¹⁵N]- F55 led to a K_D of 251 μM. NMR titrations were performed in duplicate.

¹⁵N-HSQC Titration Studies with PAR1_{GED} (49-62) Labeled at E53 and D58

The success in evaluating the binding affinity of a hydrophobic residue ([¹⁵N]-F55) led to interest in exploring anionic residues which might be involved in effective interactions with ABE I of thrombin. Gandhi *et al.*, had previously shown that PAR1 E53 is involved in hydrogen bonding with thrombin T74 and Y76.^{49,85} The acidic PAR1 E53 residue is also in close vicinity of the thrombin ABE I residue R75. Interactions involving T74, R75, and Y76 supported our idea of ¹⁵N labeling E53 to probe the 70 loop of (pro)-ABE I. The published X-ray crystal structures of PAR1 bound to thrombin were unable to detect the electron density for the acidic C-terminal tail of PAR1 (⁵⁸DEEKN⁶²).⁸⁴ Solution NMR would provide an alternative strategy to probe this region of PAR1 by first labeling PAR1 D58.

1D line broadening studies revealed that PAR1 E53 and D58 both showed some proton line broadening with ProT. By contrast, both [¹⁵N]-E53 and [¹⁵N]-D58 did not exhibit any chemical shift movement during the full 1D and 2D ¹⁵N HSQC titration series with ProT. These results indicated minor interaction with pro-ABE I of ProT but no real changes in chemical environment relative to that of free peptide. After ABE I maturation, PAR1_{GED} [¹⁵N]-E53 still did not exhibit any change in chemical shift position with PPACK-IIa (Figure 42A,42B, 43A and 43B, Table 4). By contrast, the 1D ¹⁵N HSQC spectra of the PAR1_{GED} [¹⁵N]-D58 peak started to show line broadening and an upfield chemical shift already at higher PPACK-IIa: ligand ratios. This effect was confirmed with 2D HSQC spectra, where changes in chemical shift position for PAR1_{GED} [¹⁵N]-D58 were clearly observed for the 4:1 to 1:1 PPACK-IIa to PAR1_{GED} ratios. This result provided valuable information about a flexible C-terminal region whose electron density could not

be defined by X-ray crystallography. The NMR titration series revealed that PAR1_{ED} [15N]-D58 is likely in fast exchange with PPACK-IIa with K_D of $38 \pm 6.6 \mu\text{M}$ and a maximal chemical shift difference ($\Delta\omega_{\text{max}}$) of $0.41 \pm 0.05 \text{ ppm}$ (Figures 42A, 42B, 43B and 43C, Table 4).

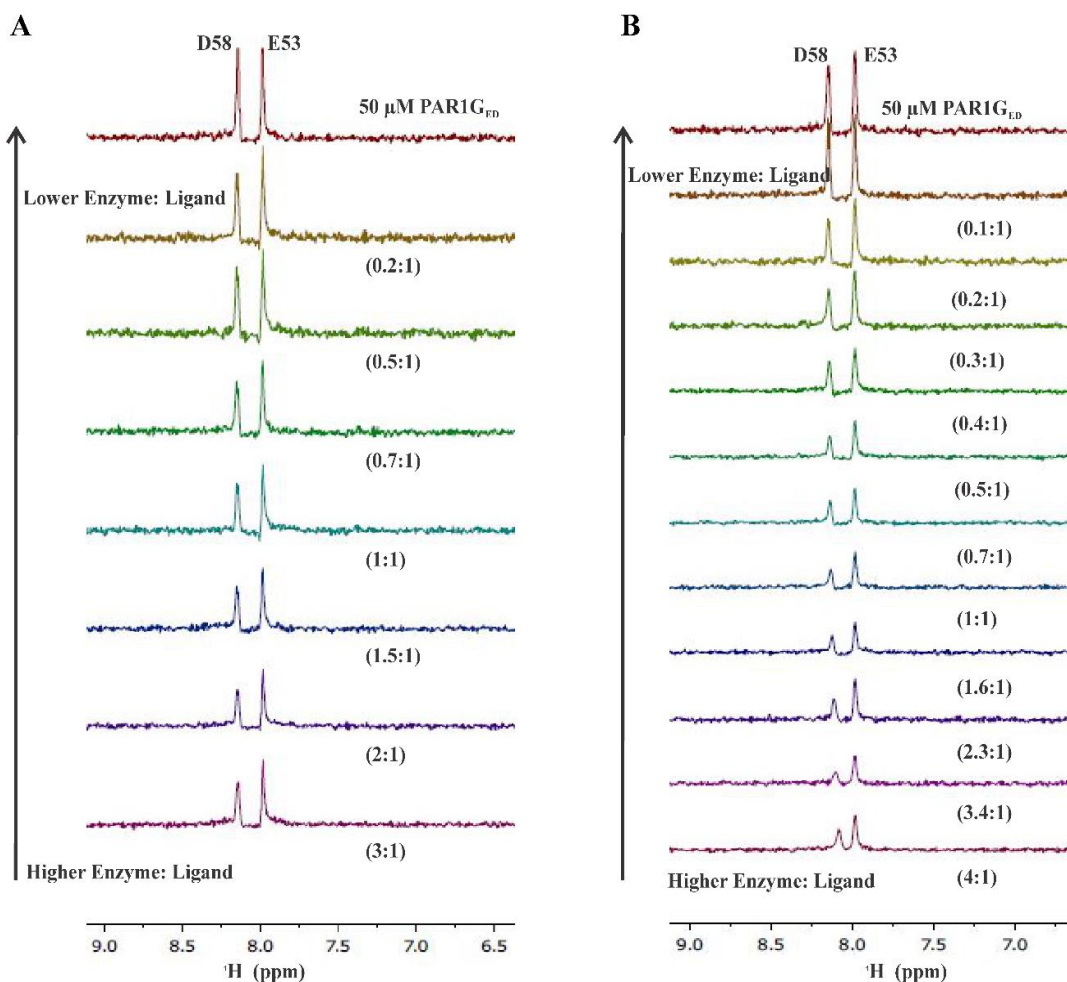


Figure 42: 1D HSQC NMR titrations of PAR1_{ED} (49-62) in the presence of ProT and PPACK-IIa. All NMR samples were in 25 mM H₃PO₄, 150 mM NaCl, 0.2 mM EDTA, and 10 % D₂O (pH 6.5). A) 1D HSQC of PAR1_{ED} binding studies with ProT, starting complexes included 50 μM PAR1_{ED} (49-62, [15N]-E53, [15N]- D58) in at least 150μM ProT. The serial dilutions resulted in ProT: PAR1_{ED} ratios that spanned from 3:1 to 0.2:1. B) 1D HSQC of PAR1_{ED} binding studies with PPACK-IIa, starting complexes included 50 μM PAR1_{ED} (49-62, [15N]-E53, [15N]- D58) in at least 200 μM PPACK-IIa. The serial dilutions resulted in PPACK: PAR1_{ED} ratios that spanned from 4:1 to 0.1:1. NMR titrations were performed in duplicate.

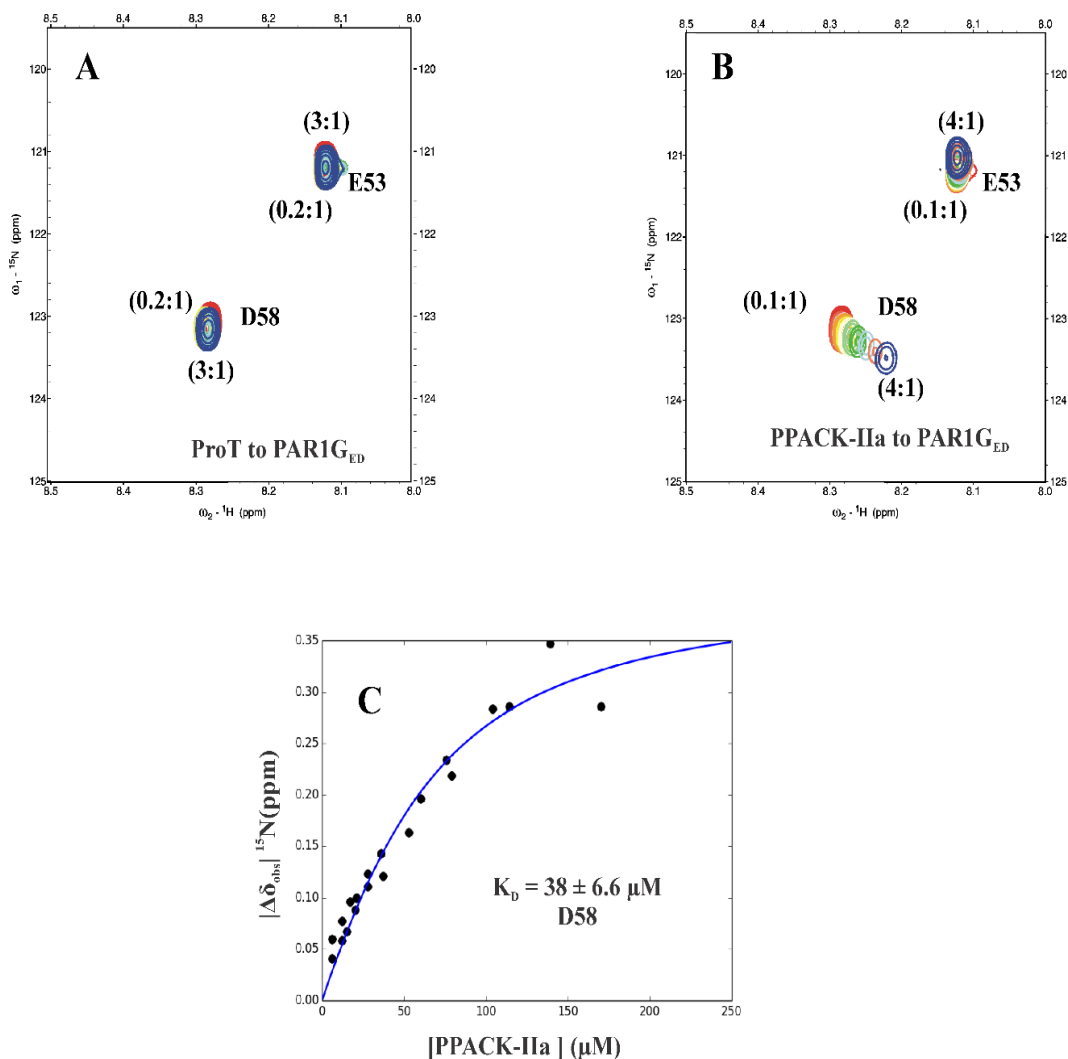


Figure 43: 2D ^1H - ^{15}N HSQC NMR titrations of PAR1_{GED} (49-62) in the presence of ProT and PPACK-IIa. All NMR samples were in 25 mM H_3PO_4 , 150 mM NaCl, 0.2 mM EDTA, and 10 % D_2O (pH 6.5). A) ^1H - ^{15}N 2D HSQC of PAR1_{GED} binding studies with ProT, starting complexes included 50 μM PAR1_{GED} (49-62), [^{15}N]-E53, [^{15}N]-D58 in at least 150 μM ProT. The serial dilutions resulted in ProT: PAR1_{GED} ratios that spanned from 3:1 to 0.2:1. B) ^1H - ^{15}N 2D HSQC of PAR1_{GED} binding studies with PPACK-IIa, starting complexes included 50 μM PAR1_{GED} (49-62), [^{15}N]-E53, [^{15}N]-D58 in at least 200 μM PPACK-IIa. The serial dilutions resulted in PPACK: PAR1_{GED} ratios that spanned from 4:1 to 0.1:1. C) Determination of the binding Affinity (K_D) for ^{15}N -labeled D58 of PAR1_{GED} interacting with PPACK-IIa led to a K_D of $38 \pm 6.6 \mu\text{M}$. NMR titrations were performed in duplicate.

^{15}N -HSQC Titration Studies with PAR1_{GKE} (49-62) Labeled at K51 and E60

The NMR mapping studies moved on to explore the binding affinity of a basic residue and a second acidic residue within the N-terminal region of PAR1 (49-62). A careful review of the PAR1 (49-62) – Ila X-ray structure (Figure 35) showed that K51 is

in close vicinity of IIa ABE I residues R73 and T74. A second acidic residue from the C-terminal segment of PAR1G (49-62) was also chosen for analysis. Like D58, the E60 residue was missing from the thrombin- PAR1 X-ray crystal structure.⁸⁵ Both [¹⁵N]-K51 and [¹⁵N]- E60 did not show any change in chemical shift position in the presence of ProT indicating little if any interaction with pro-ABE I (Figure 44A and 45A). However upon exosite maturation, the 2D HSQC studies revealed that PAR1 residue K51 showed modest changes in chemical shift in the hydrogen dimension with a K_D of $167 \pm 49.2 \mu\text{M}$ ($\Delta\omega_{\text{max}} = 0.09 \pm 0.02$) and for PAR1 E60 a K_D of $280 \mu\text{M}$ in the nitrogen dimension (Figure 44B, 45B and 46A and 46B, Table 4). Overall, both [¹⁵N]-K51 and [¹⁵N]- E60 had weak interactions with both ProT and PPACK-IIa.

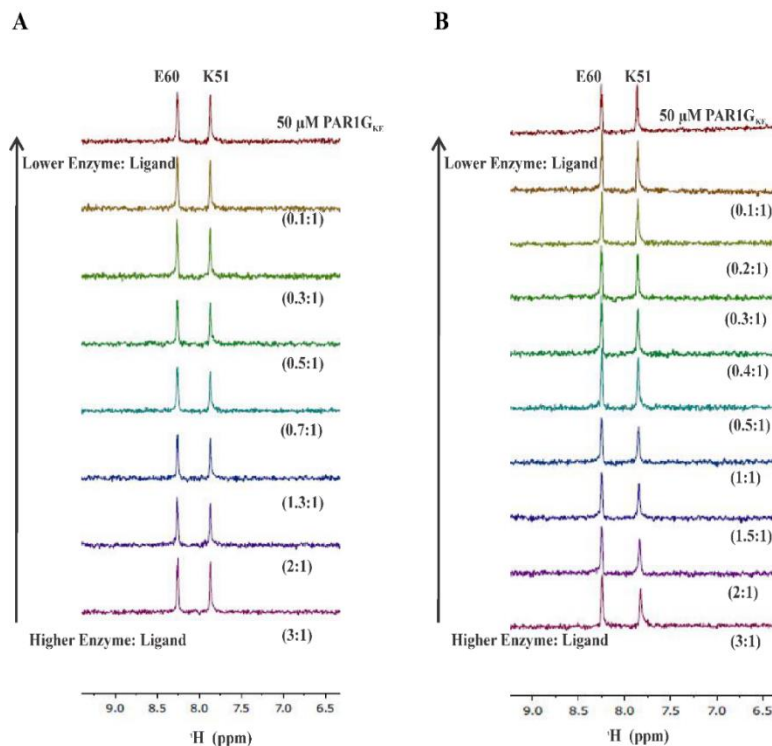


Figure 44: 1D HSQC NMR titrations of PAR1G_{KE} (49-62) in the presence of ProT and PPACK-IIa. All NMR samples were in 25 mM H₃PO₄, 150 mM NaCl, 0.2 mM EDTA, and 10 % D₂O (pH 6.5). A) 1D HSQC of PAR1G_{KE} binding studies with ProT, starting complexes included 50 μM PAR1G_{KE} (49-62), [¹⁵N]-K51, [¹⁵N]- E60) in at least 150 μM ProT. The serial dilutions resulted in ProT: PAR1G_{KE} ratios that spanned from 3:1 to 0.1:1. B) 1D HSQC of PAR1G_{KE} binding studies with PPACK-IIa, starting complexes included 50 μM PAR1G_{KE} (49-62, [¹⁵N]-K51, [¹⁵N]- E60) in at least 200 μM PPACK-IIa. The serial dilutions resulted in PPACK: PAR1G_{ED} ratios that spanned from 3:1 to 0.1:1. NMR titrations were performed in duplicate.

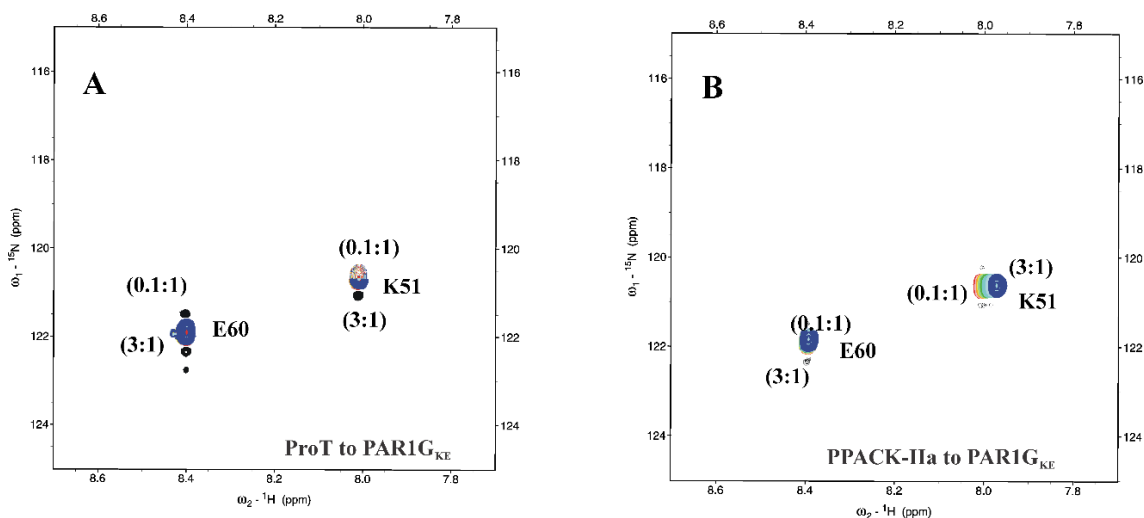


Figure 45: 2D ^1H - ^{15}N HSQC NMR titrations of PAR1G_{KE} (49-62) in the presence of ProT and PPACK-IIa. All NMR samples were in 25 mM H_3PO_4 , 150 mM NaCl, 0.2 mM EDTA, and 10 % D_2O (pH 6.5). A) 2D ^1H - ^{15}N HSQC of PAR1G_{KE} binding studies with ProT, starting complexes included 50 μM PAR1G_{ED} (49-62, [^{15}N]-K51, [^{15}N]- E60) in at least 150 μM ProT. The serial dilutions resulted in ProT: PAR1G_{KE} ratios that spanned from 3:1 to 0.1:1. B) 2D HSQC of PAR1G_{KE} binding studies with PPACK-IIa, starting complexes included 50 μM PAR1G_{KE} (49-62, [^{15}N]-K51, [^{15}N]- E60) in at least 150 μM PPACK-IIa. The serial dilutions resulted in PPACK: PAR1G_{KE} ratios that spanned from 3:1 to 0.1:1. NMR titrations were performed in duplicate.

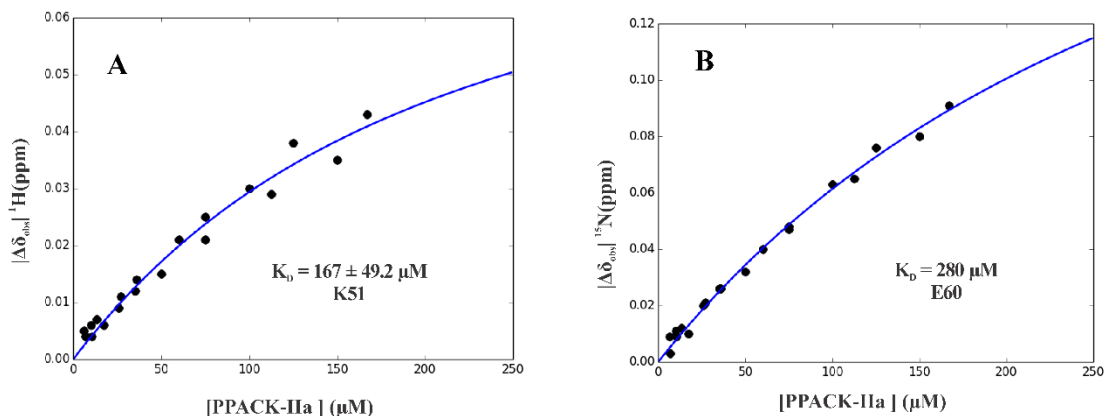


Figure 46: Determination of the binding Affinity (K_D) for ^{15}N -labeled K51 and E60 of PAR1G_{KE} interacting with PPACK-IIa led to a K_D of $167 \pm 49.2 \mu\text{M}$ and $280 \mu\text{M}$ respectively. NMR titrations were performed in duplicate. The reported K_D values were determined using in-house scripts written using Python. The term and $\Delta\delta_{\text{obs}} |^1\text{H}$ ppm = $\delta^1\text{H}_{\text{bound}} - \delta^1\text{H}_{\text{free}}$ reflects the absolute difference in chemical shift between the bound and free states of the particular ^1H -residue. NMR titrations were performed in duplicate.

1D and 2D ^1H - ^{15}N HSQC NMR Titration for Long-Range Communication Studies

Previously published HDX-MS experiments from our lab demonstrated that when a triply phosphorylated GpIb α (269-282) peptide bound to thrombin ABE II, there was a long-range influence over to the ABE I region.^{60,78} To further characterize this dual ligand binding system, NMR titration studies were carried out with complexes consisting of unlabeled GpIb α (269-282), PPACK-IIa, and two distinct ^{15}N -labeled PAR based peptides. PAR1G_{ED} and PAR3G_{EL} were selected for this study. Our previous HSQC titrations had shown that both of these PAR peptides could document information about the maturation of the 30 and 70 loops of thrombin.

The following experimental strategies were carried out to monitor dual ligand allostery. Prior to the titration, a saturated amount of triply phosphorylated GpIb α (269-282) was added to PPACK-IIa followed by the desired ^{15}N -labeled PAR peptide. Both GpIb α and PPACK-IIa were then serially diluted with constant amounts of ^{15}N -labeled peptide. The same ratios of PPACK IIa - PAR1 and PPACK IIa-PAR3 were maintained as in the single ligand experiments described earlier. Interestingly, titrations with PAR1G_{ED} revealed that E53 went from an affinity for thrombin ABE I that was too weak to detect by NMR to one with an improved K_D of $125 \pm 36 \mu\text{M}$ ($\Delta\omega_{\text{max}} = 0.32 \pm 0.05$) in the presence of GpIb α peptide (Figure 42B, 43B, 47A, 47B, 48A, Table 4 and Table 5). By contrast, PAR1 D58 did not respond much to the presence of GpIb α binding at ABE II. The K_D for D58 went from $36 \pm 6.6 \mu\text{M}$ ($\Delta\omega_{\text{max}} = 0.41 \pm 0.05$) to $75 \pm 14.9 \mu\text{M}$ ($\Delta\omega_{\text{max}} = 0.52 \pm 0.05$) (Figure 42B, 43B, 47B and 48B, Table 4 and Table 5).

The PAR3G_{EL} peptide displayed a more dramatic response to GpIb α binding at thrombin ABE II than PAR1G_{ED}. Prior studies had shown that L52 bound to ABE I with a

K_D of 124 μM and E48 had a K_D of $>200 \mu\text{M}$. With GpIb α binding to ABE II, the PAR3 peaks broadened so much there were insufficient data points for calculating the K_D values. PAR3G_{EL} had entered into the tighter binding intermediate exchange regime. From these studies, NMR could document long range influence from thrombin ABE II over to ABE I. (Figure 49A and 49B, Table 5 and Table 6).

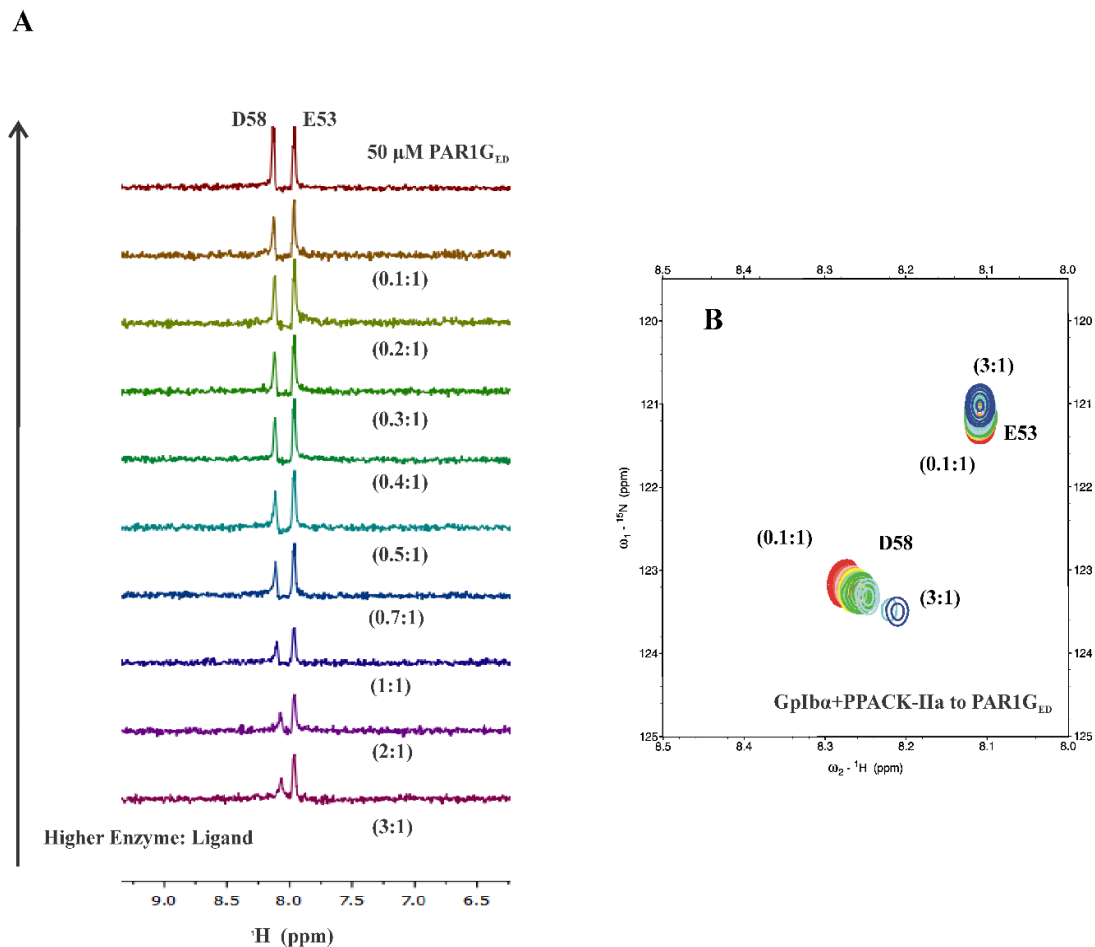


Figure 47: 1D and 2D ^1H - ^{15}N HSQC NMR titrations of PAR1G_{ED} (49-62) in the presence of saturated amounts of GpIb α (269-282) and PPACK-IIa. All NMR samples were in 25 mM H_3PO_4 , 150 mM NaCl, 0.2 mM EDTA, and 10 % D_2O (pH 6.5). A) 1D HSQC of PAR1G_{ED} binding studies with PPACK-IIa, starting complexes included 50 μM PAR1G_{ED} (49-62, [^{15}N]-E53, [^{15}N]-D58) in at least 150 μM PPACK-IIa. The serial dilutions resulted in PPACK: PAR1G_{ED} ratios that spanned from 3:1 to 0.1:1. B) 2D ^1H - ^{15}N HSQC PAR1G_{ED} binding studies with PPACK-IIa, starting complexes included 50 μM PAR1G_{ED} (49-62, [^{15}N]-E53, [^{15}N]-D58) in at least 150 μM PPACK-IIa. The serial dilutions resulted in PPACK-IIa: PAR1G_{ED} ratios that spanned from 3:1 to 0.1. (free peptide).

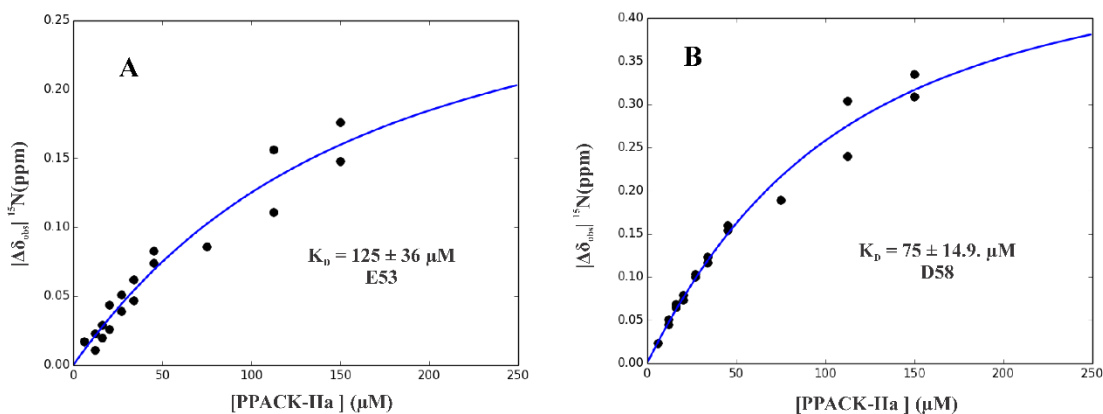


Figure 48: Determination of the binding Affinity (K_D) for ^{15}N -labeled E53 and K51 of PAR1G_{ED} interacting with GpIba (269-282) + PPACK-IIa led to a K_D of $125 \pm 36 \mu\text{M}$ and K_D of $75 \pm 14.9 \mu\text{M}$ respectively. NMR titrations were performed in duplicate. The reported K_D values were determined using in-house scripts written using Python.

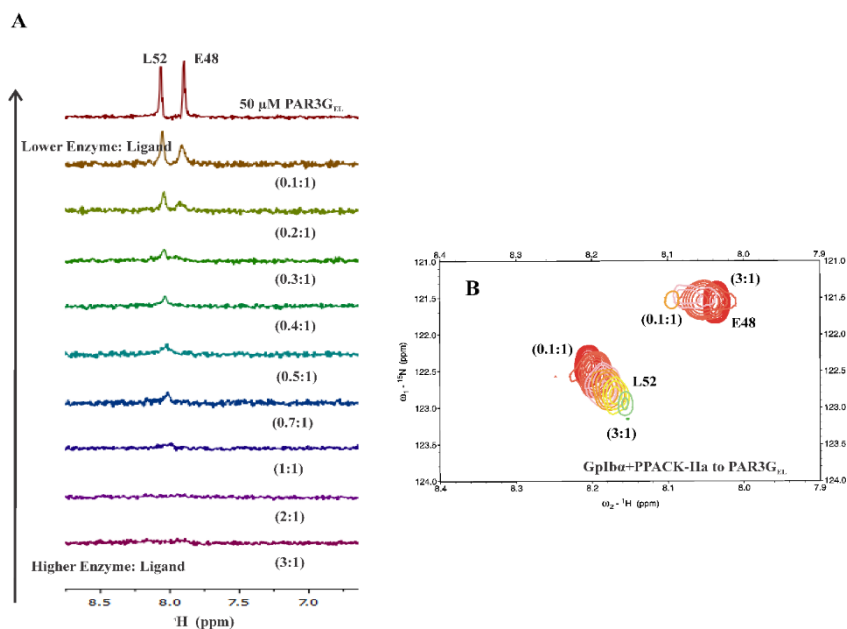


Figure 49: 1D, and 2D ^1H - ^{15}N HSQC NMR titrations of PAR3G_{EL} (44-56) in the presence of saturated amounts of GpIba (269-282) and PPACK-IIa. All NMR samples were in 25 mM H_3PO_4 , 150 mM NaCl, 0.2 mM EDTA, and 10 % D_2O (pH 6.5). A) 1D HSQC of PAR3G_{EL} binding studies with PPACK-IIa, starting complexes included 50 μM PAR3G_{EL} (44-56, ^{15}N -E48, ^{15}N -L52) in at least 150 μM PPACK-IIa. The serial dilutions resulted in PPACK: PAR3G_{EL} ratios that spanned from 3:1 to 0.1:1. B) 2D ^1H - ^{15}N HSQC PAR3G_{EL} binding studies with PPACK-IIa, starting complexes included 50 μM PAR1G_{ED} (49-62, ^{15}N -E48, ^{15}N -L52) in at least 150 μM PPACK-IIa. The serial dilutions resulted in PPACK-IIa: PAR3G_{EL} ratios that spanned from 3:1 to 0.1. (free peptide).

Peptide	Residue	[PPACK-IIa] (μM)	$ \Delta\omega_{\text{max}} $ (ppm)	IIa residues in contact with PAR1 (49-62)
PAR1G _{ED}	E53	Too weak for NMR	NA	In vicinity of T74, R75, and Y76
PAR1G _{ED} +GpIb α	E53	126 \pm 36	0.32 \pm 0.05	In vicinity of T74, R75, and Y76
PAR1G _{ED}	D58	36 \pm 6.6	0.41 \pm 0.05	Not seen in X-ray (might see R77a)
PAR1G _{ED} +GpIb α	D58	75 \pm 15	0.52 \pm 0.05	Not seen in X-ray (might see R77a)

Table 5: K_D and $|\Delta\omega_{\text{max}}|$ Values Determined from 2D HSQC Titrations for ^{15}N Labeled PAR1G_{ED} when bound to GpIb α +PPACK-IIa and PPACK-IIa

Peptide	Residue	[PPACK-IIa] (μM) ¹⁵⁴	$ \Delta\omega_{\text{max}} $ (ppm) ¹⁵⁴	IIa residues in contact with PAR3 (44-56) ⁵⁰
PAR3G _{EL} ¹⁵⁴	L52	47 \pm 6	1.84 \pm 0.08	F34, L65, I82
PAR3G _{EL} +GpIb α	L52	Too tight for NMR	NA	F34, L65, I82
PAR3G _{EL} ¹⁵⁴	E48	Too tight for NMR	Insufficient data points	R75
PAR3G _{EL} +GpIb α	E48	Too tight for NMR	NA	R75

Table 6: K_D and $|\Delta\omega_{\text{max}}|$ Values Determined from 2D HSQC Titrations for ^{15}N Labeled PAR3G_{EL} when bound to GpIb α +PPACK-IIa and PPACK-IIa.

DISCUSSION

Thrombin is a multifunctional serine protease that is originally derived from the zymogen Prothrombin. Besides the thrombin active site region, ligands and substrates also can bind to the regulatory anion binding exosites ABE I and II. PAR1 and PAR3 both have segments that target ABE I thereby providing a second anchoring point on to the thrombin surface. PAR1 and PAR3 can use their ABE I binding capabilities to help promote thrombin dependent cleavage of PAR4.^{86,166} Once activated, PARs help in platelet activation, platelet aggregation, and triggering inflammatory processes.

An important goal of the current project was to characterize the diversity of ligand binding interactions that exists as PAR residues bind to zymogen ProT versus mature thrombin. New studies with PAR1 peptides were carried out and later compared with our previously published PAR3 titrations when bound to ProT and PPACK-IIa.¹⁵⁴ Because GpIb α can function as a cofactor for PAR1 hydrolysis by thrombin, we also wanted to explore the conformational features of the ternary GpIb α -IIa-PAR1 complex. While saturated amounts of GpIb α peptide interacted at ABE II, binding affinities of ABEI-directed PAR1 (49-62) and later PAR3 (46-52) were probed. All our experiments were carried out with active site inhibited thrombin to eliminate autolysis from occurring during the long NMR titration experiments. Prior NMR relaxation studies proved that communication can still exist between the active site and ABE I when the active site is inhibited with PPACK.¹³³⁻¹³⁵ For all NMR experiments, pH was maintained at 6.5 to avoid extensive amide proton exchange with solvent.

1D ¹H line broadening studies revealed that PAR1P (49-62) and PAR1G (49-62) showed moderate line broadening with ProT, and the line broadening increased upon formation of mature thrombin (Figure 37A-F). Weaker line broadening was observed for PAR1G (49-62), containing a P54G substitution, thus suggesting this modified PAR1 sequence would work, if needed, as a lower affinity version of PAR1 (49-62). A similar strategy had been employed for our previous PAR3G project.¹⁵⁴

PAR1 peptides were synthesized with ¹⁵N amide labeling at D50, K51, E53, F55, D58, and E60. The first two residues examined included F55 and D50. The ¹⁵N-D50 of PAR1P (49-62) forms an ionic pair with thrombin R73, an important residue of the 70 loop in ABE I. PAR1 F55 is involved in hydrophobic interactions with IIa F34, L65, and

I82^{49,85}. Unfortunately, the [¹⁵N]-D50 amide proton was in fast exchange with the 10% D₂O found in the solvent and was never visible during the course of the NMR titration series at pH 6.5. More success occurred with the PAR1P F55 residue. NMR titrations revealed that [¹⁵N]-F55 was in fast exchange with the ProT protein surface and had a binding affinity of $99 \pm 39.4 \mu\text{M}$. These results indicated that pro-ABE I is already available for hydrophobic interactions with the PAR1P peptide (Figure 39A-C, Table 4). The same [¹⁵N]-F55 exhibited extensive peak broadening when bound to PPACK- Iia due to increased affinity to mature ABE I.

The fact that [¹⁵N]-F55 appeared to be in intermediate exchange with PPACK-Iia was a major hindrance to the project since K_D values could not be determined. To address this issue, the P54G replacement was chosen to help generate a weaker binding PAR1 peptide defined as PAR1G. Subsequent ¹H-¹⁵N HSQC titration studies revealed that [¹⁵N]-F55 of PAR1G_{FD} now made only modest interactions with ProT (Figure 40A and 40B) and affinity was too weak to calculate a K_D . This result contrasts with the [¹⁵N]-L52 of PAR3G_{FD} which shares common hydrophobic interactions with thrombin residues (F34, L65, and I82) (**Figure 50**). The K_D for PAR3G_{EL} [¹⁵N]-L52 binding to ProT was 124 μM . See Chapter 3 for a summary of all K_D values determined from our previous work with ¹⁵N labeled PAR3 residues.¹⁵⁴

Following ProT to thrombin maturation, [¹⁵N]-F55 of PAR1G_{FD} exhibited greater interactions with PPACK- Iia and was now in fast exchange with the ABE I surface. The broad range of chemical shifts occurring during the NMR titration is consistent with PAR1G_{FD} [¹⁵N]-F55 encountering a new binding environment. The PAR1 P54G substitution had successfully weakened the affinity into an NMR manageable range and

the binding affinity K_D was 251 μ M (Figure 41A- 41C, Table 4). These studies indicate that an improved binding environment for F55 of PAR1 G_{FD} is generated when pro-ABE I on ProT is converted to ABE I on thrombin. However, this F55 does not exhibit strong stabilizing interactions with ABE I. By contrast, the L52 in PAR3 G_{EL} had a K_D of 47 μ M towards PPACK-IIa.¹⁵⁴ The interactions with thrombin hydrophobic cluster (F34, L65, and I82) are more effective in promoting binding affinity of L52 in PAR3 G_{EL} than F55 in PAR1 G_{FD} .

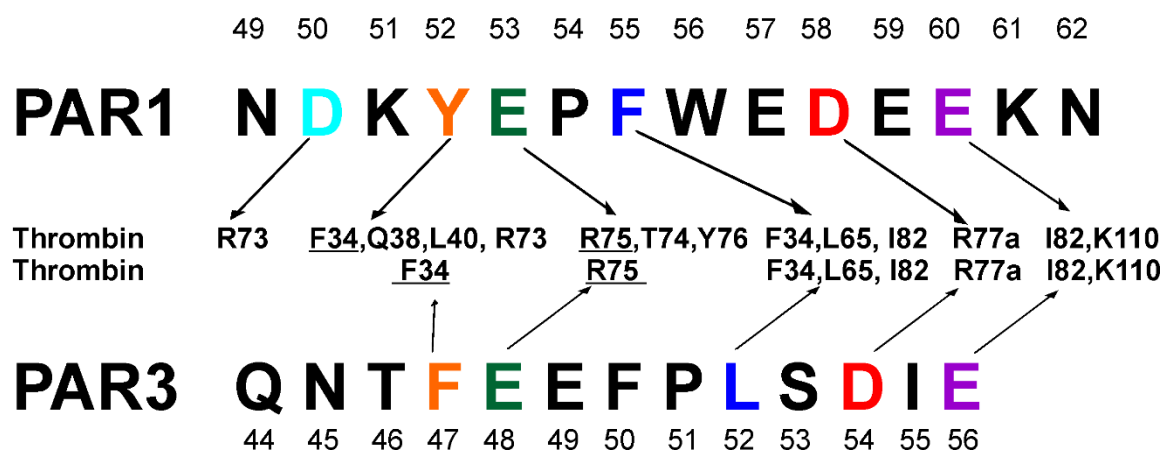


Figure 50: Interactions between thrombin ABE I (30 and 70 loop), PAR1 (49-62), and PAR3 (44-56)

As NMR is an excellent technique to probe the binding affinities of residues which are in fast exchange, we next selected E53 and D58 for 15 N labeling. PAR1 E53 is involved in hydrogen bonding with thrombin Y76 and T74 and is also in proximity to thrombin R75^{49,85}. PAR1 D58 is the first residue of a flexible acidic C-terminal tail of PAR1 (49-62) that has not been detected in X-crystal structures. The 1 H- 15 N HSQC titrations studies revealed that [15 N]-E53 of PAR1 G_{ED} showed no substantial interaction with either ProT or PPACK-IIa (Figure 42A, 42B, 43A and 43B). This E53 effect might be worsened because of replacement of the adjacent PAR1 Pro54 with Gly (P54G). As a result, E53 may be

hindered from adopting a proper orientation to promote effective interactions with (pro)-ABE I. By contrast, PAR3 E48 is known to participate in a neighboring electrostatic interaction with ABE I R75. Binding affinities went from a K_D value of $>200 \mu\text{M}$ for ProT to a too tight to calculate by NMR for thrombin (See Chapter 3).

Next, PAR1 D58 which is part of the acidic C-terminal tail segment provided valuable, new mapping information. The ^{15}N -D58 of PAR1_{GED} did not detect significant interactions with ProT. However, upon exosite maturation, ^{15}N -D58 was in fast exchange with PPACK-IIa yielding a K_D of $36 \pm 6.6 \mu\text{M}$. (Figure 42A, 42B, 43A, 43B and 43C, Table 4) Our NMR titration results thus provided the first solution-based evidence for D58 making direct contact with ABE I. Effective binding interactions occurred with the thrombin surface and a new chemical environment was encountered.

An alignment of PAR3 and PAR1 residues suggests that PAR1 D58 might be near to thrombin R77a (**Figure 50**). Consequently, thrombin R77a may help to stabilize PAR1 D58 like the strong electrostatics seen between PAR3G D54 and IIa R77a. With the PAR3 peptide, D54 exhibited a K_D of $65 \pm 12 \mu\text{M}$ with immature ProT and the affinity became too tight to calculate with mature thrombin ABE I.¹⁵⁴ Future mutations to thrombin ABE I may help confirm the key thrombin residues involved in binding of PAR1 D58.

So far, the NMR titrations studies have focused on hydrophobic and acidic residues. To check whether a basic residue of PAR1 can interact with ABE I, PAR1 K51 which is in the vicinity of thrombin R73 and T74 was selected.^{49,85} To probe another residue from the PAR1 C-terminal tail, E60 was chosen. Both ^{15}N -K51 and ^{15}N -E60 did not show significant interactions with ProT (Figures 44A and 45A). Later upon exosite maturation, the K51 amide nitrogen did not exhibit chemical shift changes but the amide hydrogen did

undergo movement in chemical shift ($K_D = 167 \pm 49.2 \mu\text{M}$, Figure 46A, Table 4). These observations highlight NMR as a sensitive technique to explore environments around different atoms such as hydrogen and nitrogen. Like PAR1 K51, the acidic C-terminal PAR1 residues [^{15}N]-E60 showed a binding interaction too weak to quantitate by NMR for ProT that later increased to a measurable K_D of $280 \mu\text{M}$ with mature PPACK-thrombin. (Figure 44A, 44B, 45A, 45B, and 46B, Table 4). With these NMR titrations results, a second residue within the X-ray invisible region could be probed. Both PAR1 acidic residues D58 and E60 could document contact with thrombin ABE I, but the affinities indicate that D58 is better anchored to ABE I than E60. In comparison to PAR1 E60, the PAR3 E56 contacts thrombin I82 and K110. Additional NMR mapping studies are needed to assess how the full C-terminal region of PAR1 interacts with thrombin ABE I. The flexibility of this PAR1 tail might have hindered the ability to promote greater binding affinity.

From our ^1H - ^{15}N -HSQC titration series, we can conclude that all ^{15}N -labeled residues of PAR1G (49-62) showed little or no interaction with ProT. However, upon exosite maturation, interactions with PPACK-IIa increased with K_D values ranging from 36 to $280 \mu\text{M}$. Interestingly, the previously published PAR3G residues were, better at binding the immature pro-ABE I region of thrombin than the PAR1 residues.¹⁵⁴ After determining individual binding affinities of labeled residues in both PAR1 (49-62) and PAR3 (44-56), we proceeded further to explore whether binding of GpIb α at ABE II would influence the affinities of ABE I ligands.

Allosteric communication between exosites and the active site is an important step in thrombin substrate specificity and catalysis.^{48,56,57,89} However, allosteric communication

between the exosites is less well explored.^{58,164} Physiologically, GpIb α bound to thrombin ABE II helps in activating the ABE I directed ligand PAR1.⁸⁰ In addition, allowing zymogen fragment F2 to bind to thrombin ABE II reduces the conversion of fibrinogen to fibrin.¹⁶⁷ The first direct evidence for direct allosteric communication between the exosites was reported by Weitz *et al* using F2 as the ABE II directed ligand and Hirudin as the ABE I directed ligand.^{58,164,168} However, Bock *et al.*, cautioned that changes in affinity could be due to competitive overlapping binding sites or additional interactions between the ligands themselves.⁵⁹

To further decipher long-range allosteric communication in thrombin, a triply phosphorylated GpIb α (269-282) was used in this project as the ABE II ligand and PAR peptides would target ABE I. With the GpIb α - PPACK-IIa complex, an increased affinity of [¹⁵N]-E53 towards ABE- I was observed. (Figure 47A, 47B, 48A, 48B, Table 4, and Table 5). The non-optimal orientation of E53 binding to ABE I may have been overcome by the introduction of GpIb α . By contrast, GpIb α did not have much of an effect on the C-terminal PAR1 residue D58 as evident from the modest change in K_D that occurred after taking error limits into account (Figure 47A, 47B, 48A, 48B, Table 4, and Table 5). Titration with PAR3G_{EL} revealed that PAR3 [¹⁵N]-E48 and [¹⁵N]-L52 both exhibited extensive peak broadening already at low PPACK-IIa: PAR3G_{EL} ratios (Figure 49A and 49B). The affinity of PAR3 [¹⁵N]-L52 for ABE I went from $47 \pm 6 \mu\text{M}$ to too tight to calculate in the presence of ABE II ligand GpIb α . PAR3 [¹⁵N]-E48 continued to remain too tight to calculate even in the presence of GpIb α . Once again GpIb α can influence affinities at distinct sites on ABE I.

When aligning the PAR3 and PAR1 sequences, GpIb α binding is shown to have influenced the conformation of a set of thrombin residues (**Figure 50**). PAR3 E48, PAR3 L52, and PAR1 E53 all underwent increased affinity in the presence of GpIb α -thrombin. The corresponding thrombin residues that interact with these PAR residues can be clustered as (F34, L65, I82) and (T74, R75, Y76). In support of the current NMR titrations, HDX-MS studies previously reported that GpIb α binding exerts a long-range solvent accessibility effect over to the thrombin 65-84 ABE I region.⁶⁰ Future studies could probe how GpIb α influences additional PAR1 and PAR3 residues. Unlike the PAR3 and PAR1 residues mentioned above, the more C-terminal PAR1 D58 which had the best PAR-thrombin K_D value was less affected by GpIb α binding. PAR1 D58 is postulated to bind in the vicinity of thrombin R77a. Binding of GpIb α at thrombin ABE II may not further promote interactions between thrombin ABE I R77a and PAR1 D58.

Overall, we conclude that although PAR1 and PAR3 both target similar areas of the thrombin 30 and 70 loop regions the individual PAR amino acids make unique contributions to the overall binding affinities. Furthermore, our novel NMR titration approach allowed us to probe such distinctions compared with previously published PAR3 (44-56) ¹H-¹⁵N-HSQC titration results.¹⁵⁴ PAR1G (49-62) exhibited weaker interactions with ProT. These results suggest that drugs that mimic PAR1G interactions may be less inclined to target immature pro-ABE I. By contrast, PAR3G interactions are tighter and could already bind to immature pro-ABE I. As a result, therapeutics based on PAR3G could help block the maturation of active thrombin. Finally, NMR studies involving the ternary complex GpIb α – PPACK-IIa -PAR1/3 provided strong evidence that GpIb α binding can exert a long-range effect over to thrombin residues F34, L65, R75, T74, Y76, and I82. In

the future, the new knowledge gained from this project may help in development of drug candidates that target specific hot spots on (pro)- ABE I and II.

CHAPTER V
SECONDARY STRUCTURE INFORMATION AS A CLUE TO EXPLAIN THE
WEAK KINETICS OF THROMBIN-CATALYZED RELEASE OF
FIBRINOPEPTIDE B

INTRODUCTION

Thrombin utilizes an active site region and two exosites ABE I and ABE II to initiate and regulate its functions. The serine protease activity of thrombin is supported by a catalytic triad composed of D102, H57, and S195 (**Figure 51A**).^{37,169} Thrombin substrate specificity is controlled by the 60s loop also known as the β -insertion loop (residues Y60a-K60f). Two critical 60s loop residues that limit substrate entrance into the active site include Y60a and W60d (**Figure 51A**). Other important thrombin residues that help accommodate substrates are part of the aryl binding pocket and include W215, I174, and L99 (**Figure 51A**). Following substrate binding at the active site, thrombin cleaves the substrate scissile bond (R/K-X) designated by the P₁-P_{1'} nomenclature.⁶¹ Substrate amino acids N-terminal of the hydrolysis site are labeled P₂, P₃, P₄ etc. whereas those that are C-terminal are labeled P_{2'}, P_{3'}, P_{4'} etc. The substrate residue at the P₁ position (R or K) forms a salt bridge with thrombin D189 at the bottom of the active site cleft. The P₂ residue makes extensive contacts with the 60s loop, the P₄ interacts with the aryl binding site, and P₃ is not so critical in binding thrombin. Figure 1B shows an example of contacts between the

P₄-P₁ segment (³⁴VVPR³⁷) of the FXIII Activation Peptide and critical residues of thrombin.⁷¹

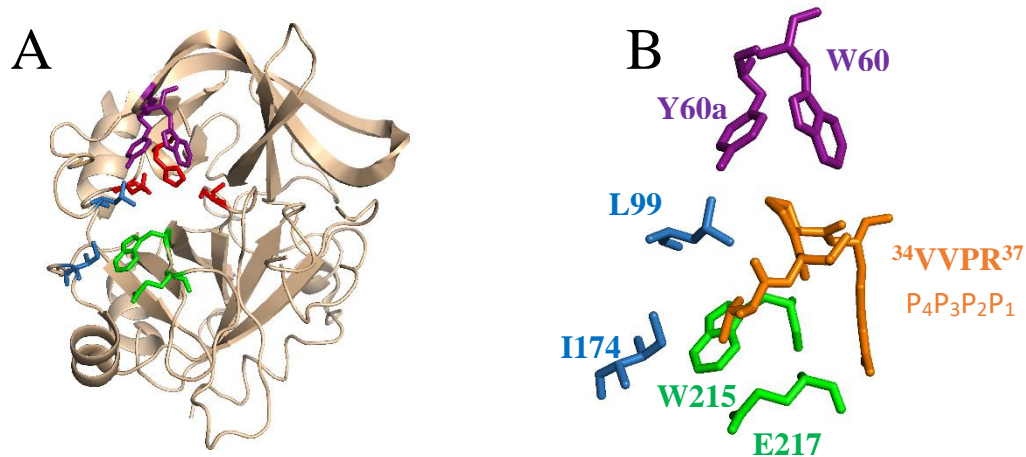


Figure 51: X-ray crystal structure of thrombin highlighting key residues that surround the active site. A) Ribbon diagram of thrombin (gray) showing selected residues as colored sticks (PDB ID: 1DE7). Residues include the catalytic triad (red), Y60a and W60d (purple), L99 and I174 (blue), W215 and E217 (green). B) The enzyme-bound FXIII AP segment (orange) (P₄-P₁) surrounded by same thrombin residues shown in figure 1A.

A key procoagulant activity of the serine protease thrombin is to convert fibrinogen (Fbg) into fibrin. Fibrinogen (340kDa) is the most abundant coagulation protein in the blood, and it consists of six polypeptide chains, two each of the A α , B β , and γ chains.^{30,33,36} The N-terminal ends of all six chains meet at the central E region, and the C-terminal ends meet at the two peripheral D regions. Thrombin first cleaves at the R16-G17 peptide bond of the Fbg A α chain to release Fibrinopeptide A (FpA) (**Figure 52**). This cleavage helps in formation of half-staggered, double stranded protofibrils involving D:E:D interactions. Later thrombin cleaves at the R14-G15 peptide bond of the Fbg B β chain to release Fibrinopeptide B (FpB).^{34,63,170}

Once both peptides are released, transglutaminase FXIIIa helps in cross linking fibrin protofibrils through isopeptide bond formations.¹⁷¹ Steady-state kinetic studies of thrombin-catalyzed hydrolysis of fibrinogen revealed that release of FpA follows a first-

order reaction. Interestingly, initial release of FpB is slow and the rate of FpB release is accelerated after protofibril formation. Hence, the release of FpB is considered “biphasic”.¹⁷²

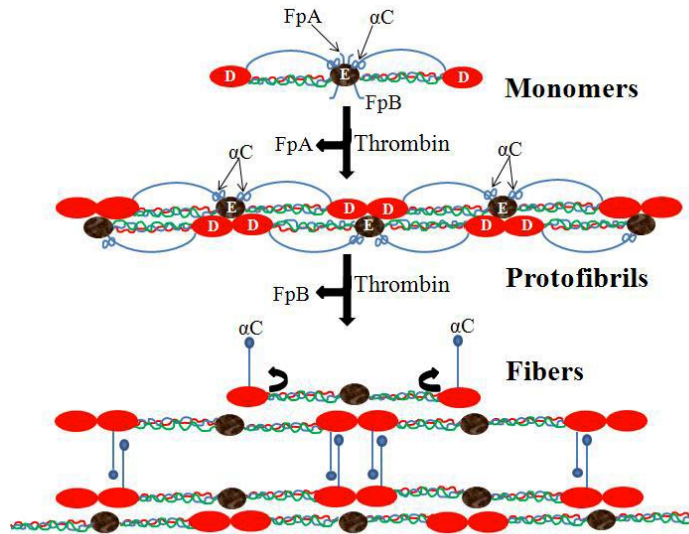


Figure 52: Fibrin clot formation is initiated by the cleavage of FpA leading to the formation of protofibrils, next the cleavage of FpB results in lateral aggregation of fibrin. Finally, FXIIIa imparts isopeptide bonds between two fibrin molecules there by stabilizing fibrin architecture. Cartoon was adapted from Weisel, J.W. (2007).

Mutations have been identified that involve fibrinogen B β chain residues or that influence this chain.^{173,174} Fibrinogen Ijmuiden (R14C) and Fibrinogen Nijmegen (R44C) mutations are common in patients with thrombophilia and have been associated with defective fibrin polymerization.¹⁷⁵ The F8Y mutation in the fibrinogen A α chain leads to preferential cleavage of Fbg B β over Fbg A α .¹⁷⁶ The X-ray crystal structure of the Fbg A α F8Y mutant revealed that the carbonyl oxygen of Y8 shifted 1.8Å relative to the original carbonyl oxygen of F8 leading to distortion of the scissile bond. As a result, the release of FpA becomes greatly hindered.

Unexpectedly when fibrinogen is adsorbed on surfaces like glass, carbon, polyethylene, and polystyrene, it takes on two kinds of orientations. One is “side-on”

(laying on the surface) occurring at low fibrinogen concentration and the other is “end-on” (standing on the surface) at high fibrinogen concentration.¹⁷⁷ For each orientation, only a portion of fibrinopeptides are accessible for thrombin cleavage. In the “side-on” orientation, 36% of FpA and 35% of FpB are released, whereas in the “end-on” orientation, 37% of FpA and a higher 64% of FpB is released.

Over the years, researchers have further explored the initial steps of fibrin formation. Using recombinant fibrinogen proteins, Mullin *et al.*, suggested that thrombin specificity is what dictates the order of fibrinopeptide release.¹⁷⁸ Based on modeling studies of the N- terminal ends of both the A α chain and the B β chains, Pechik *et al* predicted that it is the length and orientation of the chains that lead to the weaker kinetics of FpB release.¹⁷⁰ Brummel *et al.*, made the critical observation that release of FpA and activation of FXIII occur simultaneously, thus allowing FXIIIa to first cross-link the γ -chains in the newly formed fibrin protofibrils.¹⁷⁹ Later when FpB is released by thrombin, the fibrinogen α C domains become exposed and FXIIIa is responsible for additional α - α , α - γ , and higher order crosslinking of protofibrils (**Figure 52**).

All the work discussed above has been done with different lengths of Fbg A α and B β chains. None of them could provide information on the structural features of the Fbg B β segment that comes in direct contact with thrombin. Such Fbg B β interactions will dictate the orientation of the substrate- enzyme complex and thus control the ability of thrombin to cleave the FpB sequence. An important focus of the chapter was to determine individual kinetic parameters for thrombin- catalyzed hydrolysis of Fbg B β (5-16). The kinetic parameters obtained were compared with other thrombin substrates including FXIII AP (28-41) V34X,^{180,181} PAR1 (29-45),⁶⁴ and PAR4 (38-51).⁶⁵ Such comparisons led to

the conclusion that Fbg B β (5-16) had the lowest k_{cat}/K_m value thereby making it rather a poor substrate for thrombin. Solution NMR was employed to elucidate the structural features behind the weak cleavage of Fbg B β (5-16). Unlike FXIII AP (28-41) V34F, Fbg B β (5-16) does not appear to take advantage of the aromatic Phenylalanine (F) at P₄ and P₅ positions to promote improved binding interactions with thrombin. Another striking reason behind the poor kinetics is probably the smaller Alanine residue at the P₂ position that cannot serve as an additional anchor point below the thrombin 60s loop.

MATERIALS AND METHODS

Materials

Bovine thrombin was purchased from Haematologic Technologies, Inc (Essex Junction, VT). Human recombinant thrombin was a generous gift from Dr. Enrico Di Cera and Ms. Leslie Pelc, Saint Louis University, St. Louis, MO. D₂O (99.96%) was from Cambridge Isotope Laboratories (Andover, MA).

Synthetic peptide

Fbg B β (5-16) was synthesized by New England Peptides (Gardner, MA). The amino acid sequence of this peptide is as follows: (Ac-DNEEGFFSARGH-Amide). The purity of Fbg B β (5-16) was verified by high-performance liquid chromatography and matrix-assisted laser desorption ionization time-of-flight mass spectrometry. Initial stock solutions of peptide were solubilized in deionized water. The peptide was completely soluble at pH 7.0, and the concentrations were determined by quantitative amino acid analysis (AAA Service Laboratory, Inc., Damascus, OR).

Sample preparation for HPLC based kinetic assay

The HPLC based kinetics assay of Trumbo *et al.*, was employed.⁶⁹ Briefly, a 6-7 mM peptide stock solution was prepared. Later, the peptide solution was diluted into assay buffer (50 mM H₃PO₄, 100 mM NaCl, 0.1% PEG, pH 7.4) and heated to 25 °C in a heat block. The final concentrations of the Fbg B β (5-16) substrate spanned from 100 to 1500 μ M. Hydrolysis of Fbg B β (5-16) at the R14-G15 peptide bond was initiated with the addition of 134 nM of recombinant human thrombin. An aliquot of the reaction mixture was removed at 3, 5, 7, 9, 11, 13 and 17 mins and then quenched with 12.5% H₃PO₄. For all kinetic assay runs, \leq 15% of the substrate Fbg B β (5-16) was cleaved by thrombin to release the product FpB (5-14). Quenched reaction time points were analyzed by RP-HPLC using a Waters X-Bridge BEH130 C18 5 μ m column on a Waters 2695 HPLC system. Peaks for the substrate Fbg B β (5-16) and the resultant product FpB (5-14) were separated using an acetonitrile based gradient of [15% CH₃CN, 0.09% trifluoroacetic acid in dI water] to [50% CH₃CN, 0.09% trifluoroacetic acid in dI water]. Product peak areas were converted to concentration using calibration curves constructed for Fbg B β . The slopes of product concentration versus time plots were used to determine the initial velocities (in μ M/s) for the different thrombin-catalyzed reactions. The kinetic experiments were done in triplicate, and kinetic constants were determined following nonlinear regression analysis fits to the equation. $V = V_{\max} / (1 + K_m/[S])$ in Kaleidagraph (Synergy). The k_{cat} values were calculated by knowing the V_{\max} values and a final thrombin concentration of 134 nM.

Sample preparation for solution NMR experiments

All NMR experiments were performed at pH 5.6. Bovine plasma thrombin was buffer exchanged into NMR buffer- [25 mM H₃PO₄, 150 mM NaCl, 0.2 mM EDTA, (pH

5.6)] using a Vivaspin 2 ultrafiltration unit with a 5000 Da molecular weight cutoff (Sartorius, Göttingen, Germany). Thrombin concentration was determined using an extinction coefficient ($E^{1\%}_{280\text{ nm}}$) of 18.3 and a MW of 36,500 g/mol. For our 1D and 2D ^1H NMR based studies, ligand-protein complexes with ratios of at least 10:1 were then prepared. The complexes included 1600 μM Fbg B β (5-16) and 160 μM thrombin. Fbg B β at a minimum concentration of 1.5 mM was used as a free ligand control.

NMR experiments were then performed at 25 °C on a Varian Inova 700 MHz spectrometer with a triple resonance cold probe and pulsed-field Z-axis gradients. Proton chemical shift values for all the Fbg B β amino acid residues were determined using a combination of 2D TOCSY and 2D-transferred NOESY spectra. Standard TOCSY and NOESY pulse sequences were employed. Parameters for the 2D NMR experiments included nt=16, ni=512, np= 2486, gain= 20 and sweep widths of 7022.5 Hz for both direct and indirect dimensions. A mixing time of 400 msec was employed for the 2D tr-NOESY. The 1D ^1H NMR spectra were processed using Mnova NMR (Mestrelab Research software). 2D TOCSY and tr-NOESY data were processed using NMRPipe and nmrDraw and then further visualized using Sparky.

RESULTS

Thrombin-catalyzed release of Fibrinopeptide B

An HPLC based kinetic assay was employed to determine the individual kinetic constants associated with hydrolysis of Fbg B β (5-16) by human recombinant thrombin. Thrombin cleaves Fbg B β at the R14-G15 peptide bond releasing peptide fragment (5-14). As evident from the HPLC chromatogram in **Figure 53**, the substrate peak Fbg B β (5-16)

eluted first from the C18 column followed by the product (5-14). This elution order occurred because all the HPLC-based kinetic assays were done using an acetonitrile gradient with 0.09% trifluoroacetic acid. This acidic solution environment makes substrate Fbg B β (5-16) more hydrophilic (+2 charge) than the product FpB (5-14) (+1 charge). The higher hydrophilicity thus causes the substrate to elute first from the C₁₈ column.

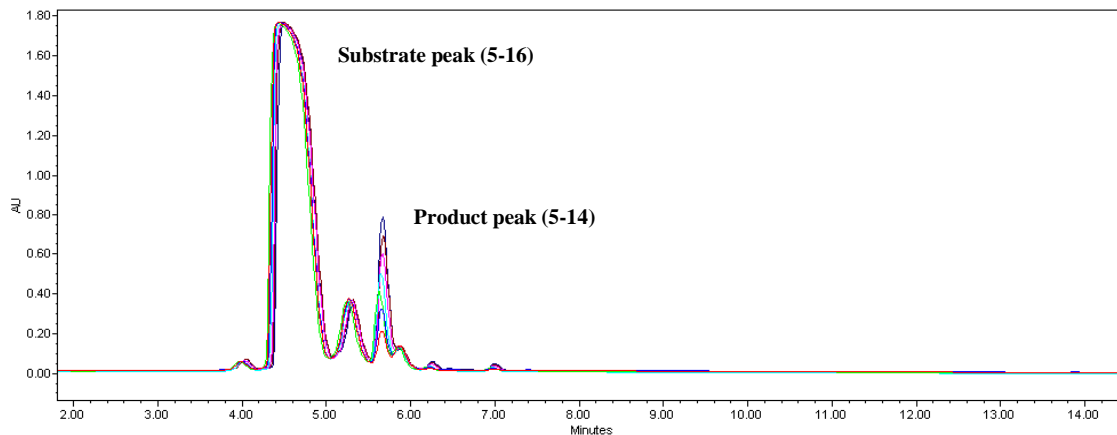


Figure 53: Hydrolysis of Fbg B β (5-16) as a function of incubation time. 500 μ M Fbg B β (5-16) was hydrolyzed by 130 nM thrombin for 3, 5, 7, 9, 11, 15 and 17 mins. Each quenched time point was run on a C18 column using a Waters HPLC system. A linear gradient of 15% acetonitrile, 0.09% trifluoroacetic acid in water to 50% acetonitrile, 0.09% trifluoroacetic acid in water in 20 min at a flow rate of 0.5 ml/min was employed. The original substrate peptide Fbg B β (5-16) eluted at approximately 4.6 mins whereas the hydrolyzed product FpB (5-14) eluted at approximately 5.7 mins.

Figure 53 corresponds to a representative 500 μ M Fbg B β (5-16) kinetic reaction. The product peak area increased over the course of the 0-17 min reaction time. Peaks neighboring the product FpB 5-14 corresponded to contaminants found in the 90% pure synthetic peptide. To allow for kinetic parameter determination, the substrate concentrations then spanned from 100 to 1500 μ M Fbg B β (5-16). Non-linear regression analysis methods were used to calculate K_m , k_{cat} , and k_{cat}/K_m values for the hydrolysis of Fbg B β (5-16). With human recombinant thrombin, the kinetic parameters included a K_m

of $1271 \pm 154 \mu\text{M}$, a k_{cat} of $1.0 \pm 0.075 \text{ s}^{-1}$, and a k_{cat}/K_m of $8.2 \times 10^{-4} \pm 1.2 \times 10^{-4} \text{ s}^{-1} \mu\text{M}^{-1}$

(Table 7 and 8).

Table 7: Human substrate sequences that target the thrombin active site region. ↓ indicates the cleavage between R-X.

	P_4	P_3	P_2	P_1	
Fibrinogen B β (5-16)	⁵ D	N	E	E	G F F S A R ↓ G H ¹⁶
Fibrinogen A α (7-20)	⁷ D	F	L	A	E G G G V R ↓ G P R V ²⁰
Factor XIII (28-41) V34 AP	²⁸ T	V	E	L	Q G V V P R ↓ G V N L ⁴¹
Factor XIII (28-41) V34F AP	²⁸ T	V	E	L	Q G F V P R ↓ G V N L ⁴¹
Factor XIII (28-41) V34W AP	²⁸ T	V	E	L	Q G W V P R ↓ G V N L ⁴¹
Factor XIII (28-41) V34L AP	²⁸ T	V	E	L	Q G L V P R ↓ G V N L ⁴¹
PAR1 (29-45)	²⁹ K	A	T	N	A T L D P R ↓ S F L L ⁴⁵
PAR4 (38-51)	³⁸ S	T	P	S	I L P A P R ↓ G Y P G ⁵¹

Table 8: Kinetic constants for the hydrolysis of Arg-Xaa by thrombin

Substrate peptides	K_m (μM)	k_{cat} (s^{-1})	k_{cat}/K_m ($\text{s}^{-1} \mu\text{M}^{-1}$)
Fibrinogen B β (5-16) ^a	1271 ± 154	1.0 ± 0.075	$8.2 \times 10^{-4} \pm 1.2 \times 10^{-4}$
Fibrinogen A α (7-20) ⁶²	569 ± 76	31.0 ± 0.005	$5.5 \times 10^{-2} \pm 7.0 \times 10^{-3}$
FXIII (28-41) V34 AP ⁶²	298 ± 42	2.6 ± 0.005	$8.6 \times 10^{-3} \pm 1.0 \times 10^{-3}$
FXIII (28-41) V34L AP ⁶²	315 ± 42	23 ± 0.003	$7.3 \times 10^{-2} \pm 1.2 \times 10^{-3}$
FXIII (28-41) V34F AP ¹⁸⁰	442 ± 93	6.3 ± 0.54	$1.4 \times 10^{-2} \pm 3.0 \times 10^{-3}$
FXIII (28-41) V34WAP ¹⁸¹	637 ± 56	7.6 ± 0.3	$1.2 \times 10^{-2} \pm 1.2 \times 10^{-3}$
PAR1 (29-45) ⁶⁴	900	35	4.0×10^{-2}
PAR4 (38-51) ⁶⁵	113 ± 19	10.2 ± 0.8	$9.0 \times 10^{-2} \pm 1.7 \times 10^{-2}$

^aThe results shown here represent averages of at least three independent experiments. Kinetic values were calculated using nonlinear regression analysis methods using Kaleidagraph. The error values correspond to standard error of the mean (SEM).

Solution NMR studies of free and thrombin bound FpB (5-16)

Chemical shift assignments for all the Fbg B β residues were derived from 2D TOCSY and 2D tr-NOESY experiments. N6NH-C α H, G9NH-C α H, G15NH-C α H, and H16NH-C α H peaks were not seen in the fingerprint region since they merged with the

solvent peaks (**Appendix 47**). The loss of the G15 and H16 peaks in the Fbg B β -thrombin sample is consistent with thrombin cleaving Fbg B β (5-16) at the R14-G15 peptide bond even at the lower NMR pH of 5.6 (**Appendix 47 and 50**). 1D ^1H line broadening experiments for free Fbg B β (5-16) (**Figure 54A, and 54B**) and Fbg B β (5-16) in the presence of bovine thrombin were acquired. Curiously, the R14-NH peak undergoes an upfield chemical shift after Ila cleavage suggesting that the R14-NH in the product peptide (5-14) encounters more shielded environment. By contrast, the proton attached to side chain ϵ nitrogen is shifted downfield.

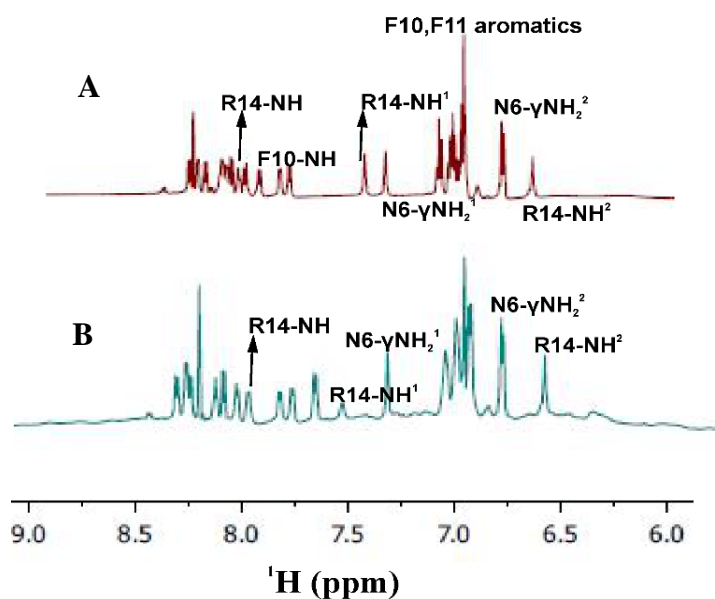


Figure 54: A) 1D Amide proton region of free Fbg B β (5-16). B) 1D amide proton region for FpB (5-14) bound to bovine thrombin.

Extensive line broadening was seen for residues A13-NH and F10-NH. NOEs are numbered from 1 to 30 in the fingerprint, aliphatic and amide regions (**Figures 55, 56, and 57**). These include several intra and inter NOEs: 1 (E8 β H-G9NH), 2 (E8 α H-G9NH), 3 (D5NH-E8 β H), 4 (A13 β H-R14NH), 5 (F11 β H-S12 β H), 6 (F11 α H-S12NH), 7 (A13 α H-R14NH), 8 (G9 α H -F10 β H), 9 (S12 α H-A13NH), 10 (S12 β H-A13NH), 11 (N6 β H-

E7NH), 12 (F11 β H-S12 β H), 13 (F10 α H- F11NH), 14 (D5 α H-N6NH), 15 (F11(2,6_H)-F11 α H), 16 (F10(2,6_H)-F10 α H), 17 (F10(2,6_H)-F11 α H), 18 (F10 α H-F11(2,6_H)), 19 (R14NH- γ CH₂), 20 (F10(2,6_H)-F10 β H), 21 (F11(2,6_H)-F11 β H), 22 (F10(3,5_H)-F11 β H), 23 (F10(3,5_H)-F10 β H), 24 (F11(3,5_H)-F11 β H), 25 (F10 β H- F11 β H), 26 (G9NH-F10NH), 27 (F10NH-F11NH), 28 (A13NH-R14NH), 29 (F11NH-S12NH), 30 (E8NH-G9NH).

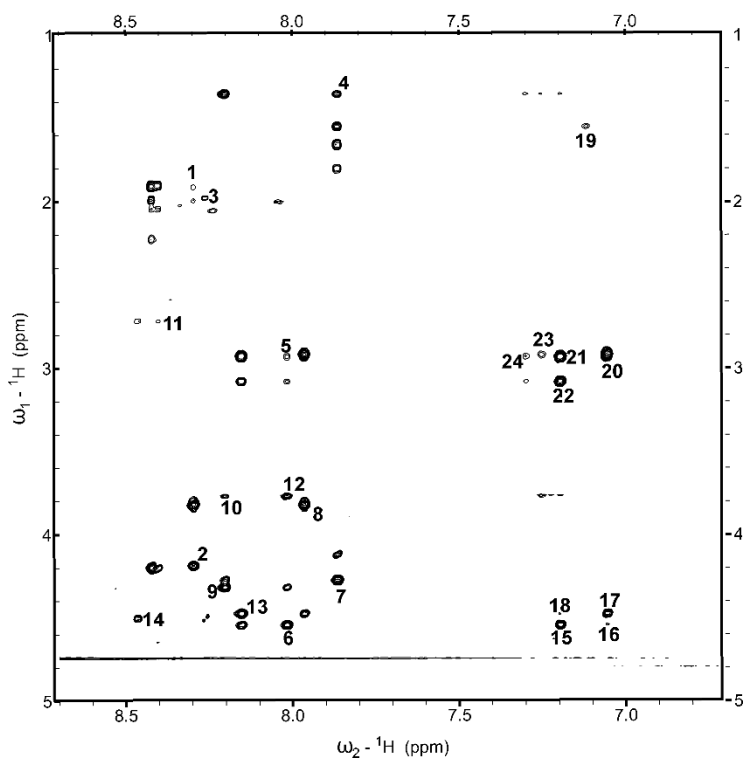


Figure 55: 2D NOESY Fingerprint region of 1.5 mM Fbg B β (5-16) and 160 μ M thrombin. Sample was prepared in 25mM H₃PO₄, 150 mM NaCl, 0.2 mM EDTA and 10 % D₂O (pH 5.6)

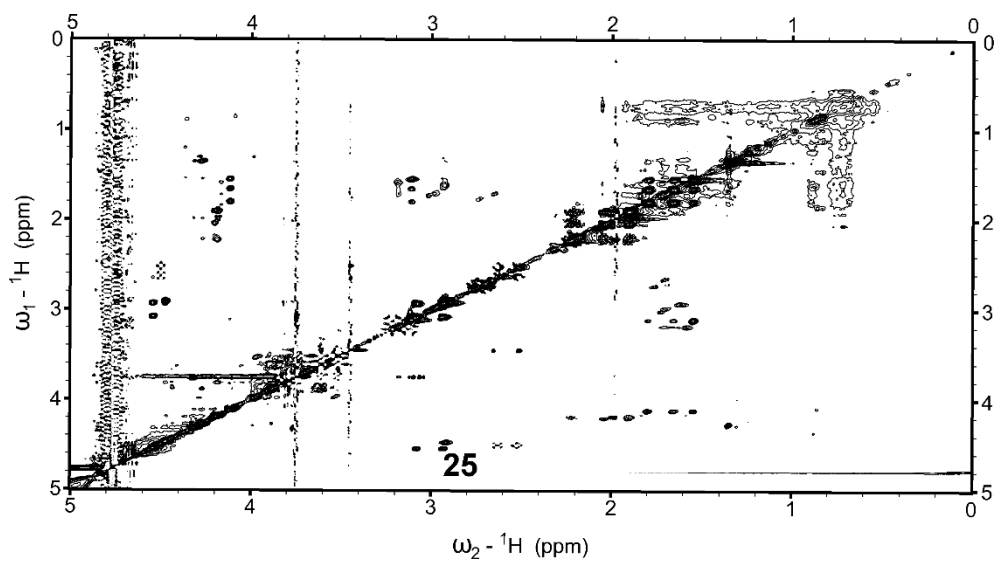


Figure 56: 2D NOESY Aliphatic region of 1.5 mM Fbg B β (5-16) and 160 μ M thrombin. Sample was prepared in 25mM H₃PO₄, 150 mM NaCl, 0.2 mM EDTA and 10 % D₂O (pH 5.6)

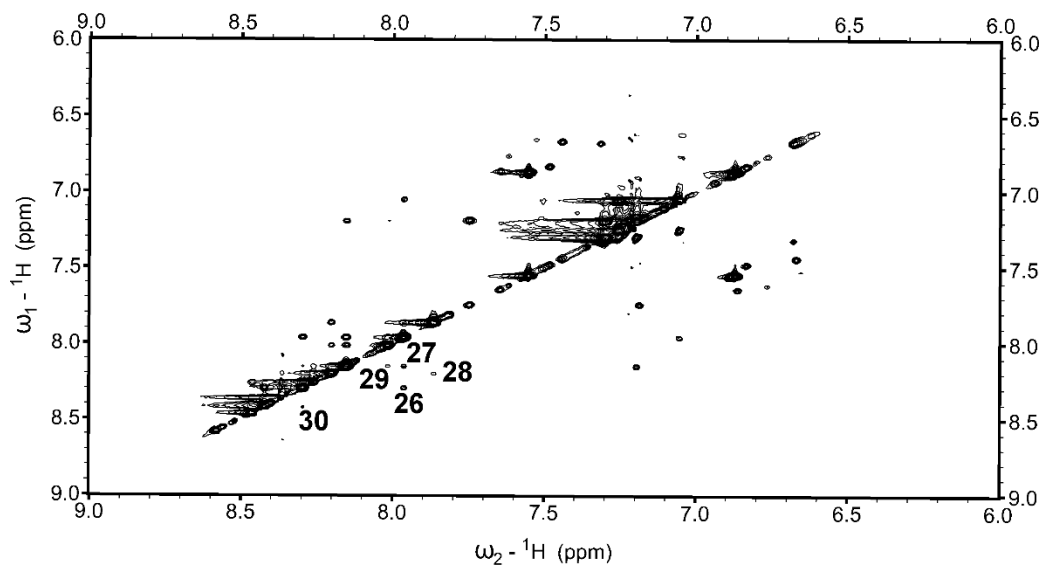


Figure 57: 2D NOESY Amide region of 1.5 mM Fbg B β (5-16) and 160 μ M thrombin. Sample was prepared in 25mM H₃PO₄, 150 mM NaCl, 0.2 mM EDTA and 10 % D₂O (pH 5.6)

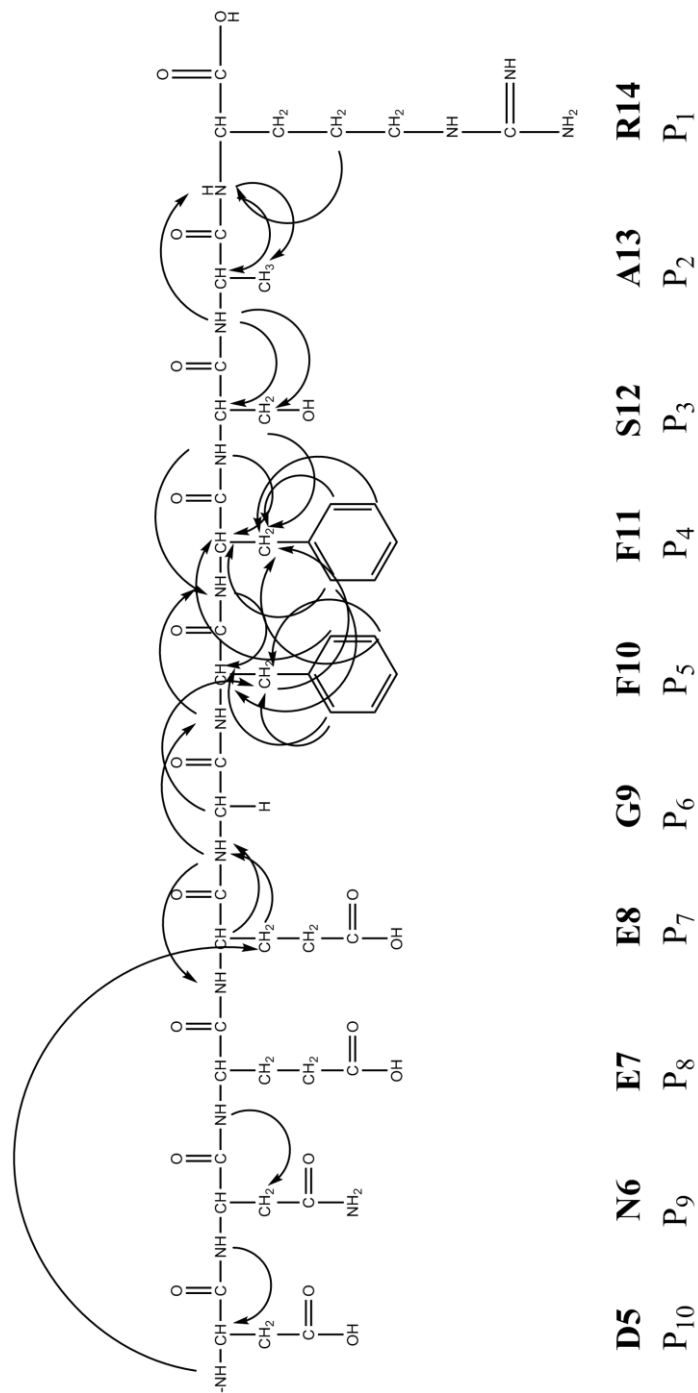


Figure 58: Cartoon showing through space interactions between the residues of Fbg Bβ (5-16) when bound to thrombin.

DISCUSSION

Much data is available on the binding of Fbg A α (7-20) to the thrombin active site from previous kinetic, NMR and X-ray crystal studies. Less is known about the binding of Fbg B β to thrombin. The focus of the current study was Fbg B β (D5-H16), a sequence that interacts with the active site region of thrombin and can be cleaved at the R14-G15 peptide bond. Kinetic parameters for thrombin-catalyzed release of FpB (5-14) were determined. In addition, 1D and 2D NMR methods were used to structurally characterize the binding of individual FpB residues to the thrombin active site region.

HPLC kinetic assay results suggest that thrombin-catalyzed hydrolysis of Fbg B β (5-16) exhibited a K_m value of $1271 \pm 154 \mu\text{M}$, a k_{cat} value of $1.0 \pm 0.075 \text{ s}^{-1}$, and a k_{cat}/K_m value of $8.2 \times 10^{-4} \pm 1.2 \times 10^{-4} \text{ s}^{-1} \mu\text{M}^{-1}$. When compared to the kinetic parameters of Fbg A α (7-20),⁶² Fbg B β (5-16) is 2-fold higher in K_m and 30-fold lower in k_{cat} value (**Table 7 and 8**). Such results reveal that binding interactions for Fbg B β (5-16) at the active site are weaker and turnover into product is greatly hindered. Fbg B β (5-16) is definitely not as well optimized to interact with thrombin as Fbg A α (7-20). Moreover, Fbg B β (5-16) exhibits the lowest k_{cat} value of the peptide substrates shown in Table 8. With its high K_m and low k_{cat} , Fbg B β (5-16) becomes the weakest peptide substrate in terms of substrate specificity (k_{cat}/K_m). A careful review of thrombin substrate sequences indicates that although the Ala 13 at the P₂ position in FpB (5-14) exhibited line broadening in the presence of thrombin, it might not be large enough to effectively promote optimal contacts with thrombin Y60a and W60d of the thrombin β -insertion loop. In addition, solution NMR studies on FpA (7-16) identified that Phe 8 at the P₉ position compensates for the absence

of a common Proline at the P₂ position by making a through space interaction with its ¹³GGV¹⁵ (P₄-P₂) region (**Table 7 and 8**).

Comparing the kinetics parameters for thrombin catalyzed hydrolysis of Fbg Bβ (5-16) with those of FXIII AP (28-41) V34F and V34W is also valuable, as both FXIII variants contain an aromatic residue at the P₄ position.^{180,181} The presence of such an aromatic residue helped both FXIII AP (28-41) V34F and V34W to improve their *k*_{cat} 3-fold relative to FXIII AP (28-41) V34 and 6-fold relative to Fbg Bβ (5-16) (**Table 7 and 8**). The presence of two Phe residues at the P₅ and P₄ positions of Fbg Bβ (5-16) clearly did not improve *k*_{cat}.

Another interesting substrate to compare is the PAR series. Even though PAR1 (29-45) has a similar *K*_m value (1271 μM vs 900 μM)⁶⁴ as Fbg Bβ (5-16), the substrate specificity (*k*_{cat}/*K*_m) of PAR1 is far higher than that of Fbg Bβ (5-16) (**Table 7 and 8**). The PAR1 L35 and P37 at the P₄ and P₂ positions interact optimally below the β insertion loop and help orient the PAR1 sequence for effective cleavage by IIa. This benefit is reflected in the 35-fold improvement in *k*_{cat} that occurs with the PAR1 sequence. The PAR4 (38-51) sequence has proline at the P₄ and P₂ positions (⁴⁴PVPR⁴⁷). This arrangement provides effective binding contacts with the thrombin active surface leading to a 10-fold improvement in *K*_m and *k*_{cat} relative to Fbg Bβ. Once again, the individual *k*_{cat} and *K*_m values of Fbg Bβ (5-16) reveal that the ¹⁰FFSAR¹⁴ segment hinders productive binding and orientation for IIa cleavage.

Solution NMR was employed in this project to further explain the weak kinetics of Fbg Bβ (5-16). The 1D proton line broadening studies revealed that A13-NH and F10-NH interacted with thrombin. The thrombin bound product FpB (5-14) did not have peaks for

G15 and H16 highlighting that thrombin catalyzed cleavage had indeed occurred at the R14-G15 peptide bond. (**Figure 55,56,57, and 58**). Furthermore, a substantial number of transferred NOEs were seen for the sequence ⁸EGFFSAR¹⁴. A prevalence of nearest neighbor NOEs indicates that there is no evidence of helices adopted by this peptide sequence when bound to thrombin. A weak NOE from D5NH-E8CβH suggests the possibility of a turn like structure within the N-terminal region of the FpB sequence.

Previously published molecular modeling studies on Fbg Bβ suggested that F10 at the P₅ position has hydrophobic interactions with thrombin Y60a and W60d.¹⁸² Such hydrophobic interactions with the thrombin 60s loop might have led to the extensive line broadening of the F10-NH. However, Fbg Bβ F11 at the P₄ position did not change peak intensity suggesting no interactions with thrombin W215 and E217. Such results agree with the *in-silico* studies, predicting that F11 projects away from thrombin surface.¹⁸² Also, no NOE cross peaks between F11 (P₄) and A13 (P₂) were observed, indicating that Fbg Bβ (5-16) does not take advantage of a P₄ to P₂ interaction to stabilize the enzyme-substrate complex. By contrast, FXIII AP (28-41) V34L,¹⁸³ and V34F¹⁸⁴ utilized P₄ to P₂ contacts to anchor better on to the IIa surface. A large number of NOEs between FpB F10 and F11 suggests that their amino acid side chains are interacting with each other through space even though both side chains may be oriented in somewhat opposite directions. Unlike FpA (7-16),^{69,183} no NOES were observed between the N-terminal portion of the FpB peptide and the P₄-P₂ region.

Overall, the HPLC based kinetic assay results that Fbg Bβ (5-16) is a relatively poor thrombin substrate because of its high K_m and low k_{cat} relative to other common thrombin substrates. Our 1D and 2D solution NMR results suggest that FpB (5-14) cannot

take advantage of stabilizing P₄ to P₂ interactions when bound to thrombin. The presence of two Phe residues at the P₅ and P₄ positions along with a small Ala at the P₂ position are proposed to hinder optimal contacts between Fbg B β (5-16) and thrombin.

CHAPTER VI

RESEARCH SUMMARY AND FUTURE DIRECTIONS

Thrombin with a catalytic triad of His 57, Asp 102, and Ser 195 is highly homologous to such serine proteases as trypsin and chymotrypsin.³⁷ Thrombin enzyme specificity is controlled through several loops including the 60s loop (or β insertion loop) and the γ loop (or autolysis loop). Another important structural feature is the Na⁺ ion binding loop which contributes to thrombin allostery. The sodium bound form of thrombin is considered to be in the “fast” state and thrombin now has procoagulant activity. In contrast, thrombin is considered “slow” and leans toward anticoagulant functions in the absence of Na⁺ ion.^{45,185} Secondary anchoring sites rich in positively charged amino acids are called anion binding exosite- I and II (ABE I and ABE II) and are present at opposite sides of the active site. ABE II interactions with ligands are mainly electrostatic; however, ABE I can have both electrostatic and hydrophobic interactions with ligands. Ligands that bind to ABE- I include the Protease Activated Receptors PAR1 (49-62),⁴⁹ PAR3 (44-56),⁵⁰ and Hirudin (54-65).^{51,161} Ligands binding to ABE-II include glycoprotein GpIb α (269-286),⁷⁹ fibrinogen γ' (410-427),⁵³ Haemadin (45-57),⁵⁴ and heparin.¹⁸⁶

Allosteric communication is possible among the two exosites and between the exosites and the active site. Amide hydrogen/deuterium exchange coupled with mass spectrometry (HDX-MS) revealed that ligand binding at the exosites exhibited both local and long-range effects but not all showed identical conformational changes to thrombin.⁶⁰

Effects of Hirudin are only restricted to the ABE I region, whereas PAR3, PAR1, and GpIb α showed both local and long-range effects.⁶⁰

Thrombin is originally produced as the 72kDa zymogen, Prothrombin (ProT). ProT is composed of Fragment-1 (1-155), Fragment-2 (156-271) and a protease domain (272-579). Fragment-1 contains a Gla domain and disulfide containing Kringle-1. Vitamin K is needed for the formation of Gla residues in Fragment -1. Fragment-2 contains Kringle-2, the A chain (272-320), and the B chain (321-579). The Thrombin A and B chains together constitute the protease domain. ProT is physiologically activated by the Prothrombinase complex consisting of a serine proteinase Factor Xa and the cofactor Factor Va, a phospholipid membrane, and Ca²⁺. ProT is anchored to the membrane surface through the Gla domain of Fragment 1 (F1).^{38,187}

In platelets, cleavage of ProT at R271 leads to the formation of the inactive precursor Prethrombin-2 (PT2) and Fragment 1.2. Subsequent cleavage at R320 gives rise to the active protease α -thrombin (36.7kDa).^{38,40} α -thrombin can also be autolysed to catalytically hindered β and γ - thrombin.^{39,41} ProT and PT2 have immature anion binding exosites called (pro)- ABE-I and II. Upon formation of α -thrombin, these exosites become more mature and are called ABE – I and II. These mature exosites help with substrate specificity and ligand binding. Unexpectedly, there are certain ligands that can already bind to pro-ABE I.¹²⁵⁻¹²⁸ The published literature has provided global K_Ds for various ligands that bind to (pro)-ABE I. Following maturation events at the single amino acid level is however missing. Solution NMR studies have revealed that thrombin is highly dynamic and there are a few residues in the thrombin ABE I region that cannot be monitored due to exchange broadening.¹³³ As a result, isotopically labeled thrombin has limitations in its

ability to understand the conformational changes of few regions that occur during thrombin activation. To decipher the missing information about maturation events and help to probe interactions between various physiological substrates, we divided our research into three projects.

The first project was to probe the maturation events of (pro)- ABE I at the single amino acid level by using various solution NMR methods on peptides based on a member of the protease activated receptor PAR family. The first peptides studied were derived from PAR3. 1D proton line broadening NMR revealed that PAR3 (44-56) and weaker binding PAR3G (44-56) could already interact with pro-ABE I on prothrombin. ^1H - ^{15}N -HSQC (Heteronuclear Single Quantum Coherence) NMR titrations were then used to probe binding of individual ^{15}N -labeled PAR3G residues (F47, E48, L52, and D54). PAR3G E48 and D54 could interact electrostatically with prothrombin and tightened upon thrombin maturation. The higher affinity for PAR3G D54 suggests the region surrounding thrombin R77a is better oriented to bind D54 than the interaction between PAR3G E48 and thrombin R75. Aromatic PAR3G F47 and aliphatic L52 also both reported on significant changes in chemical environment upon conversion of prothrombin to thrombin. The ABE I region surrounding the 30s loop was already available than the hydrophobic pocket (F34, L65, and I82). These NMR titrations demonstrate that PAR3 residues document structural rearrangements occurring during exosite maturation that are missed by reported X-ray crystal structures.^{50,154}

Later, the project was extended to better understand the diversity of PAR ligand binding interactions towards zymogen ProT vs mature thrombin. 1D proton line broadening confirmed that PAR1P (49-62) and weaker binding version PAR1G (49-62)

already exhibited line broadening with ProT and such broadening increased when bound to thrombin. 2D tr-NOESY revealed that PAR1P (49-62) when bound to pro-ABE I adopted an extended conformation with the Xaa-Pro bond existing in the *trans* conformation.

^1H - ^{15}N HSQC titrations then provided quantitative estimates of binding interactions for ^{15}N -labeled PAR peptides interacting with ProT vs thrombin. The F55 of PAR1P peptides revealed that the hydrophobic pocket of pro-ABE I (F34, L65, and I82) is available for peptide binding, and the affinity increased with mature thrombin. For both PAR3¹⁵⁴ and PAR1 peptides, a proline to glycine substitution was needed to sufficiently weaken the affinity and allow us to characterize the thrombin-peptide interactions. X-crystal structures reveal almost the same thrombin binding partners for both PAR1 (49-56) and PAR3 (44-56). However, the solution NMR methodologies demonstrated that even though the PAR residues target the same regions of (pro)- ABE I, the binding affinities of K51, E53, and E60 residues in PAR1G (49-62) are weaker than PAR3G (44-56). When bound to thrombin, the acidic C-terminal tail of PAR1 (49-62) remains unresolved by crystallography.⁴⁹ NMR titrations are making it possible, for the first time, to evaluate the binding affinities of D58 of the PAR1 ($^{58}\text{DEEKN}^{62}$) segment to pro-ABE I and ABE I.

We also found striking evidence that allosteric communication can be possible between ABE I and ABE II. When triply phosphorylated GpIb α (269-282) bound at ABE II, it affected the binding affinities of ABE I ligands. Previous HDX-MS studies revealed that GpIb α (269-282) had a long-range effect on ABE- I segment L65 to M84.⁶⁰ Our NMR protein-ligand titration studies showed that the allosteric effect of GpIb α is directed more

towards the center of the sequences in both PAR3 (44-56) and PAR1 (49-62) than towards the C-terminal end.

The final project of the dissertation was to determine kinetic parameters associated with thrombin-catalyzed hydrolysis of Fbg B β (5-16). HPLC-based kinetic assay results suggested that Fbg B β (5-16) has K_m value of $1271 \pm 154 \mu\text{M}$, k_{cat} value of $1.0 \pm 0.075 \text{ s}^{-1}$, and k_{cat}/K_m value of $8.2 \times 10^{-4} \pm 1.2 \times 10^{-4} \text{ s}^{-1} \mu\text{M}^{-1}$. A comparison of individual kinetic parameters indicates that Fbg A α (7-20),⁶² is a better substrate for thrombin than Fbg B β (5-16). Fbg B β is hindered by having both high K_m and low k_{cat} values. These limitations helped explain why FpB is released from fibrinogen later than that of FpA. FXIII AP (28-41) V34L and V34F are known to take advantage of an aromatic residue at the P₄ position to improve optimal contacts with the active site region.^{183,184} From this project, we identified that Fbg B β (5-16) was not able to utilize its two aromatic Phe residues at the P₄ and P₅ positions to help generate good kinetic parameters when compared to FXIII AP (28-41) V34F and V34L. Even though the K_m values for PAR1 (29-45)⁶⁴ and Fbg B β (5-16) are comparable, substrate specificity for PAR1 is 35-fold higher than Fbg B β (5-16). PAR1 (29-45) took advantage of Proline at the P₂ position to improve substrate orientation for thrombin-catalyzed hydrolysis at the thrombin active site surface. Our solution NMR studies then helped to further understand the weak kinetics observed for the hydrolysis of Fbg B β (5-16). Unlike PAR1, the Phe residues at P₄ and at P₅ did not show any stabilizing through space NOEs with the small Alanine residue at the P₂ position. The ¹⁰FFSAR¹⁴ sequence in Fbg B β (5-16) plays a key role in forming a stable thrombin-FpB substrate complex, however the interactions are not as effective as those found with the other physiological substrates Fbg A α , PAR1, and FXIII AP.

Preliminary results and future directions

Chapter 3 and 4 were mainly focused on calculating individual K_D values for amino acids that were hypothesized to contact critical residues of thrombin ABE I. It would also be valuable to know the global K_D s for PAR3P/G (44-56) and PAR1P/G (49-62) in the solution NMR buffer conditions of 150 mM NaCl and at pH 6.5. Literature provides global K_D s for PAR3 (2 μ M) and PAR1 (0.5 μ M) towards thrombin using a fluorescence based approach at very high concentration of NaCl (800 mM) and at pH 8.0.¹⁴⁸ We wanted to measure the global binding affinities of PAR3P/G (44-56) and PAR1P/G (49-62) using a label free technique in solution. For that, a Nano Isothermal Titration Calorimeter (ITC) from TA instruments was employed. ITC is a label -free biophysical technique which not only gives the binding affinities between a ligand and protein but also reveals the thermodynamic parameters of the complex formation. ITC works best if the binding affinities fall between the nM to low μ M range. Hence, we initiated our ITC project with a positive control DNA aptamer whose K_D was already published in the literature (64 nM).¹⁸⁸ The 15 base DNA aptamer (HD 1), GGTTGGTGTGGTTGG is documented to bind at ABE I of thrombin. Figure 59 represents our ITC binding curve between the DNA aptamer and bovine thrombin that gave a reasonable K_D of 164 nM (**Appendix 10**).

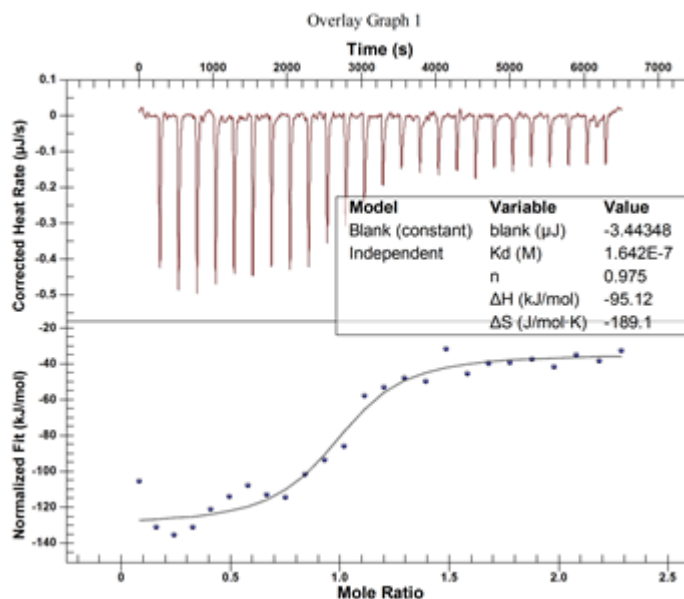


Figure 59: ITC binding curve of 2 μL injections of a 50 μM aptamer solution binding to a 7 μM solution of bovine thrombin.

With the success of ITC with the DNA aptamer and bovine thrombin, we proceeded to employ ITC for the PAR3- thrombin complex. As all our NMR titrations were performed using PPACK-thrombin, the solution conditions were matched in the ITC experiments and the PAR3 ligand was titrated into PPACK-IIa. As shown in Figure 60, the curve shape and fitting were not as good as seen with the DNA aptamer (Appendix 11). Unlike the ITC binding curve between TM and thrombin,¹⁸⁸ we found that binding of PAR3 (44-56) to thrombin generated low heats. Weak binding and lower ΔH values likely contributed to this problem. The enzyme- ligand titration system needs to be better optimized before moving on to PAR3G (44-56) or PAR1P/G (49-62) and the ternary complex consisting of GpIb α + thrombin + ABE I ligand. So far, the HSQC NMR titration was a more successful strategy for probing the affinities of PAR3 and PAR1 peptides bound to (pro)thrombin.

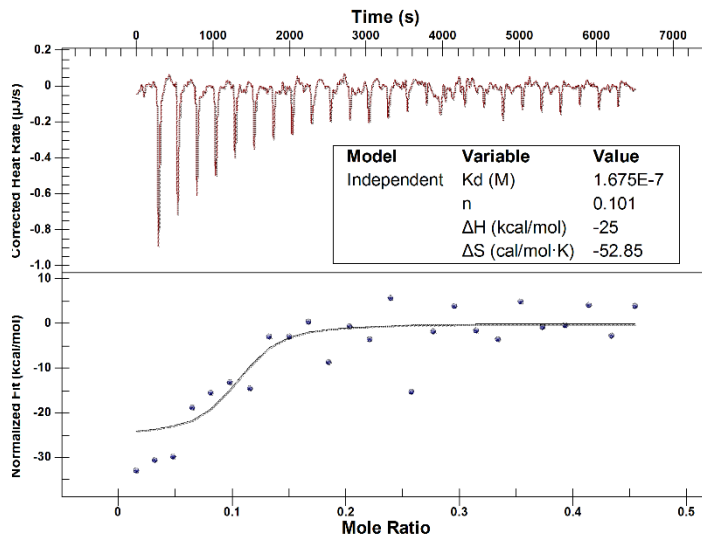


Figure 60: ITC binding curve of 2 μL injections of a 75 μM aptamer solution binding to a 50 μM solution of bovine thrombin.

The NMR titration studies from Chapter 3 and 4 revealed the roles of several individual ^{15}N - labeled amino acids from PAR3 (44-56) and PAR1 (49-62) that are involved in binding to (pro)-ABE I. There are additional residues within the sequences of PAR3 and PAR1 that are needed to be explored. A few of them would however be highly costly for custom peptide synthesis. An alternative strategy would be to express the peptides in *E. coli*. With this strategy, estimates of the binding affinities for all the individual PAR ligand amino acids could be assessed. However to study the direct thrombin-ligand contact sites and to observe long-range effects of the ligands on the thrombin, the enzyme-ligand NMR titrations should need to be switched to the protein perspective. A protocol for expressing ^{15}N -labeled thrombin has already been published¹⁸⁹ and should yield a decent amount of enzyme to carry out NMR studies. The significance of having uniformly ^{15}N labeled thrombin expression is the ability to map more thrombin-peptide contact sites and to understand the consequences of ligand-induced allostery of thrombin.

HPLC- based kinetics and solution structural information for Fbg B β (5-16) bound to thrombin in Chapter 5 indicated that Fbg B β (5-16) has weak kinetic parameters when compared to common physiological substrates like Fbg A α (7-20),⁶² FXIII (28-41) V34X,^{180,181} PAR1,⁶⁴ and PAR4.⁶⁵ An excellent strategy to compare Fbg B β binding interactions with thrombin would be to replace the Ala residue at the P₂ position of Fbg B β (5-16) with a large valine or proline. Also, the P₅ position occupied by the bulkier phenylalanine could be replaced by a slightly smaller amino acid. These substitutions may help in assessing whether there can be any improvements in the kinetic parameters and secondary structure when bound to thrombin. This information may help in assessing whether it is the thrombin specificity or the availability of Fbg B β that plays an important role in permitting Fbg A α (7-20) to be cleaved by thrombin prior to Fbg B β (5-16).

Overall, results from this dissertation project support the conclusion that thrombin is a highly dynamic enzyme that is allosterically controlled. Key regions that are affected include areas surrounding the active site, the insertion loops, and the two exosites ABE I and ABE II.^{133-135,190} Our studies have demonstrated that physiological peptide ligands based on PARs can already bind to the immature pro- ABE I of zymogen ProT. Critical maturation events not visible by X-ray crystallography have now been successfully probed through solution based NMR methodologies. For the first time, K_D values for individual ¹⁵N-labeled amino acids of PAR3¹⁵⁴ and PAR1 were estimated. As part of these studies, the changes in conformational environments that occur during the maturation events were clearly documented. Finally, long-range communication between ABE II and ABE I was proven and characterized at the single amino acid level. It would be interesting to know whether conformational changes in other clotting factors could be probed through such a

ligand perspective. A long-range goal of this research would be to develop new drugs that target unique sites within the active site region or the (pro)exosites and thereby modulate the procoagulant and anticoagulant events of thrombin.

REFERENCES

1. Donald, V., and Judith, V. G. (1995) *Biochemistry*, Wiley and Sons, Inc, New York
2. L.Nelson, D., and M.Cox, M. (2013) *Lehninger Principles of Biochemistry*, Macmillan higher education, New York
3. Schmidt, A. (1872) Neue Untersuchungen über die Faserstoffgerinnung. *Archiv für die gesamte Physiologie des Menschen und der Tiere* **6**, 413-538
4. Macfarlane, R. G. (1969) A. The blood clotting mechanism. The development of a theory of blood coagulation. *Proc R Soc Lond B Biol Sci* **173**, 261-268
5. Doolittle, R. F., Watt, K. W., Cottrell, B. A., Strong, D. D., and Riley, M. (1979) The amino acid sequence of the alpha-chain of human fibrinogen. *Nature* **280**, 464-468
6. Doolittle, R. F. (1993) The evolution of vertebrate blood coagulation: a case of Yin and Yang. *Thrombosis and haemostasis* **70**, 24-28
7. Smith, H. P., Warner, E. D., Brinkhous, K. M., and Seegers, W. H. (1938) Bleeding tendency and prothrombin deficiency in biliary fistula dogs: effect of feeding bile and vitamin k. *The Journal of experimental medicine* **67**, 911-920
8. Seegers, W. H., and Ware, A. G. (1948) Purification of prothrombin and thrombin. *Federation proceedings* **7**, 186
9. Seegers, W. H. (1949) Activation of purified prothrombin. *Proceedings of the Society for Experimental Biology and Medicine. Society for Experimental Biology and Medicine (New York, N.Y.)* **72**, 677-680
10. Laki, K., Kominz, D. R., Symonds, P., Lorand, L., and Seegers, W. H. (1954) The amino acid composition of bovine prothrombin. *Archives of biochemistry and biophysics* **49**, 276-282

11. Macfarlane, R. G. (1964) An Enzyme Cascade in the Blood Clotting Mechanism, and its Function as a Biochemical Amplifier. *Nature* **202**, 498
12. Owren, P. A. (1947) Parahaemophilia; haemorrhagic diathesis due to absence of a previously unknown clotting factor. *Lancet (London, England)* **1**, 446-448
13. Biggs, R., Douglas, A. S., and Macfarlane, R. G. (1953) The formation of thromboplastin in human blood. *The Journal of Physiology* **119**, 89-101
14. Biggs, R., Douglas, A. S., and Macfarlane, R. G. (1953) The initial stages of blood coagulation. *The Journal of Physiology* **122**, 538-553
15. Brinkhous, K. M. (1947) Clotting defect in hemophilia; deficiency in a plasma factor required for thromboplastin liberation from platelets. *Federation proceedings* **6**, 389
16. Brinkhous, K. M., and Graham, J. B. (1950) Hemophilia in the female dog. *Science (New York, N.Y.)* **111**, 723-724
17. Graham, J. B., Penick, G. D., and Brinkhous, K. M. (1951) Utilization of the antihemophilic factor during clotting of canine blood and plasma. *The American journal of physiology* **164**, 710-715
18. Brinkhous, K. M. (1954) Plasma antihemophilic factor biological and clinical aspects. *Le Sang* **25**, 738-741
19. Laki, K., and Lorand, L. (1948) On the Solubility of Fibrin Clots. *Science (New York, N.Y.)* **108**, 280
20. Chen, R., and Doolittle, R. F. (1969) Identification of the polypeptide chains involved in the cross-linking of fibrin. *Proc Natl Acad Sci U S A* **63**, 420-427
21. Davie, E. W. (2003) A brief historical review of the waterfall/cascade of blood coagulation. *The Journal of biological chemistry* **278**, 50819-50832
22. Martin, D. M., Boys, C. W., and Ruf, W. (1995) Tissue factor: molecular recognition and cofactor function. *FASEB journal : official publication of the Federation of American Societies for Experimental Biology* **9**, 852-859

23. Roberts, H. R., Hoffman, M., and Monroe, D. M. (2006) A cell-based model of thrombin generation. *Seminars in thrombosis and hemostasis* **32 Suppl 1**, 32-38
24. Monroe, D. M., Hoffman, M., and Roberts, H. R. (1996) Transmission of a procoagulant signal from tissue factor-bearing cell to platelets. *Blood coagulation & fibrinolysis : an international journal in haemostasis and thrombosis* **7**, 459-464
25. Ye, J., Liu, L. W., Esmon, C. T., and Johnson, A. E. (1992) The fifth and sixth growth factor-like domains of thrombomodulin bind to the anion-binding exosite of thrombin and alter its specificity. *The Journal of biological chemistry* **267**, 11023-11028
26. Esmon, C. T., Johnson, A. E., and Esmon, N. L. (1991) Initiation of the protein C pathway. *Annals of the New York Academy of Sciences* **614**, 30-43
27. Esmon, C. T. (2003) The protein C pathway. *Chest* **124**, 26s-32s
28. Doolittle, R. F., and Fuller, G. M. (1972) Sodium dodecyl sulfate-polyacrylamide gel electrophoresis studies on lobster fibrinogen and fibrin. *Biochimica et biophysica acta* **263**, 805-809
29. Doolittle, R. F. (1977) Structure and function of fibrinogen. *Horizons in biochemistry and biophysics* **3**, 164-191
30. Weisel, J. W. (2005) Fibrinogen and fibrin. *Advances in protein chemistry* **70**, 247-299
31. Smith, K. A., Adamson, P. J., Pease, R. J., Brown, J. M., Balmforth, A. J., Cordell, P. A., Ariens, R. A., Philippou, H., and Grant, P. J. (2011) Interactions between factor XIII and the alphaC region of fibrinogen. *Blood* **117**, 3460-3468
32. Litvinov, R. I., Yakovlev, S., Tsurupa, G., Gorkun, O. V., Medved, L., and Weisel, J. W. (2007) Direct evidence for specific interactions of the fibrinogen alphaC-domains with the central E region and with each other. *Biochemistry* **46**, 9133-9142
33. Kollman, J. M., Pandi, L., Sawaya, M. R., Riley, M., and Doolittle, R. F. (2009) Crystal structure of human fibrinogen. *Biochemistry* **48**, 3877-3886

34. Weisel, J. W., and Litvinov, R. I. (2013) Mechanisms of fibrin polymerization and clinical implications. *Blood* **121**, 1712-1719
35. Doolittle, R. F. (1973) Structural aspects of the fibrinogen to fibrin conversion. *Advances in protein chemistry* **27**, 1-109
36. Brown, J. H., Volkmann, N., Jun, G., Henschen-Edman, A. H., and Cohen, C. (2000) The crystal structure of modified bovine fibrinogen. *Proc Natl Acad Sci U S A* **97**, 85-90
37. Bode, W., Turk, D., and Karshikov, A. (1992) The refined 1.9-Å X-ray crystal structure of D-Phe-Pro-Arg chloromethylketone-inhibited human alpha-thrombin: structure analysis, overall structure, electrostatic properties, detailed active-site geometry, and structure-function relationships. *Protein science : a publication of the Protein Society* **1**, 426-471
38. Krishnaswamy, S. (2013) The transition of prothrombin to thrombin. *Journal of thrombosis and haemostasis : JTH* **11 Suppl 1**, 265-276
39. Koeppel, J. R., and Komives, E. A. (2006) Amide H/2H exchange reveals a mechanism of thrombin activation. *Biochemistry* **45**, 7724-7732
40. Dahlback, B., and Stenflo, J. (1980) The activation of prothrombin by platelet-bound factor Xa. *European journal of biochemistry* **104**, 549-557
41. Boissel, J. P., Le Bonniec, B., Rabiet, M. J., Labie, D., and Elion, J. (1984) Covalent structures of beta and gamma autolytic derivatives of human alpha-thrombin. *The Journal of biological chemistry* **259**, 5691-5697
42. Kraut, J. (1977) Serine proteases: structure and mechanism of catalysis. *Annual review of biochemistry* **46**, 331-358
43. Di Cera, E. (2009) Serine Proteases. *IUBMB life* **61**, 510-515
44. Huntington, J. A., and Esmon, C. T. (2003) The Molecular Basis of Thrombin Allostery Revealed by a 1.8 Å Structure of the "Slow" Form. *Structure* **11**, 469-479

45. Huntington, J. A. (2008) How Na⁺ activates thrombin--a review of the functional and structural data. *Biological chemistry* **389**, 1025-1035
46. Prasad, S., Cantwell, A. M., Bush, L. A., Shih, P., Xu, H., and Di Cera, E. (2004) Residue Asp-189 controls both substrate binding and the monovalent cation specificity of thrombin. *The Journal of biological chemistry* **279**, 10103-10108
47. Huntington, J. A. (2005) Molecular recognition mechanisms of thrombin. *Journal of Thrombosis and Haemostasis* **3**, 1861-1872
48. Huntington, J. A. (2012) Thrombin plasticity. *Biochimica et biophysica acta* **1824**, 246-252
49. Gandhi, P. S., Chen, Z., and Di Cera, E. (2010) Crystal structure of thrombin bound to the uncleaved extracellular fragment of PAR1. *The Journal of biological chemistry* **285**, 15393-15398
50. Bah, A., Chen, Z., Bush-Pelc, L. A., Mathews, F. S., and Di Cera, E. (2007) Crystal structures of murine thrombin in complex with the extracellular fragments of murine protease-activated receptors PAR3 and PAR4. *Proc Natl Acad Sci U S A* **104**, 11603-11608
51. Rydel, T. J., Ravichandran, K. G., Tulinsky, A., Bode, W., Huber, R., Roitsch, C., and Fenton, J. W., 2nd. (1990) The structure of a complex of recombinant hirudin and human alpha-thrombin. *Science (New York, N.Y.)* **249**, 277-280
52. Dumas, J. J., Kumar, R., Seehra, J., Somers, W. S., and Mosyak, L. (2003) Crystal structure of the GpIbalpha-thrombin complex essential for platelet aggregation. *Science (New York, N.Y.)* **301**, 222-226
53. Pineda, A. O., Chen, Z. W., Marino, F., Mathews, F. S., Mosesson, M. W., and Di Cera, E. (2007) Crystal structure of thrombin in complex with fibrinogen gamma' peptide. *Biophysical chemistry* **125**, 556-559
54. Richardson, J. L., Kroger, B., Hoeffken, W., Sadler, J. E., Pereira, P., Huber, R., Bode, W., and Fuentes-Prior, P. (2000) Crystal structure of the human alpha-thrombin-haemadin complex: an exosite II-binding inhibitor. *The EMBO journal* **19**, 5650-5660

55. Carter, W. J., Cama, E., and Huntington, J. A. (2005) Crystal structure of thrombin bound to heparin. *The Journal of biological chemistry* **280**, 2745-2749
56. Lechtenberg, B. C., Freund, S. M., and Huntington, J. A. (2012) An ensemble view of thrombin allostery. *Biological chemistry* **393**, 889-898
57. Lane, D. A., Philippou, H., and Huntington, J. A. (2005) Directing thrombin. *Blood* **106**, 2605-2612
58. Fredenburgh, J. C., Stafford, A. R., and Weitz, J. I. (1997) Evidence for allosteric linkage between exosites 1 and 2 of thrombin. *The Journal of biological chemistry* **272**, 25493-25499
59. Verhamme, I. M., Olson, S. T., Tollefsen, D. M., and Bock, P. E. (2002) Binding of exosite ligands to human thrombin. Re-evaluation of allosteric linkage between thrombin exosites I and II. *The Journal of biological chemistry* **277**, 6788-6798
60. Malovichko, M. V., Sabo, T. M., and Maurer, M. C. (2013) Ligand binding to anion-binding exosites regulates conformational properties of thrombin. *The Journal of biological chemistry* **288**, 8667-8678
61. Schechter, I., and Berger, A. (1967) On the size of the active site in proteases. I. Papain. *Biochem Biophys Res Commun* **27**, 157-162
62. Isetti, G., and Maurer, M. C. (2007) Employing mutants to study thrombin residues responsible for factor XIII activation peptide recognition: a kinetic study. *Biochemistry* **46**, 2444-2452
63. Binnie, C. G., and Lord, S. T. (1993) The fibrinogen sequences that interact with thrombin. *Blood* **81**, 3186-3192
64. Vu, T. K., Wheaton, V. I., Hung, D. T., Charo, I., and Coughlin, S. R. (1991) Domains specifying thrombin-receptor interaction. *Nature* **353**, 674-677
65. Cleary, D. B., Trumbo, T. A., and Maurer, M. C. (2002) Protease-activated receptor 4-like peptides bind to thrombin through an optimized interaction with the enzyme active site surface. *Archives of biochemistry and biophysics* **403**, 179-188

66. Mathews, II, Padmanabhan, K. P., Ganesh, V., Tulinsky, A., Ishii, M., Chen, J., Turck, C. W., Coughlin, S. R., and Fenton, J. W., 2nd. (1994) Crystallographic structures of thrombin complexed with thrombin receptor peptides: existence of expected and novel binding modes. *Biochemistry* **33**, 3266-3279
67. Schroeder, V., and Kohler, H. P. (2013) New developments in the area of factor XIII. *Journal of thrombosis and haemostasis : JTH* **11**, 234-244
68. Yee, V. C., Pedersen, L. C., Le Trong, I., Bishop, P. D., Stenkamp, R. E., and Teller, D. C. (1994) Three-dimensional structure of a transglutaminase: human blood coagulation factor XIII. *Proc Natl Acad Sci U S A* **91**, 7296-7300
69. Trumbo, T. A., and Maurer, M. C. (2000) Examining thrombin hydrolysis of the factor XIII activation peptide segment leads to a proposal for explaining the cardioprotective effects observed with the factor XIII V34L mutation. *The Journal of biological chemistry* **275**, 20627-20631
70. Muszbek, L., Yee, V. C., and Hevessy, Z. (1999) Blood coagulation factor XIII: structure and function. *Thrombosis research* **94**, 271-305
71. Sadasivan, C., and Yee, V. C. (2000) Interaction of the factor XIII activation peptide with alpha -thrombin. Crystal structure of its enzyme-substrate analog complex. *The Journal of biological chemistry* **275**, 36942-36948
72. Stieler, M., Weber, J., Hils, M., Kolb, P., Heine, A., Buchold, C., Pasternack, R., and Klebe, G. (2013) Structure of active coagulation factor XIII triggered by calcium binding: basis for the design of next-generation anticoagulants. *Angewandte Chemie* **52**, 11930-11934
73. Anokhin, B. A., Stribinskis, V., Dean, W. L., and Maurer, M. C. (2017) Activation of factor XIII is accompanied by a change in oligomerization state. *The FEBS journal* **284**, 3849-3861
74. Du, X. (2007) Signaling and regulation of the platelet glycoprotein Ib-IX-V complex. *Current opinion in hematology* **14**, 262-269
75. Clemetson, K. J. (2007) A short history of platelet glycoprotein Ib complex. *Thrombosis and haemostasis* **98**, 63-68

76. Crawley, J. T., Zanardelli, S., Chion, C. K., and Lane, D. A. (2007) The central role of thrombin in hemostasis. *Journal of thrombosis and haemostasis : JTH* **5 Suppl 1**, 95-101
77. Andrews, R. K., Gardiner, E. E., Shen, Y., Whisstock, J. C., and Berndt, M. C. (2003) Glycoprotein Ib-IX-V. *The international journal of biochemistry & cell biology* **35**, 1170-1174
78. Sabo, T. M., and Maurer, M. C. (2009) Biophysical investigation of GpIbalpha binding to thrombin anion binding exosite II. *Biochemistry* **48**, 7110-7122
79. Lechtenberg, B. C., Freund, S. M., and Huntington, J. A. (2014) GpIbalpha interacts exclusively with exosite II of thrombin. *Journal of molecular biology* **426**, 881-893
80. De Candia, E., Hall, S. W., Rutella, S., Landolfi, R., Andrews, R. K., and De Cristofaro, R. (2001) Binding of thrombin to glycoprotein Ib accelerates the hydrolysis of Par-1 on intact platelets. *The Journal of biological chemistry* **276**, 4692-4698
81. Coughlin, S. R. (1999) Protease-activated receptors and platelet function. *Thrombosis and haemostasis* **82**, 353-356
82. Coughlin, S. R. (2000) Thrombin signalling and protease-activated receptors. *Nature* **407**, 258-264
83. Schmidt, V. A., Nierman, W. C., Maglott, D. R., Cupit, L. D., Moskowitz, K. A., Wainer, J. A., and Bahou, W. F. (1998) The human proteinase-activated receptor-3 (PAR-3) gene. Identification within a Par gene cluster and characterization in vascular endothelial cells and platelets. *The Journal of biological chemistry* **273**, 15061-15068
84. Seeley, S., Covic, L., Jacques, S. L., Sudmeier, J., Baleja, J. D., and Kuliopulos, A. (2003) Structural basis for thrombin activation of a protease-activated receptor: inhibition of intramolecular liganding. *Chemistry & biology* **10**, 1033-1041
85. Gandhi, P. S., Chen, Z., Mathews, F. S., and Di Cera, E. (2008) Structural identification of the pathway of long-range communication in an allosteric enzyme. *Proc Natl Acad Sci U S A* **105**, 1832-1837

86. Nakanishi-Matsui, M., Zheng, Y. W., Sulciner, D. J., Weiss, E. J., Ludeman, M. J., and Coughlin, S. R. (2000) PAR3 is a cofactor for PAR4 activation by thrombin. *Nature* **404**, 609-613
87. Raskob, G. E., Angchaisuksiri, P., Blanco, A. N., Buller, H., Gallus, A., Hunt, B. J., Hylek, E. M., Kakkar, A., Konstantinides, S. V., McCumber, M., Ozaki, Y., Wendelboe, A., and Weitz, J. I. (2014) Thrombosis: a major contributor to global disease burden. *Arteriosclerosis, thrombosis, and vascular biology* **34**, 2363-2371
88. van der Poll, T., and Herwald, H. (2014) The coagulation system and its function in early immune defense. *Thrombosis and haemostasis* **112**, 640-648
89. Huntington, J. A. (2005) Molecular recognition mechanisms of thrombin. *Journal of thrombosis and haemostasis : JTH* **3**, 1861-1872
90. Harter, K., Levine, M., and Henderson, S. O. (2015) Anticoagulation Drug Therapy: A Review. *Western Journal of Emergency Medicine* **16**, 11-17
91. Norn, S., Permin, H., Kruse, E., and Kruse, P. R. (2014) [On the history of vitamin K, dicoumarol and warfarin]. *Dansk medicinhistorisk arbog* **42**, 99-119
92. Gray, E., Hogwood, J., and Mulloy, B. (2012) The anticoagulant and antithrombotic mechanisms of heparin. *Handbook of experimental pharmacology*, 43-61
93. Cabral, K. P., and Ansell, J. E. (2015) The role of factor Xa inhibitors in venous thromboembolism treatment. *Vascular Health and Risk Management* **11**, 117-123
94. Lee, C. J., and Ansell, J. E. (2011) Direct thrombin inhibitors. *British Journal of Clinical Pharmacology* **72**, 581-592
95. van Es, N., Bleker, S. M., Buller, H. R., and Coppens, M. (2013) New developments in parenteral anticoagulation for arterial and venous thromboembolism. *Best practice & research. Clinical haematology* **26**, 203-213
96. Bock, L. C., Griffin, L. C., Latham, J. A., Vermaas, E. H., and Toole, J. J. (1992) Selection of single-stranded DNA molecules that bind and inhibit human thrombin. *Nature* **355**, 564-566

97. Kubik, M. F., Stephens, A. W., Schneider, D., Marlar, R. A., and Tasset, D. (1994) High-affinity RNA ligands to human alpha-thrombin. *Nucleic Acids Research* **22**, 2619-2626
98. Sidhu, P. S., Liang, A., Mehta, A. Y., Abdel Aziz, M. H., Zhou, Q., and Desai, U. R. (2011) Rational design of potent, small, synthetic allosteric inhibitors of thrombin. *Journal of medicinal chemistry* **54**, 5522-5531
99. Gopinath, S. C. (2007) Methods developed for SELEX. *Analytical and bioanalytical chemistry* **387**, 171-182
100. Monteiro, R. Q., and Zingali, R. B. (2000) Inhibition of prothrombin activation by bothrojaracin, a C-type lectin from Bothrops jararaca venom. *Archives of biochemistry and biophysics* **382**, 123-128
101. Monteiro, R. Q., Bock, P. E., Bianconi, M. L., and Zingali, R. B. (2001) Characterization of bothrojaracin interaction with human prothrombin. *Protein science : a publication of the Protein Society* **10**, 1897-1904
102. Lin, H., Liu, A. P., Smith, T. H., and Trejo, J. (2013) Cofactoring and dimerization of proteinase-activated receptors. *Pharmacological reviews* **65**, 1198-1213
103. Leger, A. J., Jacques, S. L., Badar, J., Kaneider, N. C., Derian, C. K., Andrade-Gordon, P., Covic, L., and Kuliopulos, A. (2006) Blocking the protease-activated receptor 1-4 heterodimer in platelet-mediated thrombosis. *Circulation* **113**, 1244-1254
104. Rule, G. S., and Hitchens, T. K. (2006) *Fundamentals of Protein NMR Spectroscopy*, Springer, Dordrecht, The Netherlands
105. Kemp, W. (2008) *Organic Spectroscopy*, Palgrave, New York
106. Kleckner, I. R., and Foster, M. P. (2011) An introduction to NMR-based approaches for measuring protein dynamics. *Biochimica et biophysica acta* **1814**, 942-968
107. Keeler, J. (2010) *Understanding NMR Spectroscopy*, Wiley, West Sussex, United Kingdom

108. Wuthrich, K. (1986) *NMR of Proteins and Nucleic Acids*, Wiley- Interscience, United States of America
109. Ni, F. (1994) Recent developments in transferred NOE methods. *Progress in nuclear magnetic resonance spectroscopy* **26**, 517-606
110. Ni, F., and Scheraga, H. A. (1994) Use of the transferred nuclear Overhauser effect to determine the conformations of ligands bound to proteins. *Accounts of chemical research* **27**, 257-264
111. Campbell, A. P., and Sykes, B. D. (1993) The two-dimensional transferred nuclear Overhauser effect: theory and practice. *Annual review of biophysics and biomolecular structure* **22**, 99-122
112. Ni, F., Konishi, Y., and Scheraga, H. A. (1990) Thrombin-bound conformation of the C-terminal fragments of hirudin determined by transferred nuclear Overhauser effects. *Biochemistry* **29**, 4479-4489
113. Williamson, M. P. (2013) Using chemical shift perturbation to characterise ligand binding. *Progress in nuclear magnetic resonance spectroscopy* **73**, 1-16
114. Leavitt, S., and Freire, E. (2001) Direct measurement of protein binding energetics by isothermal titration calorimetry. *Current opinion in structural biology* **11**, 560-566
115. Pierce, M. M., Raman, C. S., and Nall, B. T. (1999) Isothermal titration calorimetry of protein-protein interactions. *Methods (San Diego, Calif.)* **19**, 213-221
116. Freyer, M. W., and Lewis, E. A. (2008) Isothermal titration calorimetry: experimental design, data analysis, and probing macromolecule/ligand binding and kinetic interactions. *Methods in cell biology* **84**, 79-113
117. Wiseman, T., Williston, S., Brandts, J. F., and Lin, L. N. (1989) Rapid measurement of binding constants and heats of binding using a new titration calorimeter. *Analytical biochemistry* **179**, 131-137
118. Turnbull, W. B., and Daranas, A. H. (2003) On the value of c: can low affinity systems be studied by isothermal titration calorimetry? *Journal of the American Chemical Society* **125**, 14859-14866

119. Brufatto, N., and Nesheim, M. E. (2003) Analysis of the kinetics of prothrombin activation and evidence that two equilibrating forms of prothrombinase are involved in the process. *The Journal of biological chemistry* **278**, 6755-6764
120. Pozzi, N., Chen, Z., Gohara, D. W., Niu, W., Heyduk, T., and Di Cera, E. (2013) Crystal structure of prothrombin reveals conformational flexibility and mechanism of activation. *The Journal of biological chemistry* **288**, 22734-22744
121. Pozzi, N., Bystranowska, D., Zuo, X., and Di Cera, E. (2016) Structural Architecture of Prothrombin in Solution Revealed by Single Molecule Spectroscopy. *The Journal of biological chemistry* **291**, 18107-18116
122. Wu, Q., Picard, V., Aiach, M., and Sadler, J. E. (1994) Activation-induced exposure of the thrombin anion-binding exosite. Interactions of recombinant mutant prothrombins with thrombomodulin and a thrombin exosite-specific antibody. *The Journal of biological chemistry* **269**, 3725-3730
123. Mehta, A. Y., Thakkar, J. N., Mohammed, B. M., Martin, E. J., Brophy, D. F., Kishimoto, T., and Desai, U. R. (2014) Targeting the GPIIb/IIIa binding site of thrombin to simultaneously induce dual anticoagulant and antiplatelet effects. *Journal of medicinal chemistry* **57**, 3030-3039
124. Mehta, A. Y., Mohammed, B. M., Martin, E. J., Brophy, D. F., Gailani, D., and Desai, U. R. (2016) Allosterism-based simultaneous, dual anticoagulant and antiplatelet action: allosteric inhibitor targeting the glycoprotein IIb/IIIa-binding and heparin-binding site of thrombin. *Journal of thrombosis and haemostasis : JTH* **14**, 828-838
125. Ni, F., Ning, Q., Jackson, C. M., and Fenton, J. W., 2nd. (1993) Thrombin exosite for fibrinogen recognition is partially accessible in prothrombin. *The Journal of biological chemistry* **268**, 16899-16902
126. Anderson, P. J., Nasset, A., Dharmawardana, K. R., and Bock, P. E. (2000) Characterization of proexosite I on prothrombin. *The Journal of biological chemistry* **275**, 16428-16434
127. Kretz, C. A., Stafford, A. R., Fredenburgh, J. C., and Weitz, J. I. (2006) HD1, a thrombin-directed aptamer, binds exosite 1 on prothrombin with high affinity and inhibits its activation by prothrombinase. *The Journal of biological chemistry* **281**, 37477-37485

128. Bompiani, K. M., Monroe, D. M., Church, F. C., and Sullenger, B. A. (2012) A high affinity, antidote-controllable prothrombin and thrombin-binding RNA aptamer inhibits thrombin generation and thrombin activity. *Journal of thrombosis and haemostasis : JTH* **10**, 870-880
129. Kahn, M. L., Zheng, Y. W., Huang, W., Bigornia, V., Zeng, D., Moff, S., Farese, R. V., Jr., Tam, C., and Coughlin, S. R. (1998) A dual thrombin receptor system for platelet activation. *Nature* **394**, 690-694
130. Steinberg, S. F. (2005) The cardiovascular actions of protease-activated receptors. *Molecular pharmacology* **67**, 2-11
131. Koradi, R., Billeter, M., and Wuthrich, K. (1996) MOLMOL: a program for display and analysis of macromolecular structures. *Journal of molecular graphics* **14**, 51-55, 29-32
132. Lechtenberg, B. C., Johnson, D. J., Freund, S. M., and Huntington, J. A. (2010) NMR resonance assignments of thrombin reveal the conformational and dynamic effects of ligation. *Proc Natl Acad Sci U S A* **107**, 14087-14092
133. Fuglestad, B., Gasper, P. M., Tonelli, M., McCammon, J. A., Markwick, P. R., and Komives, E. A. (2012) The dynamic structure of thrombin in solution. *Biophys J* **103**, 79-88
134. Fuglestad, B., Gasper, P. M., McCammon, J. A., Markwick, P. R., and Komives, E. A. (2013) Correlated motions and residual frustration in thrombin. *The journal of physical chemistry. B* **117**, 12857-12863
135. Handley, L. D., Fuglestad, B., Stearns, K., Tonelli, M., Fenwick, R. B., Markwick, P. R., and Komives, E. A. (2017) NMR reveals a dynamic allosteric pathway in thrombin. *Scientific reports* **7**, 39575
136. Markin, C. J., and Spyropoulos, L. (2012) Increased precision for analysis of protein-ligand dissociation constants determined from chemical shift titrations. *Journal of biomolecular NMR* **53**, 125-138
137. Marino, F., Pelc, L. A., Vogt, A., Gandhi, P. S., and Di Cera, E. (2010) Engineering thrombin for selective specificity toward protein C and PAR1. *The Journal of biological chemistry* **285**, 19145-19152

138. Teilum, K., Kunze, M. B., Erlendsson, S., and Kragelund, B. B. (2017) (S)Pinning down protein interactions by NMR. *Protein science : a publication of the Protein Society* **26**, 436-451
139. Fielding, L. (2003) NMR methods for the determination of protein-ligand dissociation constants. *Current topics in medicinal chemistry* **3**, 39-53
140. Iconaru, L. I., Ban, D., Bharatham, K., Ramanathan, A., Zhang, W., Shelat, A. A., Zuo, J., and Kriwacki, R. W. (2015) Discovery of Small Molecules that Inhibit the Disordered Protein, p27(Kip1). *Scientific reports* **5**, 15686
141. Weitz, J. I., Lensing, A. W. A., Prins, M. H., Bauersachs, R., Beyer-Westendorf, J., Bounameaux, H., Brighton, T. A., Cohen, A. T., Davidson, B. L., Decousus, H., Freitas, M. C. S., Holberg, G., Kakkar, A. K., Haskell, L., van Bellen, B., Pap, A. F., Berkowitz, S. D., Verhamme, P., Wells, P. S., and Prandoni, P. (2017) Rivaroxaban or Aspirin for Extended Treatment of Venous Thromboembolism. *The New England journal of medicine* **376**, 1211-1222
142. Connolly, S. J., Ezekowitz, M. D., Yusuf, S., Eikelboom, J., Oldgren, J., Parekh, A., Pogue, J., Reilly, P. A., Themeles, E., Varrone, J., Wang, S., Alings, M., Xavier, D., Zhu, J., Diaz, R., Lewis, B. S., Darius, H., Diener, H. C., Joyner, C. D., and Wallentin, L. (2009) Dabigatran versus warfarin in patients with atrial fibrillation. *The New England journal of medicine* **361**, 1139-1151
143. Salmeron Febres, L. M., and Cuenca Manteca, J. (2017) Direct Oral Anticoagulants in the Treatment of Venous Thromboembolic Disease. *Annals of vascular surgery*
144. Dager, W. E., and Banares, L. (2017) Reversing the anticoagulation effects of dabigatran. *Hospital practice (1995)* **45**, 29-38
145. Weitz, J. I. (2017) Reversal of Direct Oral Anticoagulants: Current Status and Future Directions. *Seminars in respiratory and critical care medicine* **38**, 40-50
146. Bock, P. E., Panizzi, P., and Verhamme, I. M. (2007) Exosites in the substrate specificity of blood coagulation reactions. *Journal of thrombosis and haemostasis : JTH* **5 Suppl 1**, 81-94
147. Kretz, C. A., Stafford, A. R., Fredenburgh, J. C., and Weitz, J. I. (2015) HD1, a thrombin-directed aptamer, binds exosite 1 on prothrombin with high affinity and

inhibits its activation by prothrombinase. *The Journal of biological chemistry* **290**, 4813

148. Krem, M. M., and Di Cera, E. (2003) Dissecting substrate recognition by thrombin using the inactive mutant S195A. *Biophysical chemistry* **100**, 315-323
149. Myles, T., Le Bonniec, B. F., Betz, A., and Stone, S. R. (2001) Electrostatic steering and ionic tethering in the formation of thrombin-hirudin complexes: the role of the thrombin anion-binding exosite-I. *Biochemistry* **40**, 4972-4979
150. Myles, T., Le Bonniec, B. F., and Stone, S. R. (2001) The dual role of thrombin's anion-binding exosite-I in the recognition and cleavage of the protease-activated receptor 1. *European journal of biochemistry* **268**, 70-77
151. Boehr, D. D., Nussinov, R., and Wright, P. E. (2009) The role of dynamic conformational ensembles in biomolecular recognition. *Nature chemical biology* **5**, 789-796
152. Tzeng, S. R., and Kalodimos, C. G. (2012) Protein activity regulation by conformational entropy. *Nature* **488**, 236-240
153. Wei, G., Xi, W., Nussinov, R., and Ma, B. (2016) Protein Ensembles: How Does Nature Harness Thermodynamic Fluctuations for Life? The Diverse Functional Roles of Conformational Ensembles in the Cell. *Chemical reviews* **116**, 6516-6551
154. Billur, R., Ban, D., Sabo, T. M., and Maurer, M. C. (2017) Deciphering Conformational Changes Associated with the Maturation of Thrombin Anion Binding Exosite I. *Biochemistry* **56**, 6343-6354
155. Ayala, Y. M., Cantwell, A. M., Rose, T., Bush, L. A., Arosio, D., and Di Cera, E. (2001) Molecular mapping of thrombin-receptor interactions. *Proteins* **45**, 107-116
156. Macfarlane, S. R., Seatter, M. J., Kanke, T., Hunter, G. D., and Plevin, R. (2001) Proteinase-activated receptors. *Pharmacological reviews* **53**, 245-282
157. McLaughlin, J. N., Patterson, M. M., and Malik, A. B. (2007) Protease-activated receptor-3 (PAR3) regulates PAR1 signaling by receptor dimerization. *Proc Natl Acad Sci U S A* **104**, 5662-5667

158. Even-Ram, S., Uziely, B., Cohen, P., Grisaru-Granovsky, S., Maoz, M., Ginzburg, Y., Reich, R., Vlodavsky, I., and Bar-Shavit, R. (1998) Thrombin receptor overexpression in malignant and physiological invasion processes. *Nature medicine* **4**, 909-914
159. Kamath, L., Meydani, A., Foss, F., and Kuliopulos, A. (2001) Signaling from protease-activated receptor-1 inhibits migration and invasion of breast cancer cells. *Cancer research* **61**, 5933-5940
160. Nieman, M. T. (2016) Protease-activated receptors in hemostasis. *Blood* **128**, 169-177
161. Rydel, T. J., Tulinsky, A., Bode, W., and Huber, R. (1991) Refined structure of the hirudin-thrombin complex. *Journal of molecular biology* **221**, 583-601
162. Li, C. Q., Vindigni, A., Sadler, J. E., and Wardell, M. R. (2001) Platelet glycoprotein Ib alpha binds to thrombin anion-binding exosite II inducing allosteric changes in the activity of thrombin. *The Journal of biological chemistry* **276**, 6161-6168
163. De Cristofaro, R., and De Filippis, V. (2003) Interaction of the 268-282 region of glycoprotein Ibalpha with the heparin-binding site of thrombin inhibits the enzyme activation of factor VIII. *The Biochemical journal* **373**, 593-601
164. Petretera, N. S., Stafford, A. R., Leslie, B. A., Kretz, C. A., Fredenburgh, J. C., and Weitz, J. I. (2009) Long range communication between exosites 1 and 2 modulates thrombin function. *The Journal of biological chemistry* **284**, 25620-25629
165. De Marco, L., Mazzucato, M., Masotti, A., and Ruggeri, Z. M. (1994) Localization and characterization of an alpha-thrombin-binding site on platelet glycoprotein Ib alpha. *The Journal of biological chemistry* **269**, 6478-6484
166. Jacques, S. L., LeMasurier, M., Sheridan, P. J., Seeley, S. K., and Kuliopulos, A. (2000) Substrate-assisted catalysis of the PAR1 thrombin receptor. Enhancement of macromolecular association and cleavage. *The Journal of biological chemistry* **275**, 40671-40678
167. Bradford, H. N., and Krishnaswamy, S. (2016) The Fragment 1 Region of Prothrombin Facilitates the Favored Binding of Fragment 12 to Zymogen and

Enforces Zymogen-like Character in the Proteinase. *The Journal of biological chemistry* **291**, 11114-11123

168. Chen, K., Stafford, A. R., Wu, C., Yeh, C. H., Kim, P. Y., Fredenburgh, J. C., and Weitz, J. I. (2017) Exosite 2-Directed Ligands Attenuate Protein C Activation by the Thrombin-Thrombomodulin Complex. *Biochemistry* **56**, 3119-3128
169. Di Cera, E. (2008) Thrombin. *Molecular aspects of medicine* **29**, 203-254
170. Pechik, I., Yakovlev, S., Mosesson, M. W., Gilliland, G. L., and Medved, L. (2006) Structural basis for sequential cleavage of fibrinopeptides upon fibrin assembly. *Biochemistry* **45**, 3588-3597
171. Schroeder, V., and Kohler, H. P. (2016) Factor XIII: Structure and Function. *Seminars in thrombosis and hemostasis* **42**, 422-428
172. Martinelli, R. A., and Scheraga, H. A. (1980) Steady-state kinetic study of the bovine thrombin-fibrinogen interaction. *Biochemistry* **19**, 2343-2350
173. Koopman, J., Haverkate, F., Lord, S. T., Grimbergen, J., and Mannucci, P. M. (1992) Molecular basis of fibrinogen Naples associated with defective thrombin binding and thrombophilia. Homozygous substitution of B beta 68 Ala----Thr. *The Journal of clinical investigation* **90**, 238-244
174. Lounes, K. C., Lefkowitz, J. B., Coates, A. I., Hantgan, R. R., Henschen-Edman, A., and Lord, S. T. (2001) Fibrinogen Longmont. A heterozygous abnormal fibrinogen with B beta Arg-166 to Cys substitution associated with defective fibrin polymerization. *Annals of the New York Academy of Sciences* **936**, 129-132
175. Koopman, J., Haverkate, F., Grimbergen, J., Engesser, L., Novakova, I., Kerst, A. F., and Lord, S. T. (1992) Abnormal fibrinogens IJmuiden (B beta Arg14----Cys) and Nijmegen (B beta Arg44----Cys) form disulfide-linked fibrinogen-albumin complexes. *Proc Natl Acad Sci U S A* **89**, 3478-3482
176. Rooney, M. M., Mullin, J. L., and Lord, S. T. (1998) Substitution of tyrosine for phenylalanine in fibrinopeptide A results in preferential thrombin cleavage of fibrinopeptide B from fibrinogen. *Biochemistry* **37**, 13704-13709

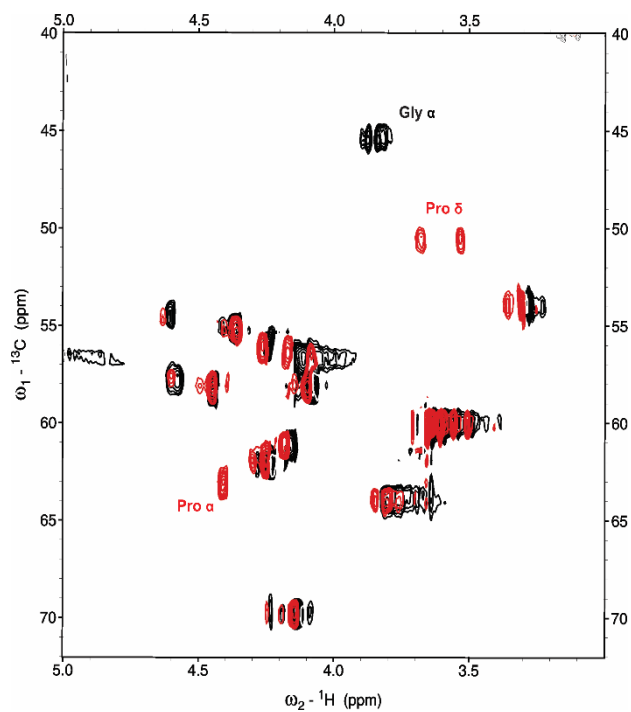
177. Riedel, T., Suttnar, J., Brynda, E., Houska, M., Medved, L., and Dyr, J. E. (2011) Fibrinopeptides A and B release in the process of surface fibrin formation. *Blood* **117**, 1700-1706
178. Mullin, J. L., Gorkun, O. V., Binnie, C. G., and Lord, S. T. (2000) Recombinant fibrinogen studies reveal that thrombin specificity dictates order of fibrinopeptide release. *The Journal of biological chemistry* **275**, 25239-25246
179. Brummel, K. E., Butenas, S., and Mann, K. G. (1999) An integrated study of fibrinogen during blood coagulation. *The Journal of biological chemistry* **274**, 22862-22870
180. Jadhav, M. A., Lucas, R. C., Goldsberry, W. N., and Maurer, M. C. (2011) Design of Factor XIII V34X activation peptides to control ability to interact with thrombin mutants. *Biochimica et Biophysica Acta (BBA) - Proteins and Proteomics* **1814**, 1955-1963
181. Jadhav, M. A., Goldsberry, W. N., Zink, S. E., Lamb, K. N., Simmons, K. E., Riposo, C. M., Anokhin, B. A., and Maurer, M. C. (2017) Screening cleavage of Factor XIII V34X Activation Peptides by thrombin mutants: A strategy for controlling fibrin architecture. *Biochimica et biophysica acta* **1865**, 1246-1254
182. Rose, T., and Di Cera, E. (2002) Three-dimensional modeling of thrombin-fibrinogen interaction. *The Journal of biological chemistry* **277**, 18875-18880
183. Trumbo, T. A., and Maurer, M. C. (2002) Thrombin hydrolysis of V29F and V34L mutants of factor XIII (28-41) reveals roles of the P(9) and P(4) positions in factor XIII activation. *Biochemistry* **41**, 2859-2868
184. Isetti, G., and Maurer, M. C. (2004) Probing thrombin's ability to accommodate a V34F substitution within the factor XIII activation peptide segment (28-41). *The journal of peptide research : official journal of the American Peptide Society* **63**, 241-252
185. Di Cera, E., Page, M. J., Bah, A., Bush-Pelc, L. A., and Garvey, L. C. (2007) Thrombin allostery. *Physical chemistry chemical physics : PCCP* **9**, 1291-1306
186. Eikelboom, J. W., and Hankey, G. J. (2002) Low molecular weight heparins and heparinoids. *The Medical journal of Australia* **177**, 379-383

187. Pozzi, N., Chen, Z., Zapata, F., Niu, W., Barranco-Medina, S., Pelc, L. A., and Di Cera, E. (2013) Autoactivation of thrombin precursors. *The Journal of biological chemistry* **288**, 11601-11610
188. Treuheit, N. A., Beach, M. A., and Komives, E. A. (2011) Thermodynamic compensation upon binding to exosite 1 and the active site of thrombin. *Biochemistry* **50**, 4590-4596
189. Johnson, D. J., Adams, T. E., Li, W., and Huntington, J. A. (2005) Crystal structure of wild-type human thrombin in the Na⁺-free state. *The Biochemical journal* **392**, 21-28
190. Gasper, P. M., Fuglestad, B., Komives, E. A., Markwick, P. R., and McCammon, J. A. (2012) Allosteric networks in thrombin distinguish procoagulant vs. anticoagulant activities. *Proc Natl Acad Sci U S A* **109**, 21216-21222

APPENDICES

APPENDIX 1

An overlay of the 2D ^{13}C - ^1H natural abundance HSQC NMR spectra of 1 mM PAR3 (44-56) and 1mM PAR3G (44-56):

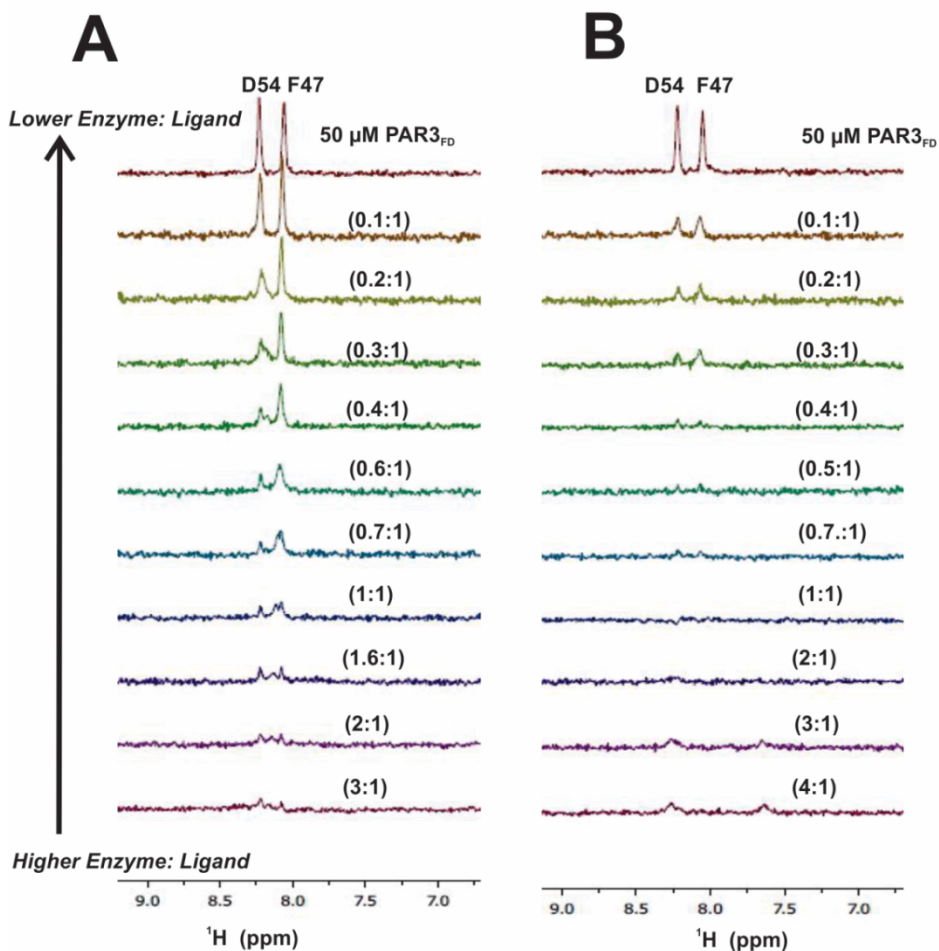


All NMR samples were in 25mM H_3PO_4 , 150 mM NaCl, 0.2 mM EDTA and 10 % D_2O (pH 6.5). The PAR3 residues are in red whereas the PAR3G are in black. The expected cross peaks for the unique residues Pro51 versus Gly51 are labeled.

APPENDIX 2

1D ^{15}N -HSQC NMR titrations of PAR3_{FD} (44-56) in the presence of ProT and

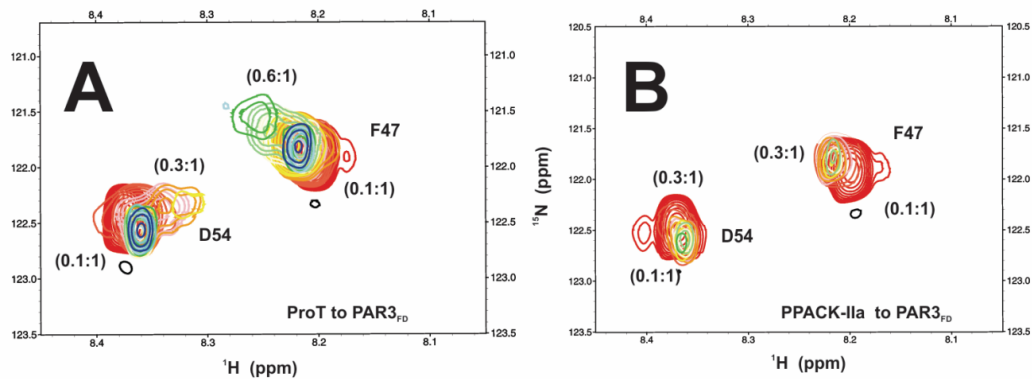
PPACK- IIa:



All NMR samples were in 25mM H_3PO_4 , 150 mM NaCl, 0.2 mM EDTA and 10 % D_2O (pH 6.5). A) For the PAR3_{FD} binding studies with ProT, starting complexes included 50 μM PAR3_{FD} (44-56, ^{15}N -F47, ^{15}N -D54) in 137 μM ProT. The serial dilutions resulted in ProT to PAR3 ratios that spanned from 3:1 to 0.1:1. B) For PPACK- IIa, starting complexes included 50 μM PAR3_{FD} (44-56, ^{15}N -F47, ^{15}N -D54) in 210 μM PPACK- IIa. The serial dilutions resulted in PPACK- IIa to PAR3_{FD} ratios that spanned from 4:1 to 0.1:1. Representative data sets are shown

APPENDIX 3

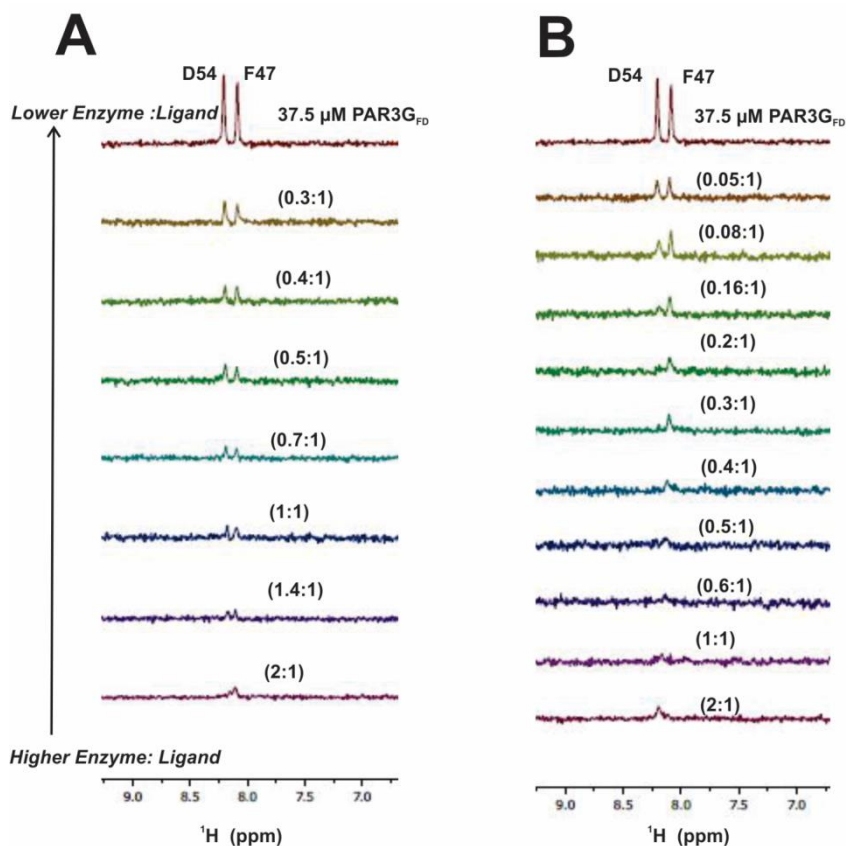
2D ^1H - ^{15}N HSQC NMR titrations of PAR3_{FD} (44-56) in the presence of ProT and PPACK-IIa:



All NMR samples were in 25mM H_3PO_4 , 150 mM NaCl, 0.2 mM EDTA and 10 % D_2O (pH 6.5). A) For the PAR3_{FD} binding studies with ProT, starting complexes included 50 μM PAR3_{FD} (44-56, ^{15}N -F47, ^{15}N -D54) in 130 μM ProT. The serial dilutions resulted in ProT to PAR3_{FD} ratios that spanned from 3:1 to 0.1:1. B) For PPACK-IIa, starting complexes included 50 μM PAR3_{FD} (44-56, ^{15}N -F47, ^{15}N -D54) in 210 μM PPACK-IIa. The serial dilutions resulted in PPACK-IIa to PAR3_{FD} ratios that spanned from 4:1 to 0.1:1. Representative data sets are shown. Colors for the HSQC crosspeaks span from blue (highest protein-peptide ratio) to red (free peptide).

APPENDIX 4

1D ^{15}N -HSQC NMR titrations of PAR3G_{FD} (44-56) in the presence of ProT and PPACK- IIa:

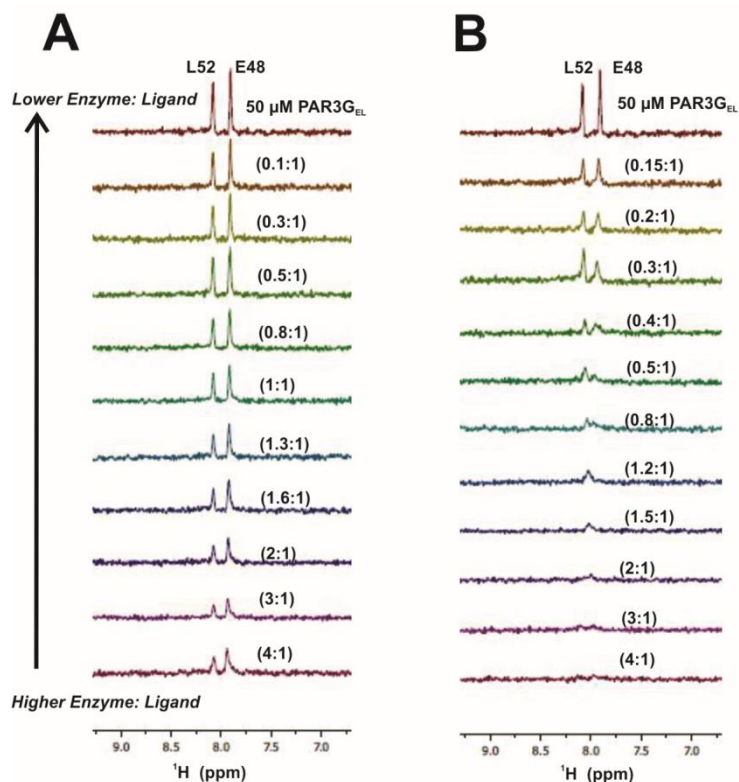


All NMR samples were in 25mM H_3PO_4 , 150 mM NaCl, 0.2 mM EDTA and 10 % D_2O (pH 6.5). A) For the PAR3G_{FD} binding studies with ProT, starting complexes included 37.5 μM PAR3G_{FD} (44-56, ^{15}N -F47, ^{15}N -D54) in 70 μM ProT. The serial dilutions resulted in ProT to PAR3G ratios that spanned from 2:1 to 0.3:1. B) For PPACK- IIa, starting complexes included 37.5 μM PAR3G_{FD} (44-56, ^{15}N -F47, ^{15}N -D54) in 70 μM PPACK- IIa. The serial dilutions resulted in PPACK- IIa to PAR3G_{FD} ratios that spanned from 2:1 to 0.05:1. Representative data sets are shown.

APPENDIX 5

^{15}N HSQC NMR titrations of PAR3G_{EL} (44-56) in the presence of ProT and

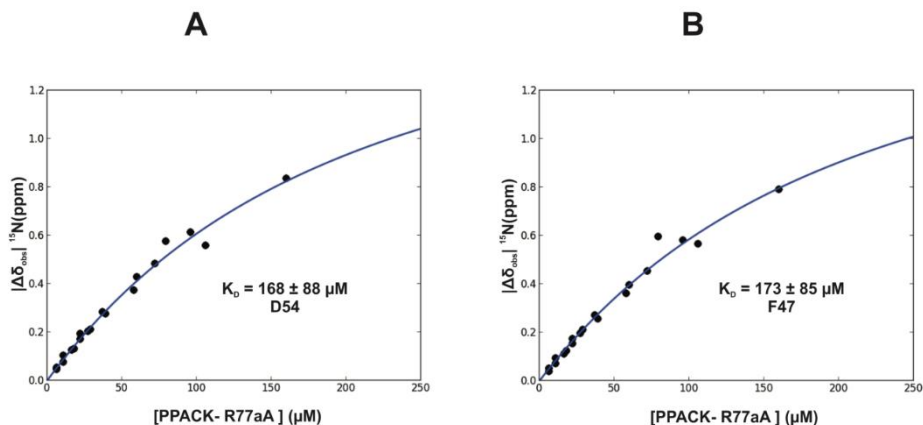
PPACK- IIa:



All NMR samples were in 25mM H_3PO_4 , 150 mM NaCl, 0.2 mM EDTA and 10 % D_2O (pH 6.5). A) For the PAR3G_{EL} binding studies with ProT, starting complexes included 50 μM PAR3G_{EL} (44-56, ^{15}N -E48, ^{15}N -L52) in 180 μM ProT. The serial dilutions resulted in ProT to PAR3G ratios that spanned from 4:1 to 0.1:1. B) For PPACK- IIa, starting complexes included 50 μM PAR3G_{EL} (44-56, ^{15}N -E48, ^{15}N -L52) in 211 μM PPACK- IIa. The serial dilutions resulted in PPACK- IIa to PAR3G_{EL} ratios that spanned from 4:1 to 0.1:1. Representative data sets are shown.

APPENDIX 6

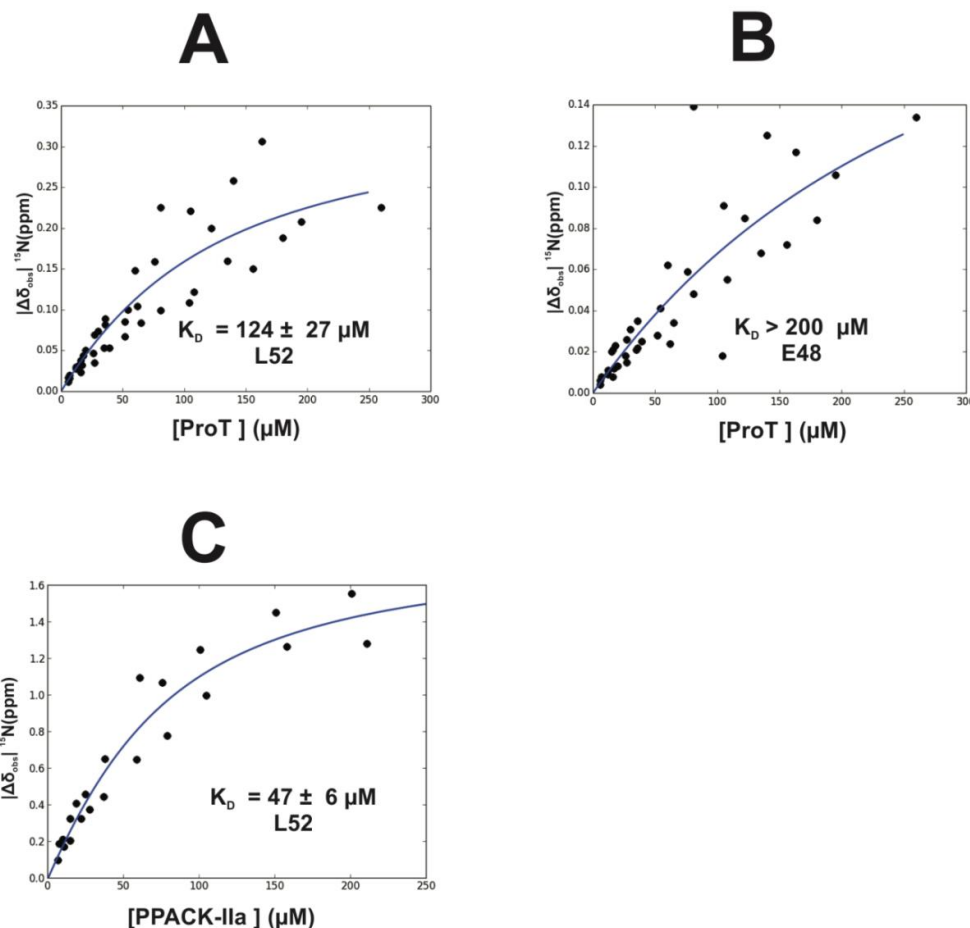
Determination of Binding Affinity (K_D) for ^{15}N -labeled F47 and D54 of PAR3G_{FD} interacting with PPACK-R77aA IIa:



For this NMR titration series, the peptide ligand concentration was kept constant and the ProT and PPACK-R77aA IIa concentrations were serially diluted. As a result, the NMR titrations were measuring the binding of protein to a defined peptide concentration. A) Interactions between PPACK-R77aA IIa and PAR3G ^{15}N -D54 led to a $K_D = 168 \pm 88 \mu\text{M}$ and B) ProT and PAR3G ^{15}N -F47 led to a $K_D = 173 \pm 85 \mu\text{M}$. NMR titrations were done in duplicate. The reported K_D values were determined using in-house scripts written using Python. The term $|\Delta\delta_{\text{obs}}|^{15}\text{Nppm} = \delta^{15}\text{N}_{\text{Bound}} - \delta^{15}\text{N}_{\text{Free}}$ reflects the absolute difference in chemical shift between the bound and free states of the particular ^{15}N -amide. Error analysis was carried out using a Monte-Carlo approach assuming a 10% error in the serially diluted protein samples. See Materials and Methods for more details.

APPENDIX 7

Determination of Binding Affinity (K_D) for ^{15}N -labeled L52 and E48 of PAR3G_{FD} interacting with Prothrombin and PPACK-IIa:



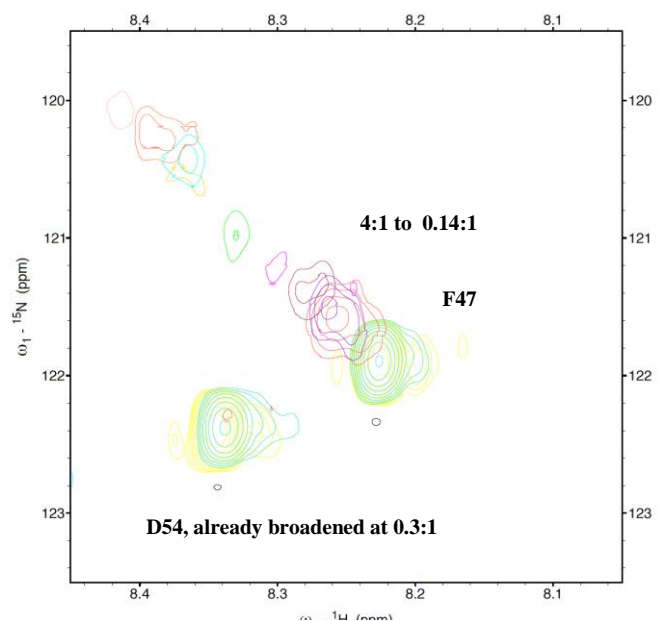
For this NMR titration series, the peptide ligand concentration was kept constant and the ProT and PPACK-IIa concentrations were serially diluted. As a result, the NMR titrations were measuring the binding of protein to a defined peptide concentration. A) Interactions between ProT and PAR3G ^{15}N -L52 led to a $K_D = 124 \pm 27 \mu\text{M}$, B) ProT and PAR3G ^{15}N -E48 led to a $K_D = > 200 \mu\text{M}$, and C) PPACK-IIa and PAR3G ^{15}N -L52 led to a $K_D = 47 \pm 6 \mu\text{M}$. NMR titrations were done in triplicate. The reported K_D values were determined using in-house scripts written using Python. The term $|\Delta\delta_{\text{obs}}|^{15}\text{Nppm} = \delta^{15\text{N}}_{\text{Bound}} - \delta^{15\text{N}}_{\text{Free}}$ reflects the absolute difference in chemical shift between the bound and free states of the particular ^{15}N -amide. Error analysis was carried out using a Monte-Carlo approach assuming a 10% error in the serially diluted protein samples. See Materials and Methods for more details.

APPENDIX 8

^1H - ^{15}N 2D HSQC titration of PAR3G_{FD} (44-56) when bound to thrombin.

Sample was prepared in 25mM H₃PO₄, 150 mM NaCl, 0.2 mM EDTA and

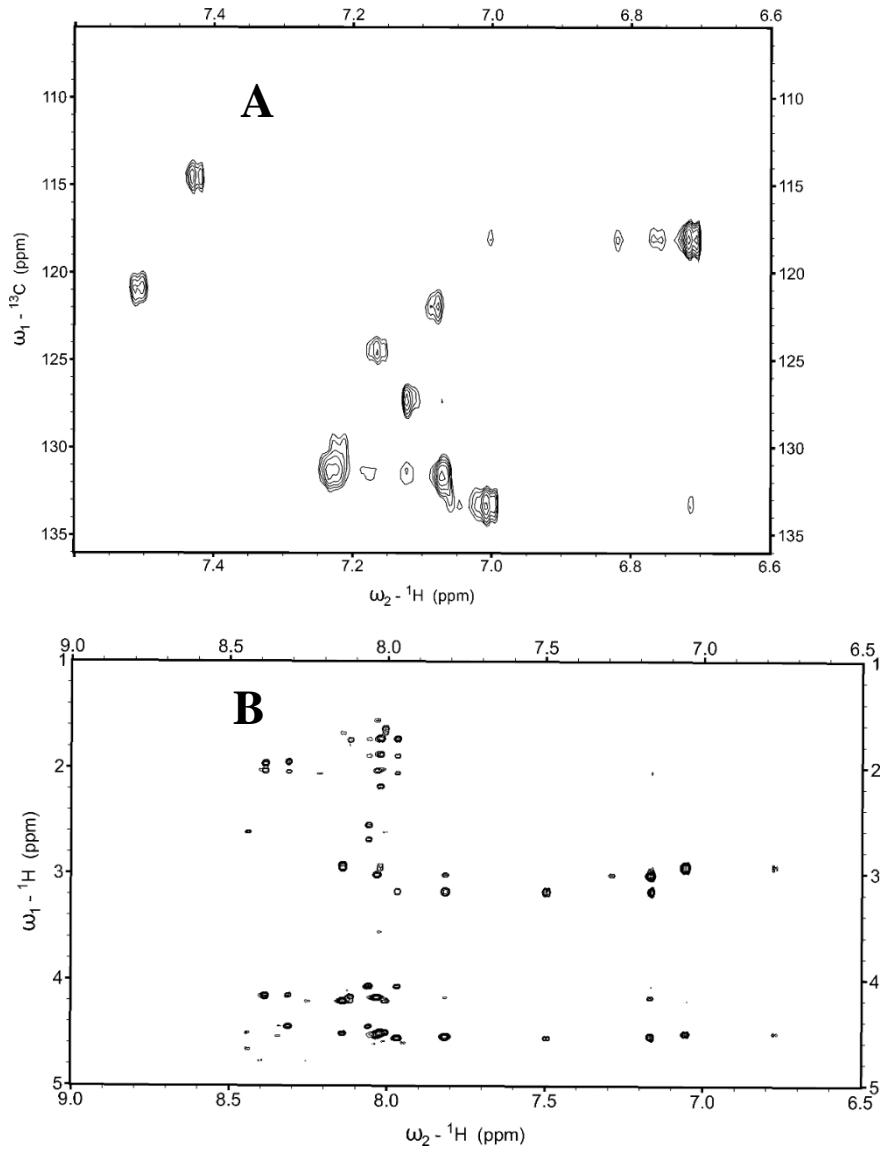
10 % D₂O (pH 6.5). This titration is done without PPACK:



APPENDIX 9

^1H - ^{13}C HSQC spectra of PAR1 (49-62) [A] used for assigning aromatics in ^1H - ^1H

2DNOESY of PAR1 (49-62) [B]:



A) ^1H - ^{13}C HSQC spectra of 1 mM PAR1 (49-62). B) ^1H - ^1H 2DNOESY of 780 μM PAR1 (49-62) when bound to 59 μM ProT.

APPENDIX 10

Procedure for ITC experiment between DNA aptamer and thrombin:

558 nmole of aptamer (HD 1, GGTTGGTGTGGTTGG) was solubilized in 500 μ L dI water. 1.12 mM aptamer was then aliquoted in 20 tubes, lyophilized, and later stored at -80°C until needed. One the day of experiment, bovine thrombin was buffer exchanged into 50 mM Bis-tris propane (pH 7.4), 150 mM NaCl through dialysis. 75 μ L of aptamer samples were reconstituted using the same buffer. 500 μ L of 7 μ M bovine thrombin was placed in the calorimetric cell of the Nano ITC (New Castle, DE). 2 μ L of DNA aptamer was added 25 times into the cell followed by an initial delay of 250 s. The final concentration of DNA aptamer in the calorimetric cell was 50 μ M. During data processing using the Nano Analyze, initial heat was masked as it resulted from the heats of dilution. The individual heats were then plotted as a function of the molar ratio, and nonlinear regression of the data was performed using Nano Analyze software supplied with the instrument. A single binding site model was used for data processing.

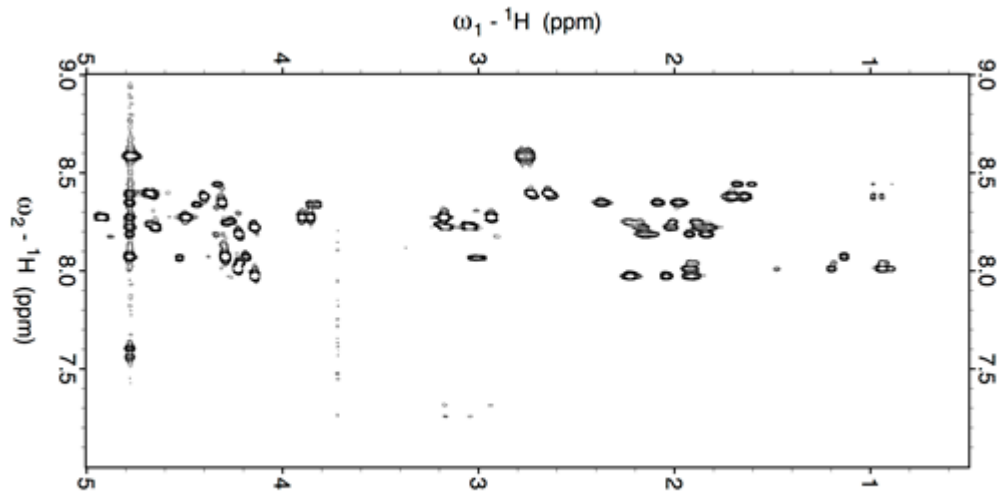
APPENDIX 11

Procedure for ITC experiment between PAR3 (44-56) and thrombin:

Prior to the titration bovine thrombin was incubated with a 4-fold excess of PPACK at 37°C for 30 mins. Later, PPACK-thrombin was buffer exchanged into 25 mM H₃PO₄, 150 mM NaCl, 0.2 mM EDTA, (pH 6.5). Lyophilized PAR3 (44-56) was solubilized into the same buffer. Since the affinity of PAR3 (44-56) for thrombin is not as strong as the DNA aptamer, quite an excess of thrombin concentration was tested. 500 µL of 50 µM bovine thrombin was placed into the calorimetric cell of the Nano ITC (New Castle, DE). 2 µL of PAR3 (44-56) was added 25 times into the cell followed by the initial delay of 250 s. The final concentration of PAR3 (44-56) was 75 µM. Same software and processing model was used to analyze the data.

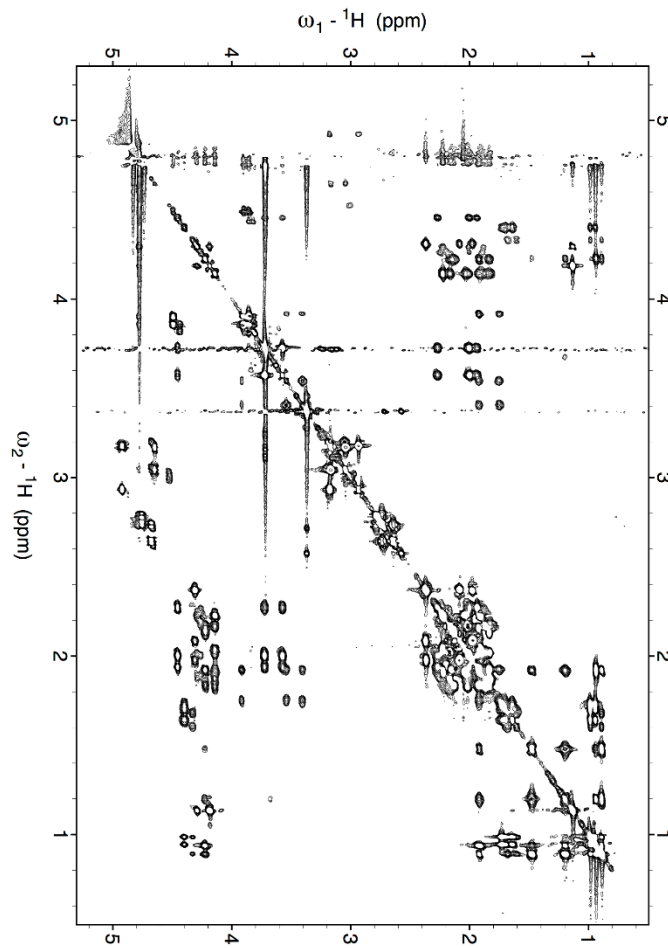
APPENDIX 12

2D TOCSY Fingerprint region of 1 mM PAR3 (44-56). Sample was prepared in 25mM H₃PO₄, 150 mM NaCl, 0.2 mM EDTA and 10 % D₂O (pH 6.5):



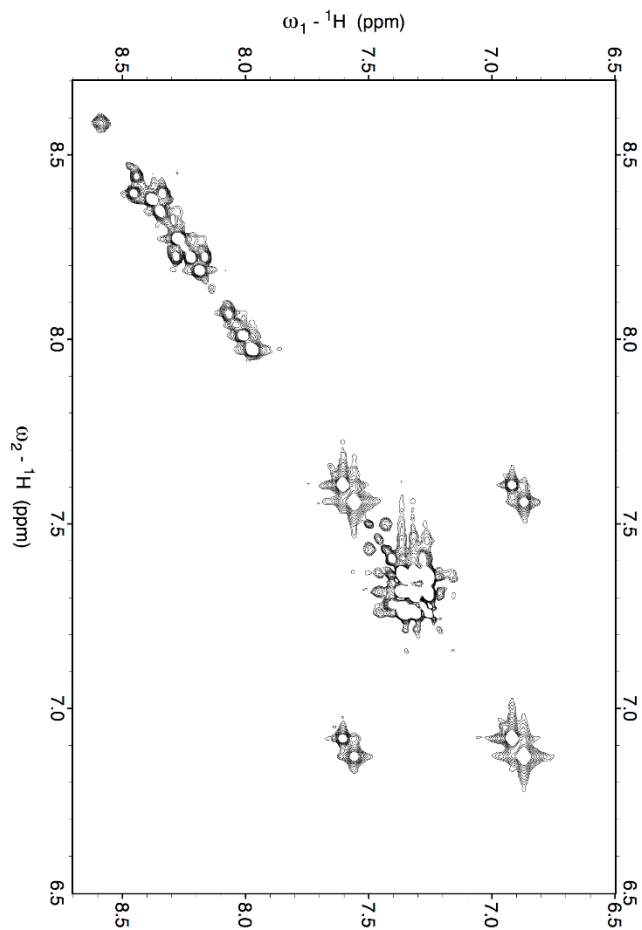
APPENDIX 13

2D TOCSY Aliphatic region of 1 mM PAR3 (44-56). Sample was prepared in 25mM H₃PO₄, 150 mM NaCl, 0.2 mM EDTA and 10 % D₂O (pH 6.5):



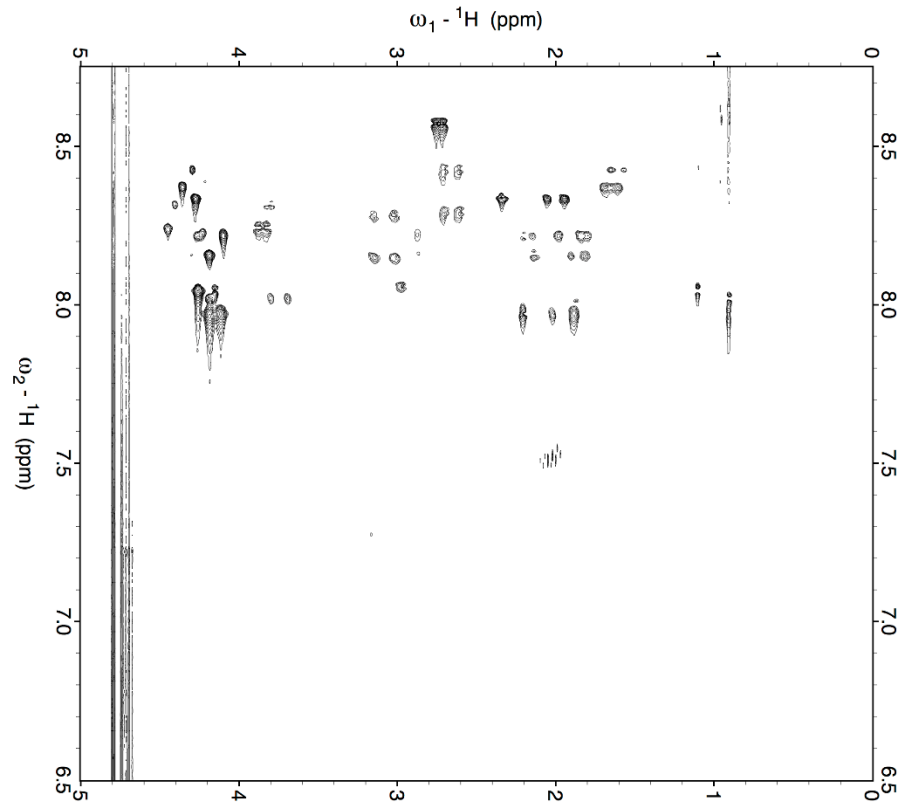
APPENDIX 14

2D TOCSY Aliphatic region of 1 mM PAR3 (44-56). Sample was prepared in 25mM H₃PO₄, 150 mM NaCl, 0.2 mM EDTA and 10 % D₂O (pH 6.5):



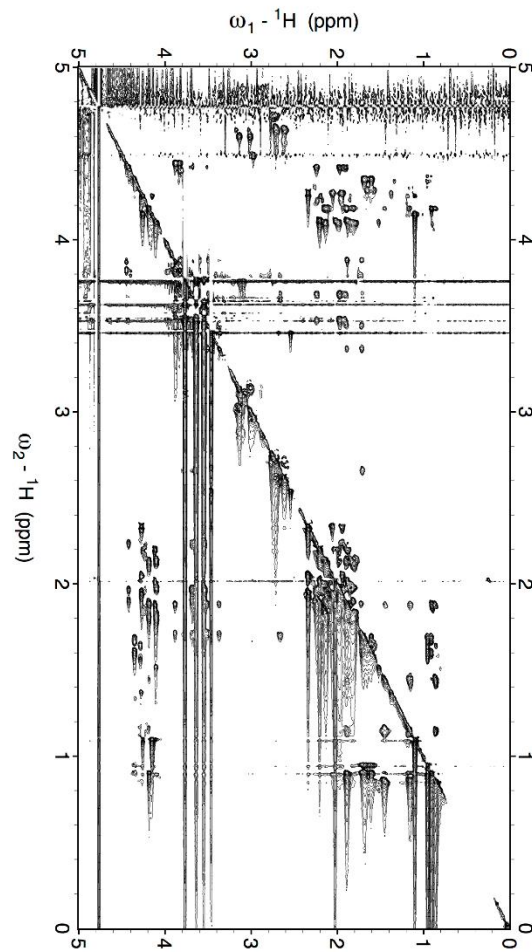
APPENDIX 14

2D TOCSY Fingerprint region of 1 mM PAR3 (44-56) + 74 μ M ProT. Sample was prepared in 25mM H_3PO_4 , 150 mM NaCl, 0.2 mM EDTA and 10 % D_2O (pH 6.5):



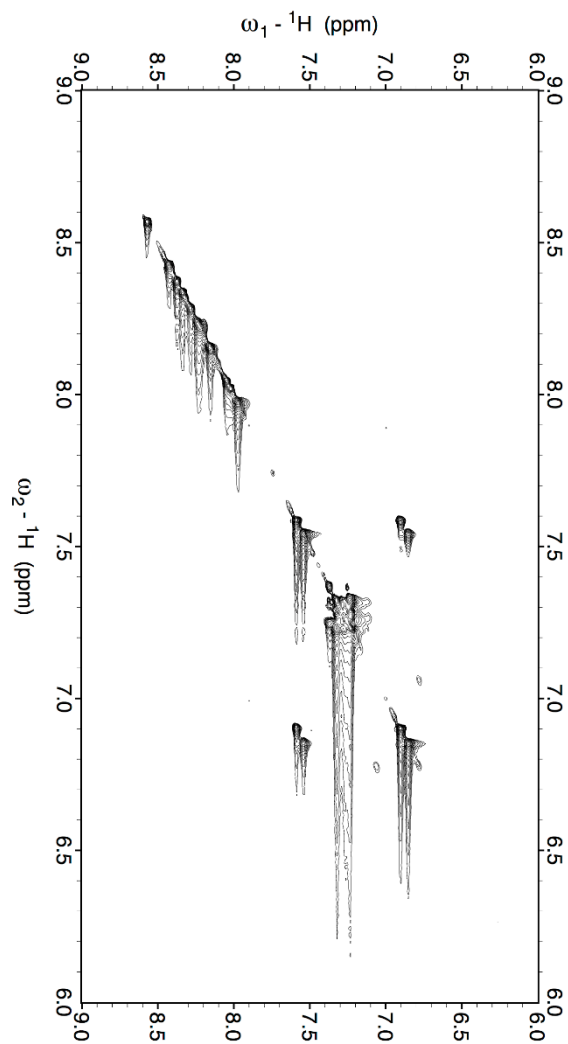
APPENDIX 15

2D TOCSY Aliphatic region of 1 mM PAR3 (44-56) + 74 μ M ProT. Sample was prepared in 25mM H_3PO_4 , 150 mM NaCl, 0.2 mM EDTA and 10 % D_2O (pH 6.5):



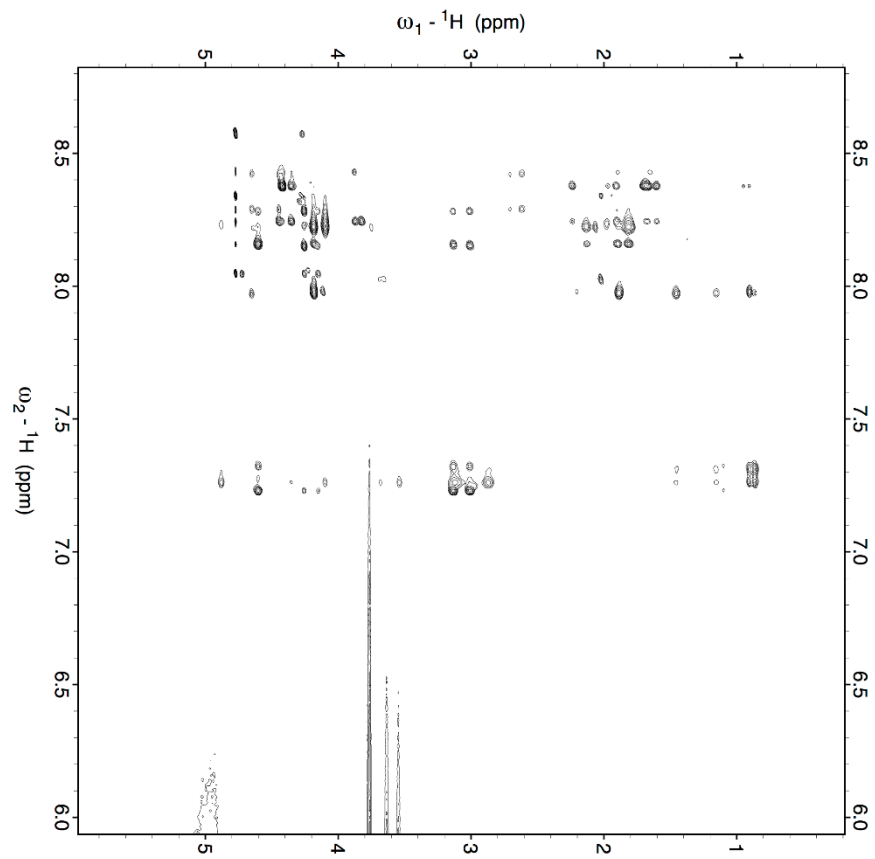
APPENDIX 16

2D TOCSY Amide region of 1 mM PAR3 (44-56) + 74 μ M ProT. Sample was prepared in 25mM H_3PO_4 , 150 mM NaCl, 0.2 mM EDTA and 10 % D_2O (pH 6.5):



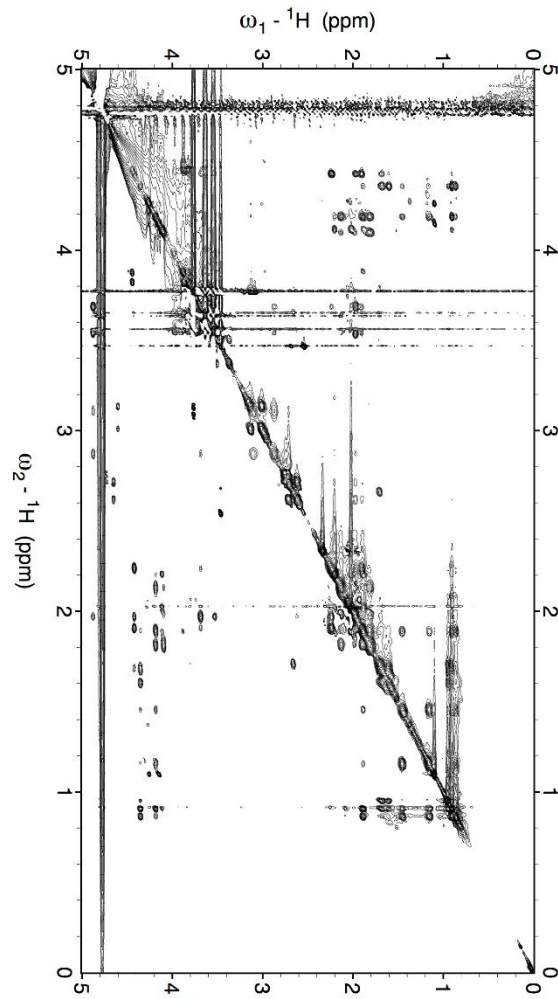
APPENDIX 17

2D tr-NOESY Fingerprint region of 1 mM PAR3 (44-56) + 74 μ M ProT. Sample was prepared in 25mM H_3PO_4 , 150 mM NaCl, 0.2 mM EDTA and 10 % D_2O (pH 6.5):



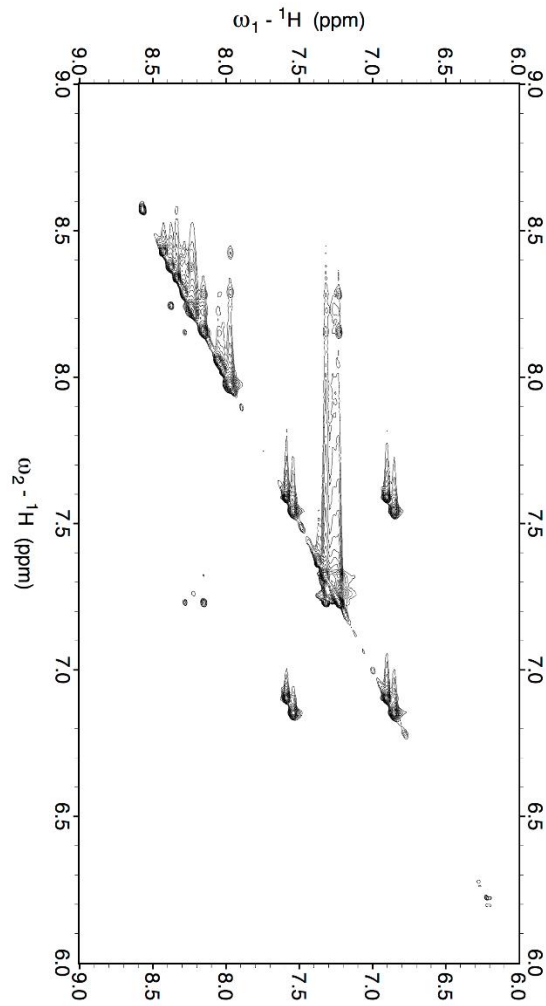
APPENDIX 18

2D tr-NOESY Aliphatic region of 1 mM PAR3 (44-56) + 74 μ M ProT. Sample was prepared in 25mM H_3PO_4 , 150 mM NaCl, 0.2 mM EDTA and 10 % D_2O (pH 6.5):



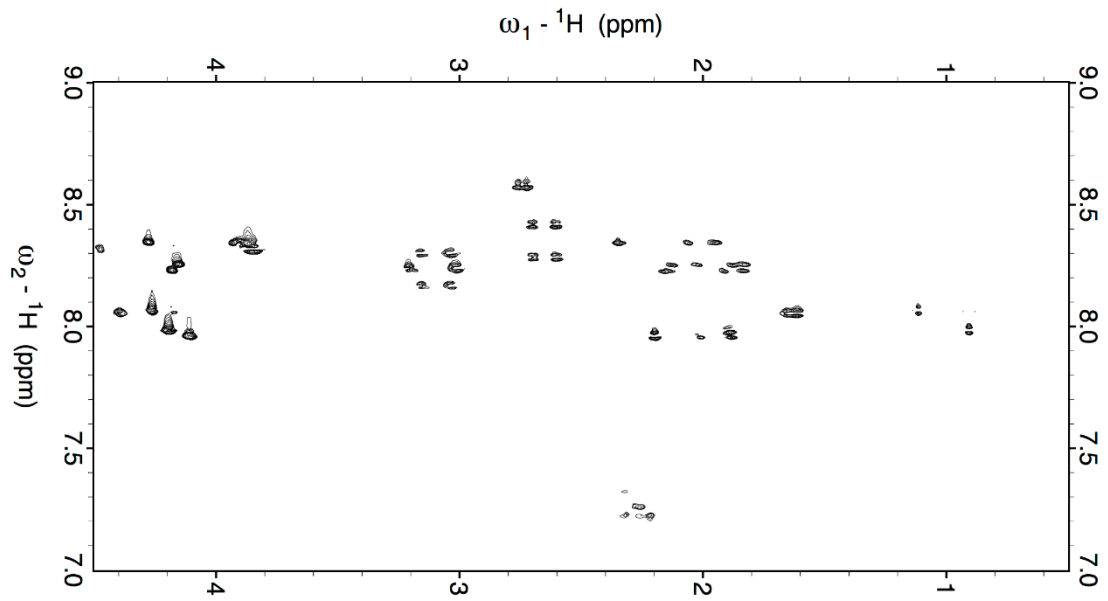
APPENDIX 19

2D tr-NOESY Amide region of 1 mM PAR3 (44-56) + 74 μ M ProT. Sample was prepared in 25mM H_3PO_4 , 150 mM NaCl, 0.2 mM EDTA and 10 % D_2O (pH 6.5):



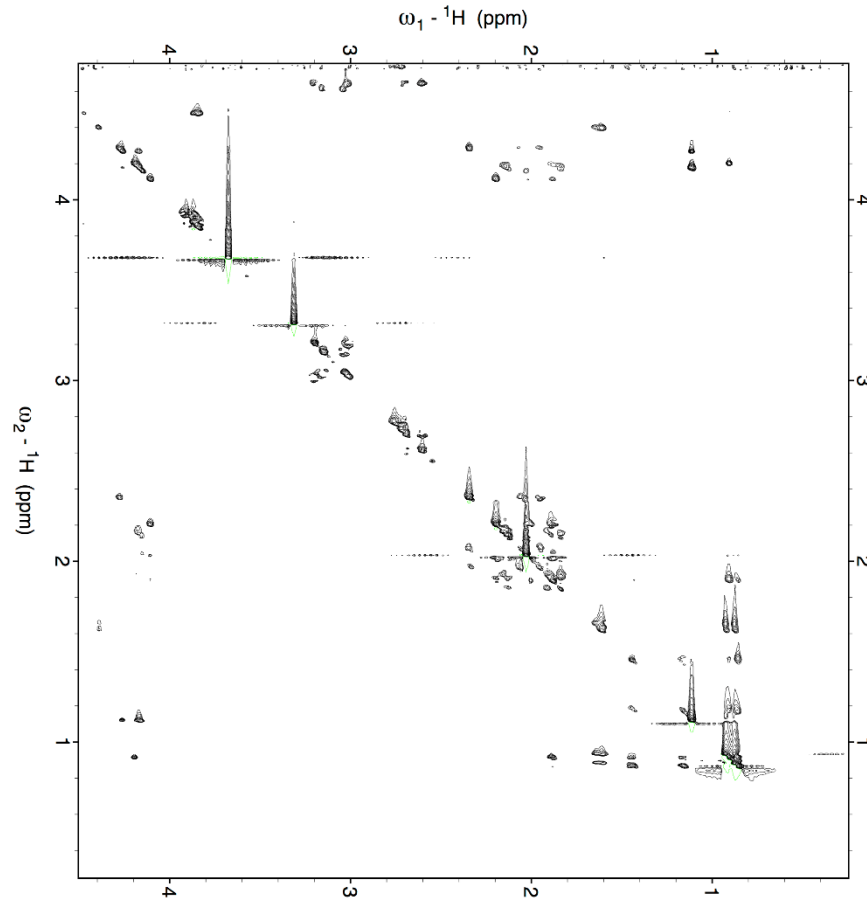
APPENDIX 20

2D TOCSY Fingerprint region of 1 mM PAR3G (44-56). Sample was prepared in 25mM H₃PO₄, 150 mM NaCl, 0.2 mM EDTA and 10 % D₂O (pH 6.5):



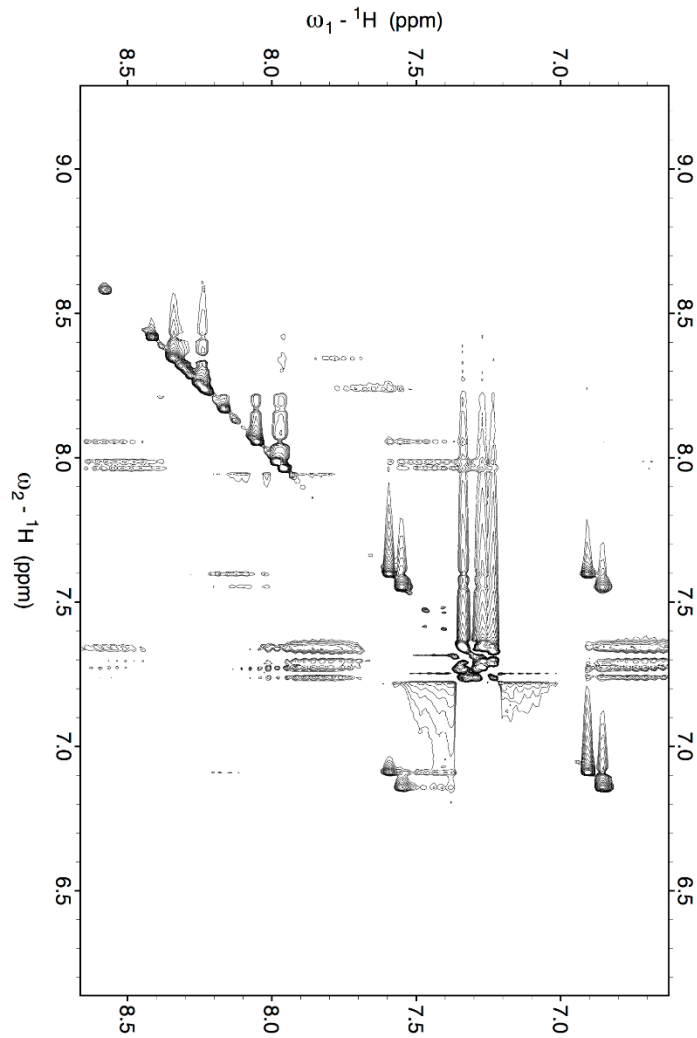
APPENDIX 21

2D TOCSY Aliphatic region of 1 mM PAR3G (44-56). Sample was prepared in 25mM H₃PO₄, 150 mM NaCl, 0.2 mM EDTA and 10 % D₂O (pH 6.5):



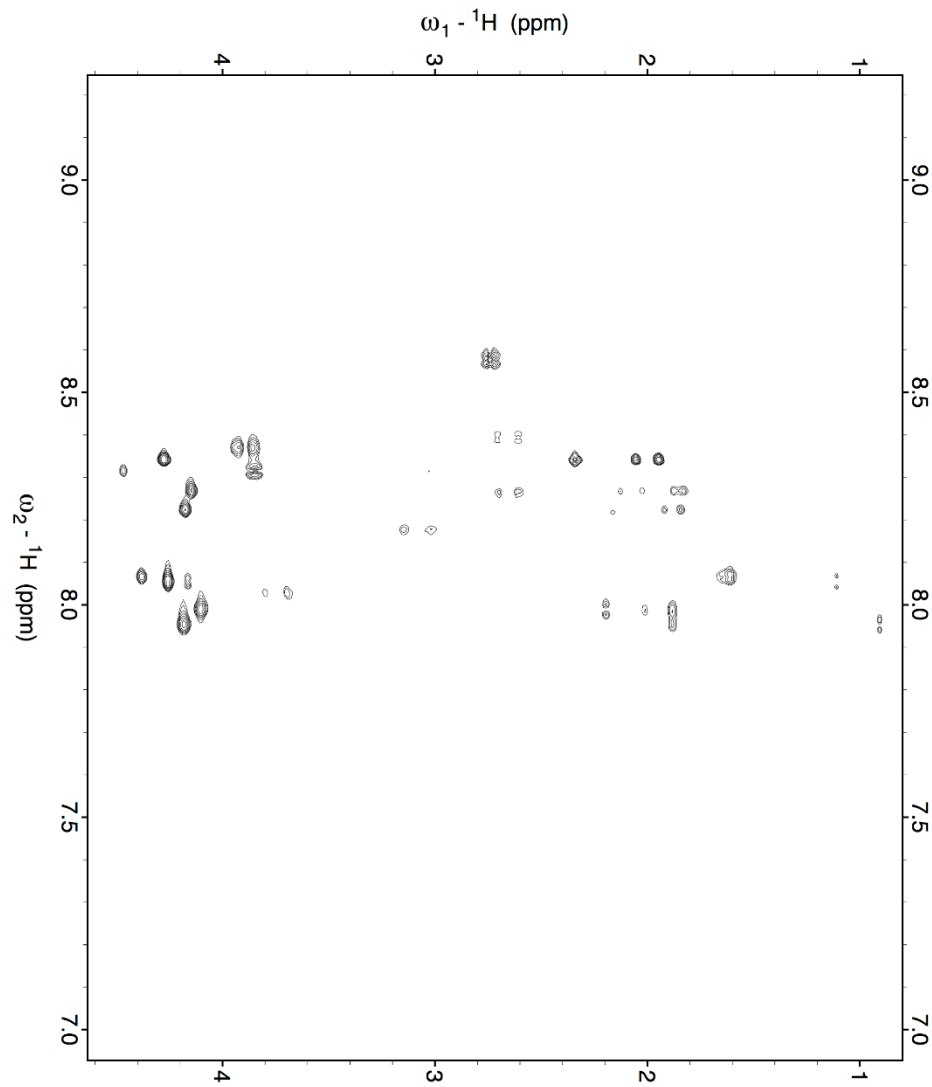
APPENDIX 22

2D TOCSY Amide region of 1 mM PAR3G (44-56). Sample was prepared in 25mM H₃PO₄, 150 mM NaCl, 0.2 mM EDTA and 10 % D₂O (pH 6.5):



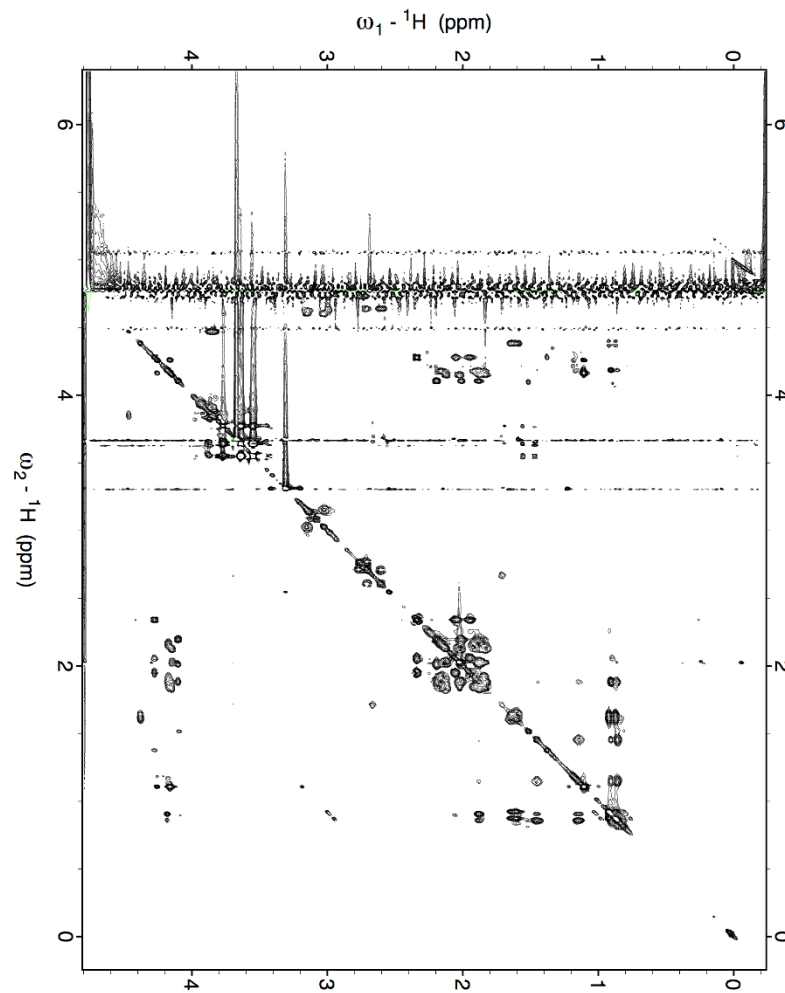
APPENDIX 23

2D TOCSY Fingerprint region of 1 mM PAR3G (44-56) + 76 μ M ProT. Sample was prepared in 25mM H_3PO_4 , 150 mM NaCl, 0.2 mM EDTA and 10 % D_2O (pH 6.5):



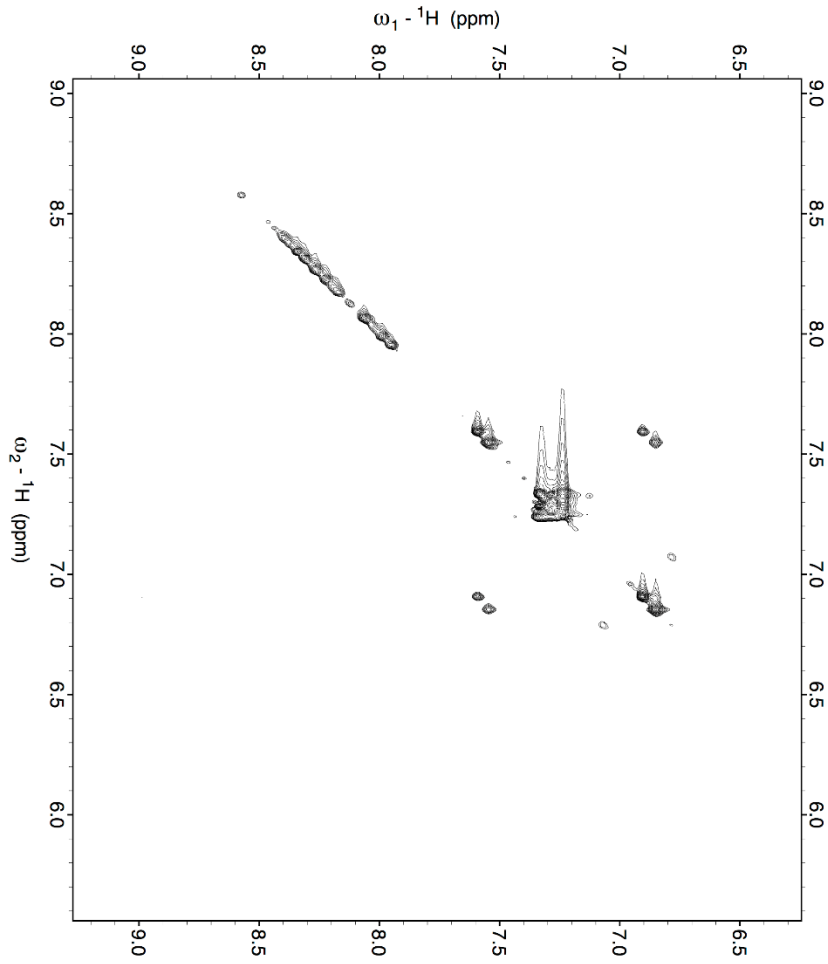
APPENDIX 24

2D TOCSY Aliphatic region of 1 mM PAR3G (44-56) + 76 μ M ProT. Sample was prepared in 25mM H_3PO_4 , 150 mM NaCl, 0.2 mM EDTA and 10 % D_2O (pH 6.5):



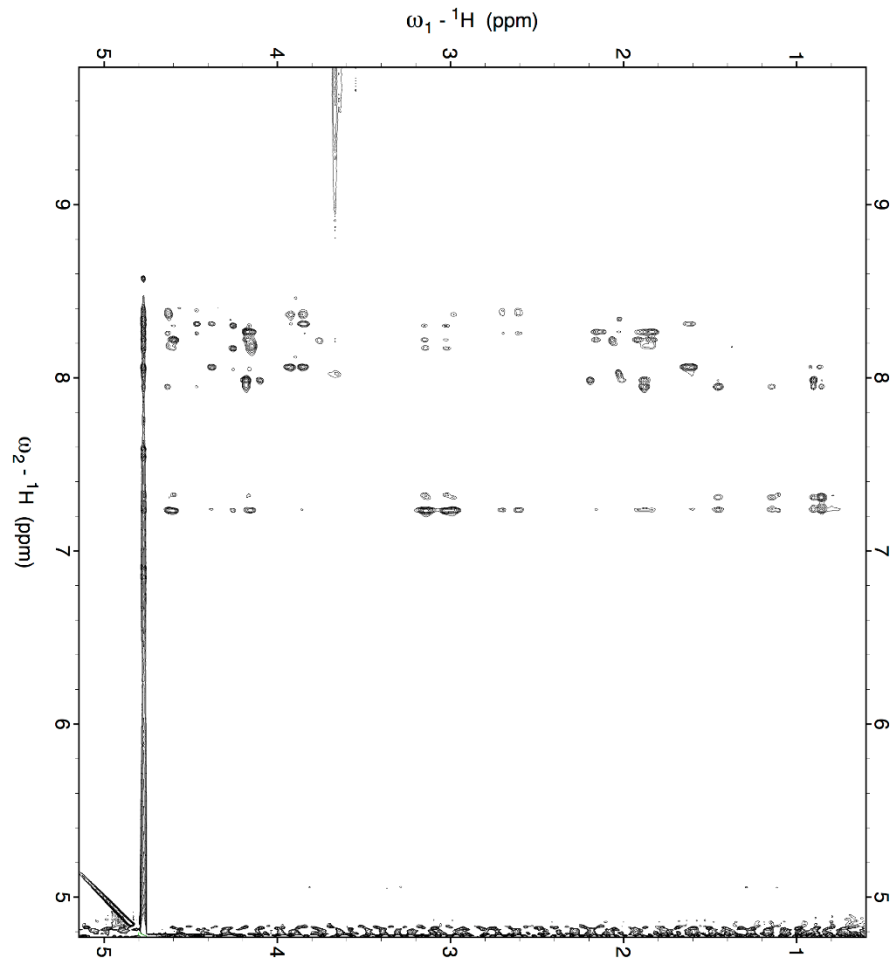
APPENDIX 25

2D TOCSY Amide region of 1 mM PAR3G (44-56) + 76 μ M ProT. Sample was prepared in 25mM H_3PO_4 , 150 mM NaCl, 0.2 mM EDTA and 10 % D_2O (pH 6.5):



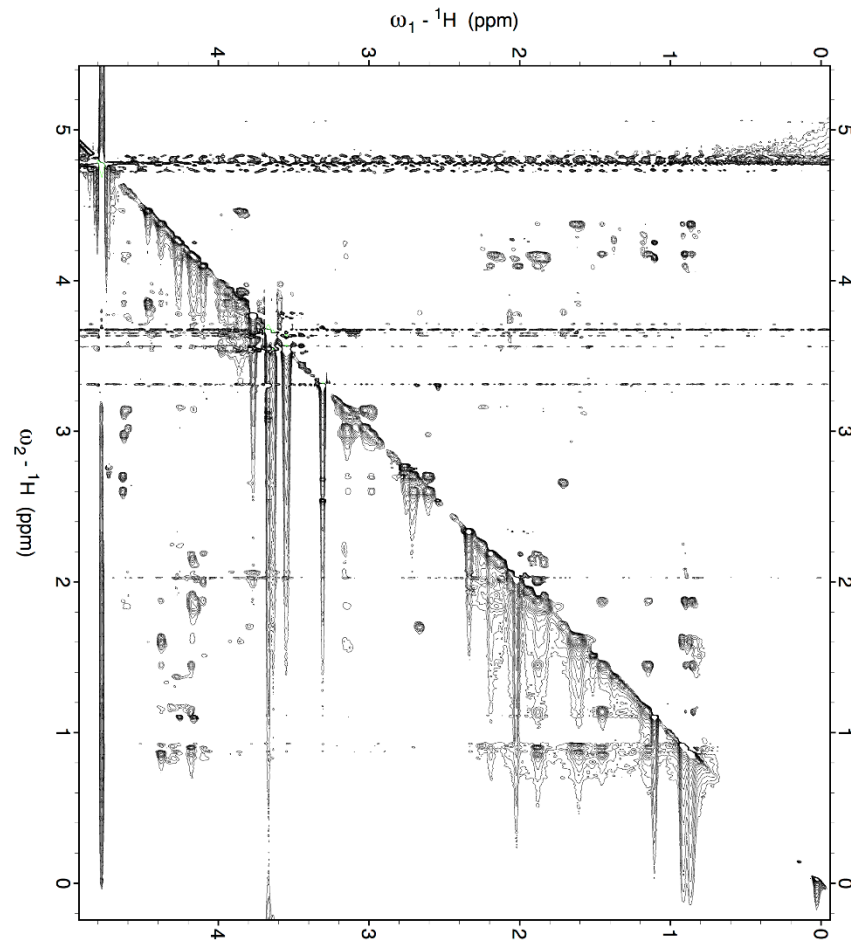
APPENDIX 26

2D NOESY Fingerprintregion of 1 mM PAR3G (44-56) + 76 μ M ProT. Sample was prepared in 25mM H_3PO_4 , 150 mM NaCl, 0.2 mM EDTA and 10 % D_2O (pH 6.5):



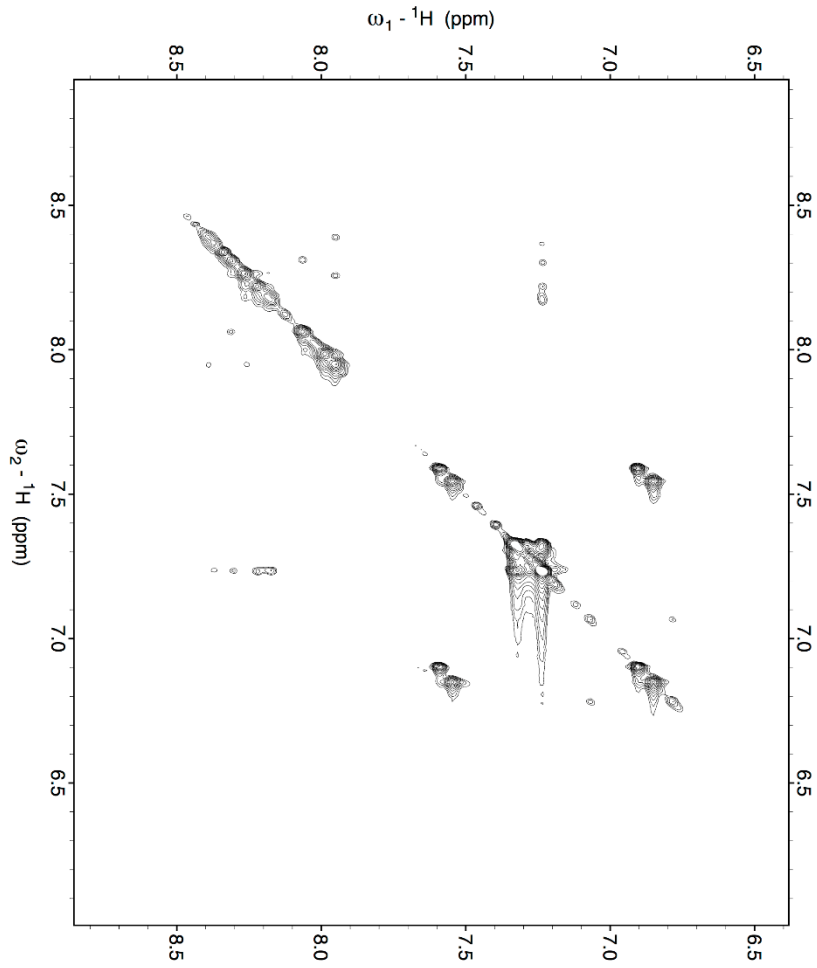
APPENDIX 27

2D NOESY Aliphatic region of 1 mM PAR3G (44-56) + 76 μ M ProT. Sample was prepared in 25mM H_3PO_4 , 150 mM NaCl, 0.2 mM EDTA and 10 % D_2O (pH 6.5):



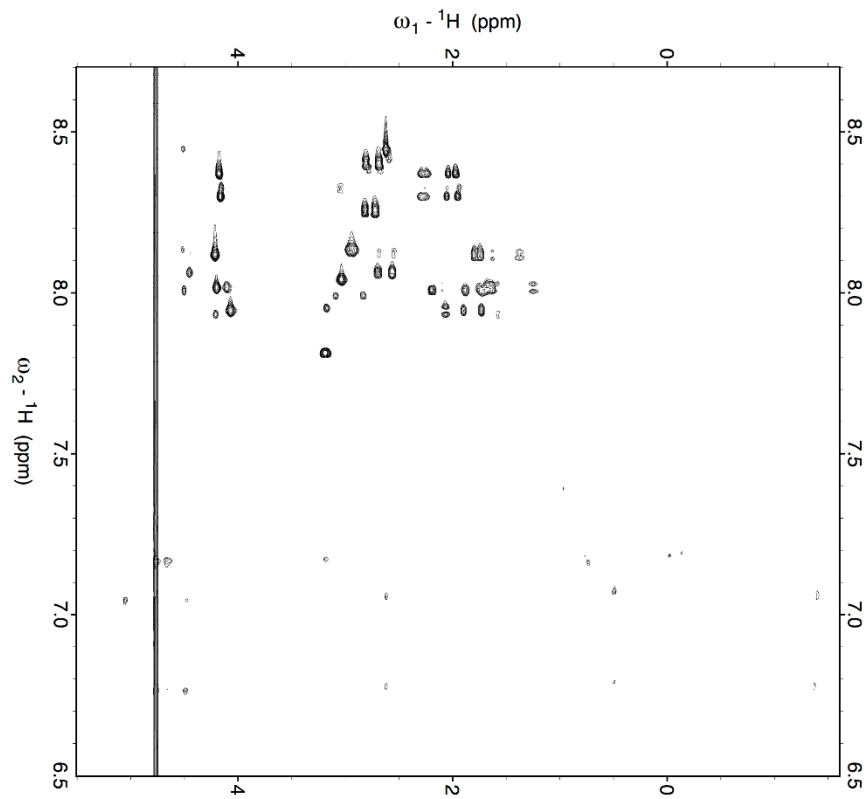
APPENDIX 28

2D NOESY Amide region of 1 mM PAR3G (44-56) + 76 μ M ProT. Sample was prepared in 25mM H_3PO_4 , 150 mM NaCl, 0.2 mM EDTA and 10 % D_2O (pH 6.5):



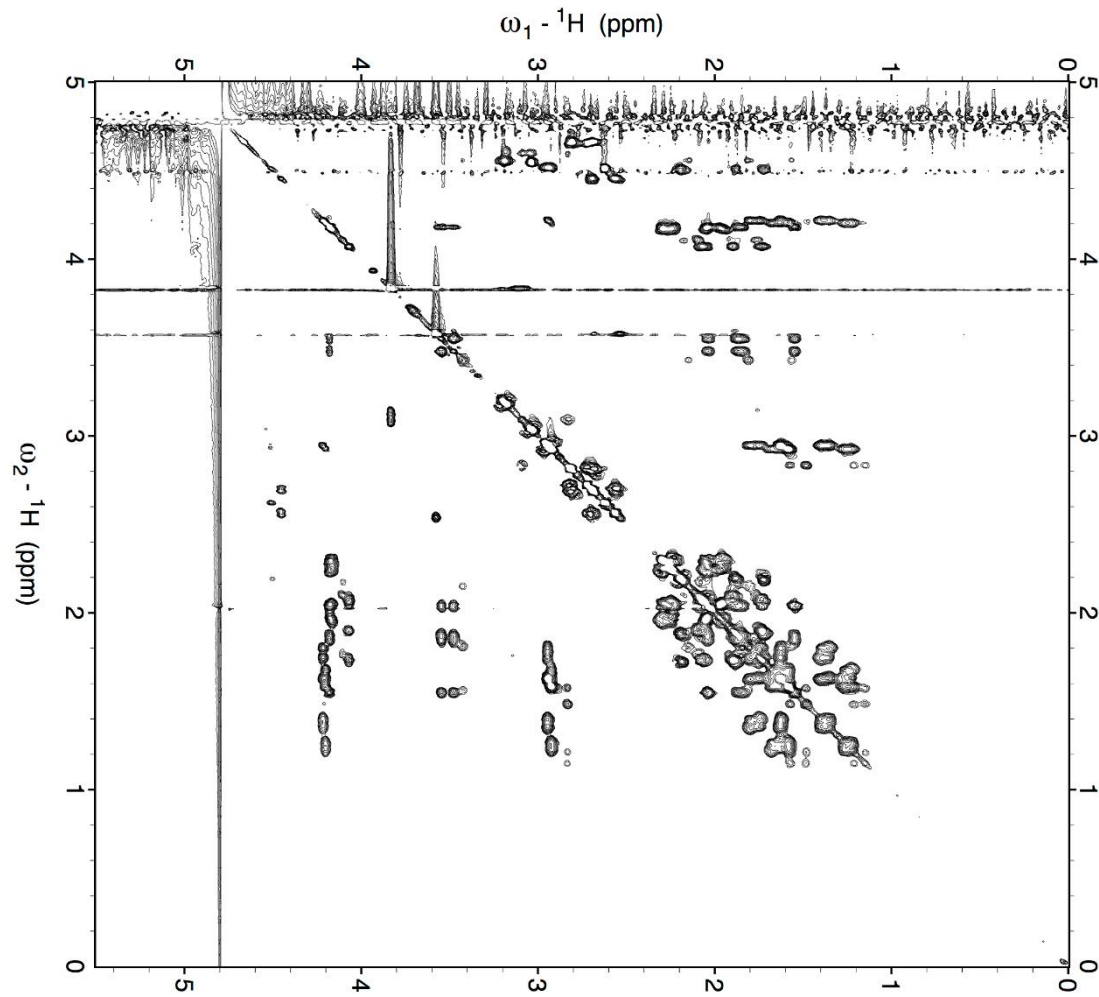
APPENDIX 29

2D TOCSY Fingerprint region of 1 mM PAR1P (49-62). Sample was prepared in 25mM H₃PO₄, 150 mM NaCl, 0.2 mM EDTA and 10 % D₂O (pH 6.5):



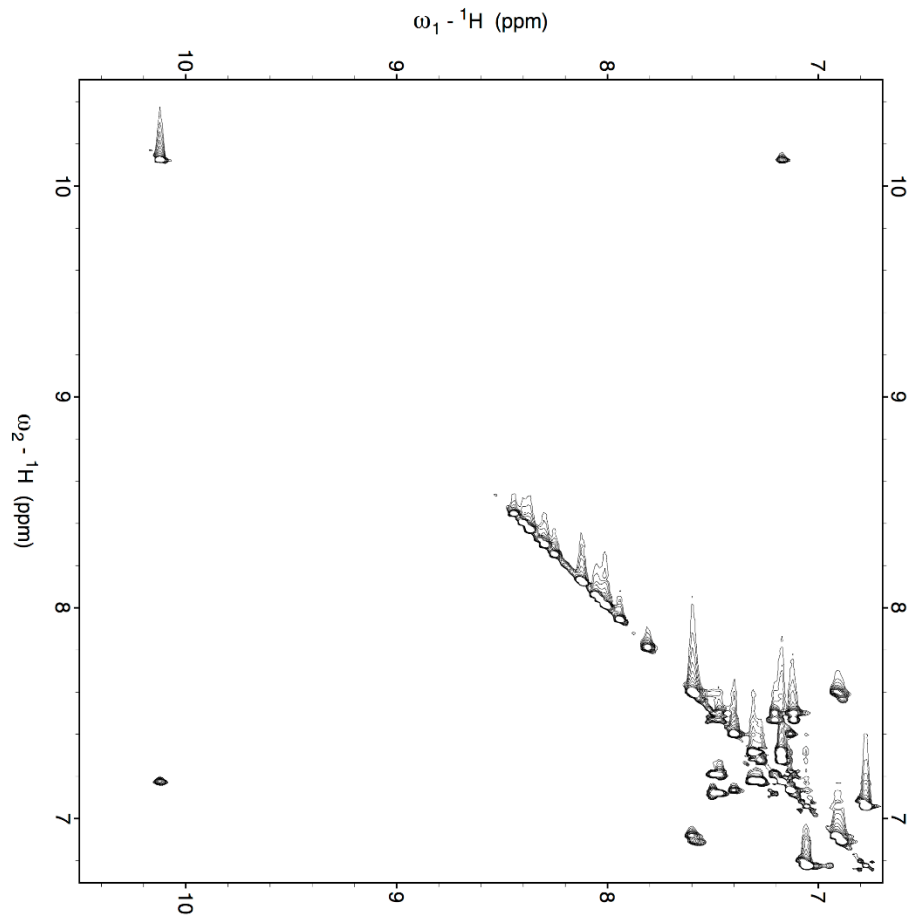
APPENDIX 30

2D TOCSY Aliphatic region of 1 mM PAR1P (49-62). Sample was prepared in 25mM H₃PO₄, 150 mM NaCl, 0.2 mM EDTA and 10 % D₂O (pH 6.5):



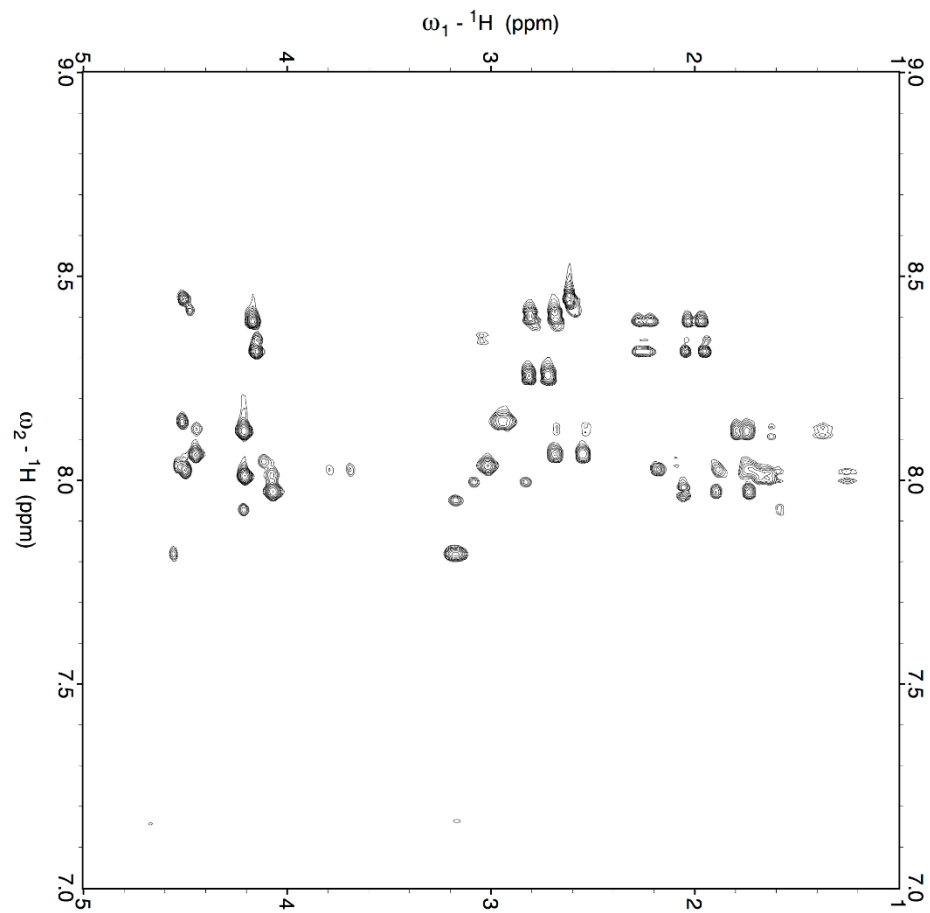
APPENDIX 31

2D TOCSY Amide region of 1 mM PAR1P (49-62). Sample was prepared in 25mM H₃PO₄, 150 mM NaCl, 0.2 mM EDTA and 10 % D₂O (pH 6.5):



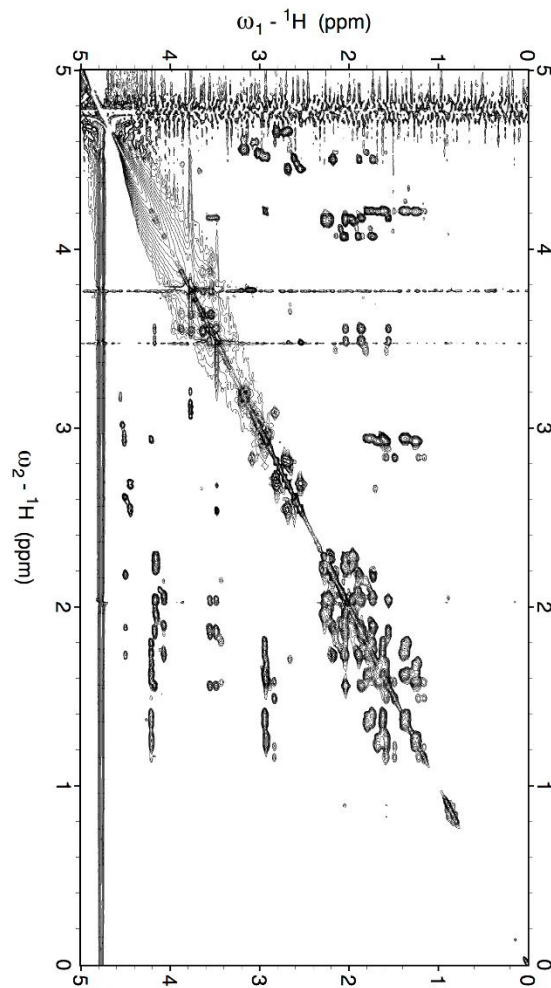
APPENDIX 32

2D TOCSY Fingerprint region of 1 mM PAR1P (49-62) + 59 μ M ProT Sample was prepared in 25mM H_3PO_4 , 150 mM NaCl, 0.2 mM EDTA and 10 % D_2O (pH 6.5):



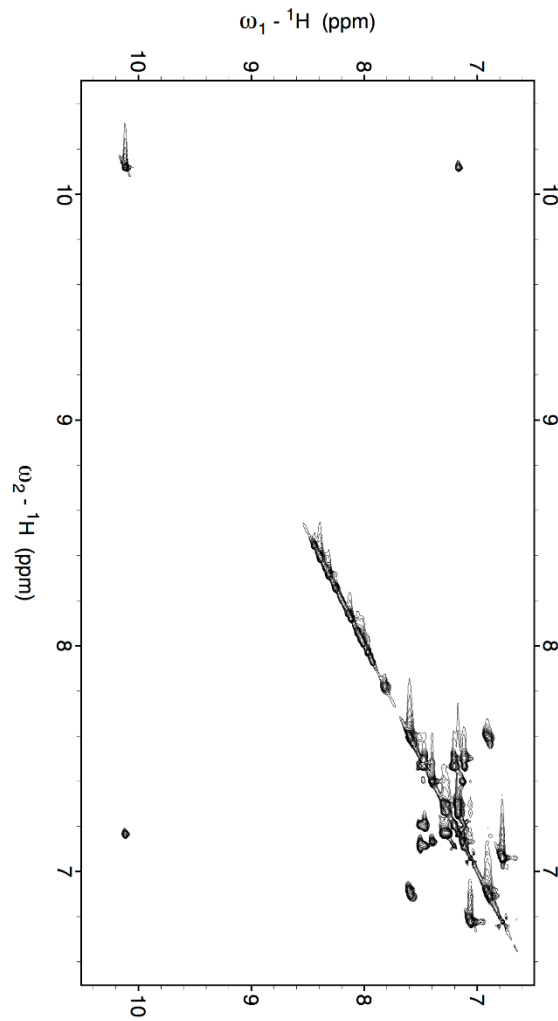
APPENDIX 33

2D TOCSY Aliphatic region of 1 mM PAR1P (49-62) + 59 μ M ProT. Sample was prepared in 25mM H_3PO_4 , 150 mM NaCl, 0.2 mM EDTA and 10 % D_2O (pH 6.5):



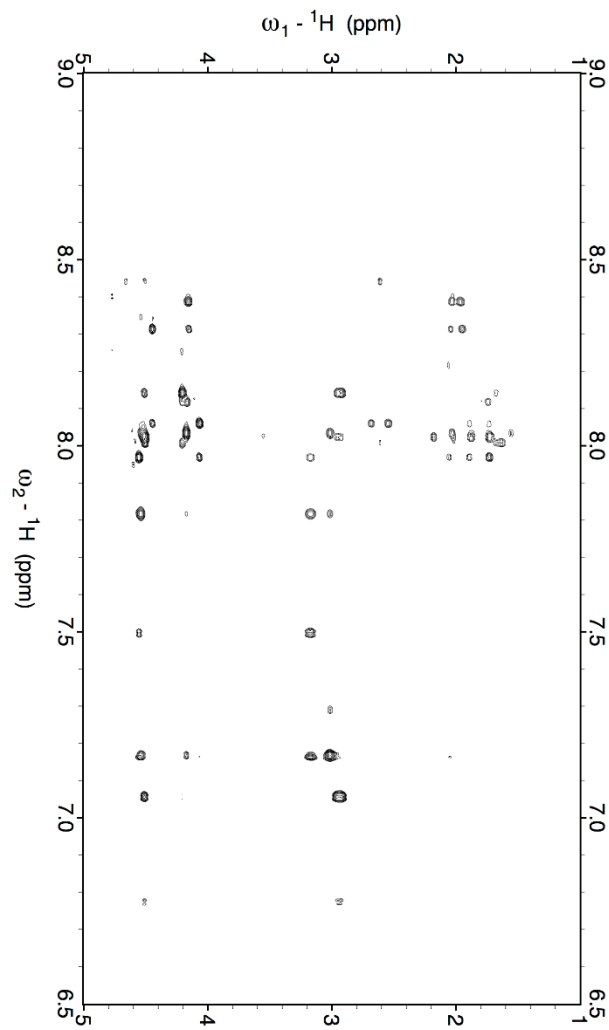
APPENDIX 34

2D TOCSY Amide region of 1 mM PAR1P (49-62) + 59 μ M ProT. Sample was prepared in 25mM H_3PO_4 , 150 mM NaCl, 0.2 mM EDTA and 10 % D_2O (pH 6.5):



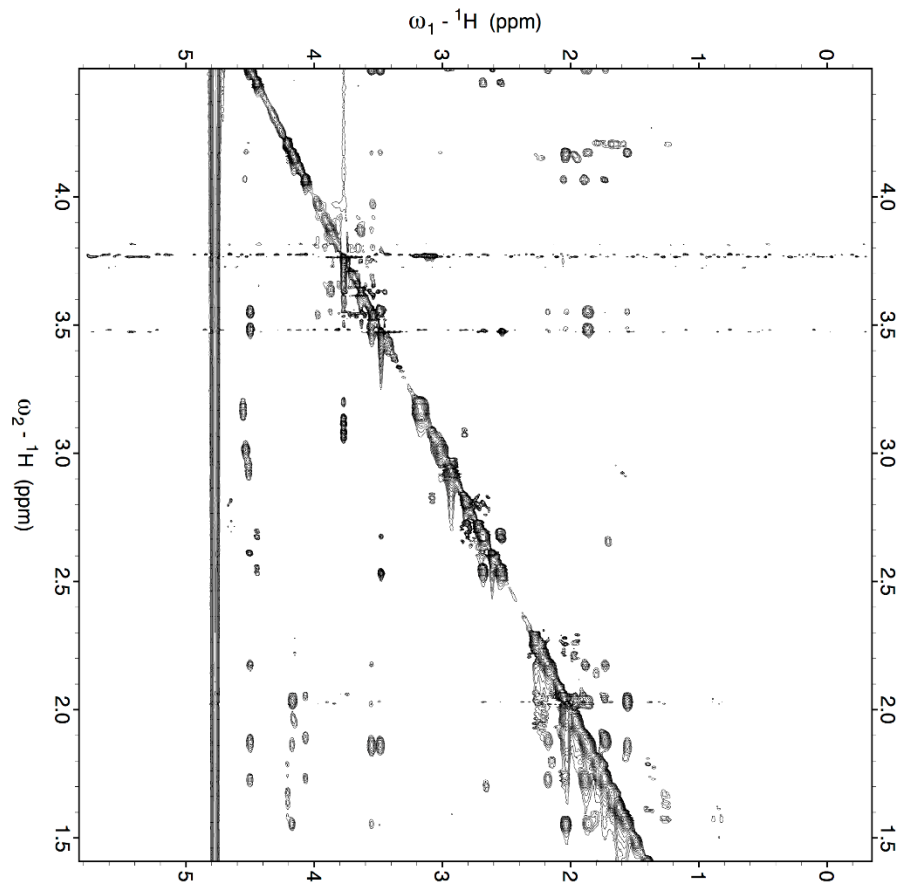
APPENDIX 35

2D NOESY Fingerprint region of 1 mM PAR1P (49-62) + 59 μ M ProT. Sample was prepared in 25mM H_3PO_4 , 150 mM NaCl, 0.2 mM EDTA and 10 % D_2O (pH 6.5):



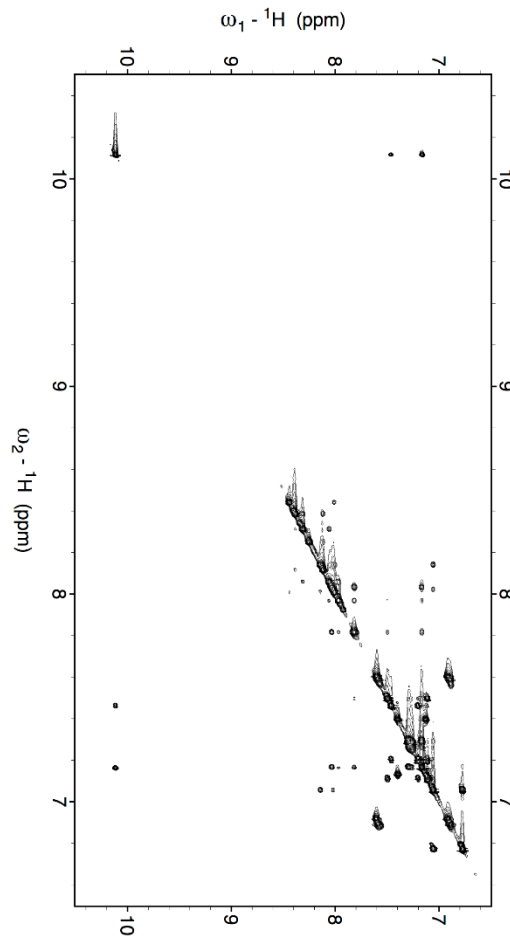
APPENDIX 36

2D NOESY Aliphatic region of 1 mM PAR1P (49-62) + 59 μ M ProT. Sample was prepared in 25mM H_3PO_4 , 150 mM NaCl, 0.2 mM EDTA and 10 % D_2O (pH 6.5):



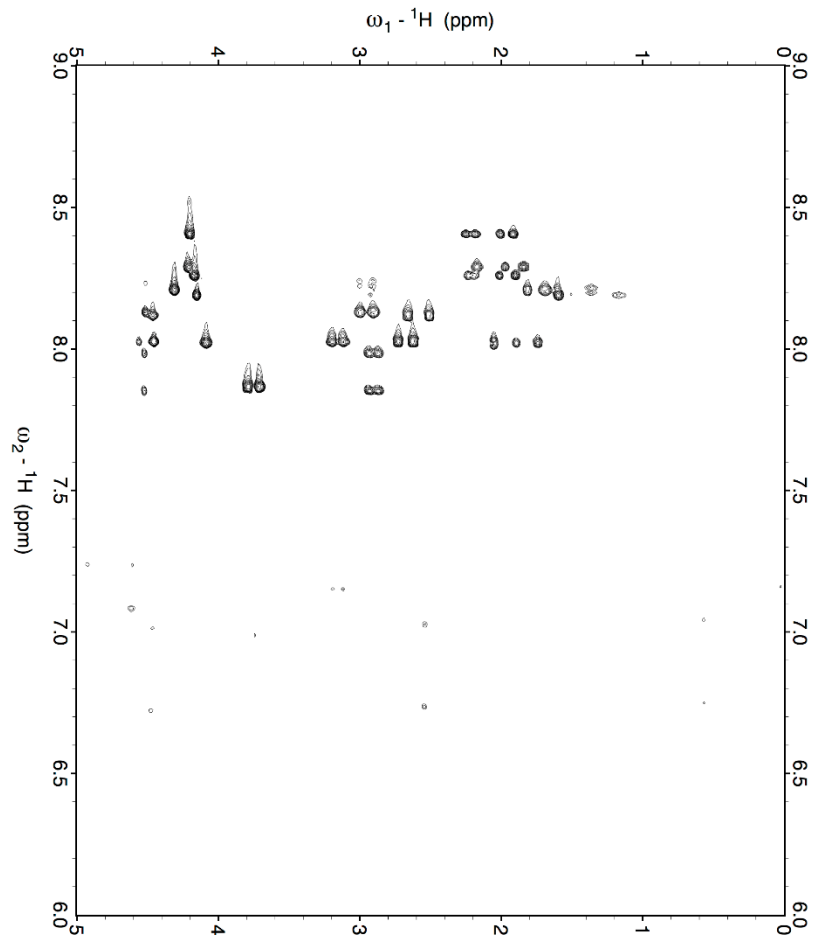
APPENDIX 37

2D NOESY Amide region of 1 mM PAR1P (49-62) + 59 μ M ProT. Sample was prepared in 25mM H_3PO_4 , 150 mM NaCl, 0.2 mM EDTA and 10 % D_2O (pH 6.5):



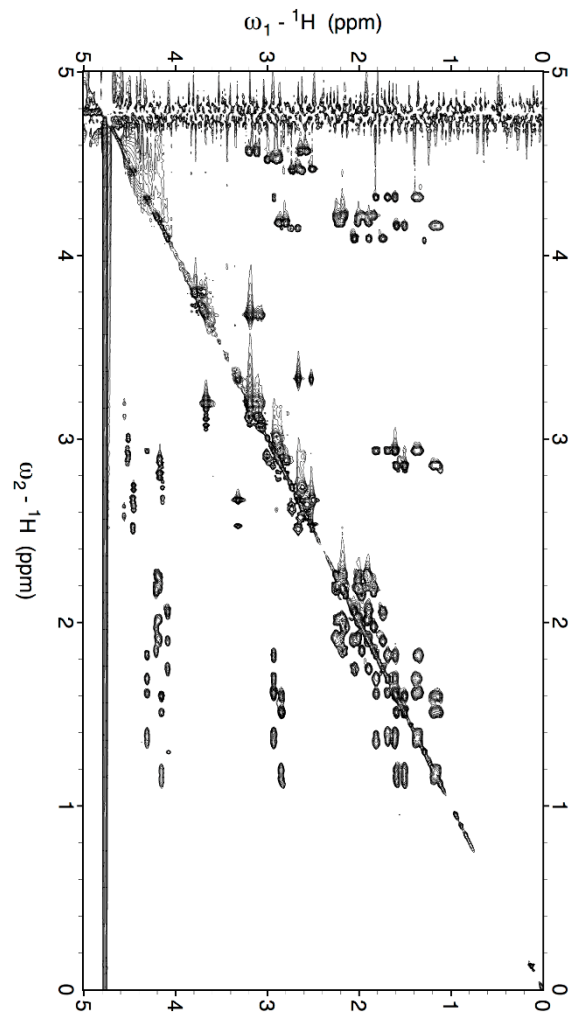
APPENDIX 38

2D TOCSY Fingerprint region of 1 mM PAR1G (49-62). Sample was prepared in 25mM H₃PO₄, 150 mM NaCl, 0.2 mM EDTA and 10 % D₂O (pH 6.5):



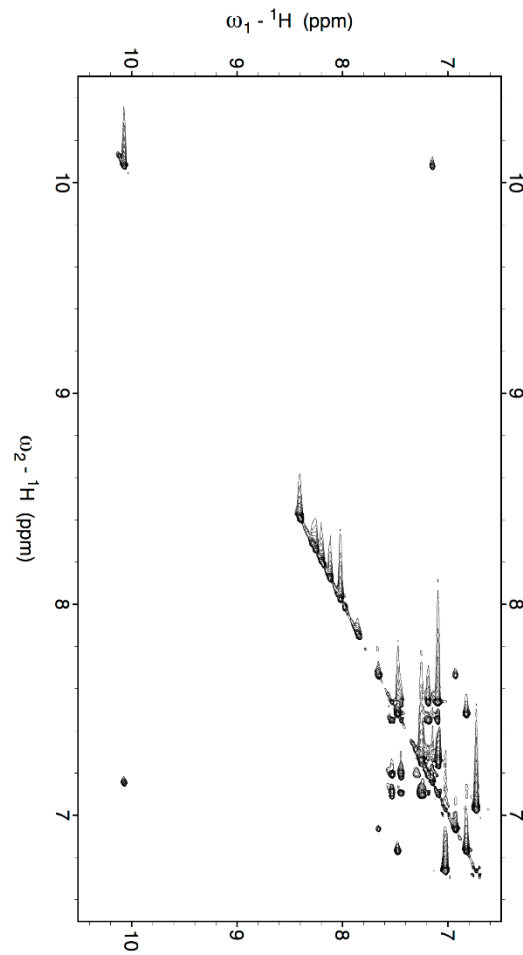
APPENDIX 39

2D TOCSY Aliphatic region of 1 mM PAR1G (49-62). Sample was prepared in 25mM H₃PO₄, 150 mM NaCl, 0.2 mM EDTA and 10 % D₂O (pH 6.5):



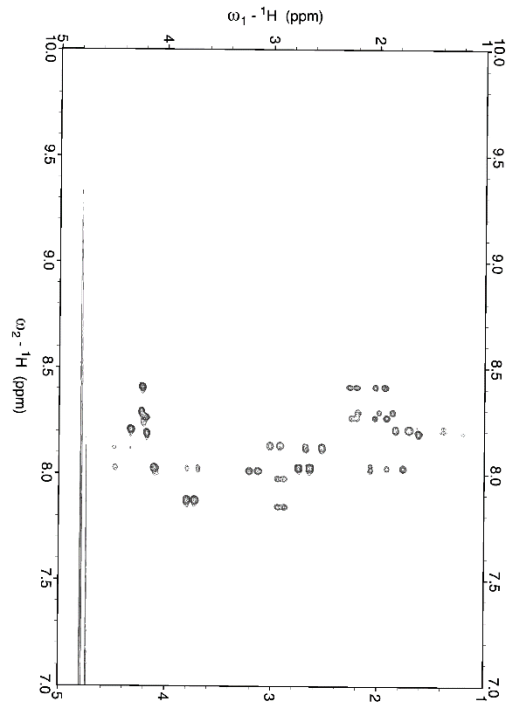
APPENDIX 40

2D TOCSYamide region of 1 mM PAR1G (49-62). Sample was prepared in 25mM H₃PO₄, 150 mM NaCl, 0.2 mM EDTA and 10 % D₂O (pH 6.5):



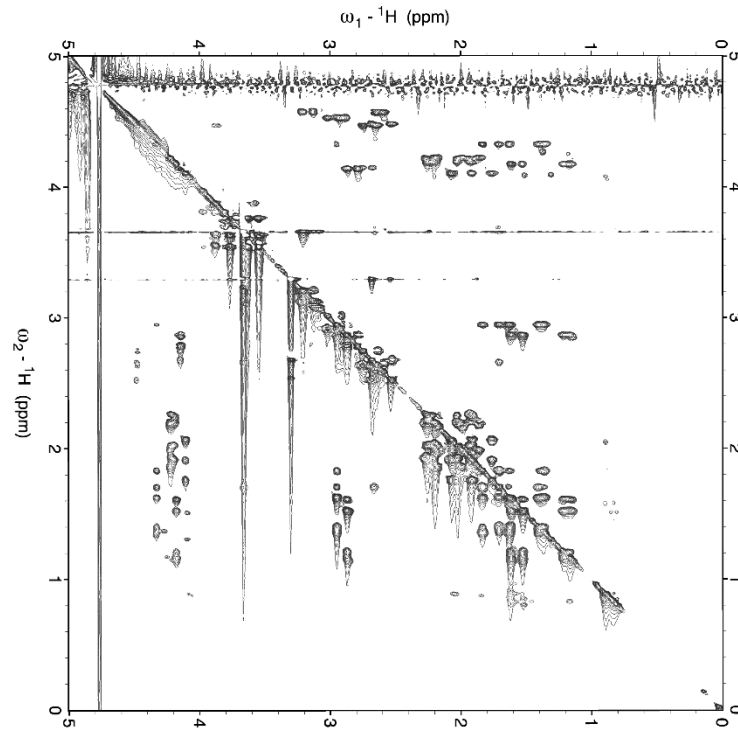
APPENDIX 41

2D TOCSY Fingerprint region of 830 μM PAR1G (49-62) + 83 μM ProT. Sample was prepared in 25mM H_3PO_4 , 150 mM NaCl, 0.2 mM EDTA and 10 % D_2O (pH 6.5):



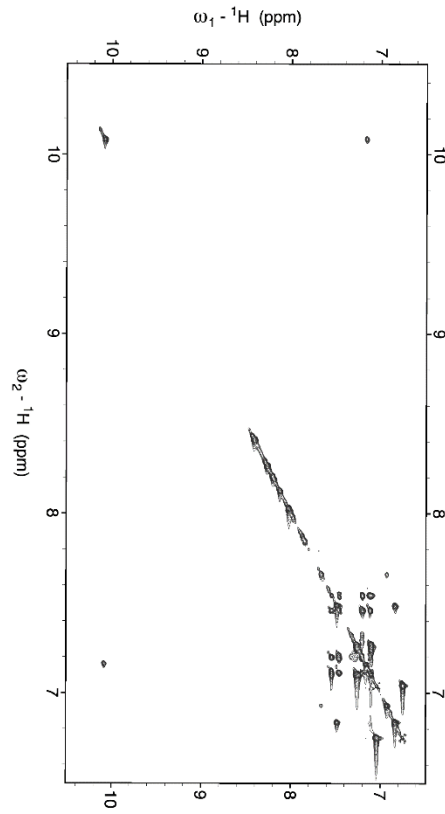
APPENDIX 42

2D TOCSY Aliphatic region of 830 μM PAR1G (49-62) + 83 μM ProT. Sample was prepared in 25mM H_3PO_4 , 150 mM NaCl, 0.2 mM EDTA and 10 % D_2O (pH 6.5):



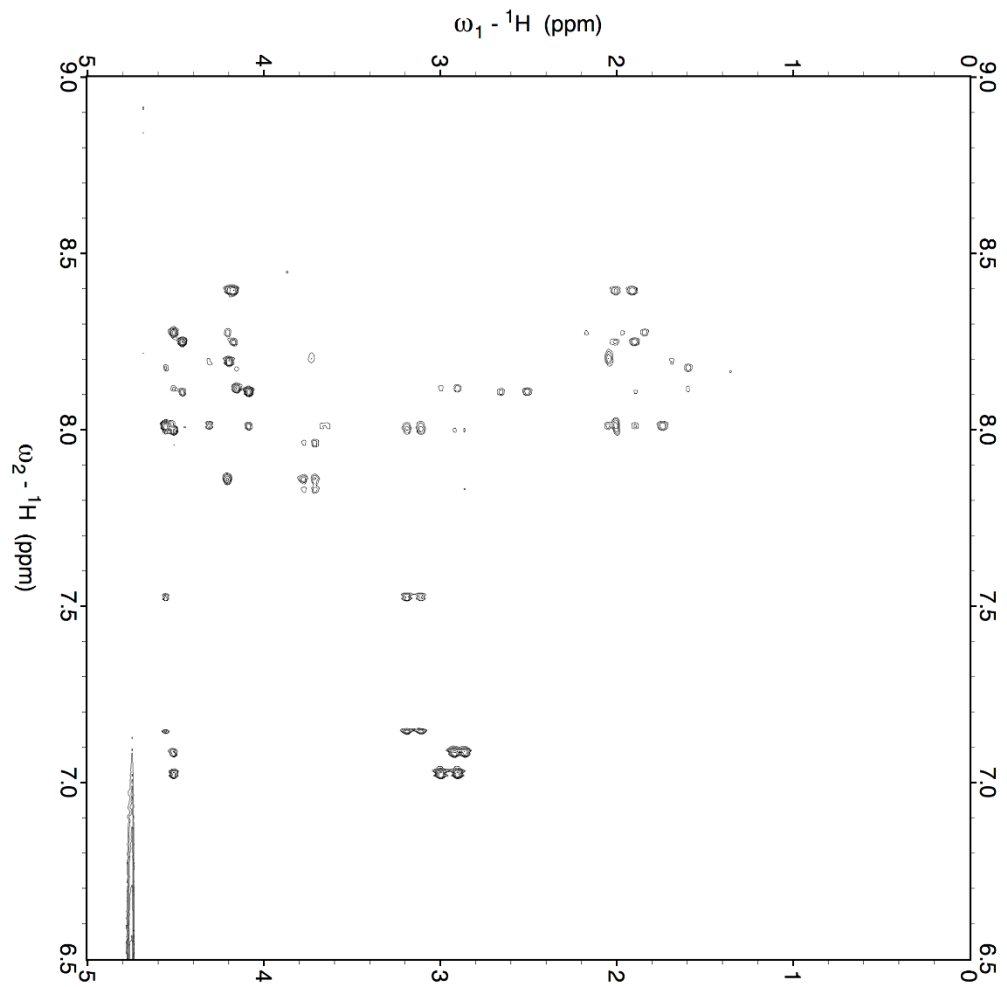
APPENDIX 43

2D TOCSY Amide region of 830 μM PAR1G (49-62) + 83 μM ProT. Sample was prepared in 25mM H_3PO_4 , 150 mM NaCl, 0.2 mM EDTA and 10 % D_2O (pH 6.5):



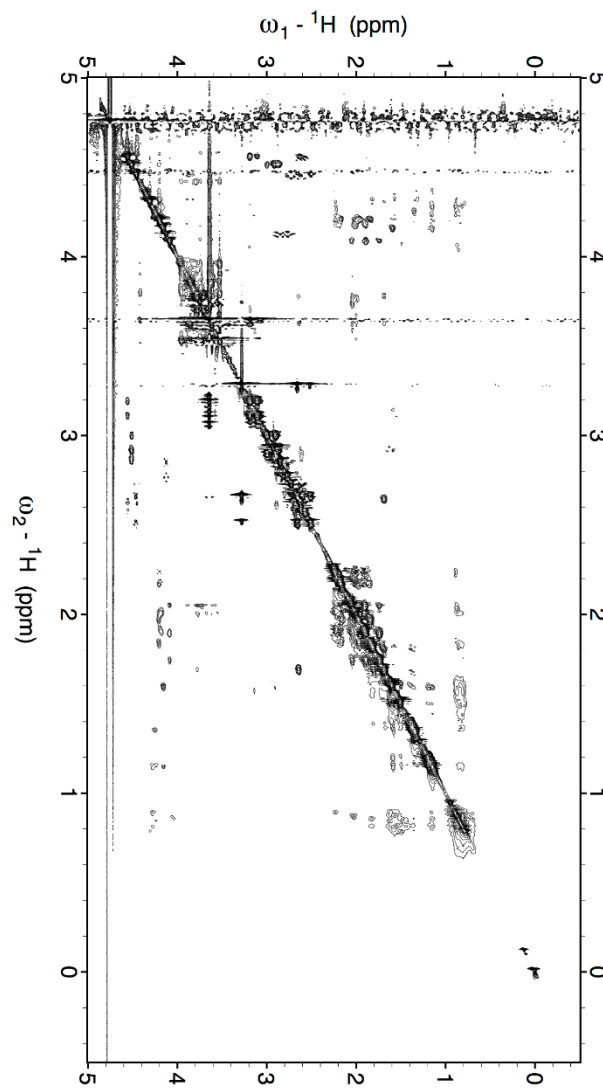
APPENDIX 44

2D NOESY Fingerprint region of 830 μM PAR1G (49-62) + 83 μM ProT. Sample was prepared in 25mM H_3PO_4 , 150 mM NaCl, 0.2 mM EDTA and 10 % D_2O (pH 6.5):



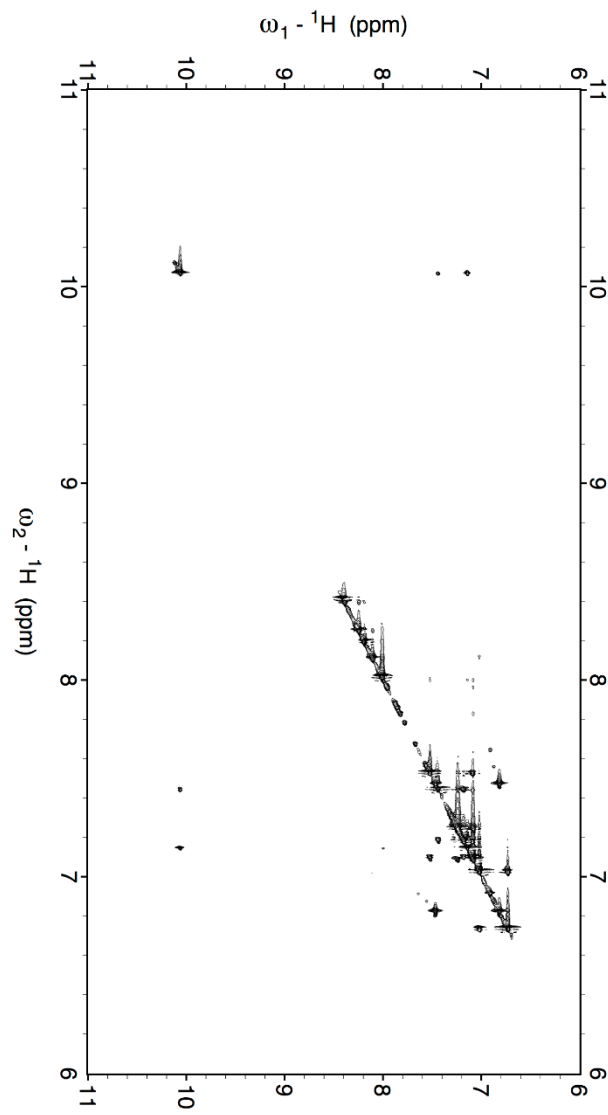
APPENDIX 45

2D NOESY Aliphatic region of 830 μM PAR1G (49-62) + 83 μM ProT. Sample was prepared in 25mM H_3PO_4 , 150 mM NaCl, 0.2 mM EDTA and 10 % D_2O (pH 6.5):



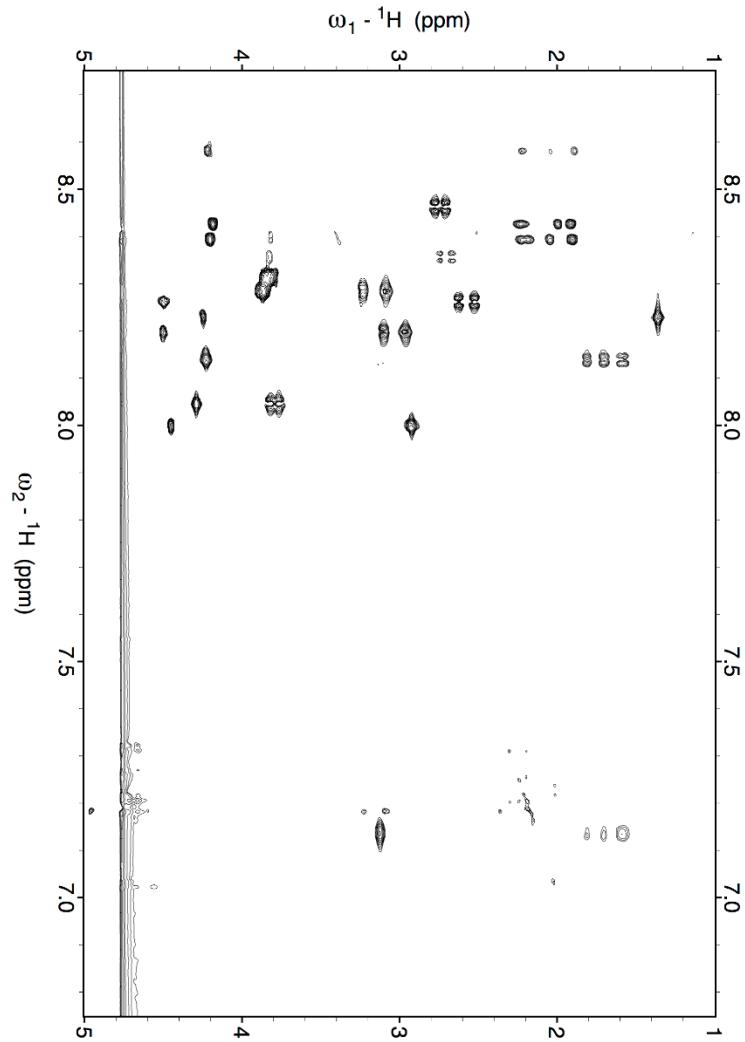
APPENDIX 46

2D NOESY Amide region of 830 μM PAR1G (49-62) + 83 μM ProT. Sample was prepared in 25mM H_3PO_4 , 150 mM NaCl, 0.2 mM EDTA and 10 % D_2O (pH 6.5):



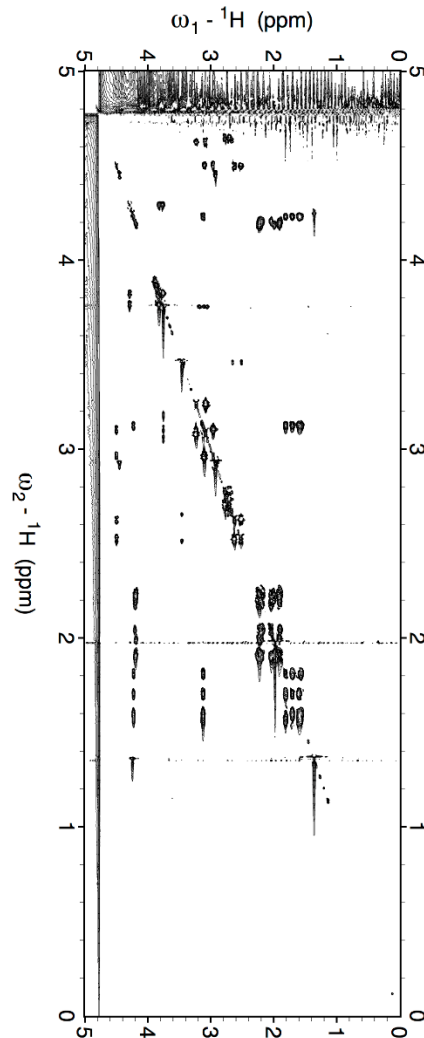
APPENDIX 47

2D TOCSY region of 1.5 mM Fbg B β (5-16). Sample was prepared in 25mM H₃PO₄, 150 mM NaCl, 0.2 mM EDTA and 10 % D₂O (pH 5.6):



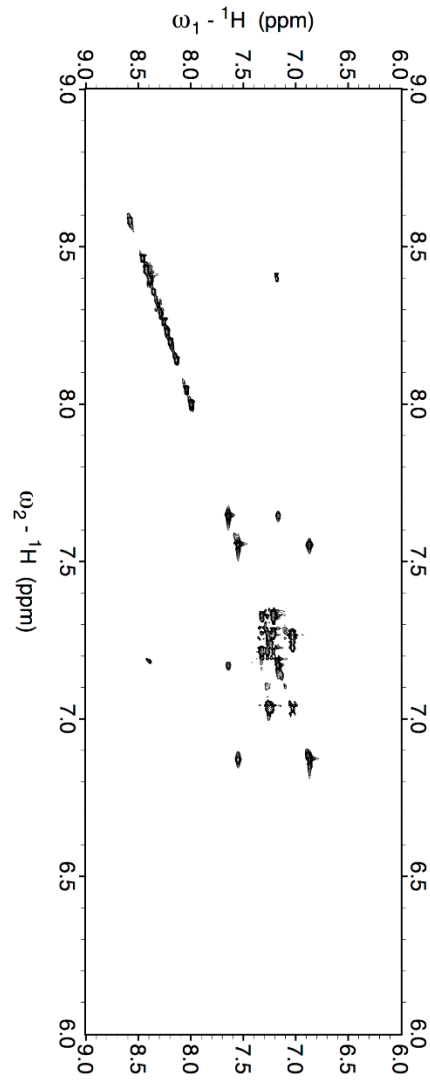
APPENDIX 48

2D TOCSY Aliphatic region of 1.5 mM Fbg B β (5-16). Sample was prepared in 25mM H₃PO₄, 150 mM NaCl, 0.2 mM EDTA and 10 % D₂O (pH 5.6):



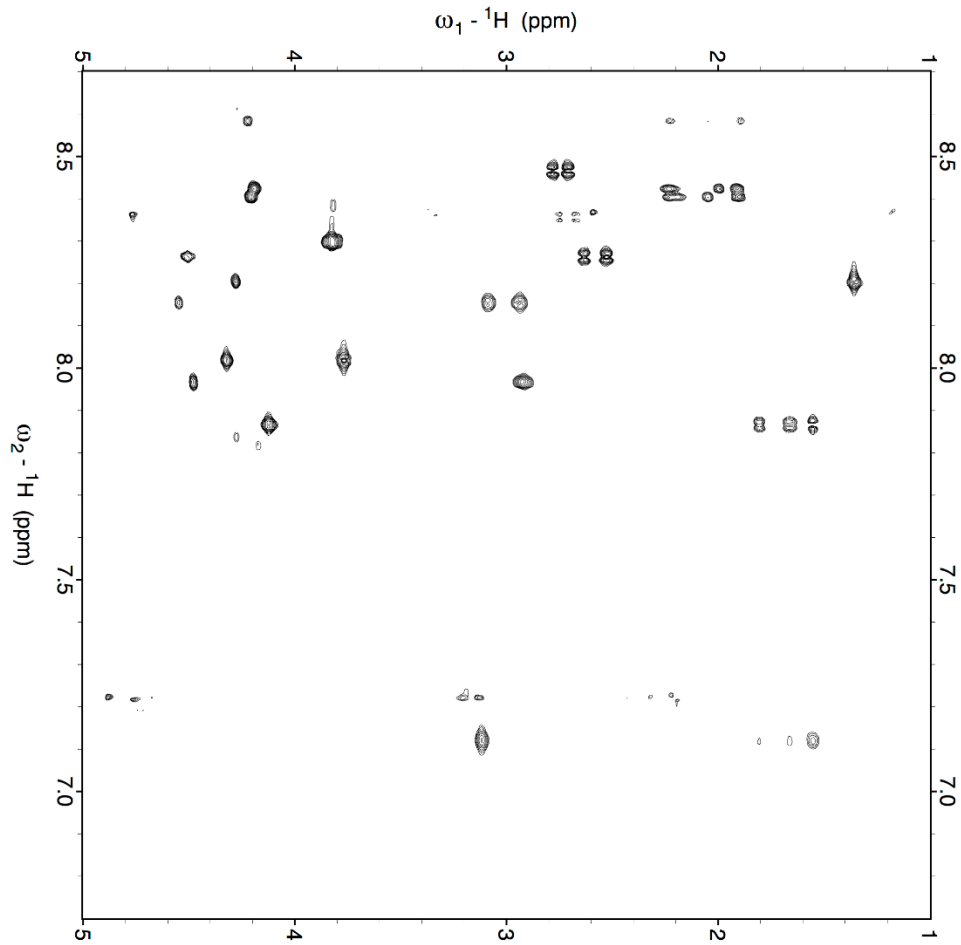
APPENDIX 49

2D TOCSY Amide region of 1.5 mM Fbg B β (5-16). Sample was prepared in 25mM H₃PO₄, 150 mM NaCl, 0.2 mM EDTA and 10 % D₂O (pH 5.6):



APPENDIX 50

2D TOCSY Fingerprint region of 1.5 mM Fbg B β (5-16) and 160 μ M thrombin. Sample was prepared in 25mM H₃PO₄, 150 mM NaCl, 0.2 mM EDTA and 10 % D₂O (pH 5.6):

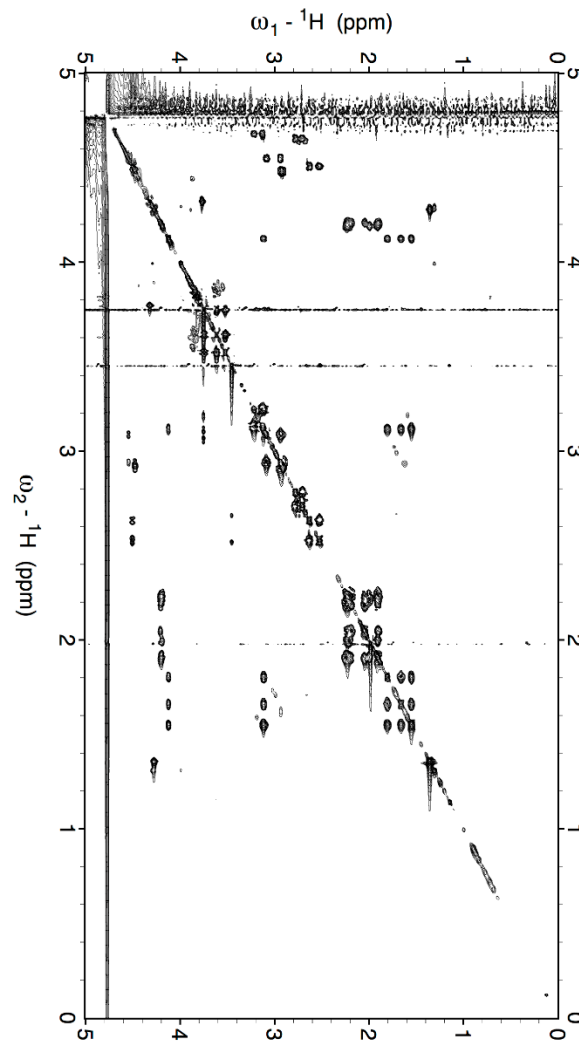


APPENDIX 51

2D TOCSY Aliphatic region of 1.5 mM Fbg B β (5-16) and 160 μ M thrombin.

Sample was prepared in 25mM H₃PO₄, 150 mM NaCl, 0.2 mM EDTA and 10

% D₂O (pH 5.6):

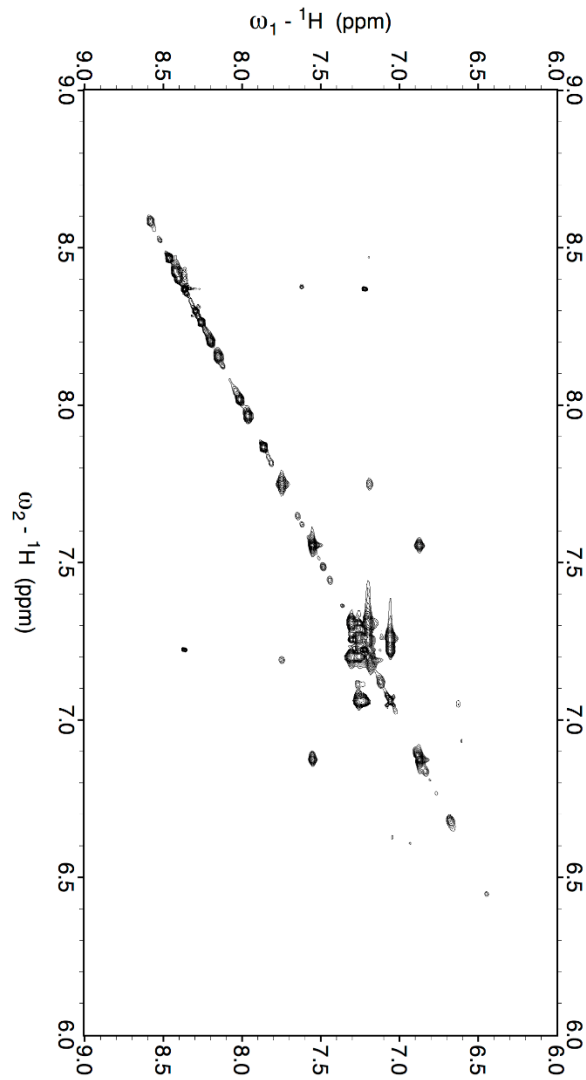


APPENDIX 52

2D TOCSY Amide region of 1.5 mM Fbg B β (5-16) and 160 μ M thrombin.

Sample was prepared in 25mM H₃PO₄, 150 mM NaCl, 0.2 mM EDTA and 10

% D₂O (pH 5.6):



APPENDIX 53

ABBREVIATIONS

ABE-I	Anion binding exosite – I
ABE-II	Anion binding exosite – II
AP	Activation peptide
AT	Antithrombin
AUC	Analytical Ultra Centrifugation
EDTA	Ethylenediaminetetraacetate
Fbg Aα	Fibrinogen A α chain
Fbg Bβ	Fibrinogen B β chain
FpA	Fibrinopeptide A
FpB	Fibrinopeptide B
FXIII	Transglutaminase FXIII
FXIII AP	Transglutaminase FXIII Activation Peptide
Gla	γ -carboxyglutamic acid
GpIbα	Glycoprotein Ib α found on the receptor
HDX-MS	Hydrogen Deuterium Exchange -Mass Spectrometry
HK/HMWK	High Molecular Weight Kininogen
His 57	Histidine at 57 th position of the thrombin sequence
HSQC	Heteronuclear Single Quantum Coherence
ITC	Isothermal Titration Calorimetry
<i>k</i>_{cat}	Product turnover/ Catalytic Constant
<i>K</i>_D	Binding affinity
<i>K</i>_m	Michaelis Constant
<i>k</i>_{cat}/<i>K</i>_m	Specificity Constant
<i>k</i>_{off}	Dissociation Rate Constant
<i>k</i>_{on}	Association Rate Constant
MALDI-TOF MS	Matrix Assisted Laser Desorption Ionization Time of Flight Mass Spectrometry
NMR	Nuclear Magnetic Resonance
PAI1	Plasminogen Activator Inhibitor 1
PAR	Protease Activated Receptor
PAR1P	Protease Activated Receptor-1 with Proline at 54 th position
PAR1G	Protease Activated Receptor-1 with Glycine at 54 th position
PAR3	Protease Activated Receptor-3
PAR3G	Protease Activated Receptor-3 with Glycine at 51 st position
PPACK	<i>D</i> -Phe-Pro-Arg chloromethyl ketone
ProT	Prothrombin
PT1	Prethrombin 1

PT2	Prethrombin 2
R	Gas constant
RP-HPLC	Reversed Phase High Performance Liquid Chromatography
R77a	Arginine at 77 th position of the thrombin sequence, “a” indicates first residue in 70 loop
R77aA	Arginine at 77 th position of the thrombin is replaced by alanine
SLEX	Systematic Evolution of Ligands by Exponential Enrichment
T	Absolute temperature
T₁	Spin-lattice Relaxation with time constant T ₁
T₂	Transverse Relaxation with time constant T ₂
TF	Tissue factor
TFPI	Tissue Factor Pathway Inhibitor
TM	Thrombomodulin
vWF	von Willebrand Factor
W60d	Trptophan at 60 th position of the thrombin sequence, “d” indicates fourth residue in 60s loop
Y60a	Tyrosine at 60 th position of the sequence, “a” indicates first residue in 60s loop
Y_P	Phosphotyrosine
1D	One Dimensional
2D	Two Dimensional
2D TOCSY	Two-Dimensional Total Correlational Spectroscopy
2D tr-NOESY	Two- Dimensional Transferred Nuclear Overhauser Spectroscopy
IIa	Thrombin
ω	Resonance Frequency
τ_c	Rotational Correlation Time
ΔH	Change in enthalpy
ΔG	Change in Gibbs Free energy
ΔS	Change in Entropy

CURRICULUM VITA

Ramya Billur
2234 South Preston Street Apt #4, Louisville, KY 40217
(502) 609-7933
r0bill01@louisville.edu | billur.ramya@gmail.com

EDUCATION

Ph.D. Candidate in Chemistry Department of Chemistry, University of Louisville, Louisville, KY	2012- 2018
M.Sc. Industrial Chemistry Jawaharlal Nehru Technological University, Hyderabad, India	2008 – 2010
B.Sc. Genetics, Chemistry, and Computer Applications Osmania University, Hyderabad, India	2005 – 2008

RESEARCH EXPERIENCE

University of Louisville, Louisville, KY

August 2013 - Present

Graduate Student with Dr. Muriel C. Maurer, Chemistry Department

- Investigating how binding interactions of platelet-derived Protease Activated Receptors (PARs) change as zymogen Prothrombin is converted to the serine protease Thrombin that contains with functional ligand binding exosites
- Using HSQC NMR titrations with ¹⁵N labeled peptides based on PAR3 (44-56) and PAR1 (49-62) to probe the conformational changes associated with maturation of Thrombin Anion binding Exosite I
- Evaluating binding affinities of individual ¹⁵N-labeled PAR residues for zymogen Prothrombin versus mature, active thrombin
- Elucidating the structural features that PAR3 (44-56) and PAR1 (49-62) adopt when complexed with Prothrombin and Thrombin using 2D TOCSY and 2D transferred NOESY NMR
- Characterizing long range interexosite communication between Thrombin Anion Binding Exosites I and II by NMR and Isothermal Titration Calorimetry (ITC) methods
- Analyzing thrombin-catalyzed hydrolysis of Fibrinopeptide B (5-16) by HPLC kinetic assay

RESEARCH EXPERIENCE (CONTD)

MNR Degree and P.G. College, Hyderabad, India April 2011-August 2011

Research Assistant with Dr. Sarabani Pal, Chemistry Department

Synthesis, purification and characterization of prodrug Chalcone and its derivatives from Paracetamol and NSAID

JNTU, Hyderabad, India November 2010- March 2011

Research Assistant with Dr. Mukkanti Khagga, Chemistry Department

- Synthesis, purification, and characterization of anticancer drug Dithiocarbamates and its derivative

JNTU, Hyderabad, India March 2010- August 2010

Research Assistant with Dr. Mukkanti Khagga, Chemistry Department

- Synthesis, purification, and characterization of potential pharmacological Indole and Aryl sulfonyl chloride derivatives

TECHNICAL SKILLS

- **Spectroscopy:** Infrared, UV-Visible, Atomic Absorption, NMR (^1H , ^{13}C , ^{15}N)
- **Protein Biochemistry:** Gel Electrophoresis, Ultrafiltration, Dialysis, Kinetic Assays, Enzyme-Ligand Titrations with NMR, and Isothermal Titration Calorimetry
- **Mass Spectrometry:** GC-MS Mass Spectrometry
- **Chromatography:** Paper, Column, HPLC, Gas Chromatography
- **Software:** NMRPipe, NMRDraw, Sparky, Mnova, CorelDraw, ChemDraw, ITCRun, NanoAnalyze, Pymol, Swiss-PdbViewer, UCSF Chimera, Kaleidagraph

CERTIFICATION COURSES

- **Grant Writing Academy** Spring 2017
School of Interdisciplinary and Graduate Studies, University of Louisville, KY
- **A Practical Approach to Microcalorimetry** Spring 2017
TA Instruments Webinar Training series

PUBLICATIONS

- **Ramya Billur**, T. Michael Sabo, Muriel C. Maurer “Binding Interactions of PAR1 and PAR3 for Thrombin and Dissecting the Allosteric Linkage Between Exosites” (*Manuscript in preparation*)
- **Ramya Billur**, Muriel C. Maurer “Secondary Structure Information as a Clue to Explain the Weak Kinetics of Thrombin-Catalyzed Release of Fibrinopeptide B” (*Manuscript in preparation*)

PUBLICATIONS (CONTD)

- **Ramya Billur**, David Ban, T. Michael Sabo, Muriel C. Maurer. (2017) “Deciphering the Conformational Changes Associated with the Maturation of Thrombin Anion Binding Exosite I”, *Biochemistry*, 56, 6343- 6354.
- Kavitha Kankanala, **Ramya Billur**, Vangala Ranga Reddy, Khagga Mukkanti & Sarbani Pal. (2012) “TFAA-H₃PO₄ Mediated Rapid and Single-step Synthesis of Mutual Prodrugs of Paracetamol and NSAIDs”, *Green Chemistry Letters and Reviews*, 5(3), 421-432.

POSTER AND ORAL PRESENTATIONS

- **R. Billur**, T. Michael Sabo, Muriel C. Maurer (2018) “Evaluating How Binding Interactions for PARs change as Prothrombin is Converted to Thrombin” 62nd Annual Meeting of the Biophysical Society, San Francisco, CA
- **R. Billur**, T. Michael Sabo, Muriel C. Maurer (2017) “Evaluating How Binding Interactions for PARs change as Prothrombin is Converted to Thrombin” Second Gateway NMR Conference, Columbus, OH
- **R. Billur**, M.C. Maurer (2016) “Probing Anion Binding Exosite Development as a Strategy to Understand Thrombin Activation” First Gateway NMR Conference, Louisville, KY
- **R. Billur**, M.C. Maurer (2016) “Probing Anion Binding Exosite Development as a Strategy to Understand Thrombin Activation” Research Louisville, Louisville, KY
- R. Billur, **M.C. Maurer** (2016) “Probing Anion Binding Exosite Development as a Strategy to Understand Thrombin Activation” Gordon Research Conference: Hemostasis, Stowe, VT
- **R. Billur**, M.C. Maurer (2016) “Anion Binding Exosites as a Target to Understand the Activation of Thrombin” 60th Annual Meeting of the Biophysical Society, Los Angeles, CA
- **R. Billur**, M.C. Maurer (2015) “Ligand Binding to Anion Binding Exosites as Prothrombin is Converted to Active Thrombin, IMD3 Fall Fest, University of Louisville, Louisville, KY, (ORAL)
- **R. Billur**, M.V. Malovichko, M.C. Maurer (2015) “Ligand Binding to Anion Binding Exosites as Prothrombin is Converted to Active Thrombin, 4th Bluegrass Molecular Biophysics Symposium, University of Kentucky, Lexington, KY
- **R. Billur**, M.V. Malovichko, M.C. Maurer (2015) “Ligand Binding to Anion Binding Exosites as Prothrombin is Converted to Active Thrombin, 59th Biophysical Society Meeting, Baltimore, MD
- Kavitha Kankanala, **R. Billur**, Vangala Ranga Reddy, Khagga Mukkanti, Sarbani Pal (2011) “Mild, Alternative Protocol for Synthesis of Chalcones Mediated by TFAA-H₃PO₄”, National Seminar on Recent Trends in Pharmaceutical Chemistry, Krishna University, Machilipatnam, India

POSTER AND ORAL PRESENTATIONS (CONTD)

- Katari Naresh Kumar, R. Billur, **Kintali Sreeramamurthy**, Khagga Mukkanti, Parthasarathi Das (2011) “Dithiocarbamate Promoted a Practical Synthesis of N-Aryl-2-Aminobenzazoles: Synthesis of Novel Aurora- A Kinase inhibitor”, National Conference on Recent Trends in Organic Chemistry and Natural Products, Adikavi Nannaya University, Rajamundry, India
- **Katari Naresh Kumar**, R. Billur, Khagga Mukkanti, Parthasarathi Das (2011) “An Efficient one-pot Synthesis of Various Substituted Aryl Dithiocarbamic Acid Methyl Esters”, National Conference on Recent Trends in Organic Chemistry and Natural Products, Adikavi Nannaya University, Rajamundry, India
- T. Vanishri, **R. Billur** and Sarbani Pal (2010) “Synthesis and Characterization of Substituted Carbazoles by Using Microwave Condition”, AP Science Congress, Jawaharlal Nehru Technological University, Hyderabad, India

AWARDS

- Graduate Research Assistant, NIH - Fall 2017 to May 2018
- Department of Chemistry Travel Award, (\$ 200) - 2017
- International Student Tuition Support, (\$ 500) - 2017
- Graduate Student Council Travel Award, (\$ 350) - 2017
- GNAS Travel Award, (\$ 250) - 2017
- Graduate Teaching Assistant, UofL - Fall 2012 to July 2017
- IMD3Travel Award, (\$ 600) -2016
- Graduate Student Council Travel Award, (\$ 350) - 2016
- IMD3Travel Award, (\$ 600) -2015
- Graduate Student Council Travel Award, (\$ 350) - 2015
- Best poster award, Krishna University, Machilipatnam, India – 2011

TEACHING EXPERIENCE

Graduate Teaching Assistant Fall 2012 – Summer 2017
Department of Chemistry, University of Louisville, KY

- Biochemistry Laboratory (CHEM 546)
- Organic Chemistry Laboratory I (CHEM 343)
- Chemical Analysis Laboratory IV (CHEM 210)
- Chemical Analysis Laboratory III (CHEM 209)
- Chemical Analysis Laboratory II (CHEM 208)
- Chemical Analysis Laboratory I (CHEM 207)
- Assisted Chemistry professors in organizing, proctoring, and grading exams

Lecturer September 2011- June 2012

- Engineering Chemistry (JNTUH, EC)

PROFESSIONAL MEMBERSHIP

- Golden Key International Honor Society - Lifetime member
- Biophysical Society - 2017 to 2018
- American Heart Association - 2017
- Biophysical Society - 2014 to 2016
- American Chemical Society - 2012-2013